

Copy No. 312
RM No. A6K15

RESTRICTED



RESEARCH MEMORANDUM

AN INVESTIGATION OF THE LOW-SPEED STABILITY AND CONTROL
CHARACTERISTICS OF SWEPT-FORWARD AND SWEPT-BACK WINGS
IN THE AMES 40- BY 80-FOOT WIND TUNNEL

By

Gerald M. McCormack and Victor I. Stevens, Jr.

Ames Aeronautical Laboratory
Moffett Field, Calif.

CLASSIFIED DOCUMENT

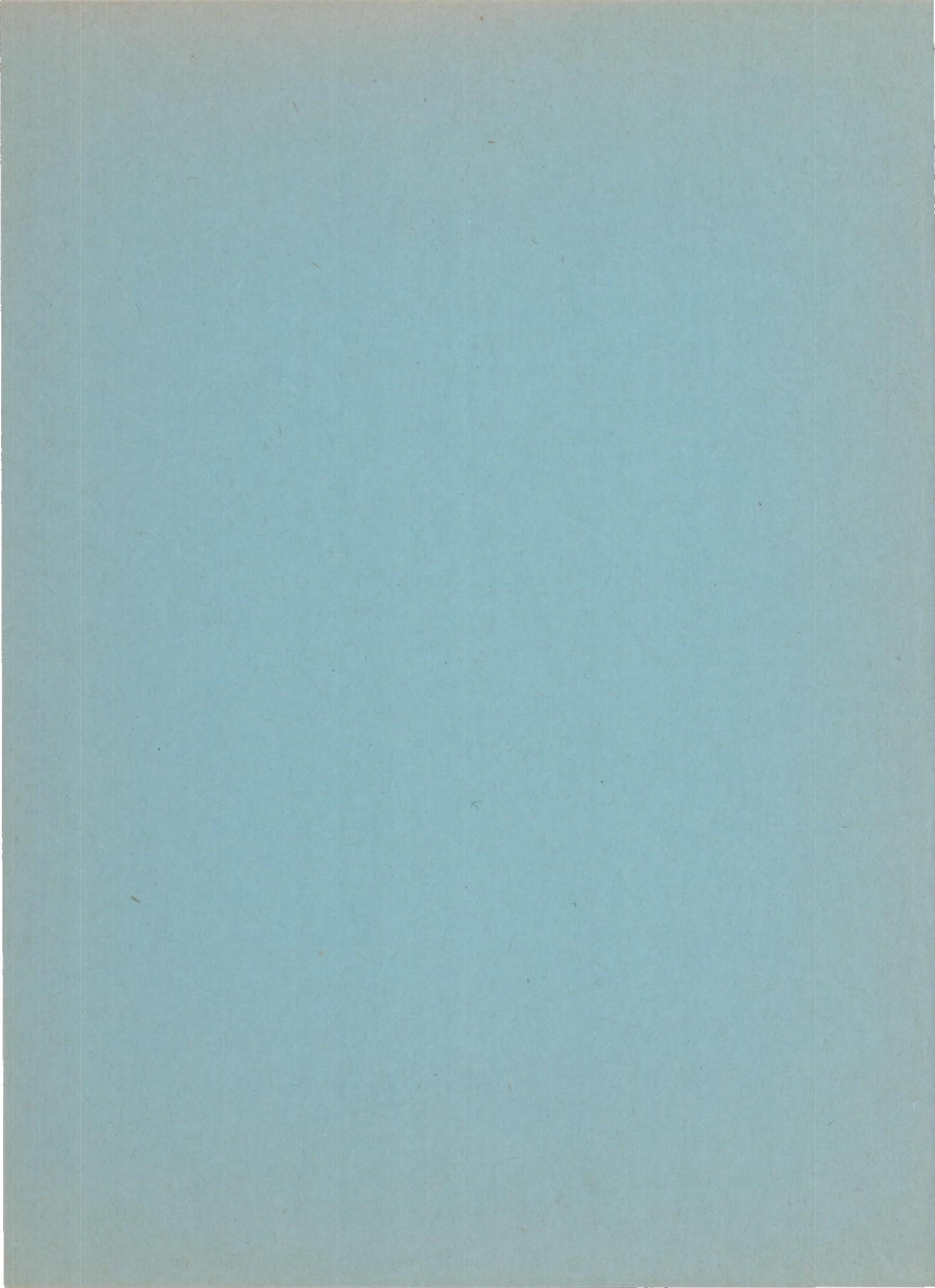
This document contains classified information affecting the National Defense of the United States within the meaning of the Espionage Act, USC 50:31 and 32. Its transmission or the revelation of its contents in any manner to an unauthorized person is prohibited by law. Information so classified may be imparted only to persons in the military and naval services of the United States, appropriate civilian officers and employees of the Federal Government who have a legitimate interest therein, and to United States citizens of known loyalty and discretion who of necessity must be informed thereof.

NATIONAL ADVISORY COMMITTEE
FOR AERONAUTICS

WASHINGTON

June 10, 1947

RESTRICTED



NATIONAL ADVISORY COMMITTEE FOR AERONAUTICS

RESEARCH MEMORANDUM

AN INVESTIGATION OF THE LOW-SPEED STABILITY AND CONTROL
CHARACTERISTICS OF SWEPT-FORWARD AND SWEPT-BACK WINGS
IN THE AMES 40- BY 80-FOOT WIND TUNNEL

By Gerald M. McCormack and Victor I. Stevens, Jr.

SUMMARY

An investigation has been made at large scale of the characteristics of highly swept wings. Data were obtained at several angles of sideslip on wings having angles of sweep of $\pm 45^\circ$, $\pm 30^\circ$, and 0° . The airfoil sections of the wings varied from approximately NACA 0015 at the root to NACA 23009 at the tip. Each wing was investigated with flaps undeflected, partial-span split flaps deflected 60° , full-span split flaps deflected 60° and split-flap-type ailerons deflected $\pm 15^\circ$. Values of maximum lift were obtained at Reynolds numbers ranging from 5.7 to 9.2×10^6 . In this report the summarized results are compared with the predictions made by use of the simplified theory for the effect of sweep and with existing small-scale data. The basic wind-tunnel results from which these summary data were taken are included in an appendix.

The primary problems accompanying the use of sweep as revealed by this investigation are the loss in maximum lift, the high effective dihedral, and the sharp reduction in lateral-control effectiveness. In general, simple theory enables good predictions to be made of the gross effects of sweep but further

refinements are necessary to obtain the accuracy required for design purposes. In cases where comparisons can be made, the indications are that, as sweep increases, scale effects diminish and large-scale results approach small-scale results.

INTRODUCTION

Theory indicates and experiment has shown that the prime aerodynamic effect of wing sweep is to reduce by the cosine of the angle of sweep the effective flight velocity experienced by the airfoil sections of the wing. This then enables increases in maximum flight speed to be attained before serious compressibility effects are encountered. Theory and experiment also show that wing sweep introduces a number of stability and control problems, the seriousness of which becomes accentuated at low flight speeds.

Small-scale tests have pointed out the general nature of these problems and indicated those which must be overcome if the high-speed benefits of sweep are to be realized. They have also suggested that boundary-layer flow and, hence, Reynolds number has a profound influence on measured characteristics and that the value of small-scale tests remain somewhat doubtful until the extent of this influence is understood.

Since no large-scale data were available for wings with large angles of sweep, an investigation of the effects of sweep was conducted in the Ames 40- by 80-foot wind tunnel and the results are reported herein. It is believed that

these data will go far towards establishing the datum required to estimate the effects of scale on highly swept wing plan forms. With this knowledge at hand it is evident that the value of future small-scale tests will be considerably increased.

This report discusses a summary of the basic results and compares them with simple swept-wing theories and, where possible, with existing small-scale data (references 1, 2, and 3). To make the basic data available for further analyses they are included as an appendix to this report.

DESCRIPTION OF MODELS

The five models tested were composed of wing panels from an available airplane which were given the desired plan form and sweep by individually fabricated tips and center sections. The resulting angles of sweep were 0° , 30° , and 45° sweepforward, and 30° , and 45° sweepback (measured with reference to the quarter-chord line of the airfoil sections). Aside from the angle of sweep, the prime plan-form variable was considered to be aspect ratio. The tips and center sections were constructed to give the smallest variation of this parameter possible without modification of the airplane wing panels. No special attempt was made to control the variation of taper ratio, area or span. Photographs of the wings and plan-form drawings with pertinent dimensions are shown in figures 1 and 2. The geometric characteristics of the five wings tested are listed in table I.

The airfoil sections of the swept wings were dictated by the sections of the airplane wing panels (an NACA 0015 at the inboard end and an NACA 23009 at the outboard end of the panel). The profiles of the center sections and tips were simply extensions of the wing-panel airfoil. To expedite construction, three tips only were fabricated: one for the swept-forward wings, one for the straight wing, and one for the swept-back wings. Thus for the swept-forward and swept-back wings compromise tips were used which were misaligned $7\frac{1}{2}^{\circ}$ to the air stream. The twist in the chord plane of the wing panels was approximately $1/4^{\circ}$ of washout. The dihedral of the chord-plane leading edge was kept at 0° .

No attempt was made to improve the fairness of the wing panels beyond the original manufacturing condition. Thus, due to presence of various access plates, panel joints, etc., the wings were rough to a greater degree than that normally associated with latest construction requirements.

Partial-span and full-span split flaps were tested on all models. The flaps were 0.20 chord and were deflected 60° .¹ The span of the partial-span flaps was 0.623 wing span for all models; the span of the full-span flaps varied slightly from full-span (in no case more than 0.064 wing span) as shown in table I.

Ailerons were simulated by attaching the outboard portion of one of the flaps to the right wing and deflecting it $\pm 15^{\circ}$ (up-deflection was obtained by attaching the flap to the upper surface of the wing). Thus the ailerons as tested were

¹Except where noted, all chords and spans used in this report were measured parallel and perpendicular to the plane of symmetry. Flap deflection angles were measured in a plane perpendicular to the flap hinge line.

0.20-chord split-flap-type ailerons.

The wings were mounted on a faired sting which in turn was attached to the three-strut support system. Photographs of the wing installations are shown in figure 1.

COEFFICIENTS AND SYMBOLS

The data are presented in the form of standard NACA coefficients and symbols as defined in figure 3 and the following tabulation. All forces and moments are presented about the stability axes with their origin located on the root chord, or root chord projected and at the same fore and aft location as the quarter H.A.C.

C_L	lift coefficient (lift/qS)
C_D	drag coefficient (drag/qS)
C_m	pitching-moment coefficient ($\frac{\text{pitching moment}}{qSc}$)
C_l	rolling-moment coefficient ($\frac{\text{rolling moment}}{qSb}$)
C_n	yawing moment coefficient ($\frac{\text{yawing moment}}{qSb}$)
C_Y	side-force coefficient ($\frac{\text{side force}}{qS}$)
$C_{L\alpha}$	rate of change of lift coefficient with angle of attack, per degree
ΔC_L	increment of lift coefficient due to deflecting flaps
$C_{L_{\max}}$	maximum lift coefficient
$C_{l\beta}$	rate of change of rolling-moment coefficient with sideslip, per degree
C_{l_p}	rate of change of rolling-moment coefficient with wing-tip helix angle, per radian

$C_{n\beta}$	rate of change of yawing-moment coefficient with sideslip, per degree
$C_{l\delta_a}$	rate of change of rolling-moment coefficient with aileron angle, per degree
$\frac{\partial C_l}{\partial C_L}$	rate of change of C_l with lift coefficient where lift is increased by changing angle of attack
$\Delta C_l / \Delta C_L$	rate of change of C_l with lift coefficient where lift is increased by deflecting flaps
$\frac{\partial C_{n\beta}}{\partial C_L^2}$	rate of change of $C_{n\beta}$ with the lift coefficient squared
L/D	ratio of lift to drag
q	dynamic pressure, pounds per square foot
V	velocity along flight path, feet per second
α	angle of attack, degrees
β	angle of sideslip, degrees
Λ	angle of sweep of quarter chord line of airfoil sections, degrees (Sweepback is positive and sweepforward is negative.)
Γ_e	effective dihedral, degrees
δ	control surface deflection, degrees
A	aspect ratio based on span ($\frac{b^2}{s}$)
A'	aspect ratio based on length of quarter chord line ($\frac{b^2}{s \cos^2 \Lambda}$)
E	Jones' edge-velocity correction
λ	taper ratio, ratio of tip chord to root chord ($\frac{c_t}{c_r}$)
S	wing area, square feet

- c mean aerodynamic chord of wing measured parallel
to plane of symmetry, feet
- b wing span measured perpendicular to the plane of
symmetry, feet
- c_t wing-tip chord
- c_r wing-root chord

TESTS AND RESULTS

For each of the model configurations six-component force and moment data were obtained through an angle-of-attack range at each of several angles of sideslip. The data were obtained at dynamic pressures which range from 5 to 75 pounds per square foot ($R = 2.8 \times 10^6$ to $R = 18.0 \times 10^6$)²; most of the data were obtained at dynamic pressures of 10 to 20 pounds per square foot ($R = 4.0 \times 10^6$ and $R = 9.3 \times 10^6$, respectively).

The basic data obtained from the wind-tunnel tests of the five swept wings are described in the appendix. Also included in the appendix is a description of the corrections and tares applied to the data.

DISCUSSION

In this discussion an evaluation is made of the effect of wing sweep on the more important aerodynamic parameters and of the consequent effect on airplane performance and stability.

²These Reynolds numbers are based upon the M.A.C. as a reference length and are the minimum and maximum limits of the variation including the change in chord length with sweep.

Also, the accuracy with which the simplified sweep theory may be used to predict the characteristics of swept wings is evaluated by a comparison with the experimental data. Finally, an attempt is made to compare at least qualitatively the values of the various characteristics as obtained at small-scale ($R < 1.5 \times 10^6$) and full-scale Reynolds numbers. The summary data on which this discussion is based have been extracted (for a test dynamic pressure of 20 lb/sq ft) from the measured characteristics included in the appendix.

The concepts advanced by Betz in reference 4 form the groundwork for the theory of the aerodynamic effects of incorporating sweep in a wing plan form. These concepts are based on the assumption that for an infinite-span wing only the velocity component normal to the quarter-chord line influences the pressures over a wing; the spanwise component of velocity is neglected. Thus, if the velocity components are resolved perpendicular and parallel to the quarter-chord line of a wing, the effective dynamic pressure over the wing will decrease in proportion to the square of the cosine of the angle of sweep and the effective angle of attack will increase in proportion to the reciprocal of the cosine of the angle of sweep. These changes in effective dynamic pressure and angle of attack brought about by wing sweep form the basis for the existing simplified sweep theory.

In interpreting the comparisons to be made between the simplified theory and experimental results, the limitations

of the simplified theory must be borne in mind. Over the root section of highly swept finite-span wings, particularly highly tapered low aspect ratio wings, the basic assumption that the wing reacts only to air velocities normal to the quarter-chord line probably does not hold. It should also be noted that simplified theory in its present form applies only to wings which generate an additional loading due to angle-of-attack change that is rectangular in form. Therefore appreciable deviations from rectangular loading such as produced by taper will result in discrepancies between the theoretical and experimental results.

Lift Characteristics

Lift-curve slope.— The simplified theory indicates a decrease in lift-curve slope proportional only to $\cos\Lambda$. To account for induction effects, a correction must also be made for any variations of aspect ratio. Hence, the effect of sweep on lift-curve slope, when corrected for aspect ratio, will be in accordance with the relation:

$$(c_{L\alpha})_\Lambda = (c_{L\alpha})_{\Lambda=0} \cos\Lambda \frac{[A/(A+2)]_\Lambda}{[A/(A+2)]_{\Lambda=0}}$$

In conformity with standard nomenclature, aspect ratio is based on the span of the wings; however, there is some contention that since only air flow perpendicular to the quarter-chord

line is considered to affect the aerodynamic characteristics, aspect ratio should be based on the length of the quarter-chord line. Such an assumption is used in the analysis included in reference 1. In figure 4, the experimental results (taken from the linear portion of the lift curve) are shown together with the predictions based on theory for both concepts of aspect ratio³. For swept-back wings, basing the aspect ratio on the length of the quarter-chord line gives the better agreement; whereas for swept-forward wings, basing the aspect ratio on the conventional span gives the better agreement.

It is believed that neither of these aspect ratio concepts gives a correct picture of the induction effects of the vortex pattern on swept wings. It can be shown that if a wing is swept back, the induction influences of the trailing vortices on the wing should be reduced, and conversely, if a wing is swept forward, the induction influences on the wing should be increased. That is, the effective aspect ratio increases with sweepback and decreases with sweepforward for wings of constant geometric aspect ratio (b^2/S).

The lift-curve slopes for the wings of this report have been estimated using the method of Falkner (reference 5) which

³It is recognized that a further aspect ratio correction, namely, Jones' edge-velocity correction should be used. The effect is small, however, compared to the errors resulting from the use of simple sweep theory. It has been omitted, therefore, in an effort to indicate clearly the adequacy of simple sweep theory in indicating the lift-curve slope of highly swept wings.

takes into consideration the induction effects of the swept vortex system in a more precise manner. In applying this method the section lift-curve slope for these wings ($c_{l\alpha} = 0.103$) was used rather than the theoretical value ($c_{l\alpha} = \frac{2\pi}{57.3}$) used in reference 5. The results are shown in figure 4. The predicted values of $C_{L\alpha}$ and their variation with sweep closely approximate the experimental results. This indicates that, when induction effects are properly accounted for, accurate predictions of lift-curve slope can be made. It can be inferred then that the failure of simple theory to accurately indicate the effect of sweep on lift-curve slope is a result of improper induction effects.

Taper appears to have a strong effect on lift-curve slope due to its inherent influence on induction effects. As previously mentioned, the simplified theory strictly applies only to rectangular loading and hence the taper of the wings of the subject investigation may account for some of the discrepancy between theoretical and experimental results. In an attempt to correlate the effect of taper on the lift-curve slope of swept wings, data from previous investigations of swept wings having different taper ratios (references 1, 2, 3, 6, and 7) are shown in figure 5. For most of the investigations the wing aspect ratio (defined as b^2/S) and taper ratio did not vary with sweep. For those cases where aspect ratio (b^2/S) varied with sweep, the data were corrected to the aspect ratio (b^2/S) for the unswept wing.

Examination of the data in figure 5 will reveal that, as taper ratio is decreased, the maximum value of lift-curve slope occurs at greater angles of sweepback. The relation between taper ratio and the angle of sweep at which the maximum value of lift-curve slope occurs is shown in figure 6. The figure discloses that in order to obtain maximum lift-curve slope the taper ratio should be reduced from 1.0 as the wing is swept back and, by inference, increased from 1.0 as the wing is swept forward.

A comparison of figures 4 and 5 shows that values of lift-curve slope determined from large-scale tests show no better or poorer agreement with simple theory than values from small-scale tests. It appears that the principal disagreement between theory and experiment lies in failure of the theory to properly account for the induction effects on swept wings and that in comparison the effects of scale are relatively small.

Examination of the nonlinear portion of the lift curves and comparison with small-scale data shows that no consistent effects exist which could be attributed directly to scale effect. Those differences which do exist are small and erratic in nature and probably result from differences in plan form, wing section, and local wing roughness.

Flap effectiveness.-- According to simple sweep theory, flap effectiveness decreases as $\cos^2\Lambda$. An additional correction to account for induction effects must be applied

when comparing flap effectiveness on wings of different aspect ratio. The comments previously made regarding the effects of induction on lift-curve slope apply equally well to flap effectiveness. In fact when α' , $C_{L\alpha}'$, and δ are measured perpendicular to the quarter-chord line, the effectiveness parameter $\alpha'\delta$ is unaffected by sweep and the lift increment produced by flap deflection is directly proportional to $C_{L\alpha}'$ or to $C_{L\alpha} \cos\Lambda$. Hence the theoretical effect of sweep on flap lift increment may be written either in terms of sweep and aspect ratio:

$$(\Delta C_L)_\Lambda = (\Delta C_L)_{\Lambda=0} \cos^2\Lambda \frac{[A/(A+2)]_\Lambda}{[A/(A+2)]_{\Lambda=0}}$$

or in terms of sweep and lift-curve slopes:

$$(\Delta C_L)_\Lambda = (\Delta C_L)_{\Lambda=0} \cos\Lambda \frac{(C_{L\alpha})_\Lambda}{(C_{L\alpha})_{\Lambda=0}}$$

where α is the angle of attack of the root chord.

In figure 7 the experimental results are shown together with predictions made in accordance with both the foregoing relations⁴. It can now be seen that predictions of flap lift increment made in terms of aspect ratio deviate from experiment the same as did the predictions of lift-curve slope. However when predictions are made in terms of lift-curve

⁴Note that in correcting for aspect ratio, the aspect ratio was based on the span. As in the case of $C_{L\alpha}$, if aspect ratios were based on the length of the quarter-chord line better agreement in flap lift increment would have been obtained for swept-back wings and poorer agreement for swept-forward wings.

slopes, the agreement with experiment is almost exact. Thus the control which C_{L_a} has on flap effectiveness emphasizes the importance of fully understanding the effect on C_{L_a} of the many factors involved; this is especially significant when flap effectiveness is considered in terms of airplane control and performance.

Since the flap lift increment is dependent upon lift-curve slope, the conclusions concerning the effect of scale on lift-curve slope apply equally well to flap lift increment. In general, it can be said that sweep introduces no new scale effect on flap lift increments measured at low angles of attack.

Maximum lift.-- The effect of sweep on maximum lift of the wing without flaps, with 0.623 span flaps deflected 60°, and with full-span split flaps deflected 60° is shown in figure 8. Attention is called to the fact that the wings tested were composed largely of production wing panels with normal roughness and irregularities such as caused by access plates. As a result of the roughness, maximum lifts measured on these wings may be somewhat lower than those measured on smooth wings. However, since the measured values on the unswept wing appear to be reasonably high for the particular airfoil sections, it is believed that the roughness was not sufficient to seriously reduce the maximum lift measured.

As shown in figure 8, sweep in wing plan form produces serious losses in maximum lift. However, for all but one of

the wing configurations the measured maximum lift was equal to or greater than simple theory would indicate, that is, $C_{L_{max}}$ did not in general decrease proportional to $\cos^2\Lambda$. Furthermore, the geometric angle of attack for $C_{L_{max}}$ (fig. 9) does not decrease as

$$\cos\Lambda \frac{[A/(A+2)]_{\Lambda=0}}{[A/(A+2)]_{\Lambda}}$$

which would be predicted by simple theory. It is probable that spanwise boundary-layer flow prevents stall from spreading from tip to root on the swept-back wing and from root to tip on the swept-forward wing. It is also possible that this intense boundary-layer drain allows certain sections of the wing to reach abnormally high angles of attack prior to stall.

On the unswept wing the gain in maximum lift coefficient due to flap deflection is equal to the flap lift increment at low angles of attack; whereas on the swept wings the gains in maximum lift coefficient are somewhat less than the flap lift increments realized at low angles of attack. This is particularly true for the outboard portion of full-span flaps on the swept-back wings and the inboard flaps on the swept-forward wings. (For sweepback angles greater than 30° , full-span flaps produce no greater $C_{L_{max}}$ than do partial-span flaps.) Such decreases in flap effectiveness with sweep are disappointing but not surprising, since near stall the air flow is separated on the outboard section of swept-back wings and the inboard section of swept-forward wings.

The measured loss in $C_{L_{max}}$ due to sweep seriously limits airplane performance. With either partial or full-span flaps, the loss in $C_{L_{max}}$ due to 45° of sweep would require increases in landing speed of approximately 20 percent.

Because of differences in taper ratio and airfoil sections of models used for small- and large-scale tests to date, no quantitative conclusions can be drawn regarding the effects of scale on $C_{L_{max}}$ at various angles of sweep. In general, however, it can be inferred that as the angle of sweep is increased the effects of scale become smaller. For instance a comparison of figure 8 of this report with figure 7 of reference 8 shows that an increase in $C_{L_{max}}$ of 0.25 is obtained at 0° of sweep when going from small- to large-scale tests. In contrast, increases of only 0.10 and 0.08 in $C_{L_{max}}$ are gained with 30° and 45° sweepback. The increase in $C_{L_{max}}$ at 0° of sweep is in general accord with what past experience has shown to be a reasonable effect of scale; whereas the increases for the swept wings fall far short of what would be anticipated from experience on straight wings. These data indicate that large-scale tests show a much more rapid decrease of $C_{L_{max}}$ with sweep than do model tests. This seems true whether flaps are deflected or not. Since large-scale results tend to approach small-scale results at large angles of sweep, considerable care should be taken in trying to estimate large-scale airplane performance from swept-wing model tests. Expectations of improving $C_{L_{max}}$ commensurate with that experienced at zero sweep are not likely to be fulfilled. The importance of this problem would indicate a pressing need for swept-wing tests of a number of given models throughout the full Reynolds number range.

~~before~~ It should be noted that the above inferences have been drawn from results of tests of wings using conventional airfoil sections. It may well be that when sufficient data become available to make similar comparisons on wings using laminar-flow sections, the effects of roughness and Reynolds number may be markedly different.

L/D ratio. - The variation of L/D with lift coefficient is shown in figure 10 for each of the five wings with partial and with full-span flaps. That part of the drag attributed to induced drag has been corrected to the aspect ratio⁵ (b^2/S) of the unswept wing, that is, an aspect ratio of 4.62. The L/D values for conditions where the drag coefficient was less than 0.1 are not shown because it is believed possible inaccuracies due to lack of precise drag tare values would invalidate any conclusion drawn from such results. This excluded study of the most important flight speed range for plain wings and hence the L/D values for plain wings are not shown. It is believed, however, that the results shown for the wings with flaps are sufficiently accurate to allow useful conclusions to be drawn as to the effect of sweep on L/D ratios for that region of the most interest, centering around gliding and landing.

The results show that at lift coefficients near a maximum lift coefficient of 0.8 the L/D for the swept wings

⁵The use of aspect ratio based upon the span of wing rather than the length of the quarter-chord line is justified on the basis of results quoted in reference 6.

approximates that for the unswept wing. As stall is approached the L/D ratios of the swept-back wings remain at least as high as those for the unswept wing; whereas the L/D ratios of the swept-forward wings show a rapid decrease.

Longitudinal Characteristics

The effects of sweep on the pitching-moment characteristics of the plain wing, wing with partial-span flaps, and with full-span flaps are shown in figures 11 to 13. The remarks which follow are based upon the data obtained on the plain wing (fig. 11) but in general apply also to the wings with partial- or full-span flaps (figs. 12 and 13).

For lift coefficients less than 0.5, the pitching-moment coefficients vary almost linearly with lift coefficient and indicate that forward sweep moves the aerodynamic center forward (4 percent M.A.C. at -45° sweep), while sweepback moves the aerodynamic center rearward (5 percent M.A.C. at 45° sweep). At higher lift coefficients the $\pm 45^\circ$ swept wings, and to a lesser degree the -30° swept wing, exhibit an abnormal diving tendency. Similar diving tendencies of highly swept wings have been reported previously (reference 1). Such irregularities in moment characteristics do not appear serious if considered only in terms of the elevator power available with a conventional tail. However, the effect upon static stability and the abrupt variation of elevator position and of stick force with speed may prove objectionable to pilots. In

the case of a tailless design these irregularities would be more serious. For instance, if the 45° swept-back wing were considered a possible design with the 0.40-span ailerons used for longitudinal control (elevons) and with neutral stability at low lift coefficients, over 30° up-elevon travel would be required to maintain trim even if the elevon effectiveness at low lift coefficients were maintained. For the 45° swept-forward wing a similar but less extreme condition existed. Smaller control angles would be required but the data indicate an abruptness of control motion which, because of the low damping in pitch, might be serious in tailless designs. In considering the longitudinal stability it should be remembered that the effects of fuselage, tip shape, slots, etc., have been disregarded. It may be, and unpublished data so indicate, that minor configuration changes will remove the diving tendency and its associated problems.

For lift coefficients just less than $C_{L_{max}}$, the swept wings tested, with the exception of the 30° swept-forward wing, exhibited a strong climbing moment. This characteristic is obviously undesirable since it makes inadvertent stall quite likely. In reference 8 a chart was presented which defined, on the basis of small-scale data, the boundaries of aspect ratio and sweep angle which would give a wing either a climbing or a diving tendency near stall. This chart is reproduced herein as figure 14. Also shown on this figure are the data obtained in this investigation. Based upon these data, it appears that the chart as set forth in reference 8

applies as well to large-scale as to small-scale wings; furthermore, the chart applies to swept-forward as well as swept-back wings. Insofar as the over-all shape of the pitching-moment curve is concerned large-scale tests agree generally with small-scale results with the exception of minor differences. Again it should be noted that these comparisons have been made from examination of results of investigations on wings using conventional sections. The validity of the statements regarding these comparisons is as yet unsubstantiated in cases where laminar-flow sections are involved.

Lateral Characteristics

Dihedral effect.—The variation with lift coefficient of the rolling moment due to sideslip is shown in figure 15 for the plain wings and in figure 16 for the wings with flaps. The powerful influence of sweep on the dihedral effect is immediately apparent. (A scale of effective dihedral for the unswept wing has been shown on the figures to allow convenient comparisons.) Within limits, the dihedral effect due to sweep increases in proportion to lift coefficient.

Both the 30° and 45° plain swept-back wings reached a maximum value of $C_{l\beta}$ of -0.0034 (17° effective dihedral) at lift coefficients of 1.15 and 0.85, respectively. In the case of the swept-forward wing the maximum value of $C_{l\beta}$ increased with angle of sweep, being 0.0014 for the -30° swept wing and 0.0020 for the -45° swept wing. These maximum values for the swept-forward wings occurred in both cases near a lift coefficient of 0.9. It should be noted that while the swept-back wings show much greater dihedral effect than do the swept-forward wings, this is due largely to the dihedral effect of

the unswept wing. The incremental dihedral effect is roughly of the same order of magnitude for either direction of sweep.

The maximum dihedral effect of the wing with flaps deflected is considerably higher, about 32° for the 45° swept-back wing with full-span flaps. Such extreme dihedral would make maintenance of a wings-level attitude in the landing approach almost impossible because of extreme sensitivity in roll to slight angles of sideslip. Even with adequate lateral control it is felt that a pilot would have difficulty in reacting sufficiently fast to prevent reaching excessive angles of bank.

For the case where lift is changed by changing angle of attack (flap deflection constant), simple sweep theory gives the following relation for the parameter $\frac{\partial C_{l\beta}}{\partial C_L}$:

$$^e \quad (\frac{\partial C_{l\beta}}{\partial C_L})_A = (\frac{\partial C_{l\beta}}{\partial C_L})_{A=0} - \frac{1}{4} \frac{\tan A}{57.3}$$

^eIt is recognized that both of the terms on the right side of this equation should be modified further by a correction involving aspect ratio and edge velocity. Simple theory shows that, where asymmetrical lift exists, the corrections would be the form $A/(AE+4)$. Again the question arises as to what the value of aspect ratio should be. Obviously the choice is more complex than simply deciding whether the span should be based on conventional span or quarter-chord-line length. In attempting to correlate the subject data as well as other swept-wing data both these approaches were used. Since neither proved consistently superior to the other or to simple theory, it was decided to delete the correction entirely. It is possible that additional study of existing data together with future tests will reveal a means of determining an effective aspect ratio which when used in this connection will more accurately predict asymmetric loading conditions. It should be noted, then, that throughout the sections of this report dealing with asymmetric loading conditions (sideslip or ailerons deflected) no corrections for aspect ratio changes have been applied to the predictions for the effect of sweep.

This relation has been used to estimate the values of $\delta C_{l\beta}/\delta C_L$ for the five wings tested and the results are compared with experimental values in figure 17. Reasonably good agreement is shown except in the case of the 45° sweep-forward wing which had a somewhat lower value of $\delta C_{l\beta}/\delta C_L$ than was predicted.

For the case where lift is changed by changing flap deflection (angle of attack constant), the theoretical effect of sweep on $\delta C_{l\beta}/\delta C_L$ is twice that given by the foregoing expression, that is,

$$(\delta C_{l\beta}/\delta C_L)_A = (\delta C_{l\beta}/\delta C_L)_{A=0}^{-\frac{1}{2}} \frac{bf}{b} \frac{\tan A}{57.3}$$

where bf/b is the ratio of flap span to wing span. The estimated and experimental results for this case are also shown in figure 17. The agreement between theory and experiment in this case is only fair. The discrepancy is probably due in great measure to failure of the theory to properly account for the spanwise center of load. Theory indicates rectangular loading - that is, that the center of additional load is applied at mid-semispan of wing or flap. Movement of the center of load inboard as much as 20 percent of the wing semispan would be required to make the discrepancy between theory and experiment vanish.

Thus, relations obtained by means of the simplified theory appear to estimate at least the gross effects of sweep on the parameter $\delta C_{l\beta}/\delta C_L$. A notable exception is the case of the

45° swept-forward wing which exhibits a dihedral effect much less than theory would indicate but still greater than the 30° swept-forward wing.

Since the problem of determining the value of $\delta C_{l\beta} / \delta C_L$ and the maximum value of $C_{l\beta}$ is probably the most serious one faced by the designer of swept-wing airplanes, a considerable effort has been made to evaluate the effects of scale on swept-back wings from the data. Unfortunately, such an evaluation could not be obtained. Only the generalization can be made that the effects of scale appear much less important than the effects of wing geometry. Both large- and small-scale swept-back-wing tests show very similar characteristics. That is, the value of $\delta C_{l\beta} / \delta C_L$ approximates that predicted by theory, with a maximum value of $C_{l\beta}$ being reached prior to the stall, and followed by a reduction in $C_{l\beta}$ as the stall is approached. Note that these and the following considerations regarding the effects of scale apply to plain swept-back wings only.

As previously noted, the value of $\delta C_{l\beta} / \delta C_L$ indicated by simple theory is based upon the assumption that the additional load is concentrated at the mid-semispan. Therefore marked differences in this parameter would be expected where nonrectangular loading was known to exist. In comparing experimental results with the theory such was found to be the case. Reference 1 showed that for the rectangular swept-back wings the measured value was as much as 14 percent more than

the predicted value. The tests reported herein gave experimental results less (as much as 14 percent less) than the predicted value. Such differences might be anticipated since theory shows that sweepback tends to shift the load center towards the tips, and taper ratios less than 1.0 tend to shift the load center towards the root. A complete understanding of this action cannot be had until more thorough studies are made of the effects of sweep and taper on load center. A first approximation (probably an overcorrection) of the answer can be reached, however, by simply adjusting the load center to correspond to the area center. If this is done, theory would fall within 10 percent of the results shown in this report while, of course, the discrepancies of reference 1 would be unchanged. Such a procedure applied to the results of reference 3 would slightly overcorrect for the effects of taper that are shown. From this it can be concluded that the value of $\delta C_{l_f} / \delta C_L$ can be approximated to within 15 percent by simple theory; that a closer approximation can be had - probably within 10 percent - if the centroid of load is assumed to lie on the centroid of area. It is believed that the effects of scale fall within this latter error and probably are of the same general magnitude as the effects of section or tip shape. No data could be found to aid in a quantitative evaluation of those effects.

With regard to the maximum values of C_{l_f} likely to be encountered with a highly swept wing, it appears impossible to

conclude more than the fact that a maximum value exists for every wing and that this maximum value tends to decrease with taper ratio. The data of this report and reference 1 show very nearly the same maximum value ($C_{l\beta_{max}} = 0.0035$ to 0.0038) for both swept-back wings. Reference 3 shows a very similar maximum for the untapered wings but shows the maximum decreasing with both taper and sweep for other wings. No relation seems to exist between the lift coefficient at which the maximum $C_{l\beta}$ occurs and the maximum lift coefficient of the wing. Since, however, the value of $\partial C_{l\beta} / \partial C_L$, in general, increases more rapidly with sweep than $C_{L_{max}}$ decreases, the maximum value of $C_{l\beta}$ occurs at progressively lower percentages of $C_{L_{max}}$ as sweep is increased. For instance, for a 45° sweptback wing, $C_{l\beta_{max}}$ occurs at $0.55 C_{L_{max}}$ in reference 3, $0.61 C_{L_{max}}$ in reference 1, and $0.70 C_{L_{max}}$ in the data of this report; whereas $C_{l\beta_{max}}$ for a 30° swept-back wing occurs at $0.80 C_{L_{max}}$, $0.82 C_{L_{max}}$, and $0.91 C_{L_{max}}$ for the same data, respectively. Since the phenomenon which causes the value of $C_{l\beta}$ to peak are not completely understood at the present time, an accurate prediction of its value is impossible. Examination of all available data leads, however, to the conclusion that if a maximum value of -0.0038 is chosen the choice can be considered conservative, but for the present, wind-tunnel tests must be relied upon to give the exact answer. Certainly this problem is worthy of additional study. Until the governing factors are more clearly defined it remains

impossible to determine to what extent $C_{l\beta_{max}}$ is affected by scale.

In the case of swept-back wings with flaps deflected the amount of correlation possible between large- and small-scale data is extremely limited and the results far less amenable to interpretation. For most cases examined theory gave at least a slightly conservative value of $\Delta C_{l\beta}/\Delta C_L$ where the change in lift coefficient was due either to a flap deflection at constant angle of attack or a change of angle of attack with flaps deflected. All the data, large and small scale showed or indicated that a value of $C_{l\beta_{max}}$ existed and that it increased with sweep. While no systematic variation of $C_{l\beta_{max}}$ with wing geometry could be ascertained, none of the data showed a value greater than -0.007. For the present, therefore, if wind-tunnel tests are not available the best approach to predicting $C_{l\beta}$ characteristics of swept wings with flaps is to use simple theory to predict $\Delta C_{l\beta}/\Delta C_L$ and to consider -0.007 $C_{l\beta}$ as the maximum.

No correlation was attempted with the swept-forward-wing data because of the scarcity of low-scale tests.

Aileron effectiveness.- The variation of aileron effectiveness with lift coefficient is shown in figure 18. The values of aileron effectiveness shown in figure 18 were obtained as the ΔC_l produced by -15° or 15° of aileron deflection and hence are $\Delta C_l/\Delta\delta_a$ rather than a true $C_{l\delta_a}$. It is immediately apparent that aileron effectiveness decreases with sweep,

decreasing as much as 50 percent for 45° of sweep. The effectiveness of the ailerons on the swept-back wings decreased with lift coefficient, rapidly at high lift coefficients. This is due to a loss in effectiveness of the upward deflected aileron which is in the wake of the separated flow and hence contributes little or nothing to the rolling moment. The ailerons on the swept-forward wings show a general increase in effectiveness with lift coefficient, probably due to a favorable effect of the spanwise boundary-layer drain.

According to the simplified theory, as a wing is swept, the aileron effectiveness will decrease, as for any flap, in proportion to the $\cos^2\Lambda$. That is, when corrections for aspect ratio are ignored the value of $C_{l\delta_a}$ is given by the following relation: (See footnote 6, p. 21)

$$(C_{l\delta_a})_\Lambda = (C_{l\delta_a})_0 \cos^2\Lambda$$

This relation has been used to predict the variation of aileron⁷ effectiveness with sweep for the five wings tested, and the results are compared in figure 19 with the experimental data cross-plotted from figure 18 for zero lift.

⁷The ailerons on the wings of this investigation varied both in the relative amount of wing area affected and in the relative spanwise location of the center of pressure of the area affected. In comparing theory and experiment, these variations were accounted for by correcting the theoretical values of aileron effectiveness in proportion to the ratio of the relative area and spanwise center of pressure of the swept wing to the relative area and spanwise center of pressure of the unswept wing.

For either sweepforward or sweepback the experimental values of aileron effectiveness are as much as 20 percent lower than the theoretical values.

The foregoing results show that aileron effectiveness is reduced by wing sweep and that on swept-back wings the aileron effectiveness is further reduced at high lift coefficients. Insofar as rolling control at low lift coefficient is concerned, theory shows that C_{l_p} is reduced in proportion to $\cos\Lambda$; whereas $C_{l\delta_a}$ is reduced in proportion to $\cos^2\Lambda$ and hence $pb/2V$ will be reduced in proportion to $\cos\Lambda$ for a given size of aileron. In general, therefore, it appears that, to maintain a given value of $pb/2V$, aileron size must be increased as wings are swept. As higher lift coefficients are reached the lateral-control problem becomes particularly pronounced. Not only must powerful lateral control be provided to overcome great dihedral effects but the results reported herein show that available lateral control, at least for swept-back wings, decreases seriously with lift coefficients. For example, with the 45° swept-back wing equipped with full-span flaps and flying near $C_{L_{max}}$, 13° of total aileron deflection would be required to hold the wings level for only 1° of sideslip. The need for development of adequate aileron control or a means to reduce aileron control requirements is obvious.

Directional Characteristics

The variation with lift coefficient of the yawing moment due to sideslip is shown in figure 20 for the plain wings and in figure 21 for the wings with partial- and full-span flaps. Sweepback increased the directional stability and sweepforward decreased the stability; however, due to the initial positive stability of the unswept wing the stability of the swept-forward wings became negative only at higher lift coefficients and then only slightly so.

The theoretical effect of sweep on the directional stability is in accordance with the following relation:

$$\left(\frac{\partial C_{n\beta}}{\partial C_L^2} \right)_A = \left(\frac{\partial C_{n\beta}}{\partial C_L^2} \right)_{A=0} + \frac{\tan A}{2\pi A \times 57.3}$$

The directional stability estimated on the basis of this equation is compared with experimental results in figure 22. Although precise agreement is not obtained, the trend of the experimental data is indicated by theory.

The directional characteristics of the swept wings tested should not present any serious problems of a purely low-speed static directional stability and control nature since adequate stability and control should be obtainable by use of fins and rudders of normal proportions combined with normal tail lengths. However a dynamic problem arises from the fact that $C_{l\beta}$ increases with sweep more rapidly than $C_{n\beta}$. This unbalance between $C_{l\beta}$ and $C_{n\beta}$ leads to the dutch-roll type

of instability which has been discussed in reference 8. The data obtained in the investigation reported herein substantiate previous tests conducted on small-scale models and consequently indicate that means must be found to balance $C_{l\beta}$ and $C_{n\beta}$.

CONCLUDING REMARKS

Large-scale tests indicate that the primary problems to be overcome before successful use can be made of high angles of sweep are (1) high dihedral effects accompanied by poor lateral control at high lift coefficients, (2) low maximum lift value together with low flap effectiveness, and (3) rapid shift in neutral point in the moderate to high lift-coefficient range coupled with a possibility of strong stalling moment at maximum lift resulting from poor plan-form choice.

In general, simple theory enables good predictions to be made of the gross effects of sweep on wing characteristics, but it is felt that the accuracy is inadequate for purposes of design. It appears that the majority of the inaccuracies result from an incomplete understanding of the effects of aspect ratio.

Where it has been found possible to compare large-scale data with small-scale data a comparison has shown that where scale effects exist at low angles of sweep, scale effects

tend to vanish at high angles of sweep with large -scale results approaching small-scale results.

Ames Aeronautical Laboratory,
National Advisory Committee for Aeronautics,
Moffett Field, Calif.

Gerald M. McCormack,
Mechanical Engineer.

Victor I. Stevens, Jr.
Victor I. Stevens, Jr.
Aeronautical Engineer.

Approved:

Harry J. Goett
for John F. Parsons,
Aeronautical Engineer.

APPENDIX

Description of Basic Wind-Tunnel Test Results

For each swept wing, six-component force data were obtained at several angles of sideslip and several values of dynamic pressure. (See fig. 23 for variation of Reynolds number with dynamic pressure.) At each angle of sideslip, several model configurations were tested including plain wing, wing with partial-span split flaps, wing with full-span split flaps and wing with split-flap-type aileron. The data obtained are presented in figures 24 to 91 in terms of the variation of the measured characteristics with lift coefficient. Table II forms an index of these figures presenting the basic data.

All the data are referred to the stability axes whose origin is located at a point on the root chord or root chord projected and at the same fore and aft location as the quarter M.A.C. The test results are presented in the form of standard NACA coefficients as defined in the section Coefficients and Symbols.

All the basic wind-tunnel data have been corrected for air stream inclination and for wind-tunnel-wall effects. A brief analysis of the effect of sweep on tunnel-wall corrections indicated that the average correction either with or without sweep was approximately the same for the tunnel wing configurations considered. Hence the standard corrections for unswept wings were applied.

Force tests made with the sting support alone in the tunnel showed that its tare should be negligible except in the case of pitching moment, drag and yawing moment. Measured pitching-moment tares are believed reliable and were applied to all the data. While the drag tares are appreciable (approximately 0.02 in the case of the unswept wing where the area is small and decreasing for the swept wings where the area is larger), it is felt that they could not be determined with sufficient accuracy to warrant application. Hence no drag tares have been applied. Since the measured yawing-moment tares (fig. 92) were small, they were not applied to the basic data. However, in analysis of the data it was found that the tares were relatively large when compared to the effects of sweep. In order then to properly assess the effects of sweep, it was necessary to apply tares to the summary data which is, therefore, shown fully corrected in figures 20, 21, and 22.

REFERENCES

1. Letko, William, and Goodman, Alex: Preliminary Wind-Tunnel Investigation at Low Speed of Stability and Control Characteristics of Swept-Back Wings. NACA TN No. 1046, 1946.
2. Jacobs, W.: Six-Component Measurements on Three Back-Swept Wings. Ger. FB 1629. ZWB P31 II.
3. Jacobs, W.: Six-Component Measurements on Four Trapezoidal Wings With Sweepback. Ger. UI 2069. ZWB P31 II.
4. Betz, A.: Applied Airfoil Theory. Unsymmetrical and Non-Steady Types of Motion. Vol. IV of Aerodynamic Theory, div. J, ch. IV, sec. 4, W. F. Durand, ed., Julius Springer (Berlin), 1935, pp. 94 - 107.
5. Falkner, V. M.: The Calculation of Aerodynamic Loading on Surfaces of any Shape. R. & H. No. 1910, British A.R.C., 1943.
6. Falkner, V. M.: The Effect of Sweepback on the Aerodynamic Loading on a V Wing. Rep. No. 7786, British A.R.C., 1944.
7. Anderson, Raymond F.: Determination of the Characteristics of Tapered Wings. NACA Rep. No. 572, 1936.
8. Soulé, Hartley A.: Influence of Large Amounts of Wing Sweep on Stability and Control Problems of Aircraft. NACA TN No. 1088, 1946.

TABLE I.-- GEOMETRIC CHARACTERISTICS OF THE FIVE SWEPT WINGS

Angle of sweep (deg)	Span (ft)	Area, S (sq ft)	Aspect ratio, b^2/S	Taper ratio, c_t/c_r	¹ Mean aerodynamic chord, c (ft)	² Span of partial-span flaps (% b)	² Span of full-span flaps (% b)	² Span of ailerons (% b)
-45	32.38	335.5	3.12	0.38	11.32	62.3	97.0	34.7
-30	36.39	282.3	4.69	.40	8.44	62.3	93.2	30.9
0	30.53	201.8	4.62	.55	6.92	62.3	92.5	30.2
30	36.06	268.4	4.84	.44	7.97	62.3	97.0	34.7
45	33.56	309.6	3.64	.42	10.00	62.3	96.2	33.9

¹All chords were measured parallel to the air stream.

²Flaps and ailerons were 20 percent chord.

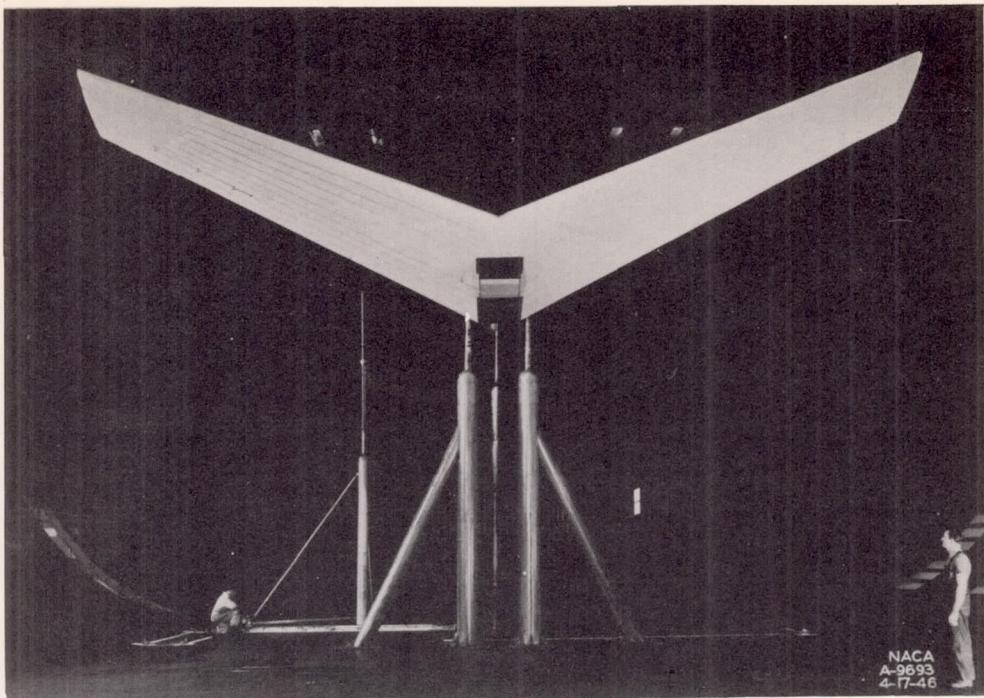
TABLE II.- INDEX TO THE BASIC DATA FIGURES

Figure number					¹ Nominal angle of sideslip	Configuration	Data presented
$\Lambda = -45$	$\Lambda = -30$	$\Lambda = 0$	$\Lambda = 30$	$\Lambda = 45$			
24	36	50	64	78	0	Plain wing	$C_D, \alpha, C_m, C_l, C_n, C_Y$ vs C_L
25	37	51	65	79	0	Plain wing + partial-span flaps	$C_D, \alpha, C_m, C_l, C_n, C_Y$ vs C_L
26	38	52	66	80	0	Plain wing + full-span flaps	$C_D, \alpha, C_m, C_l, C_n, C_Y$ vs C_L
27	39	53	67	81	0	Plain wing + ailerons	α, C_m, C_l vs C_L
28	40	54	68	82	-5	Plain wing	$C_D, \alpha, C_m, C_l, C_n, C_Y$ vs C_L
29	41	55	69	83	-5	Plain wing + partial-span flaps	$C_D, \alpha, C_m, C_l, C_n, C_Y$ vs C_L
30	42	56	70	84	-10	Plain wing	$C_D, \alpha, C_m, C_l, C_n, C_Y$ vs C_L
31	43	57	71	85	-10	Plain wing + partial-span flaps	$C_D, \alpha, C_m, C_l, C_n, C_Y$ vs C_L
--	44	58	72	86	-10	Plain wing + full-span flaps	$C_D, \alpha, C_m, C_l, C_n, C_Y$ vs C_L
32	45	59	73	87	-10	Plain wing + ailerons	α, C_m, C_l vs C_L
33	46	60	74	88	5	Plain wing	$C_D, \alpha, C_m, C_l, C_n, C_Y$ vs C_L
34	47	61	75	89	5	Plain wing + partial-span flaps	$C_D, \alpha, C_m, C_l, C_n, C_Y$ vs C_L
--	48	62	76	90	5	Plain wing + full-span flaps	$C_D, \alpha, C_m, C_l, C_n, C_Y$ vs C_L
35	49	63	77	91	5	Plain wing + ailerons	α, C_m, C_l vs C_L

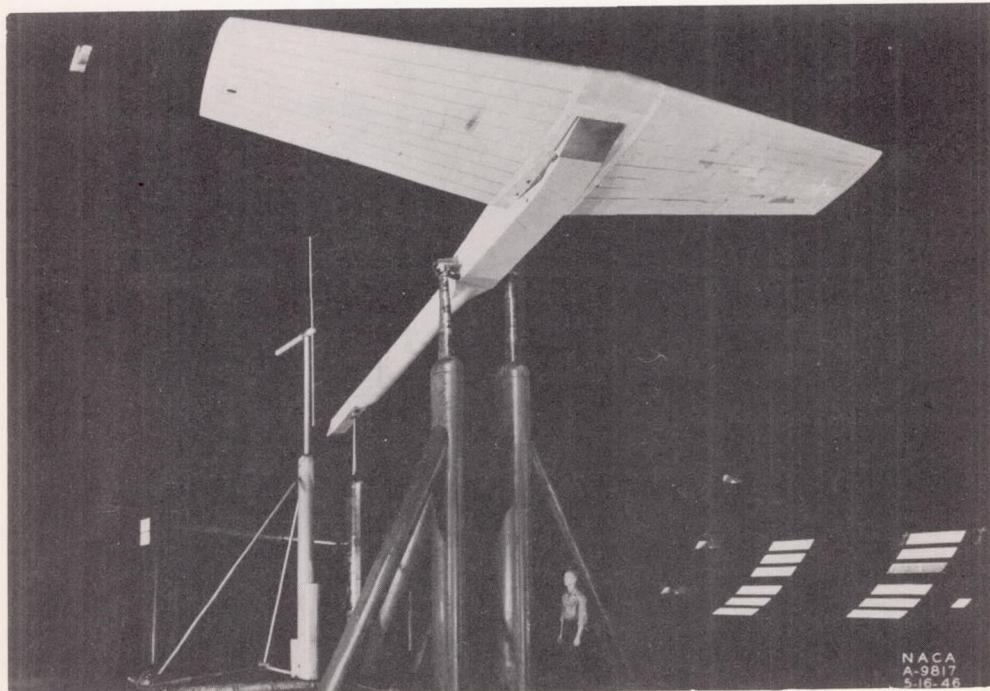
¹Actual angle of sideslip is noted on each curve sheet.

NACA RM No. A6K15

Fig. 1a,b



(a) The 45° swept-forward wing.



(b) The unswept wing.

Figure 1.- Photographs of three of the swept wings mounted in the Ames 40- by 80-foot wind tunnel.

NACA RM No. A6K15

Fig. 1c

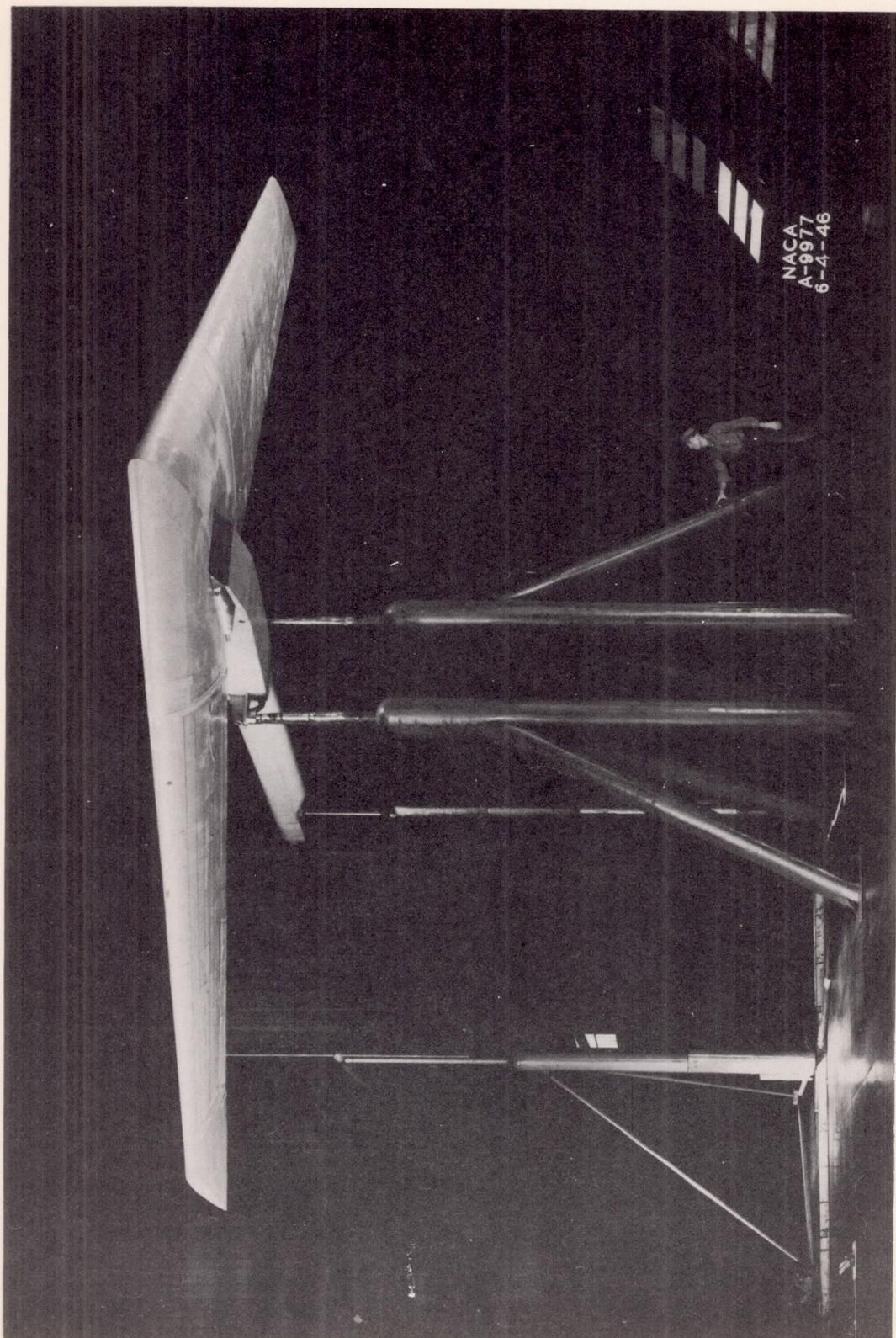
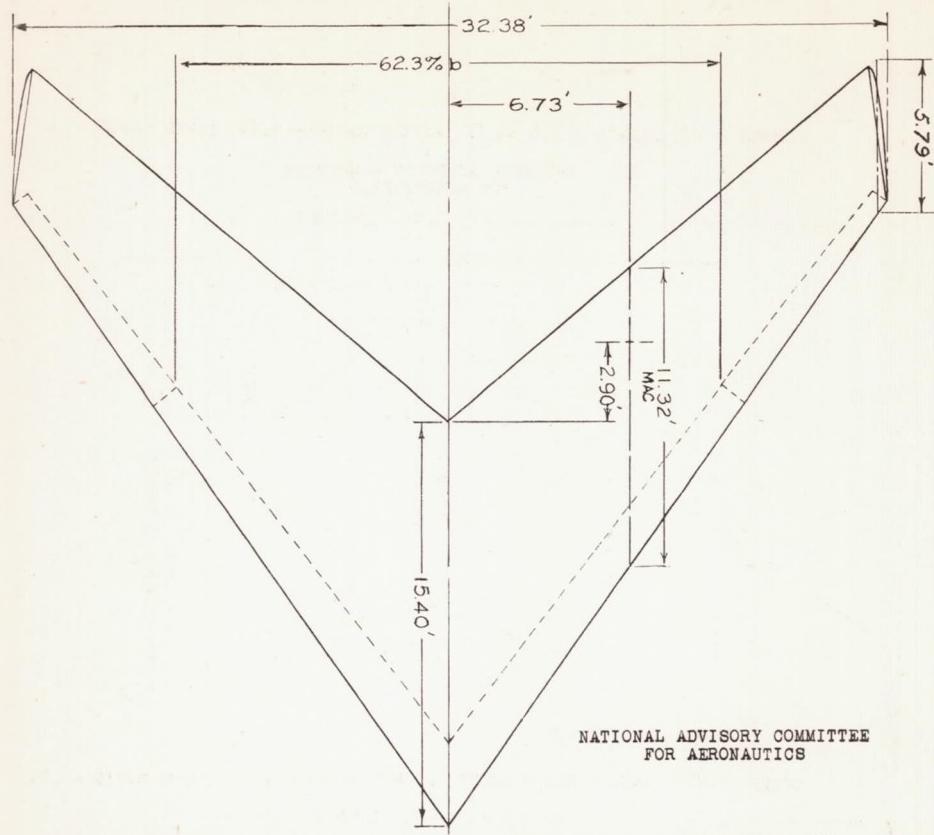
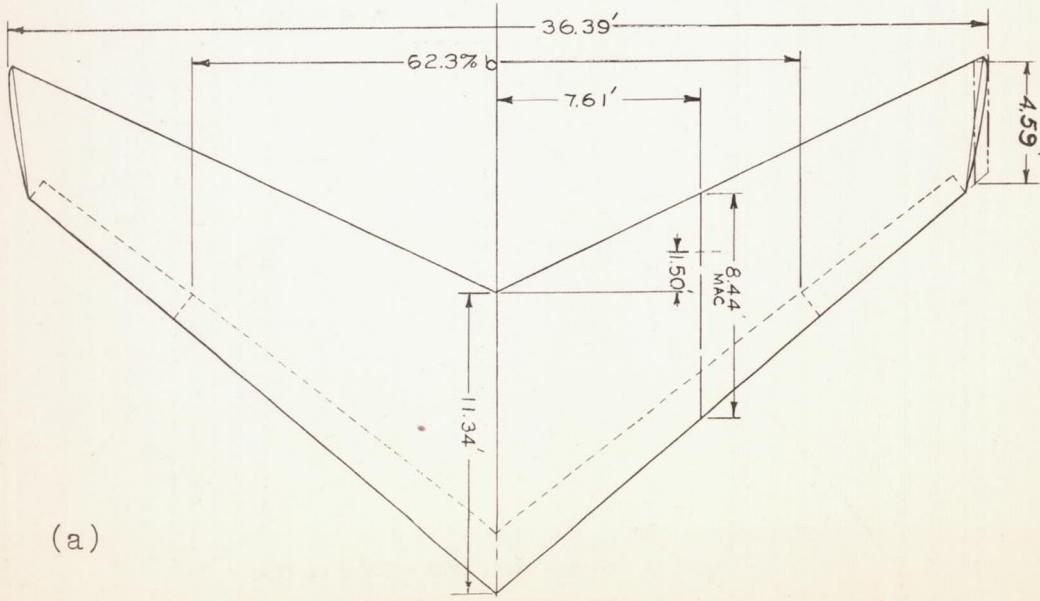


Figure 1.- Concluded. (c) The 45° swept-back wing.

NOTES: 1.- SWEEP ANGLES GIVEN ARE REFERRED TO QUARTER CHORD LINE OF AIRFOIL SECTIONS.
 2.- FORE AND AFT LOCATION OF ROOT CHORD IS REFERRED TO .25 MAC.
 3.- CHORD AT FLAPS AND AILERONS IS .20 OF WING CHORD MEASURED PARALLEL TO AIRSTREAM.



SWEEP = -45° , AREA = 335.5 SQ FT, ASPECT RATIO = 3.12, TAPER RATIO = .38

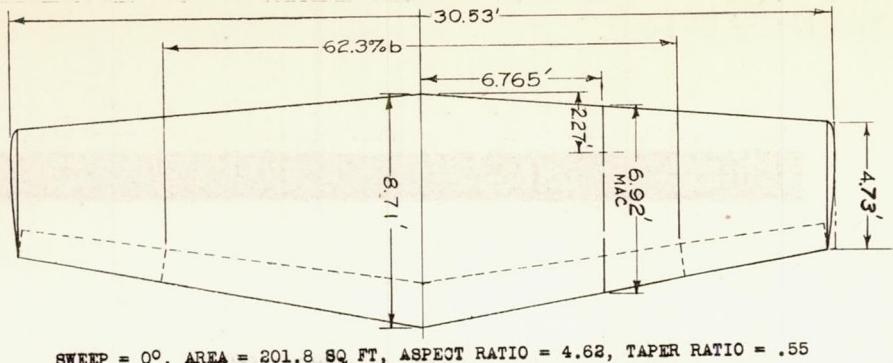
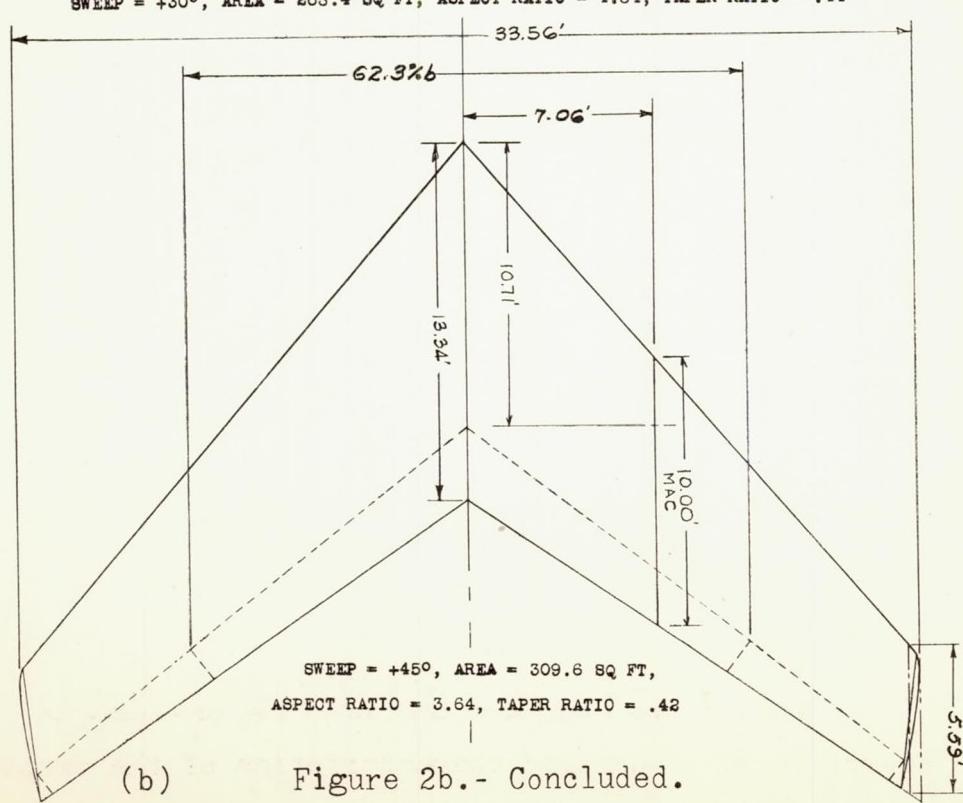
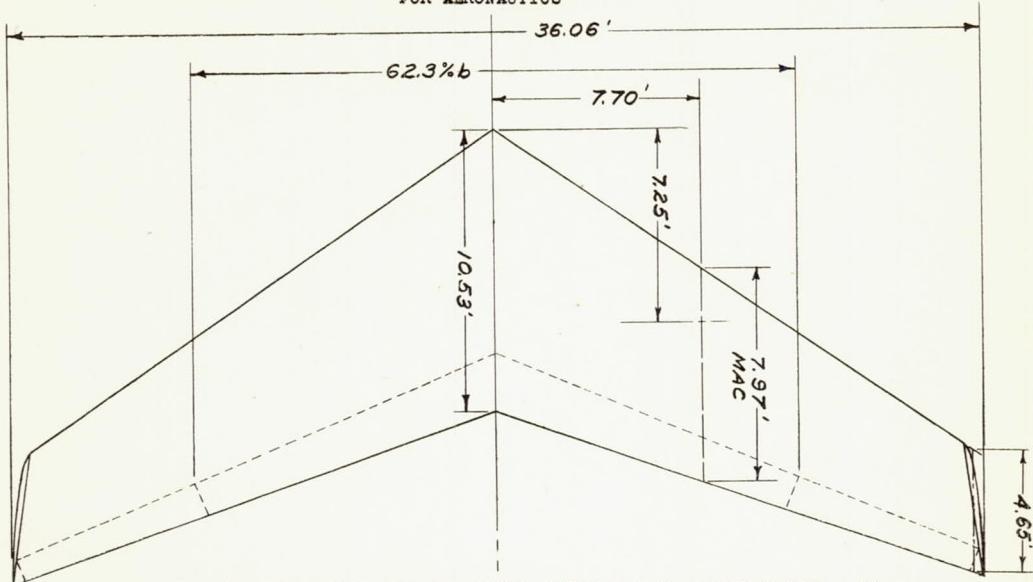


SWEEP = -30° , AREA = 282.3 SQ FT, ASPECT RATIO = 4.69, TAPER RATIO = .40

Figure 2a,b.- Geometric characteristics of the swept wings.

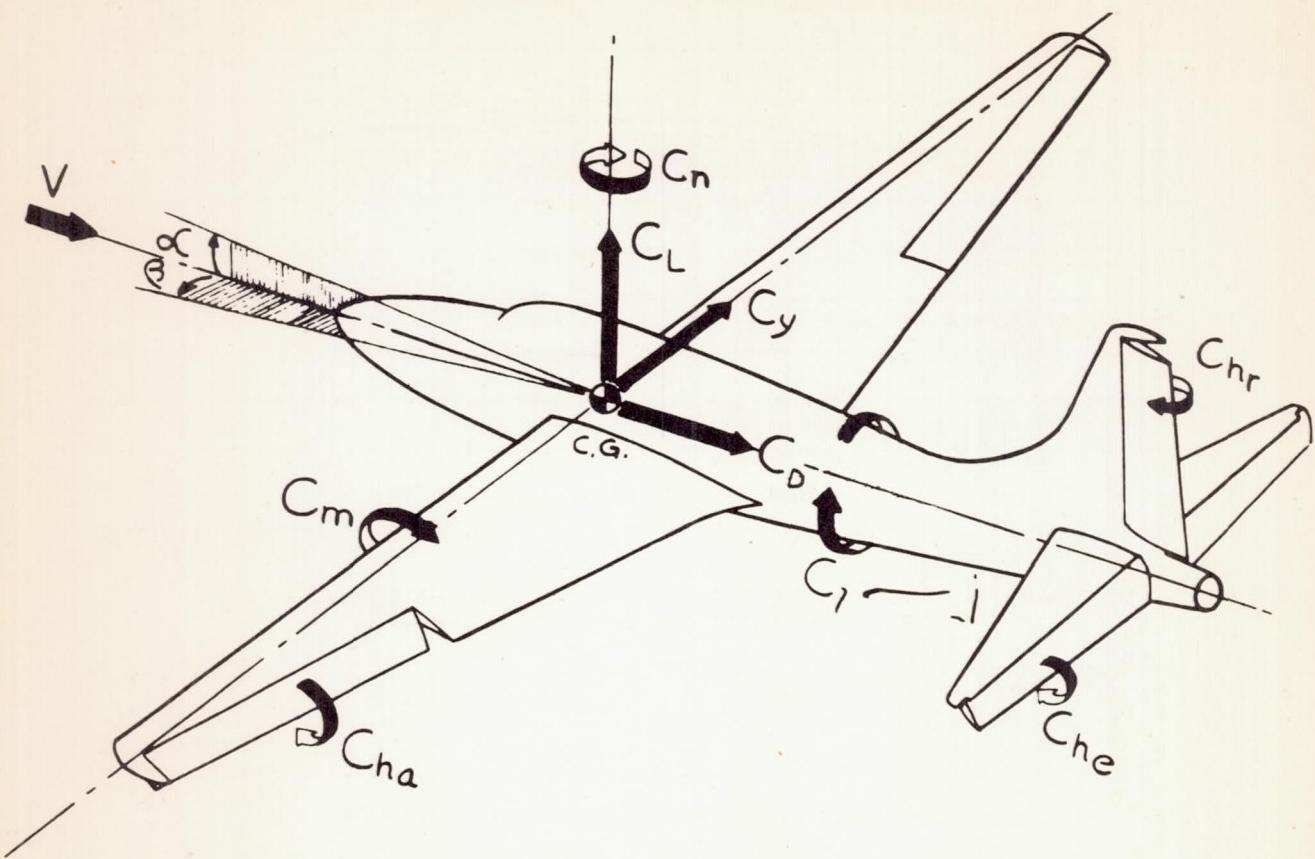
Fig. 2b

NACA RM No. A6K15

NATIONAL ADVISORY COMMITTEE
FOR AERONAUTICS

(b)

Figure 2b.- Concluded.



NATIONAL ADVISORY COMMITTEE
FOR AERONAUTICS

Figure 3.- Sign convention for the standard NACA coefficients.
All forces, moments, angles, and control surface deflections are shown as positive.

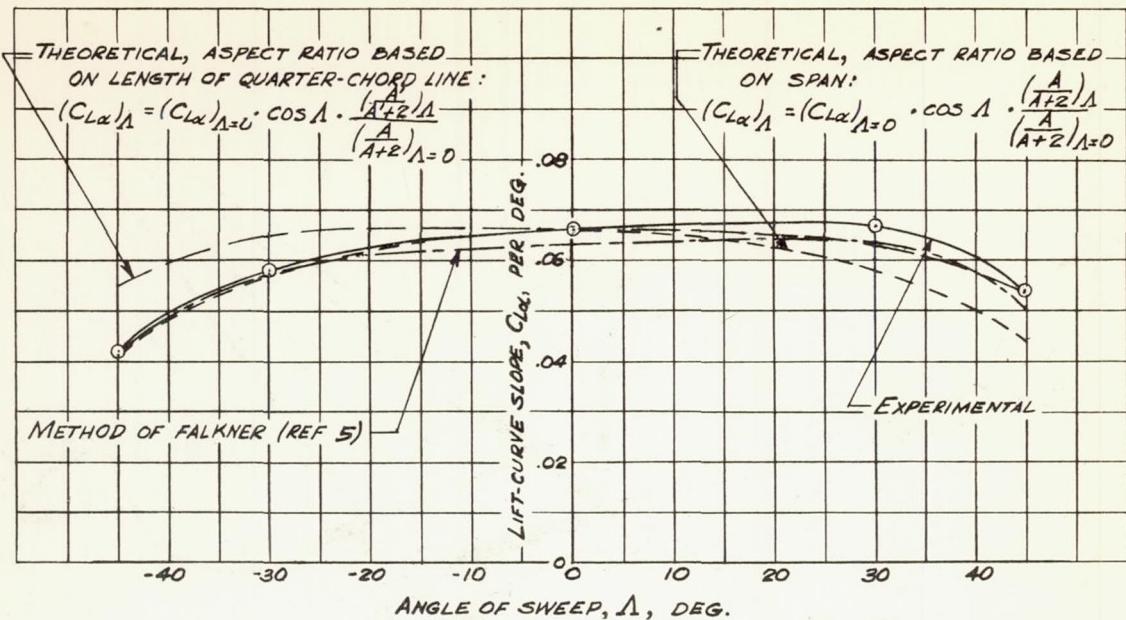
NATIONAL ADVISORY COMMITTEE
FOR AERONAUTICS

FIGURE 4.-COMPARISON BETWEEN THEORETICAL AND EXPERIMENTAL EFFECTS OF SWEEP ON LIFT-CURVE SLOPE

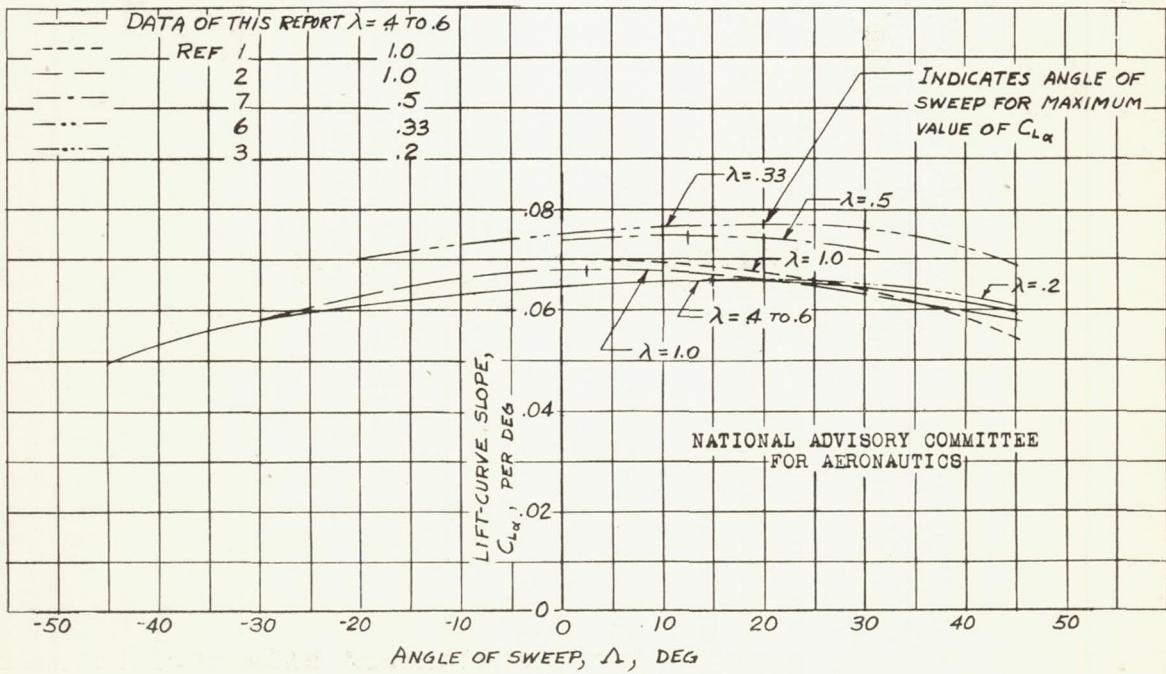


FIGURE 5.-EFFECT OF SWEEP ON LIFT-CURVE SLOPE

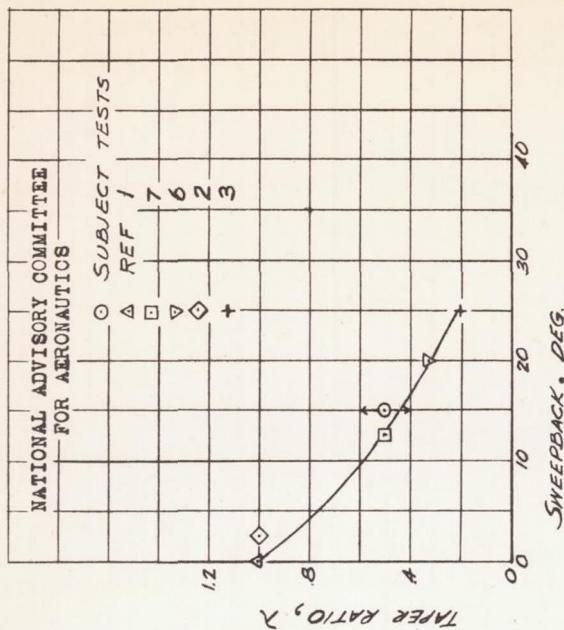
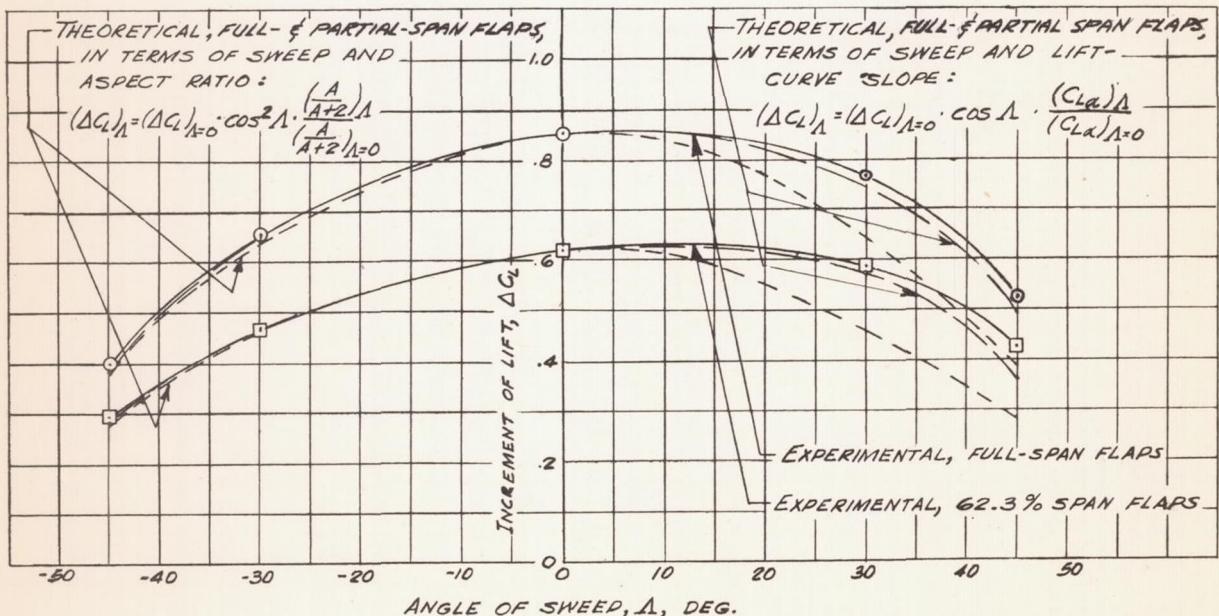


FIGURE 6.—CHART SUMMARIZING THE EFFECT
OF TAPER ON THE ANGLE OF SHEEP-
BACK AT WHICH THE MAXIMUM
VALUE OF LIFT-CURVE SLOPE OCCURS.



NATIONAL ADVISORY COMMITTEE
FOR AERONAUTICS

FIGURE 7.—COMPARISON BETWEEN THE THEORETICAL AND EXPERIMENTAL
EFFECTS OF SWEEP ON THE INCREMENT OF LIFT OBTAINABLE
AT 0° ANGLE OF ATTACK BY DEFLECTING FULL-SPAN AND
PARTIAL-SPAN SPLIT FLAPS 60°.

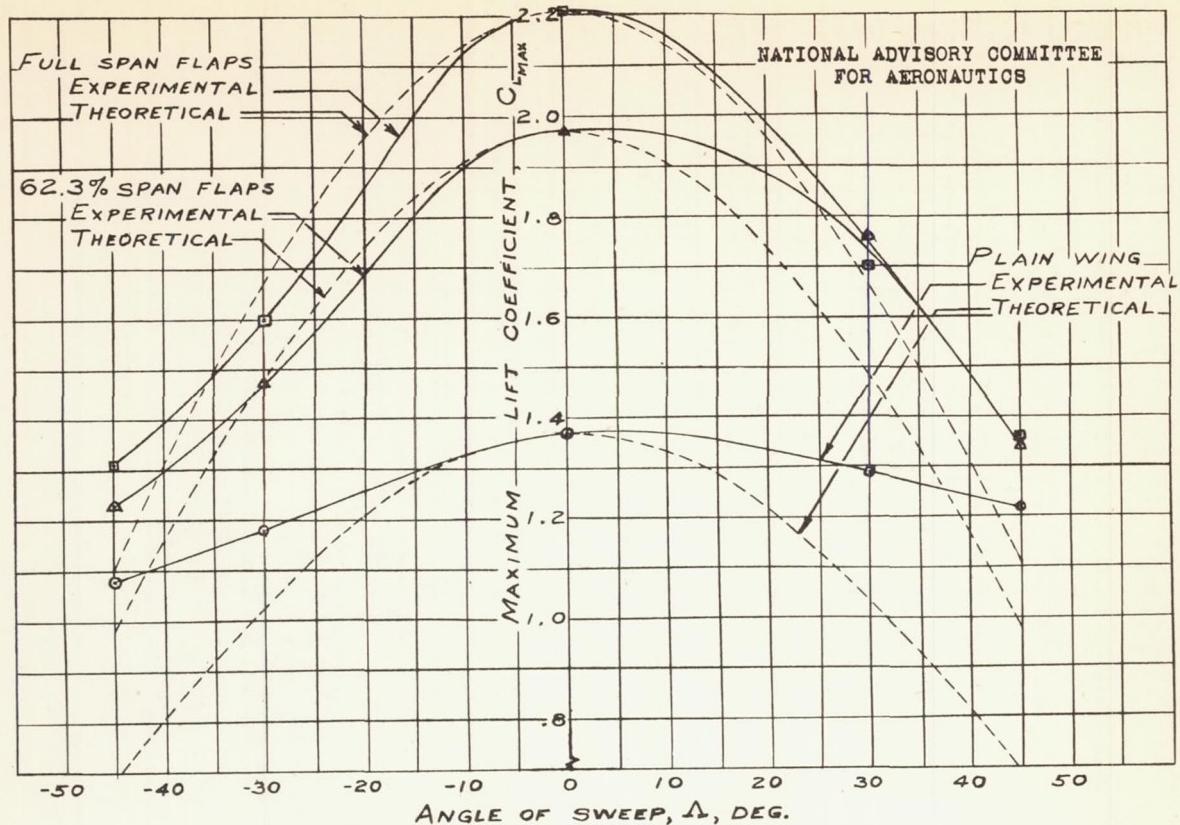


FIGURE 8.—EFFECT OF SWEEP ON THE MAXIMUM LIFT COEFFICIENT.

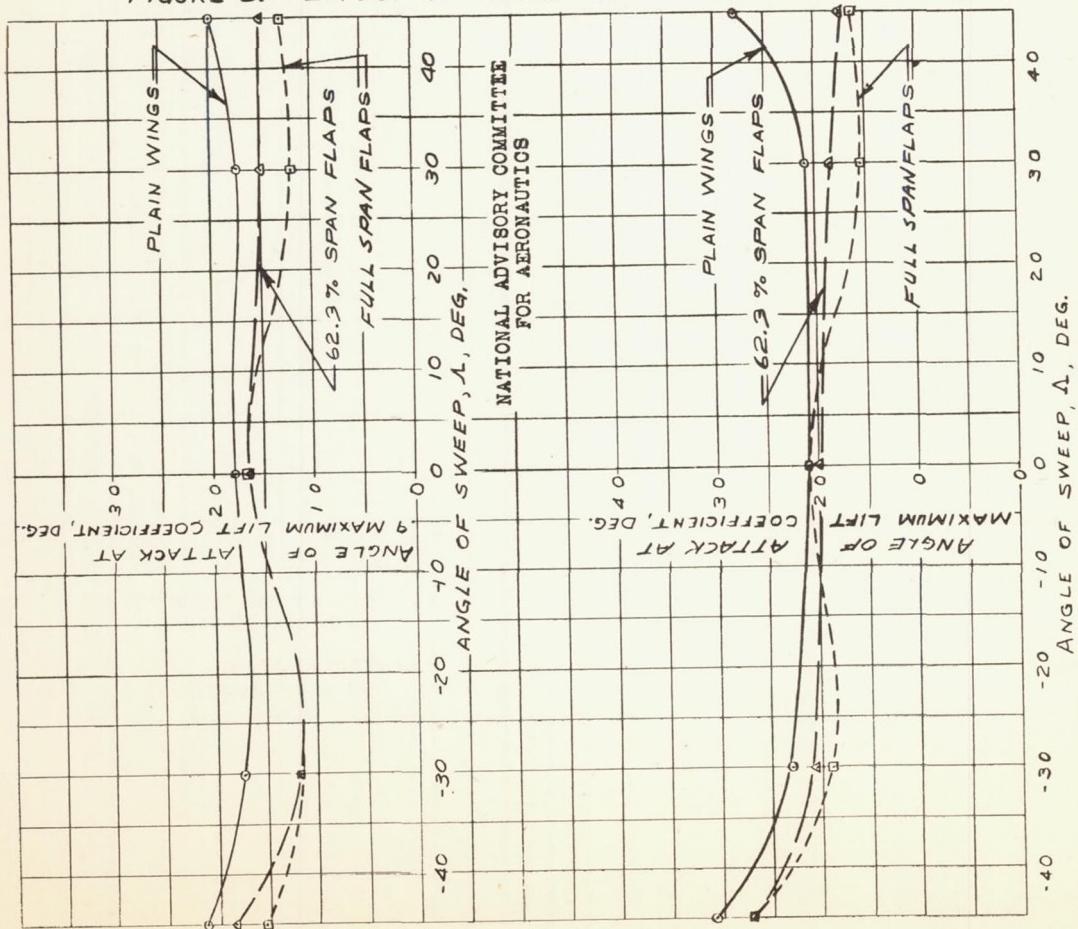


FIGURE 9.—EFFECT OF SWEEP ON ANGLE OF ATTACK FOR 0.5 MAXIMUM LIFT.

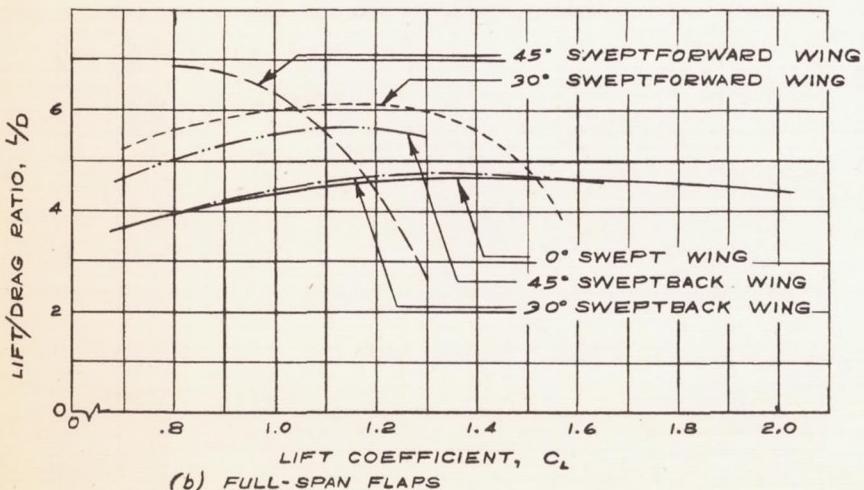
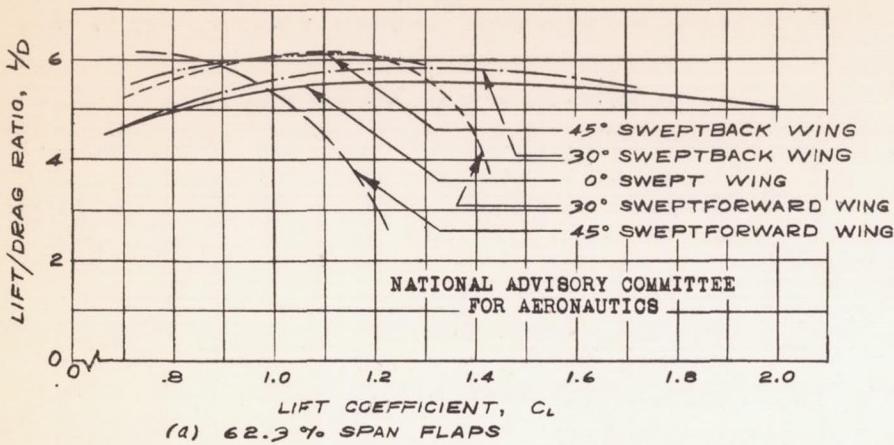


FIGURE 10.— VARIATION WITH LIFT COEFFICIENT OF LIFT-DRAG RATIO OF THE FIVE SWEPT WINGS.

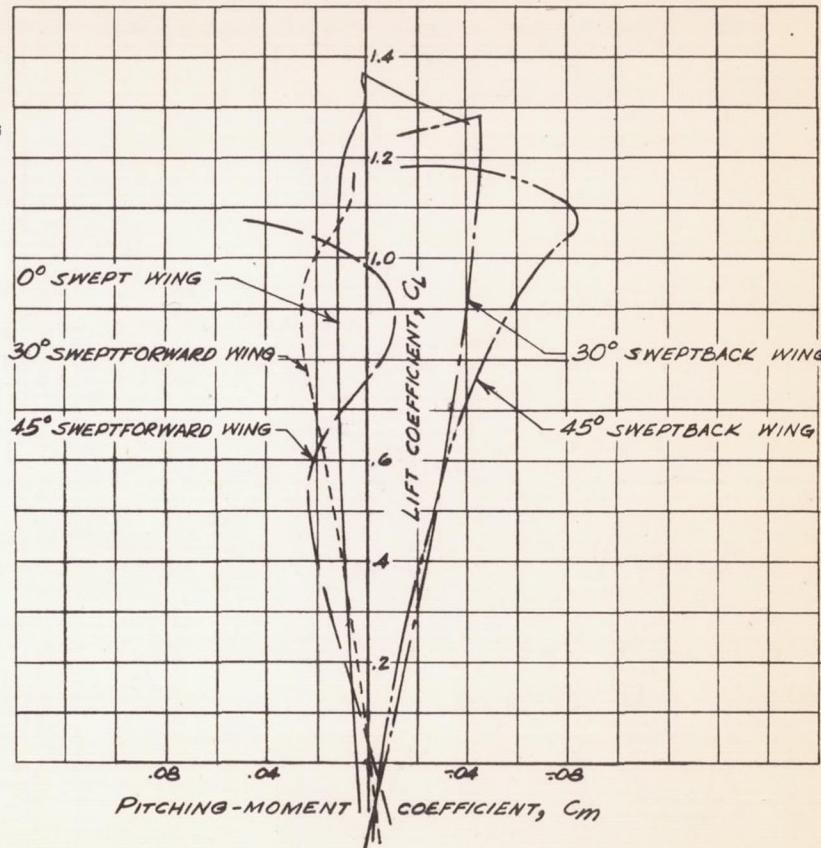


FIGURE 11.— PITCHING-MOMENT CHARACTERISTICS OF THE FIVE SWEPT WINGS. PLAIN WING CONFIGURATIONS.

Figs. 12,13

NACA RM No. A6K15

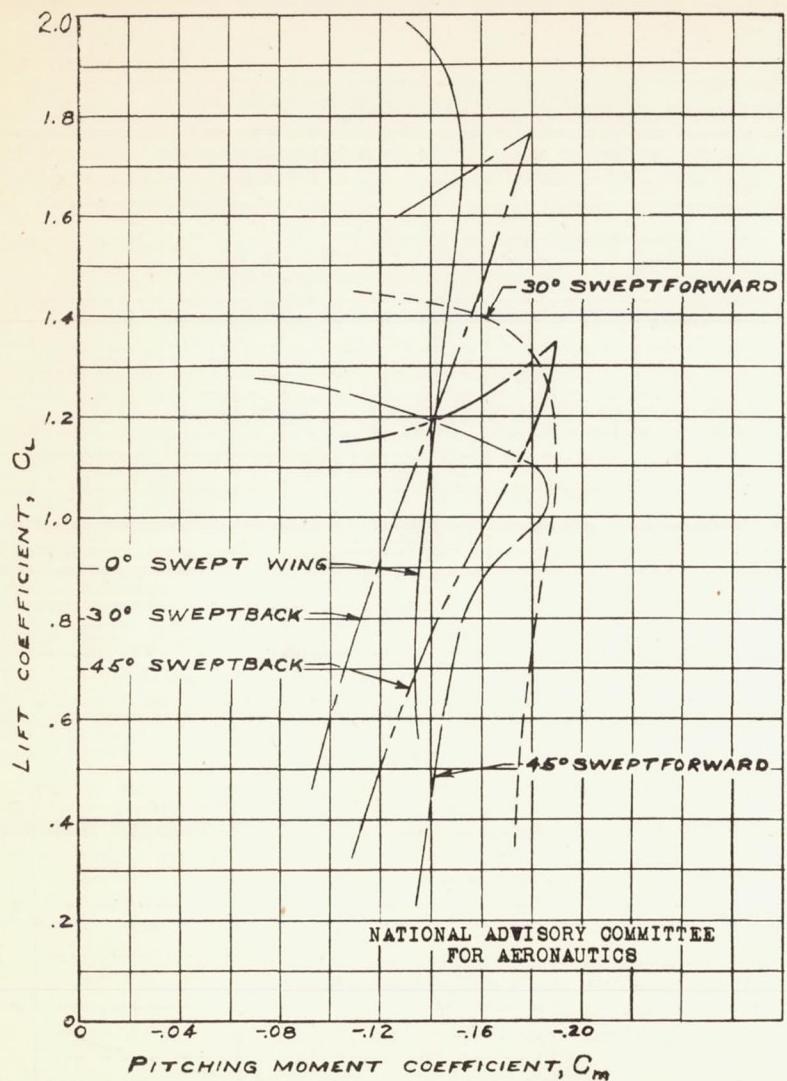


FIGURE 12.- PITCHING-MOMENT CHARACTERISTICS
OF THE FIVE SWEPT WINGS, 62.3% SPAN
SPLIT FLAPS DEFLECTED 60° .

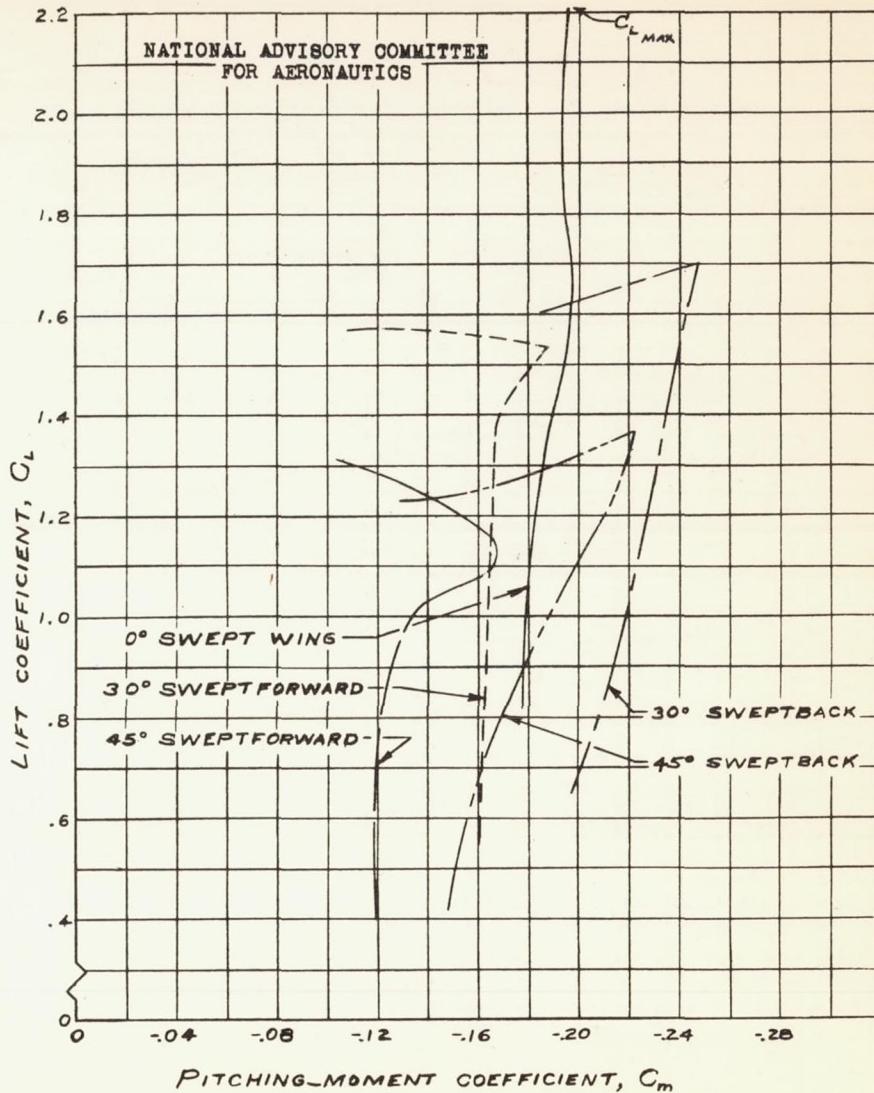
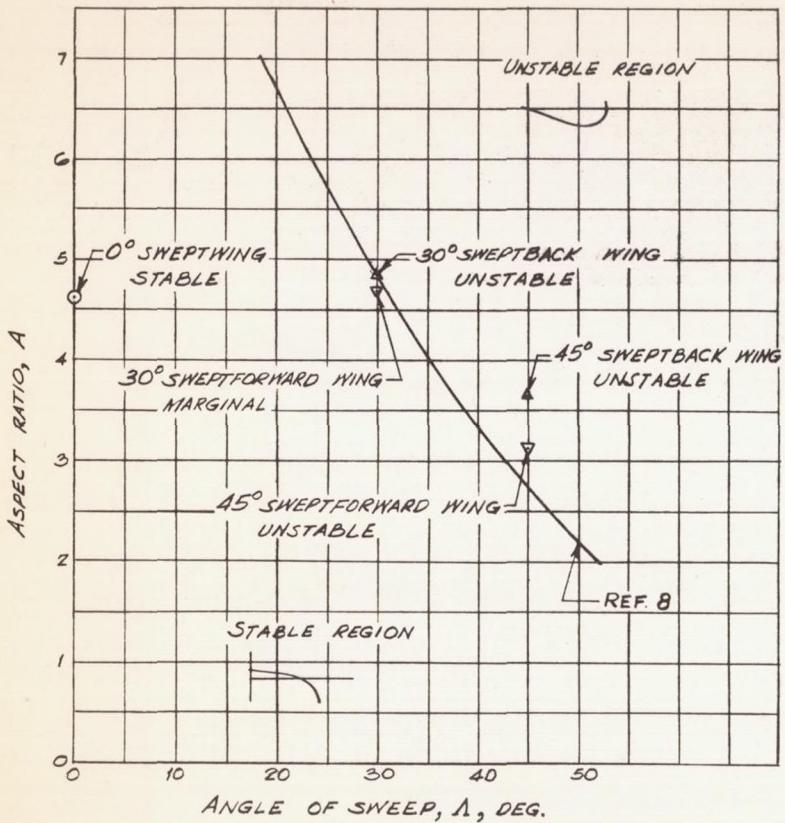


FIGURE 13.- PITCHING-MOMENT CHARACTERISTICS
OF THE FIVE SWEPT WINGS, FULL-SPAN
SPLIT FLAPS DEFLECTED 60° .



NATIONAL ADVISORY COMMITTEE
FOR AERONAUTICS

FIGURE 14.—CHART SUMMARIZING THE EFFECT OF ASPECT RATIO ON THE PITCHING-MOMENT CURVE OF SWEPTBACK WINGS AT THE STALL.

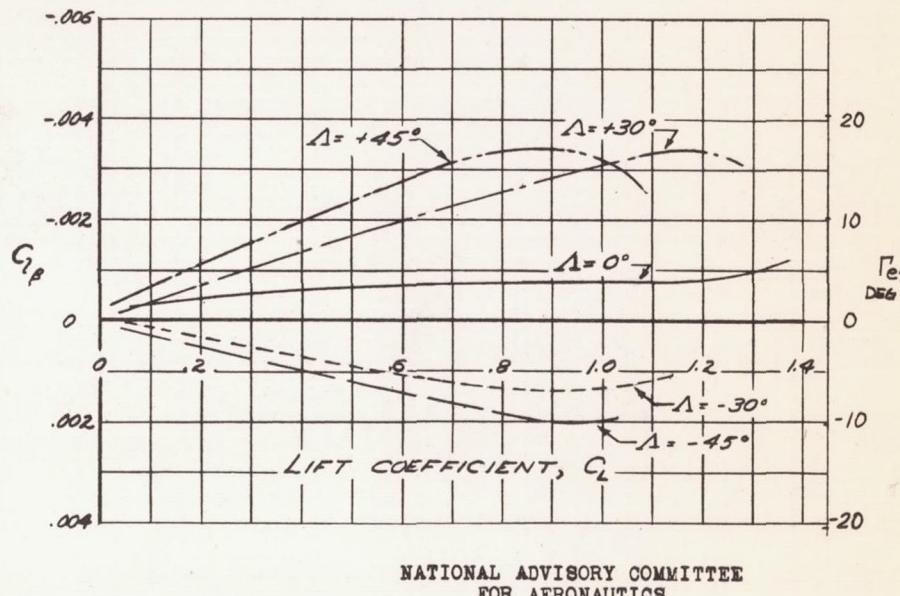


FIGURE 15.—THE EFFECT OF SWEET ON THE VARIATION OF DIHEDRAL EFFECT WITH LIFT COEFFICIENT. PLAIN WING.

Figs. 16,17

NACA RM No. A6K15

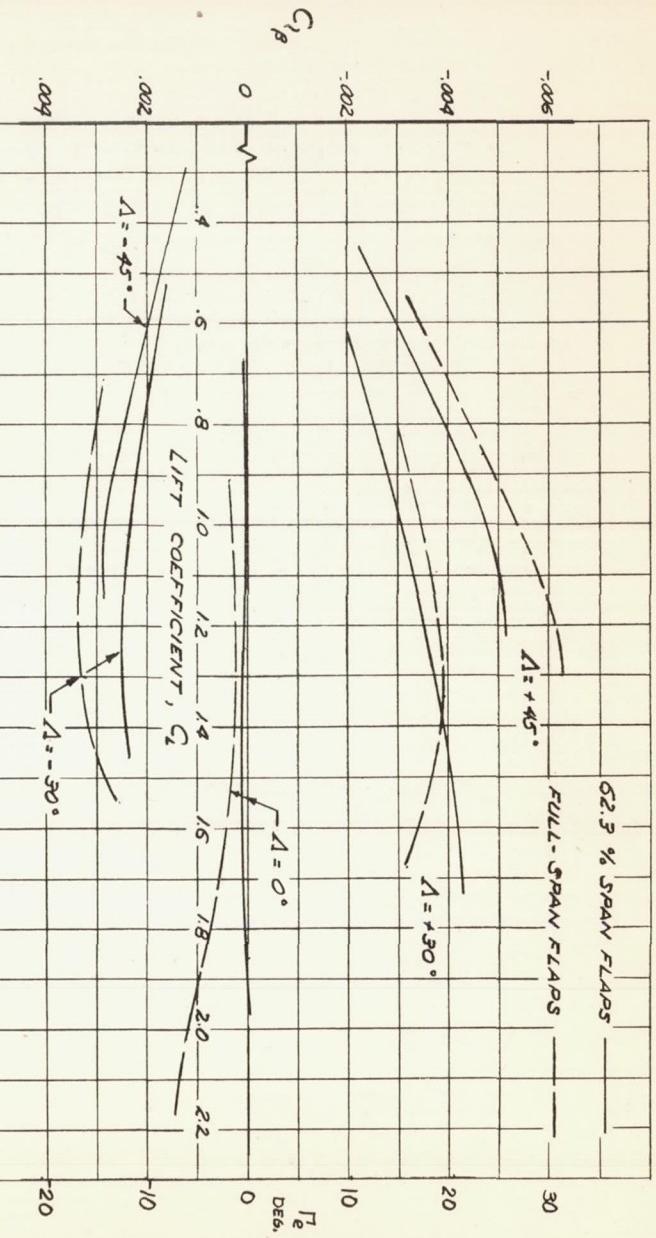


FIGURE 16.—THE EFFECT OF SWEET ON THE VARIATION OF DIHEDRAL EFFECT WITH LIFT COEFFICIENT. 20 % CHORD SPAN FLAP DEFLECTED 60°.

NATIONAL ADVISORY COMMITTEE FOR AERONAUTICS

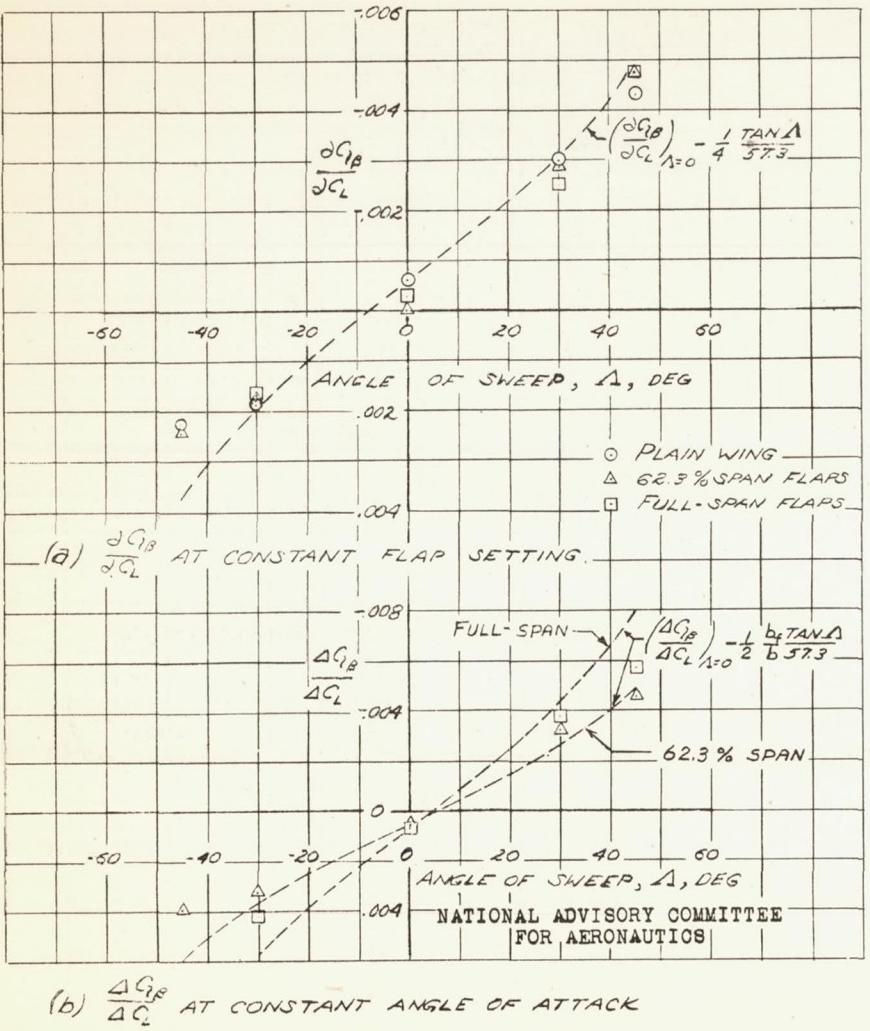


FIGURE 17.—VARIATION WITH SWEET OF THE ESTIMATED AND EXPERIMENTAL VALUES OF $dC_L/d\alpha$

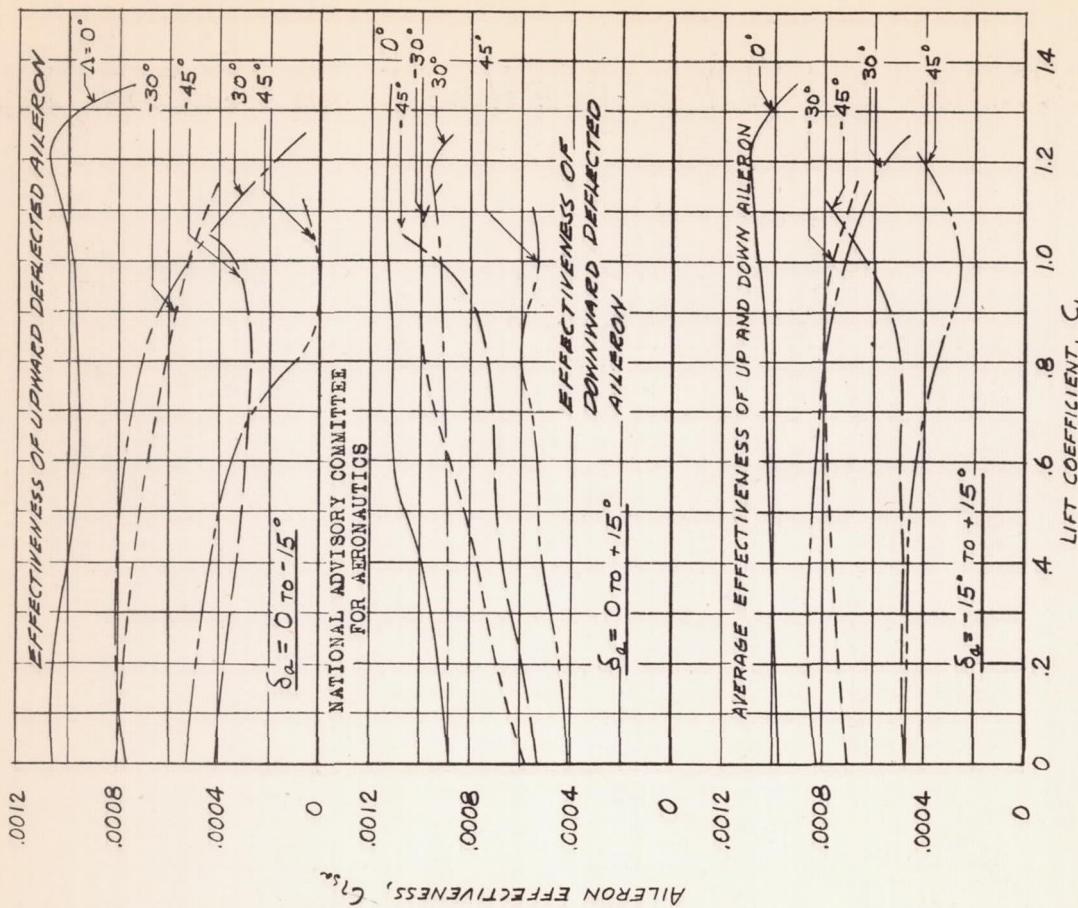


FIGURE 18.—VARIATION WITH LIFT COEFFICIENT OF
AILERON EFFECTIVENESS BASED ON
 $\pm 15^\circ$ AILERON DEFLECTION.

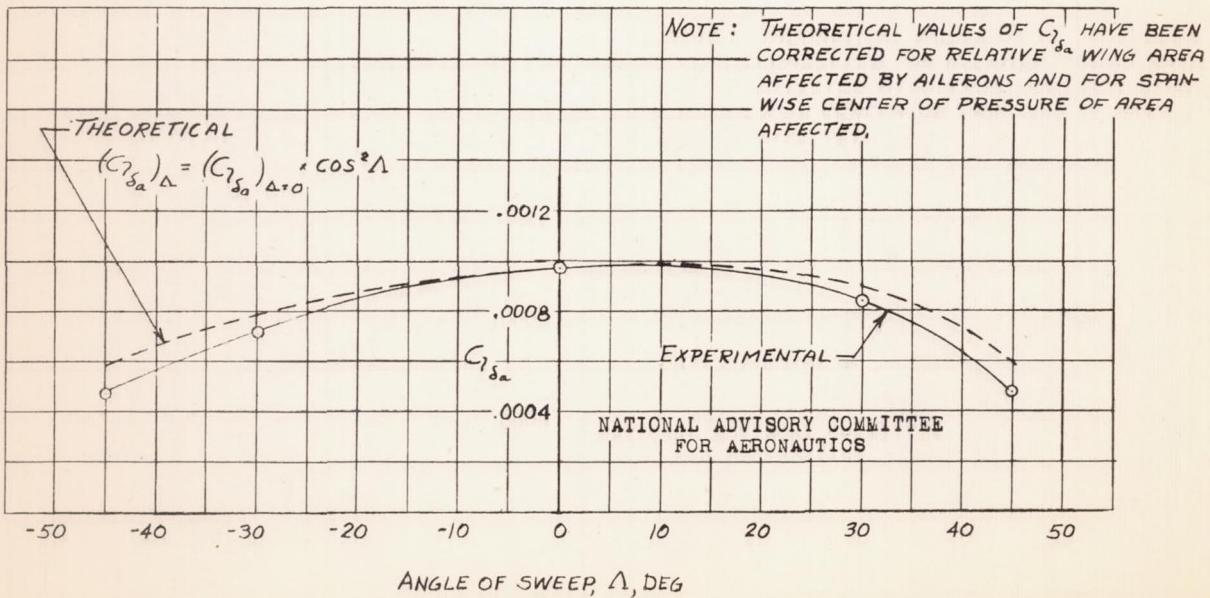


FIGURE 19.—EFFECT OF SWEEP ON THE AILERON EFFECTIVENESS FOR
THE PLAIN WING AT ZERO LIFT.

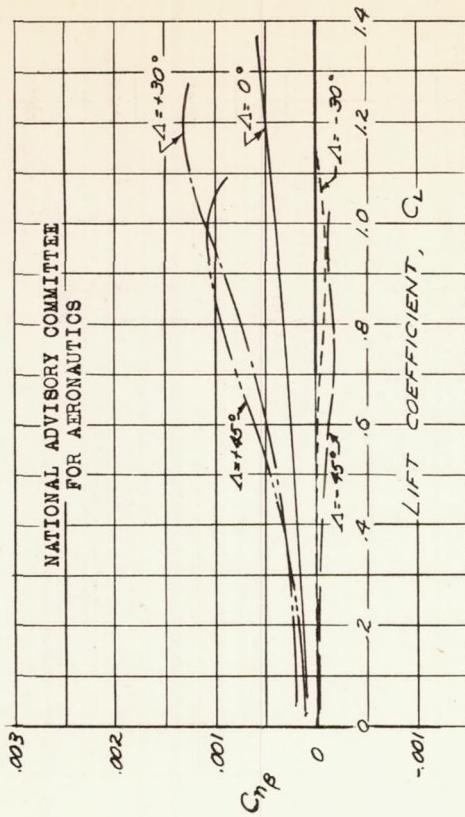


FIGURE 20.— THE EFFECT OF SWEET ON THE VARIATION OF DIRECTIONAL STABILITY WITH LIFT COEFFICIENT. PLAIN WING.

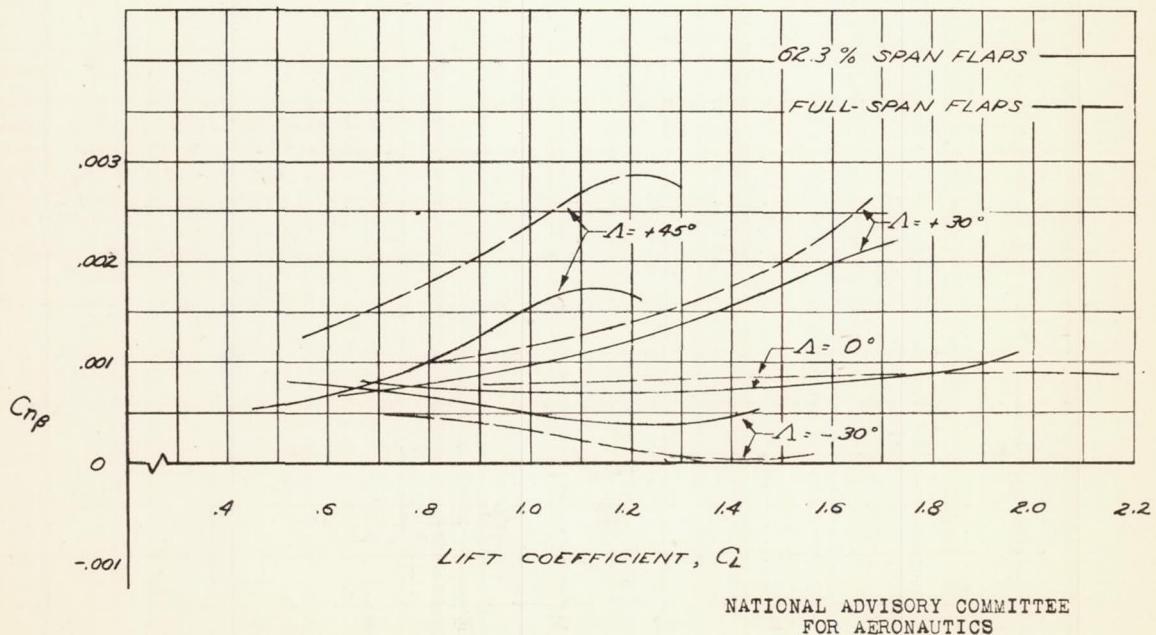
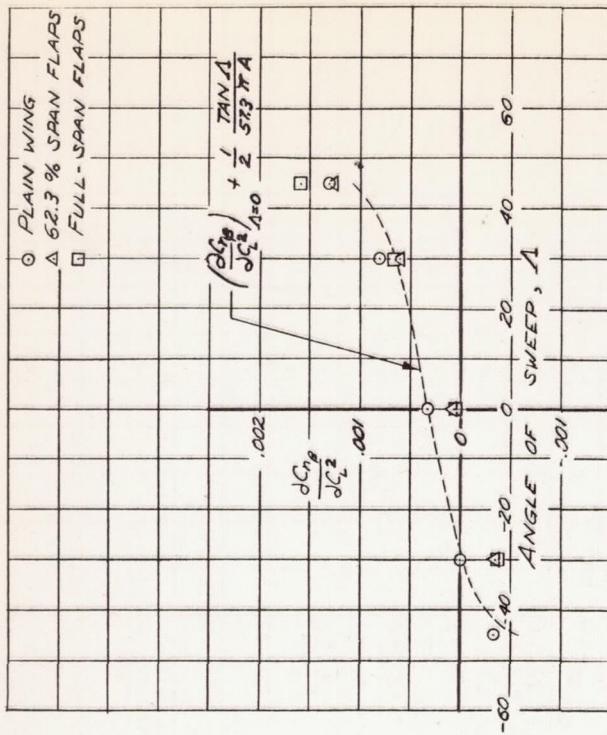


FIGURE 21.— THE EFFECT OF SWEET ON THE VARIATION OF DIRECTIONAL STABILITY WITH LIFT COEFFICIENT. 20 % CHORD SPLIT FLAPS DEFLECTED 60° .



NATIONAL ADVISORY COMMITTEE
FOR AERONAUTICS

FIGURE 22.— VARIATION WITH SWEET OF THE ESTIMATED
AND EXPERIMENTAL VALUES OF $\frac{dC_L}{dA}$.

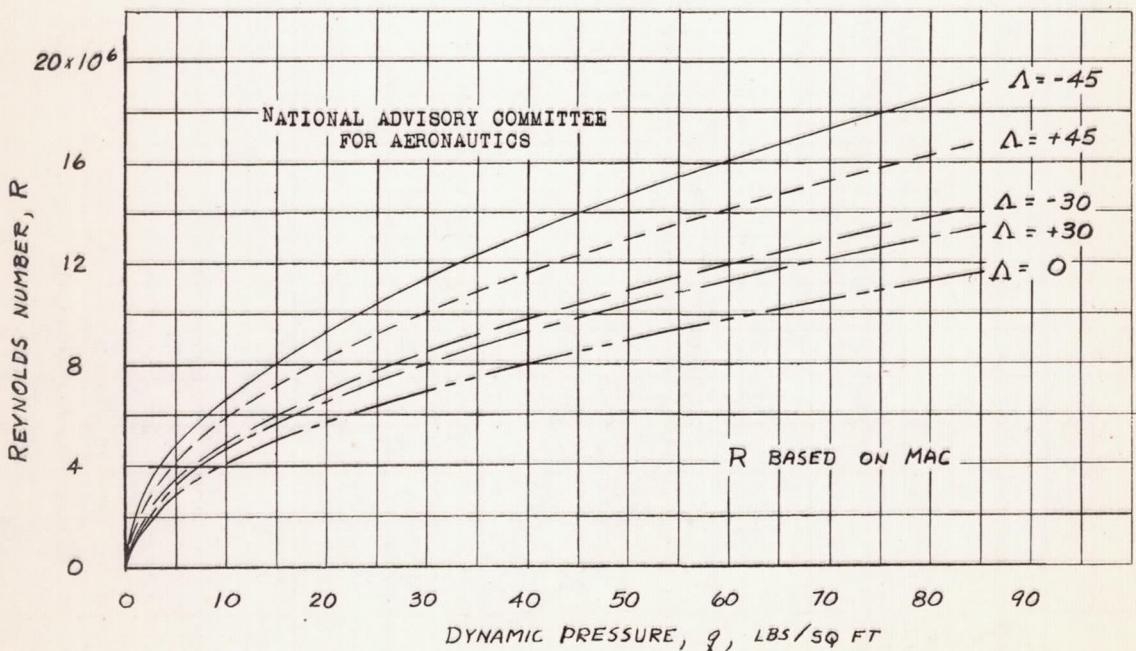
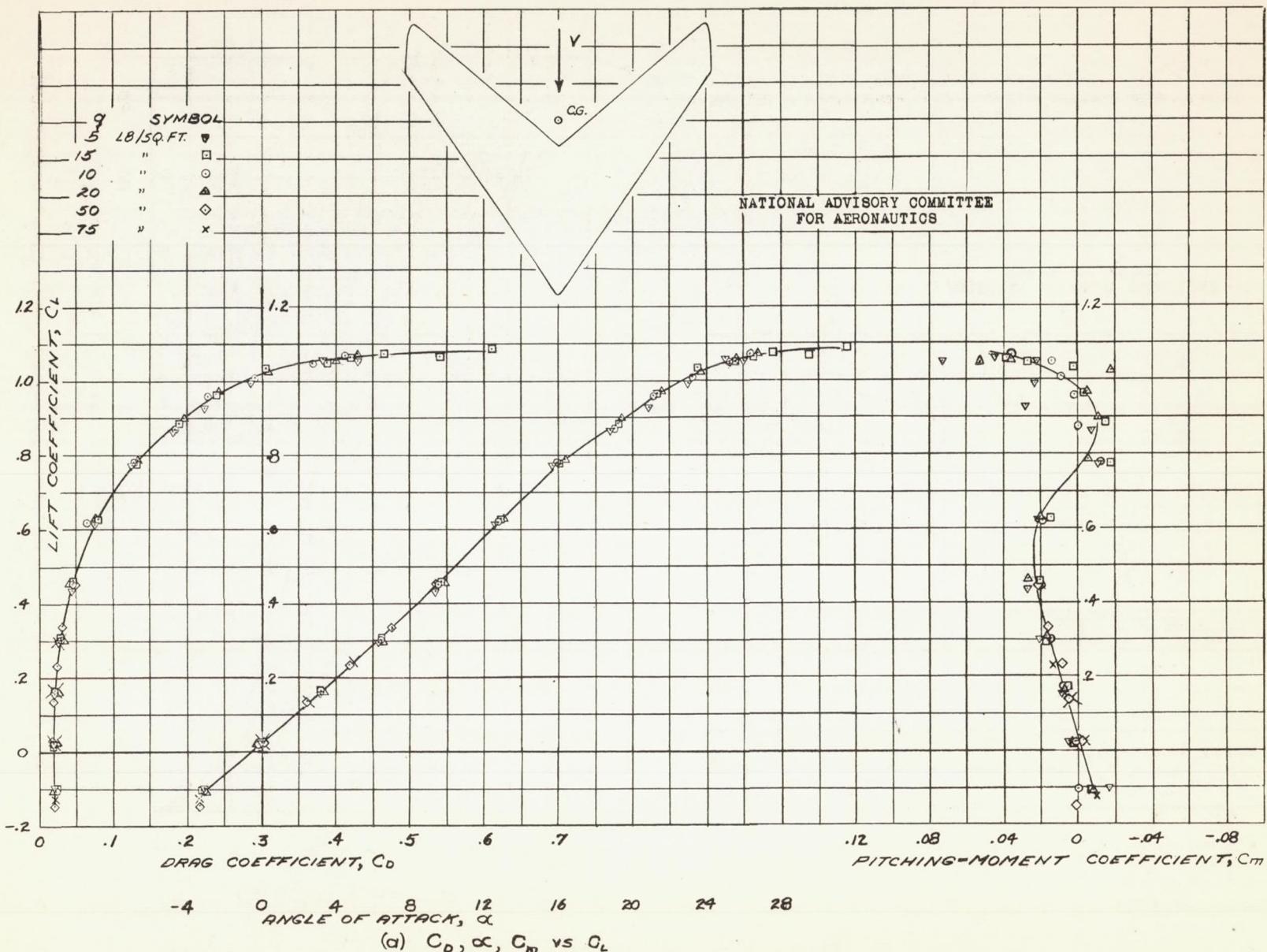


FIGURE 23.— VARIATION OF REYNOLDS NUMBER WITH DYNAMIC PRESSURE
FOR WINGS TESTED

Fig. 24a

NACA RM No. A6K15



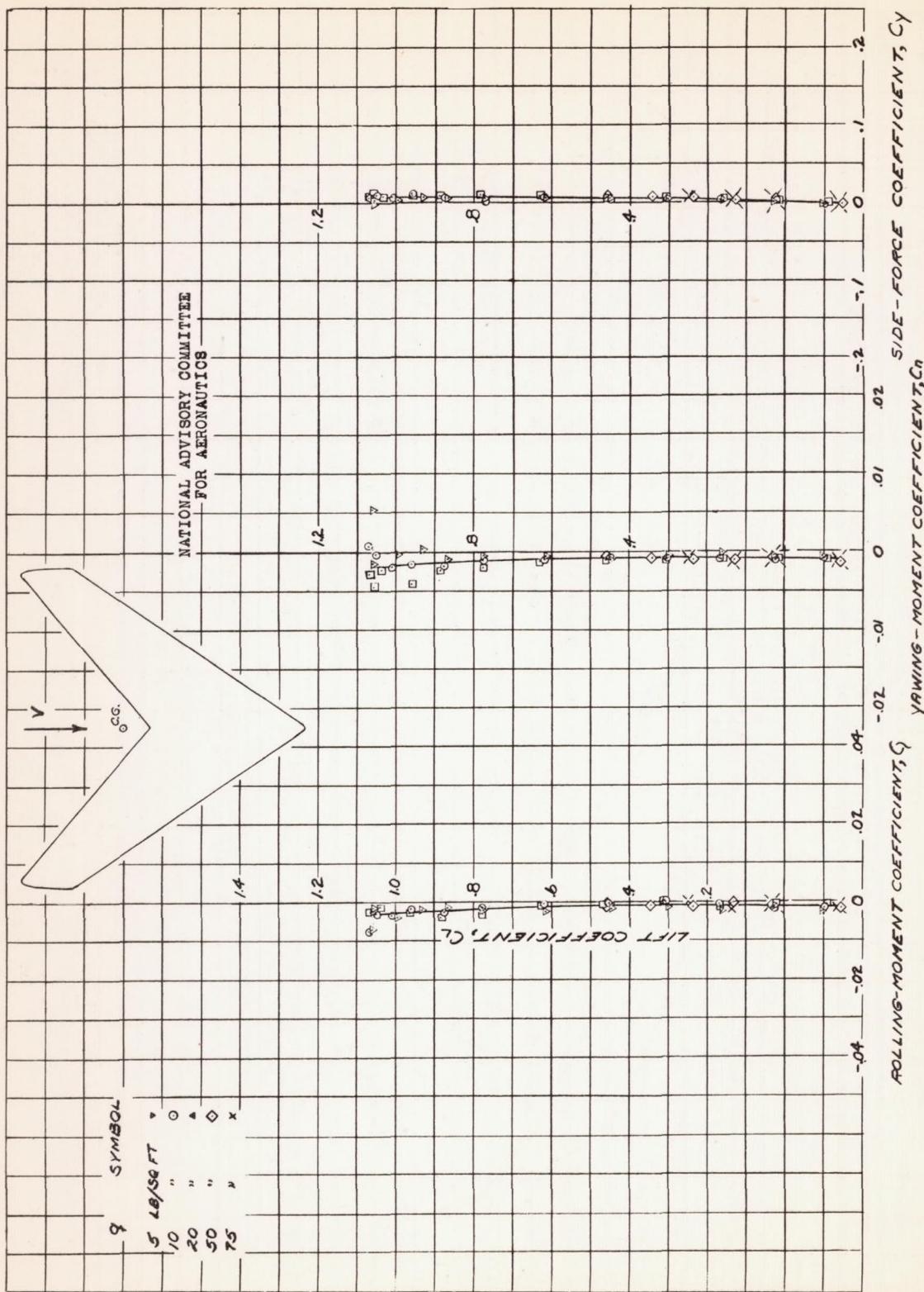
(b) C_l , C_m , C_y vs C_L

FIGURE 24.- CONCLUDED.

Fig. 25a

NACA RM No. A6K15

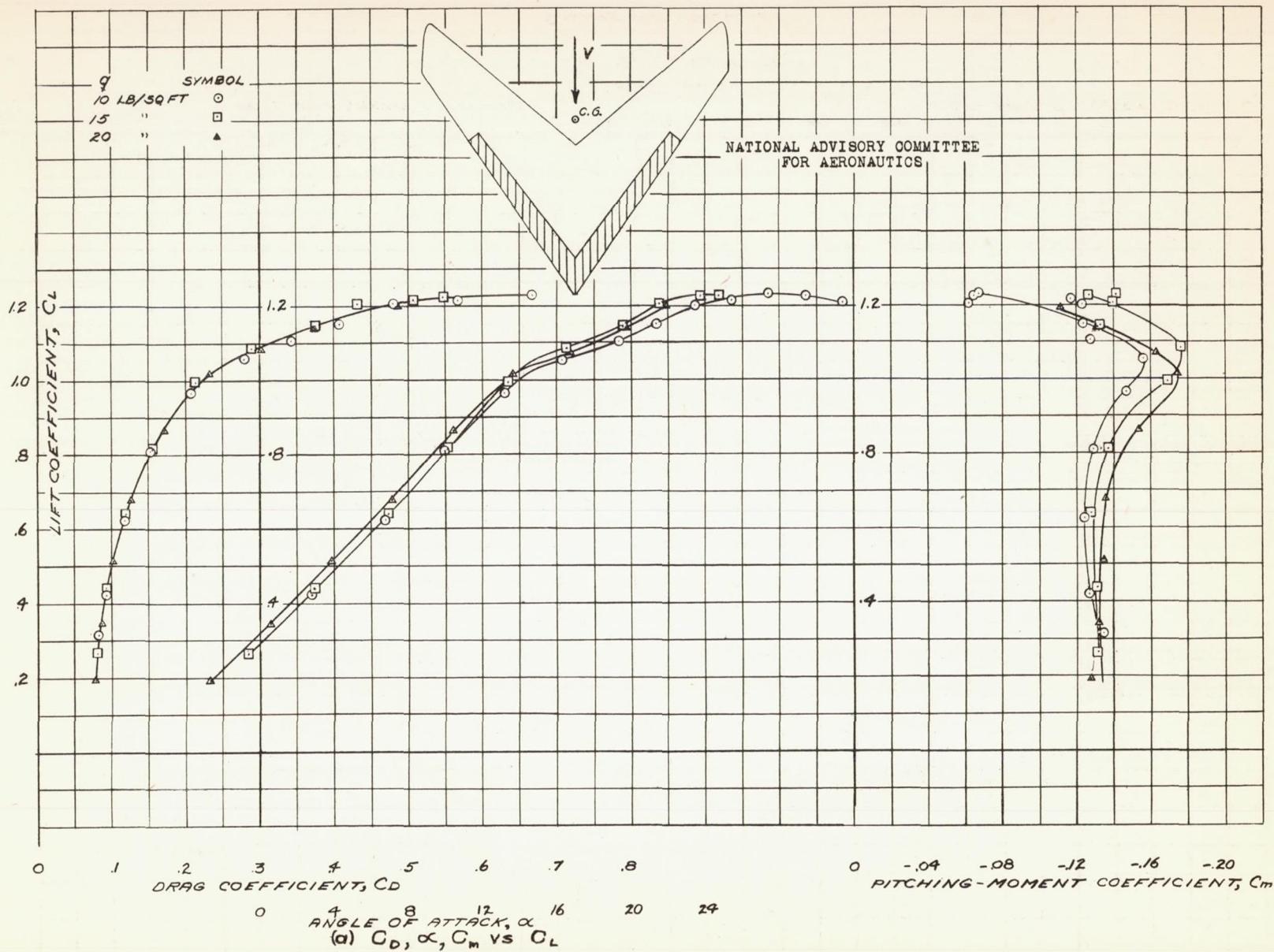


FIGURE 25.- AERODYNAMIC CHARACTERISTICS OF THE 95° SWEEPTFORWARD WING AT +0.2° SIDESLIP.
20% CHORD, 62.3% SPAN SPLIT
FLAPS DEFLECTED 60°

Fig. 25b

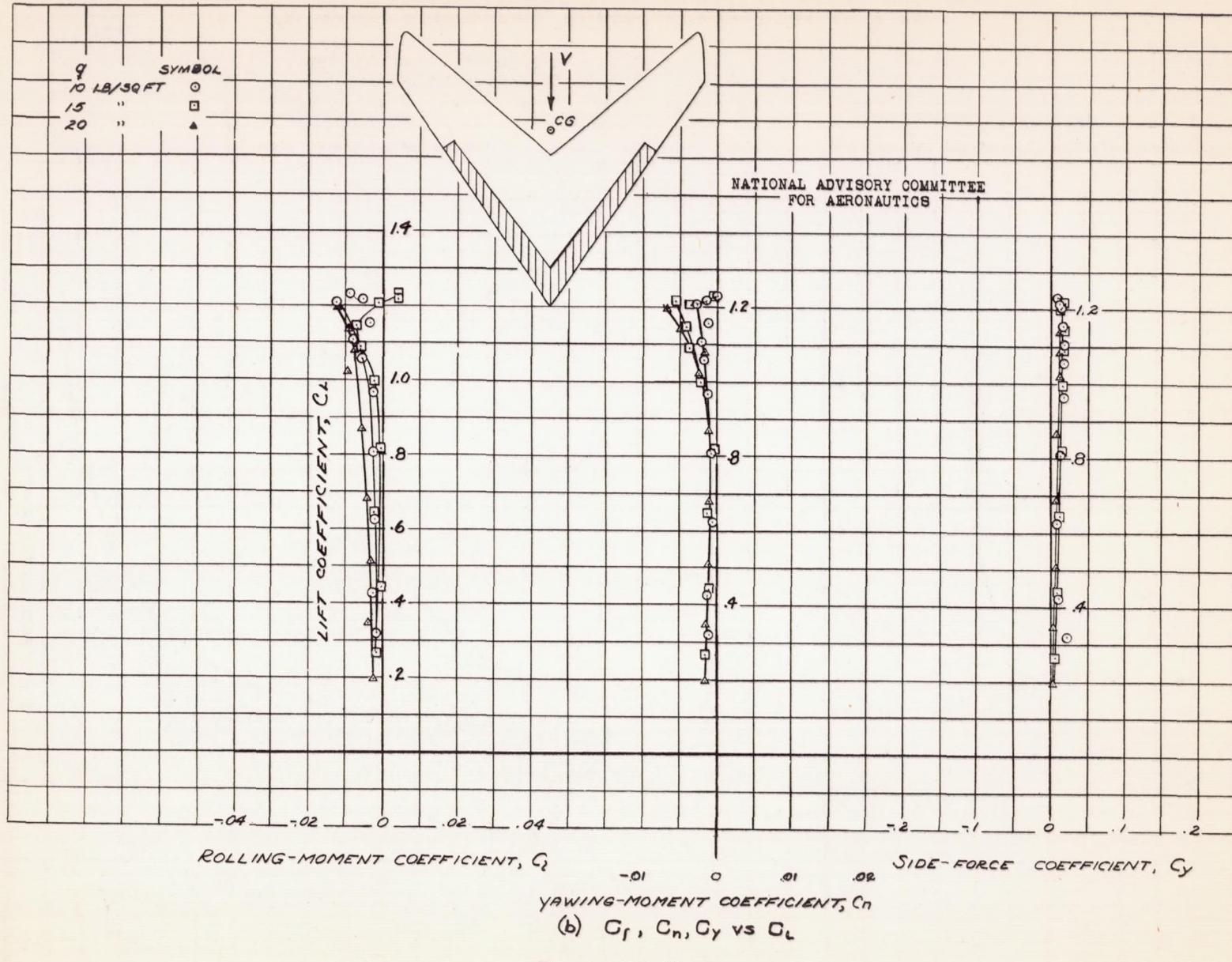


Fig. 26a

NACA RM No. A6K15

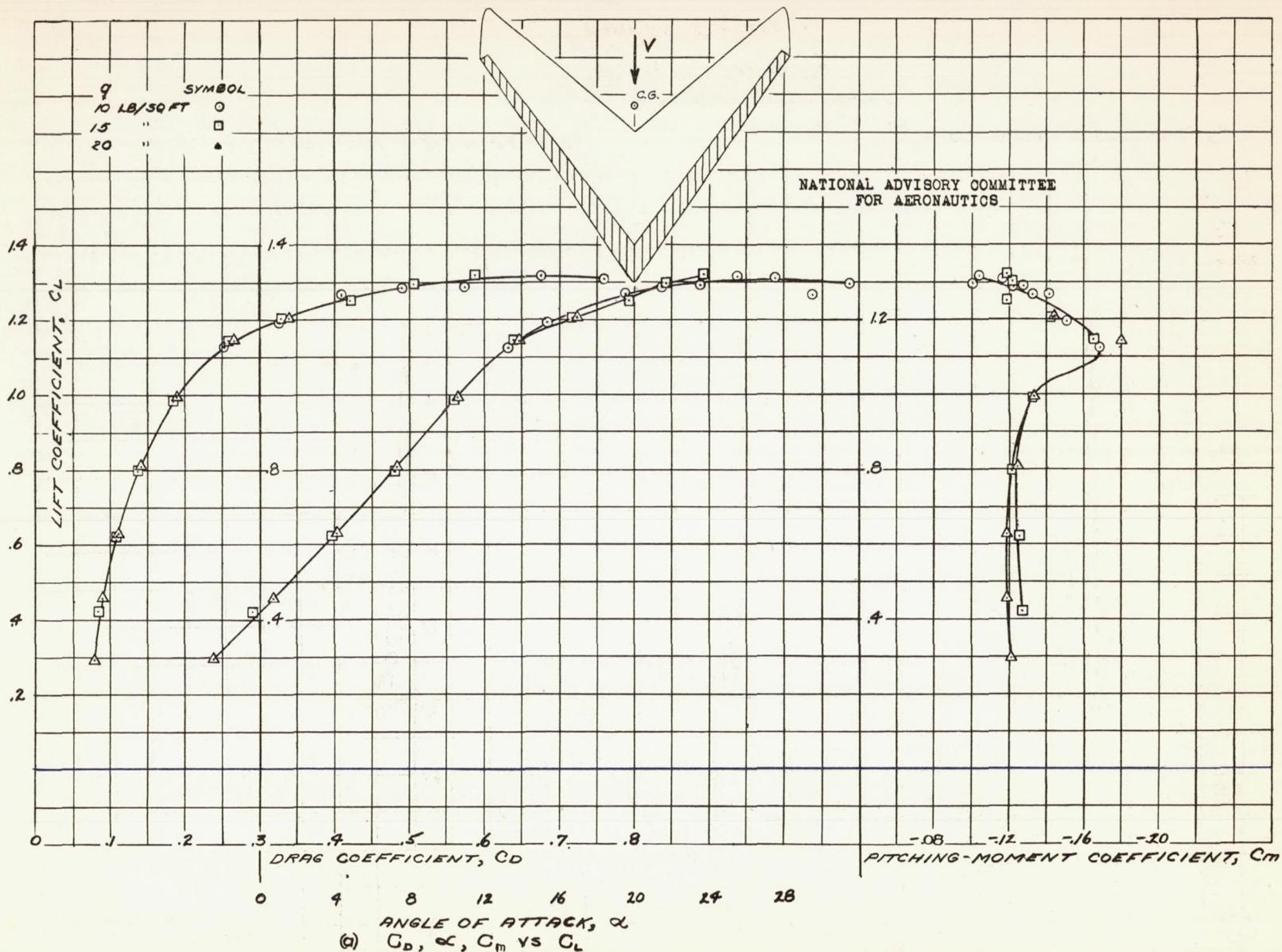


FIGURE 26.—AERODYNAMIC CHARACTERISTICS OF THE 95° SWEEP FORWARD WING AT +0.2° SIDESLIP. 20% CHORD FULL-SPAN SPLIT FLAPS DEFLECTED 60°.

Fig. 26b

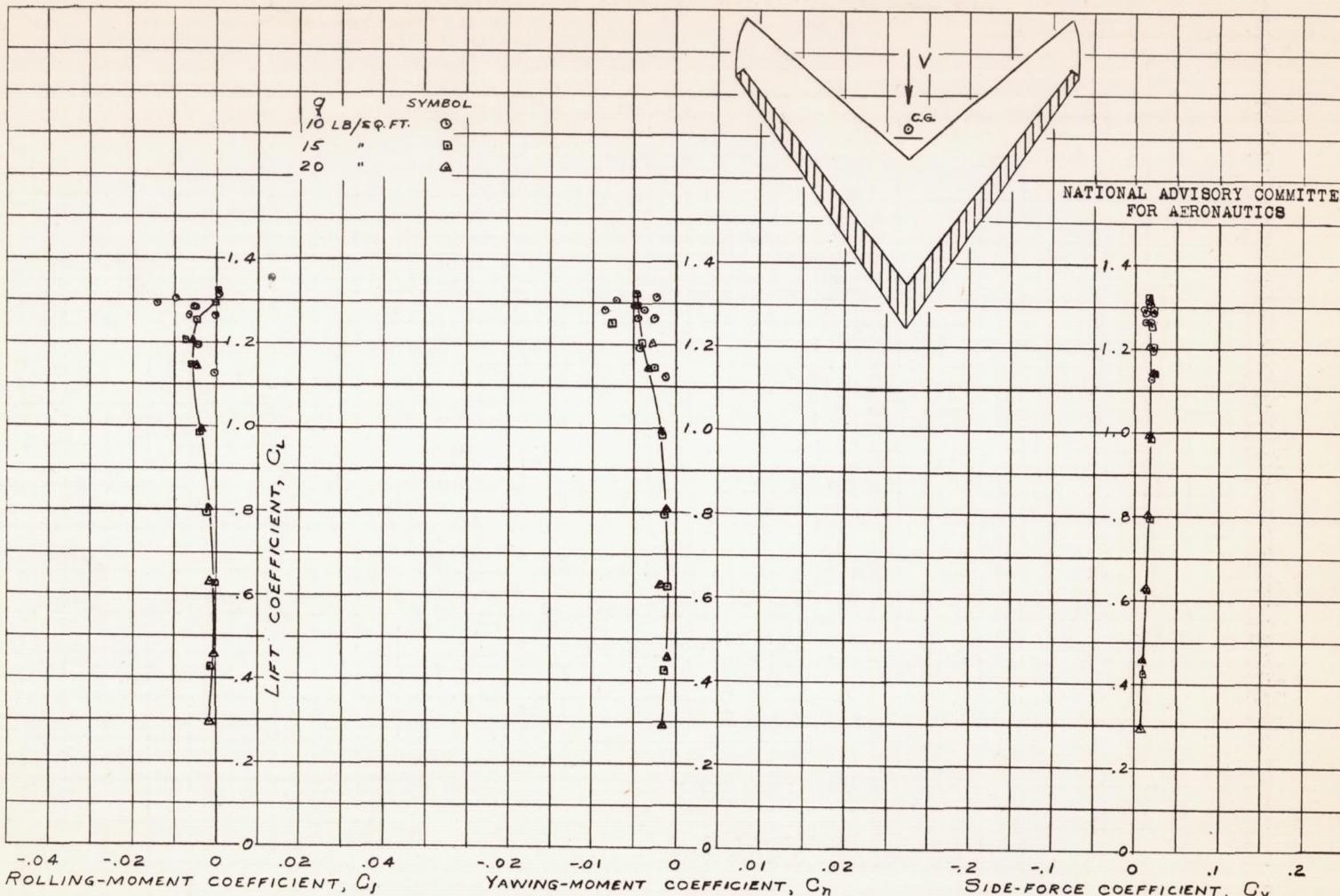
(b) C_s , C_n , C_y vs C_l

FIGURE 26.- CONCLUDED

Fig. 27

NACA RM NO. A6K15

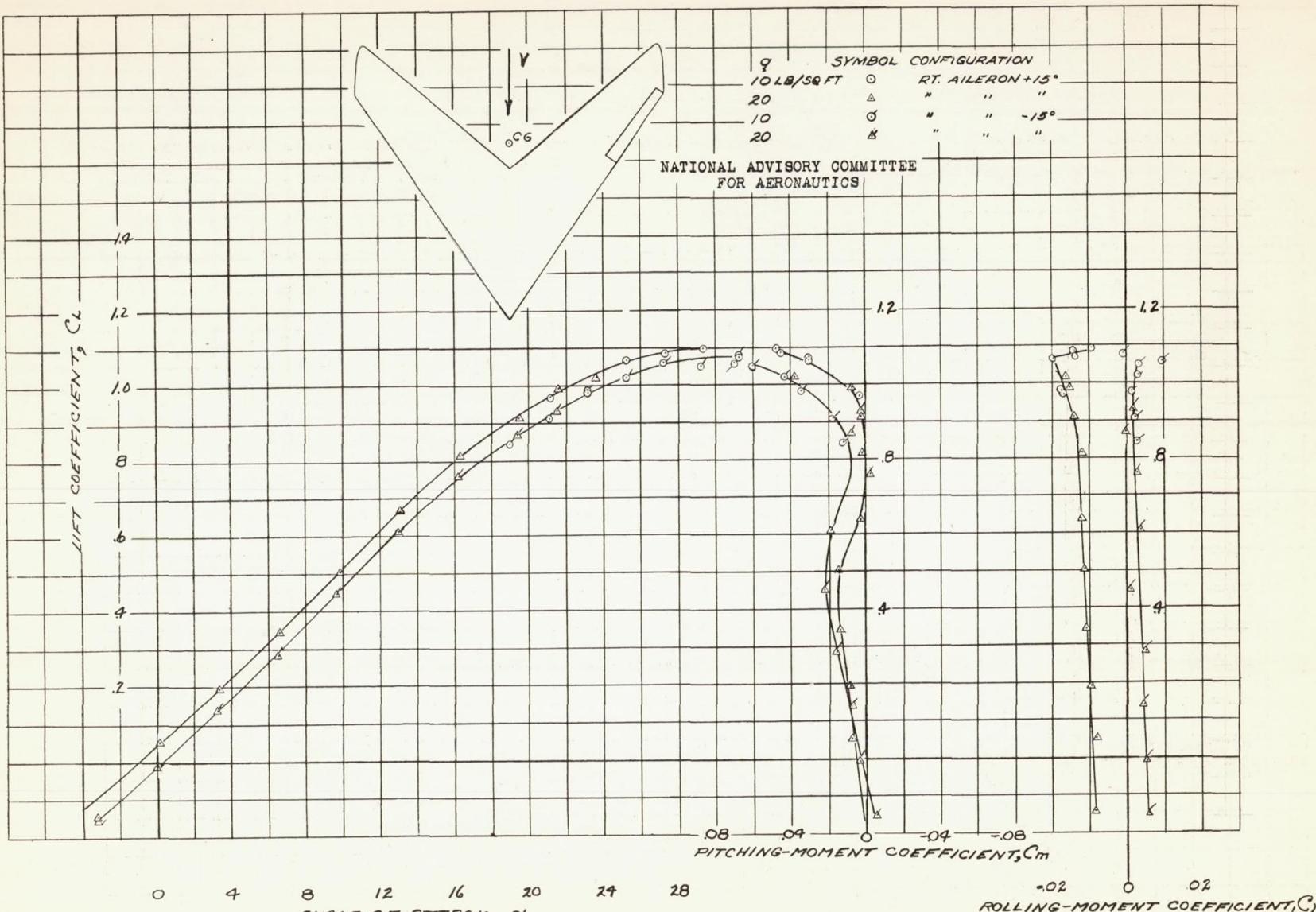


FIGURE 27.-AERODYNAMIC CHARACTERISTICS OF THE 95°
SWEEP FORWARD WING AT +0.2° SIDESLIP. 20% CHORD
34.6% SPAN SPLIT FLAP TYPE AILERON
ON RIGHT WING DEFLECTED $\pm 15^\circ$

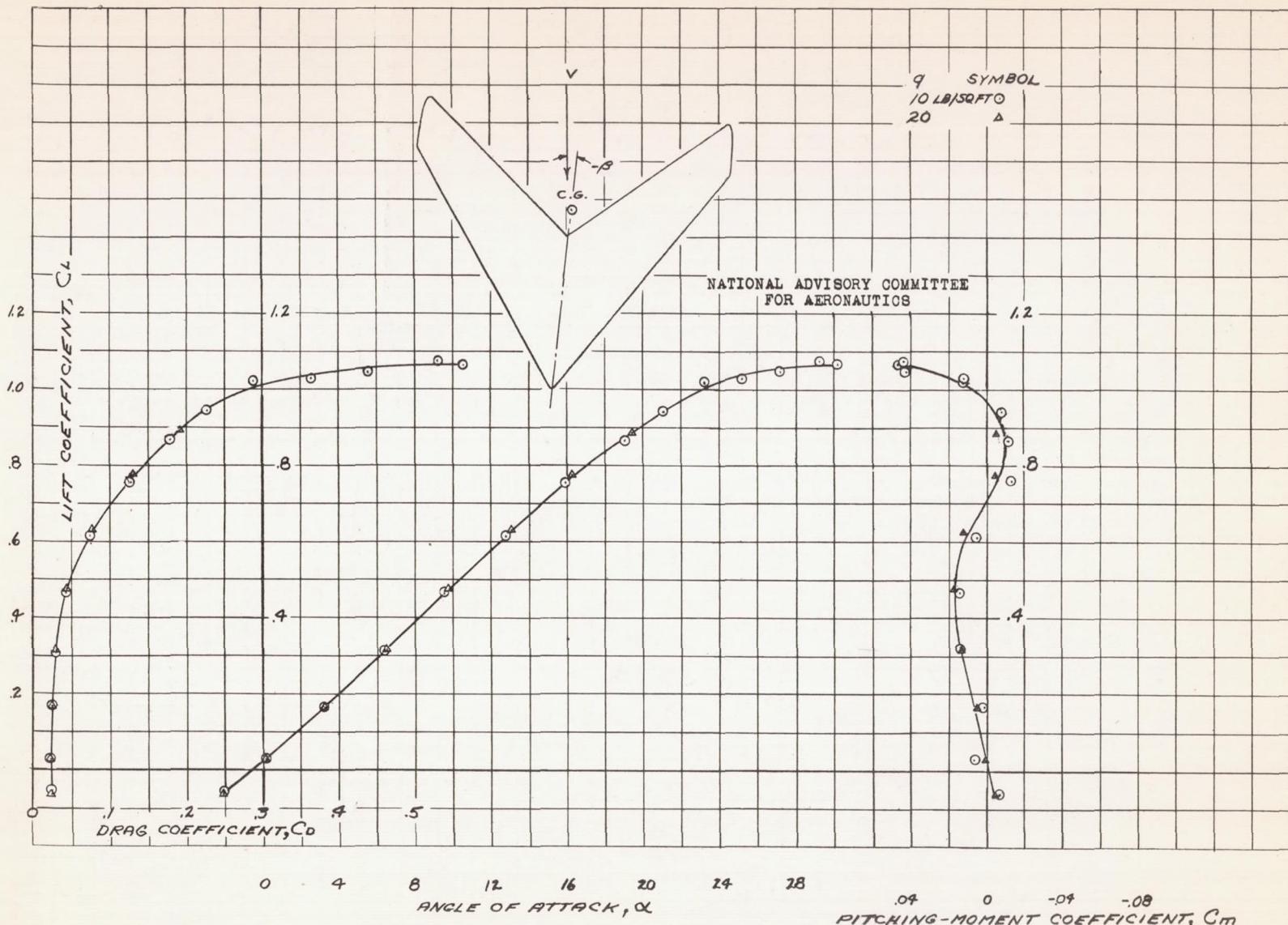


FIGURE 28-AERODYNAMIC CHARACTERISTICS OF THE 95° SWEEPFORWARD WING AT -5.3° SIDESLIP.
PLAIN WING.

Fig. 28b

NACA RM No. A6K15

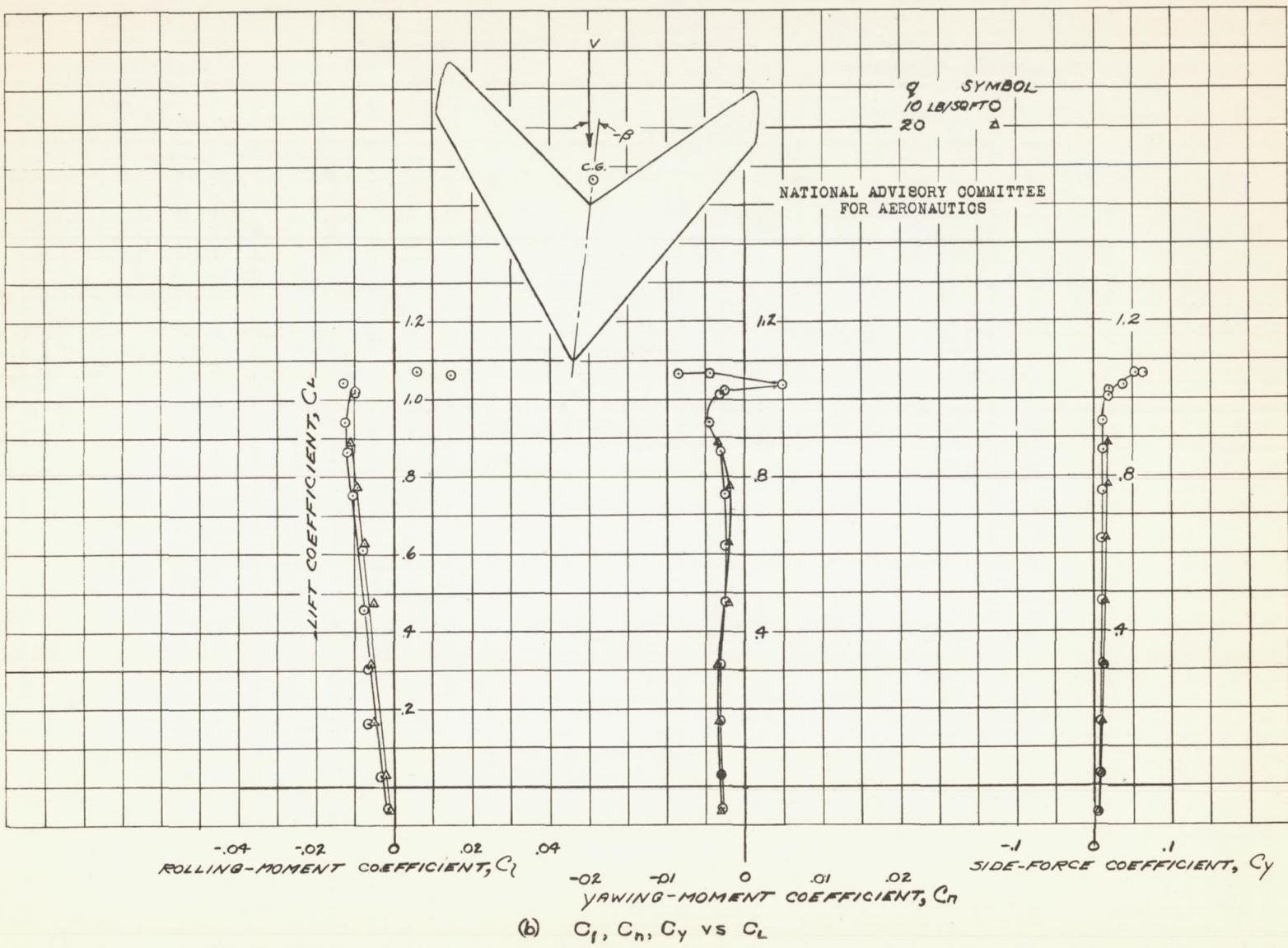


FIGURE 28.- CONCLUDED.

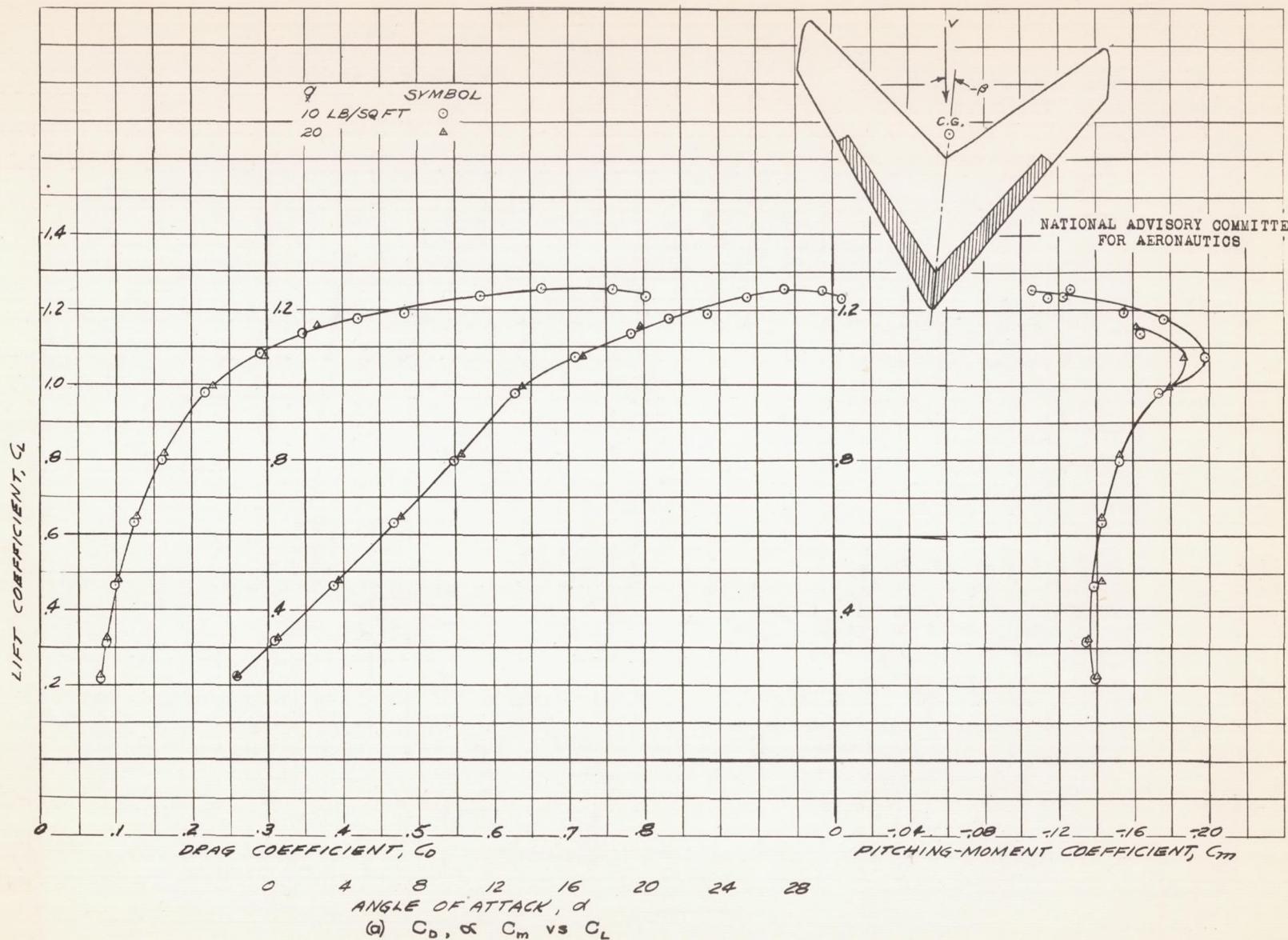


FIGURE 29.-AERODYNAMIC CHARACTERISTICS OF THE 95° SWEEPTFORWARD WING AT -5.3° SIDESLIP.
20% CHORD, 62.3% SPAN SPLIT FLAPS DEFLECTED 60° .

Fig. 29b

NACA RM No. A6K15

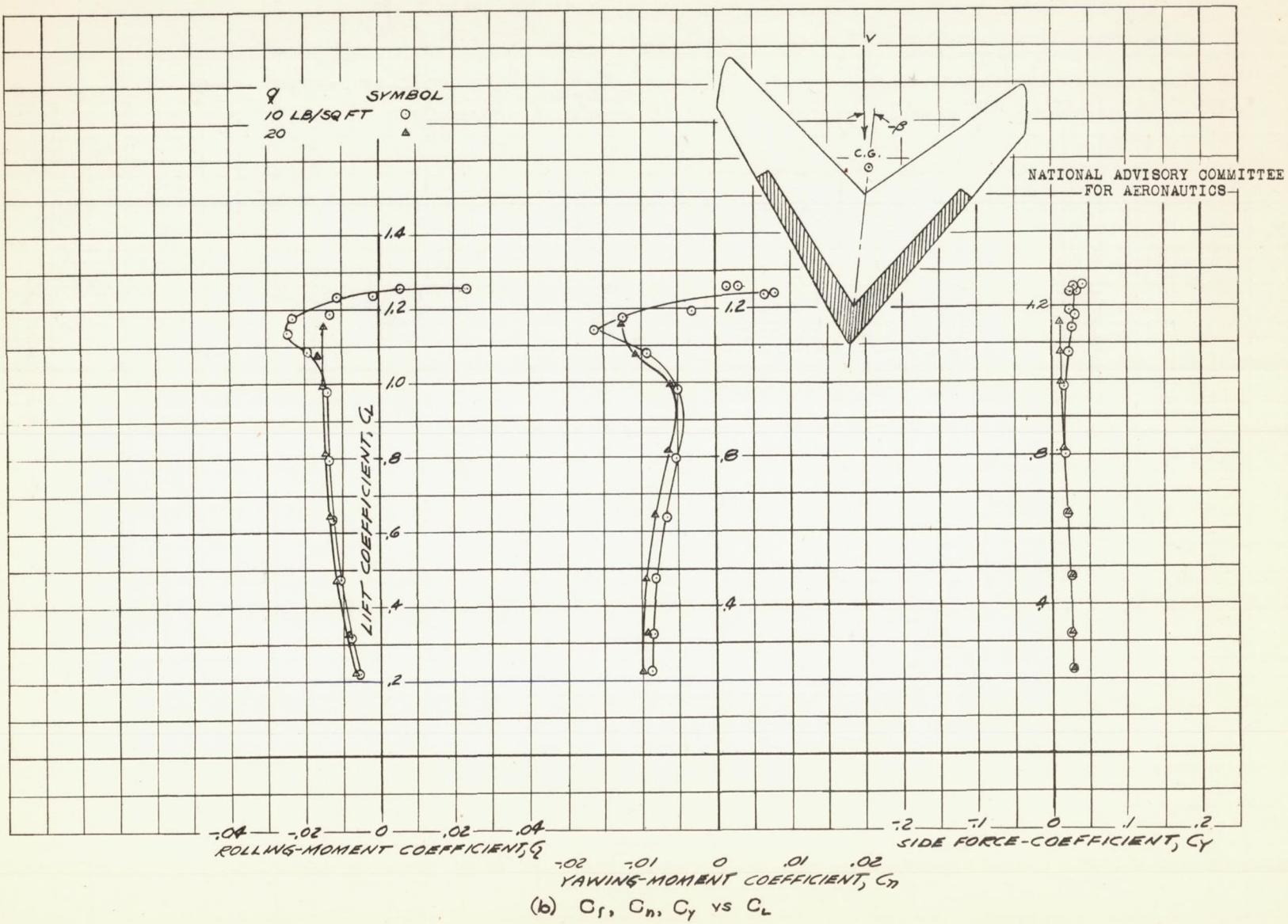


FIGURE 29.-CONCLUDED.

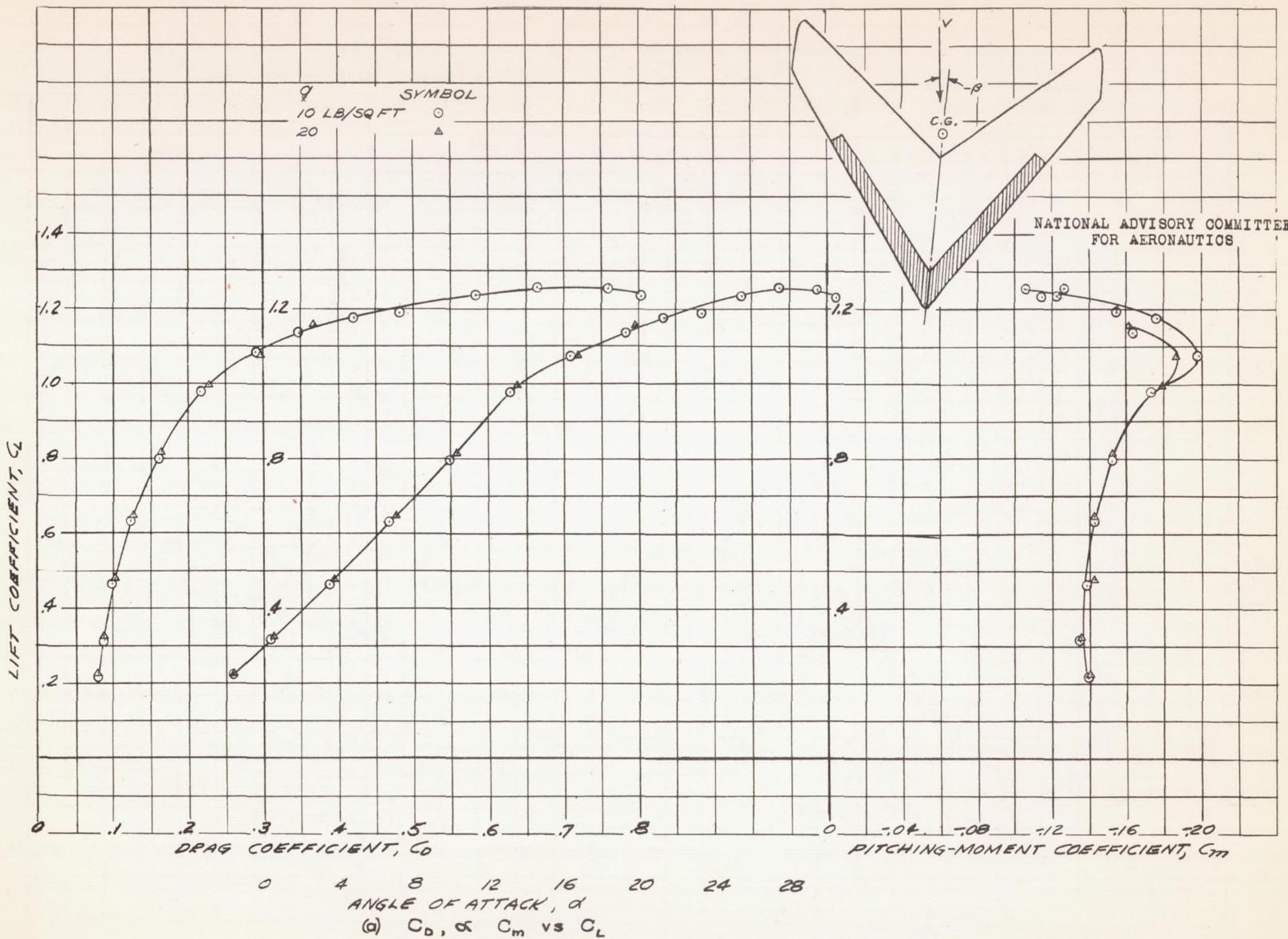


FIGURE 29.-AERODYNAMIC CHARACTERISTICS OF THE 95° SWEEPED-FORWARD WING AT -5.3° SIDESLIP.
20% CHORD, 62.3% SPAN SPLIT FLAPS DEFLECTED 60° .

Fig. 29b

NACA RM No. A6K15

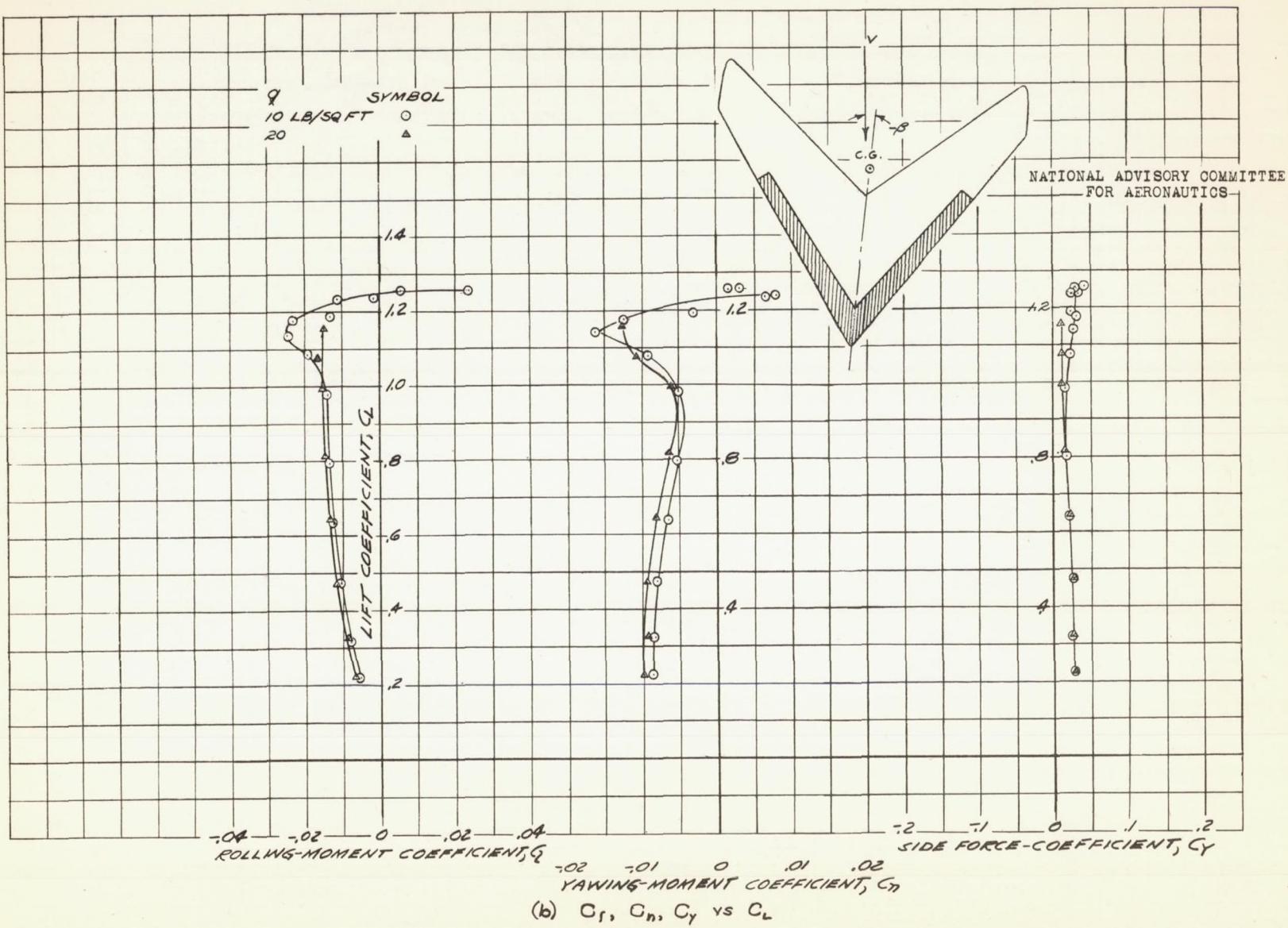


FIGURE 29.-CONCLUDED.

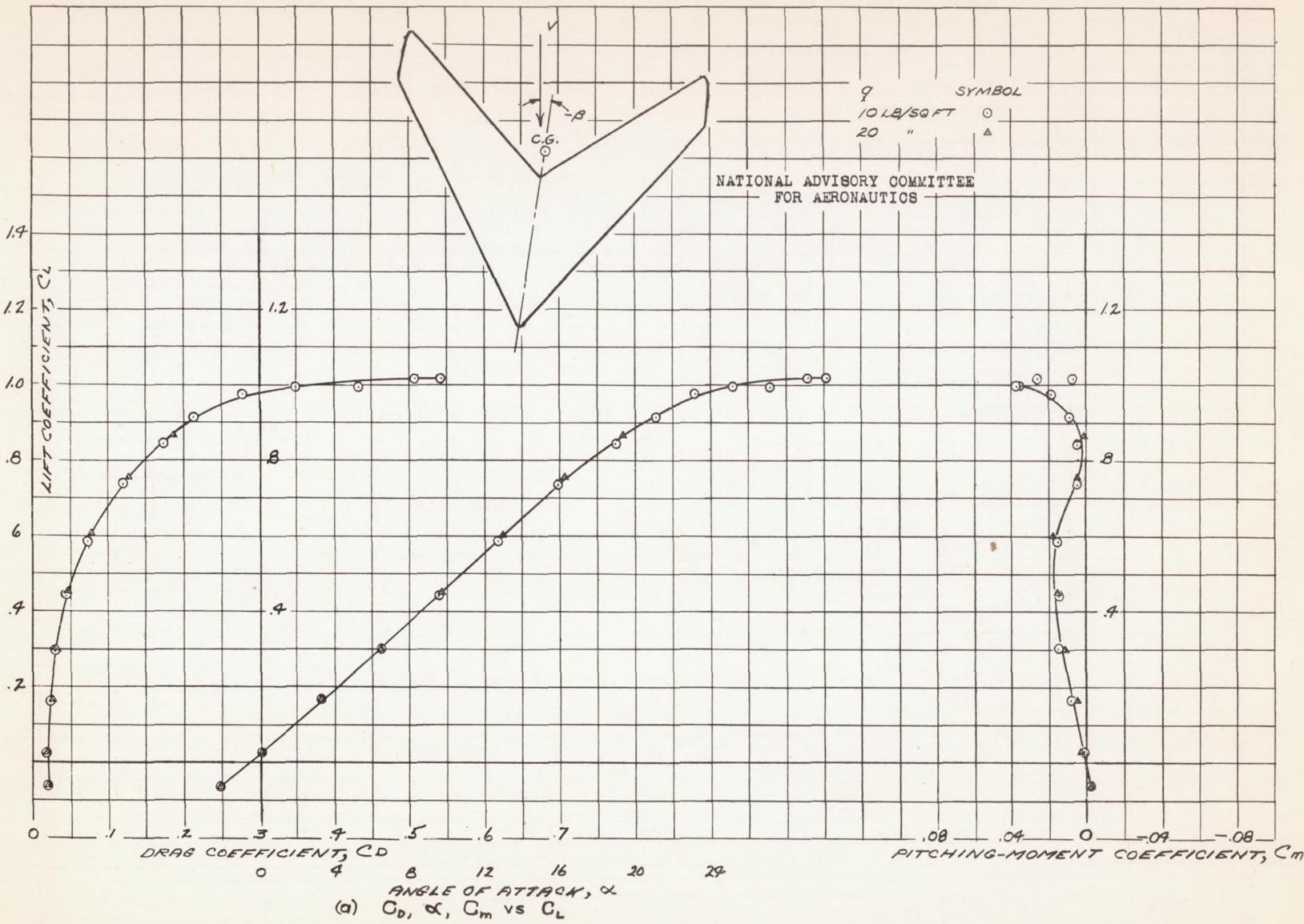


FIGURE 30.- AERODYNAMIC CHARACTERISTICS OF THE 95° SWEEP FORWARD WING AT -9.9° SIDESLIP.
PLAIN WING.

Fig. 30b

NACA RM No. A6K15

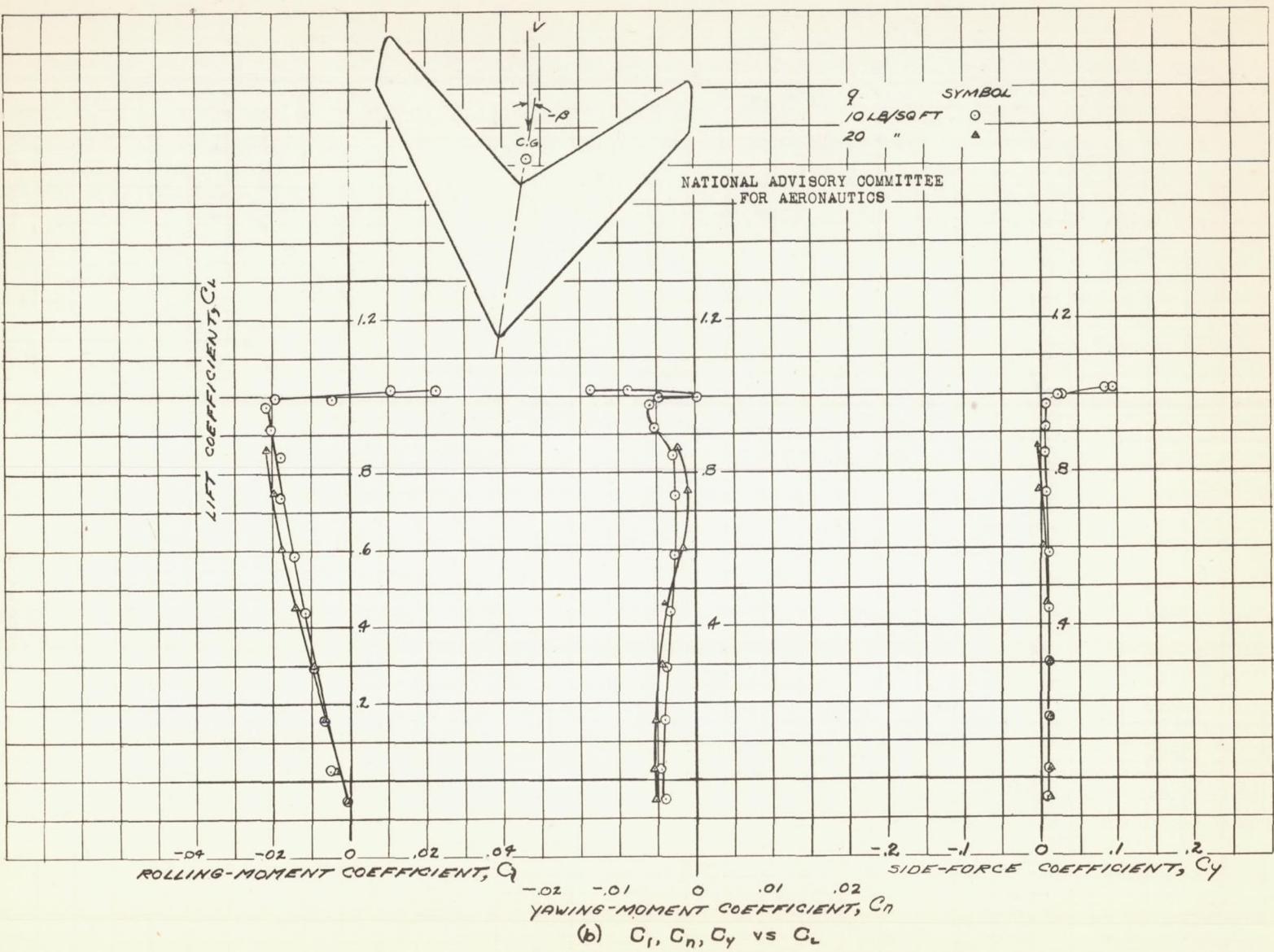


FIGURE 30.-CONCLUDED.

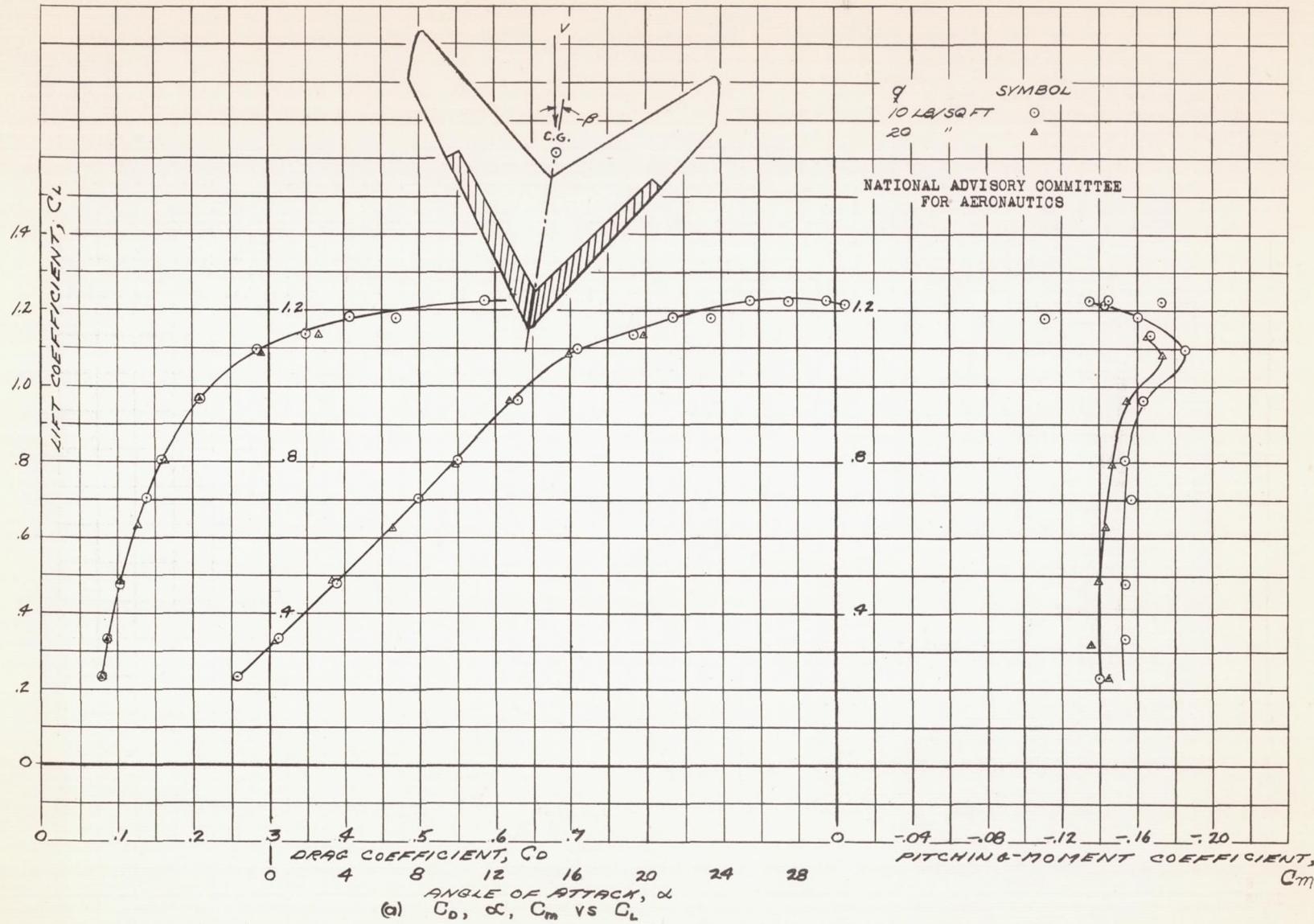


Fig. 31a

FIGURE 31.— AERODYNAMIC CHARACTERISTICS OF THE 95° SWEEP-FORWARD WING AT -9.9° SIDESLIP
20% CHORD, 62.3% SPAN SPLIT FLAPS DEFLECTED 60°

Fig. 31b

NACA RM No. A6K15

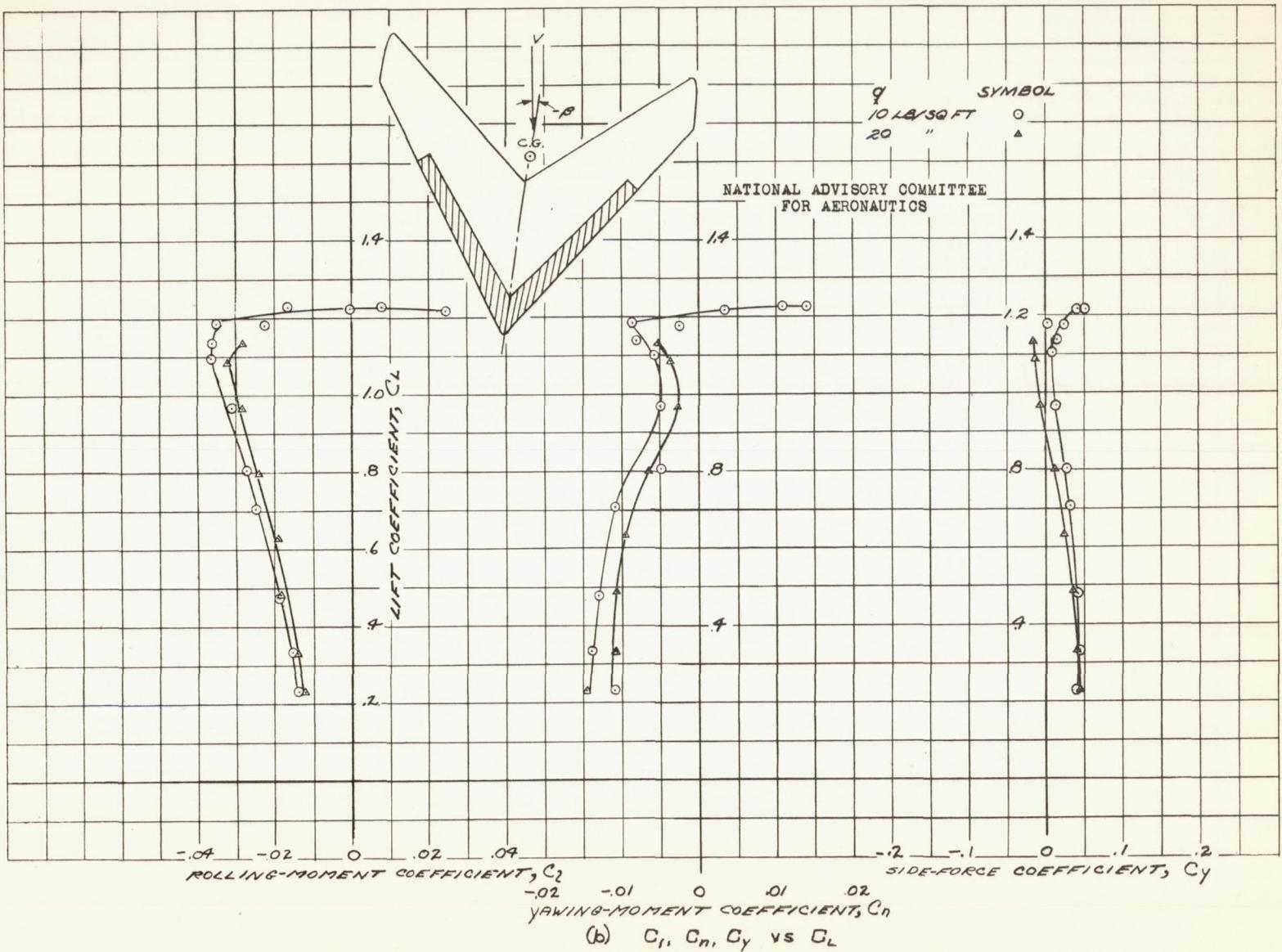


FIGURE 31.- CONCLUDED.

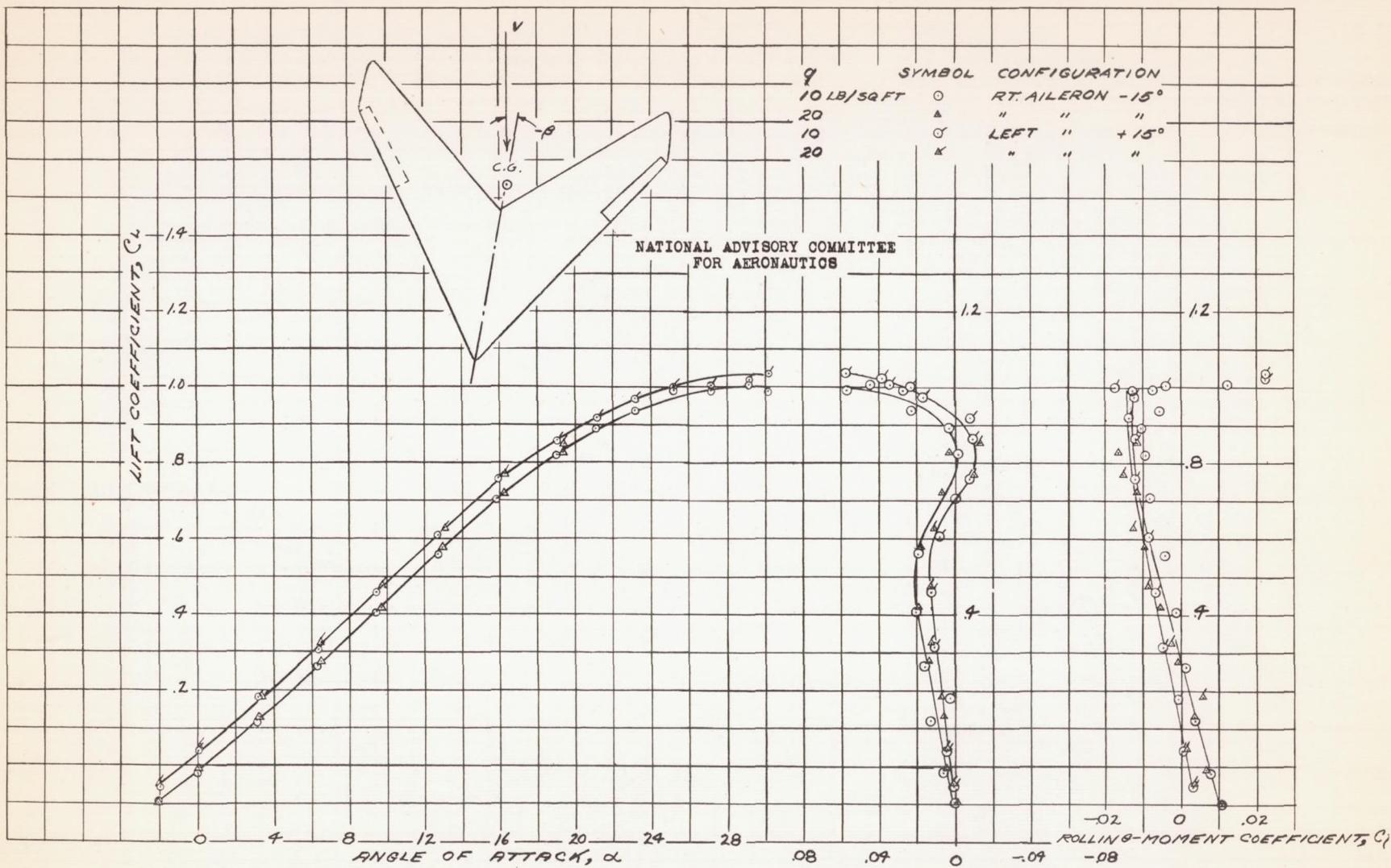


FIGURE 32.—AERODYNAMIC CHARACTERISTICS OF THE 95° SWEEP-FORWARD WING AT -9.9° SIDESLIP, 20% CHORD, 34.6% SPAN SPLIT FLAP TYPE AILERONS, DEFLECTED $\pm 15^\circ$.

Fig. 33a

NACA RM NO. A6K15

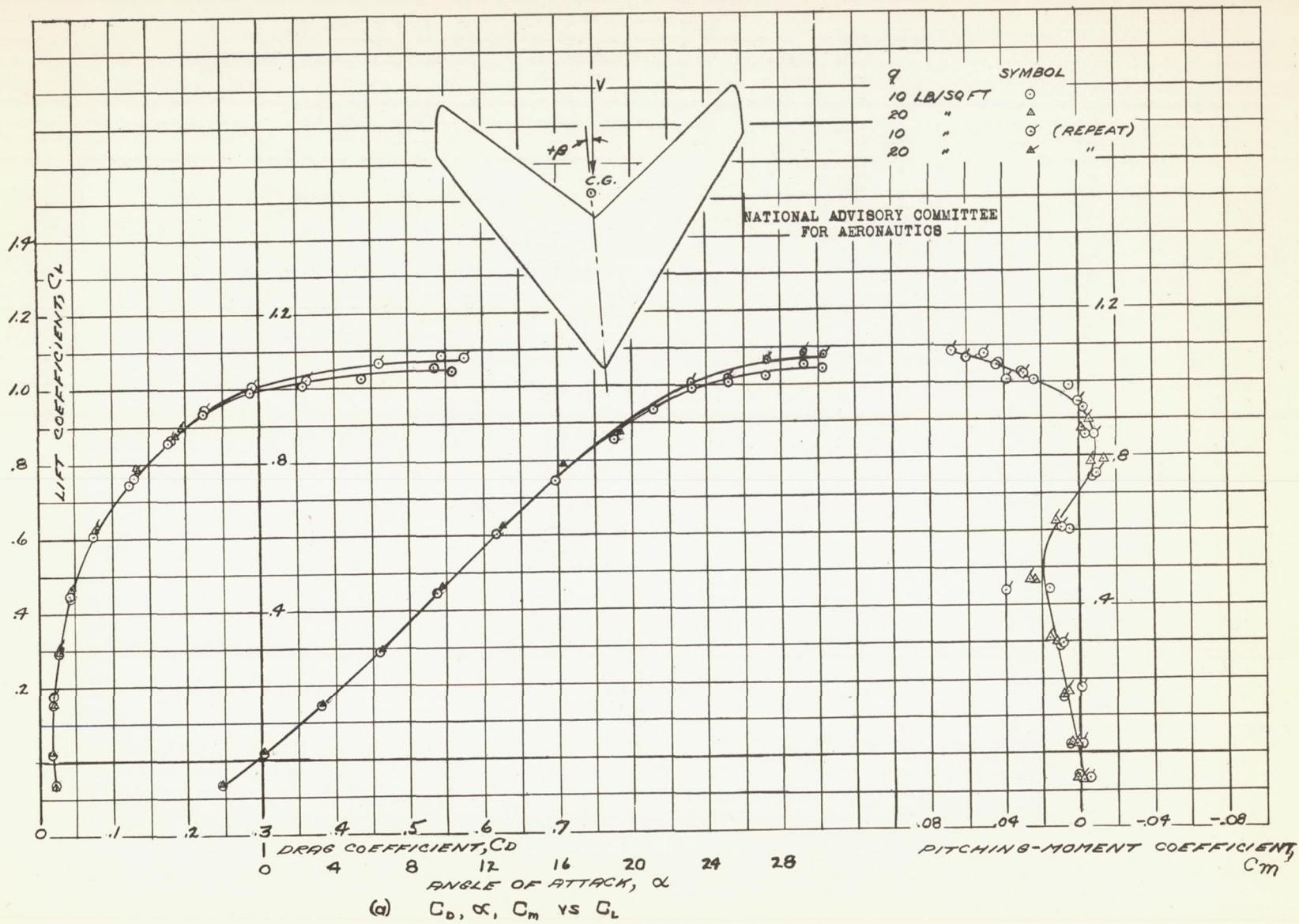


FIGURE 33.—AERODYNAMIC CHARACTERISTICS OF THE 95° SWEEP FORWARD WING AT +9.5° SIDE-SLIP.
PLAIN WING.

Fig. 33b

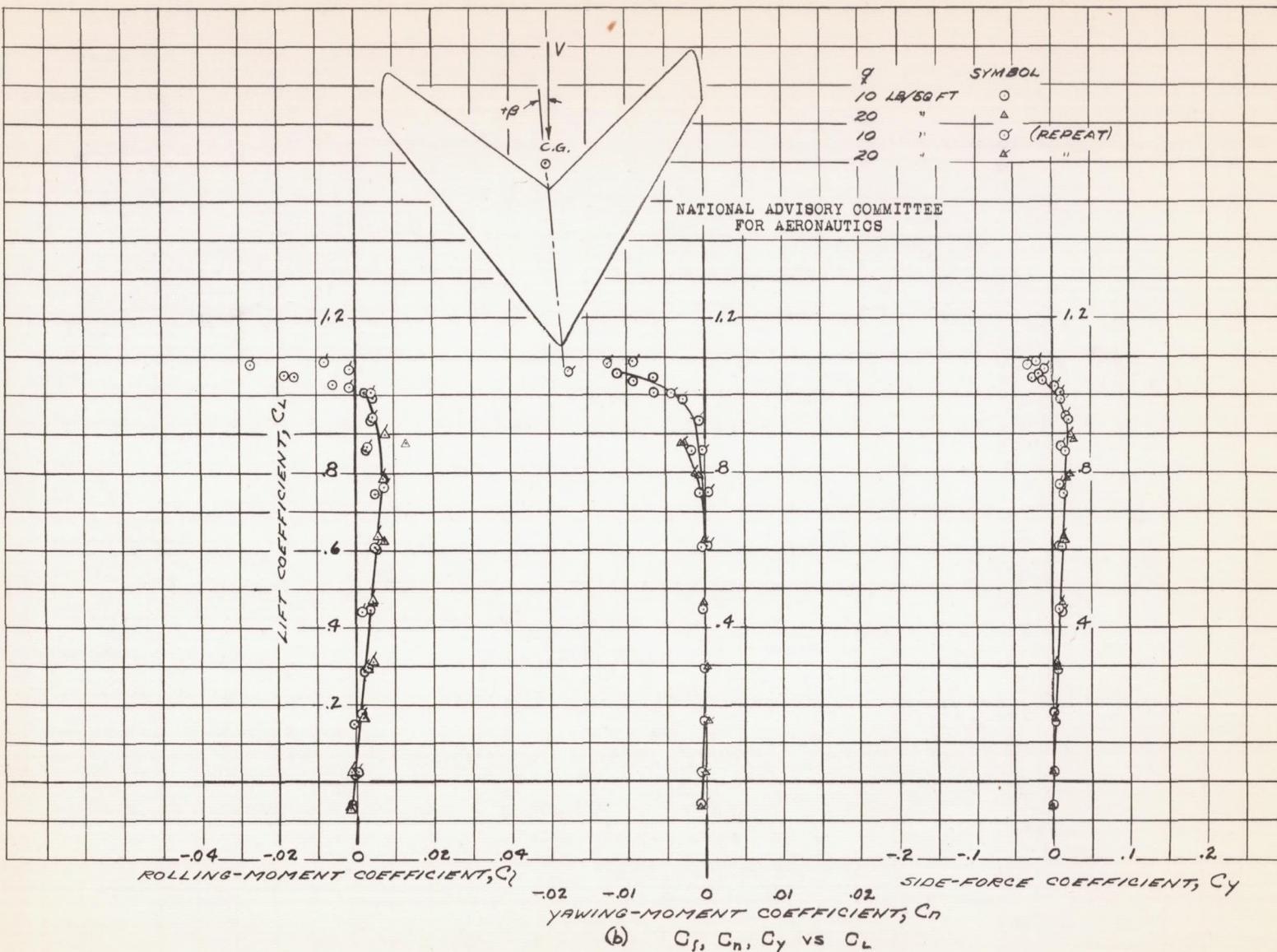


FIGURE 33.- CONCLUDED.

Fig. 34a

NACA RM NO. A6K15

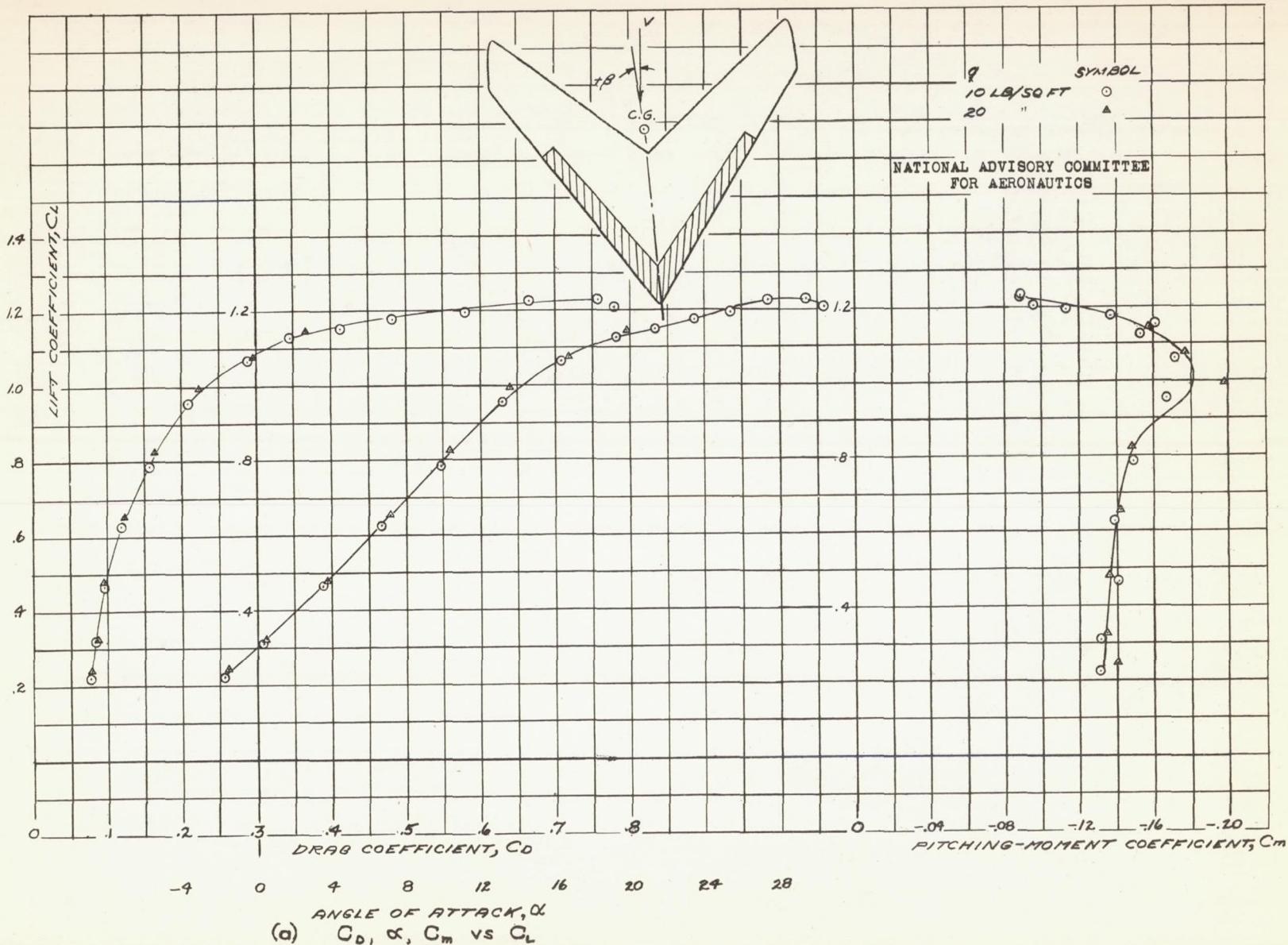


FIGURE 34.—AERODYNAMIC CHARACTERISTICS OF THE 95° SWEEP FORWARD WING AT $+9.5^\circ$ SIDESLIP
20% CHORD, 62.3% SPAN SPLIT FLAPS DEFLECTED 60° .

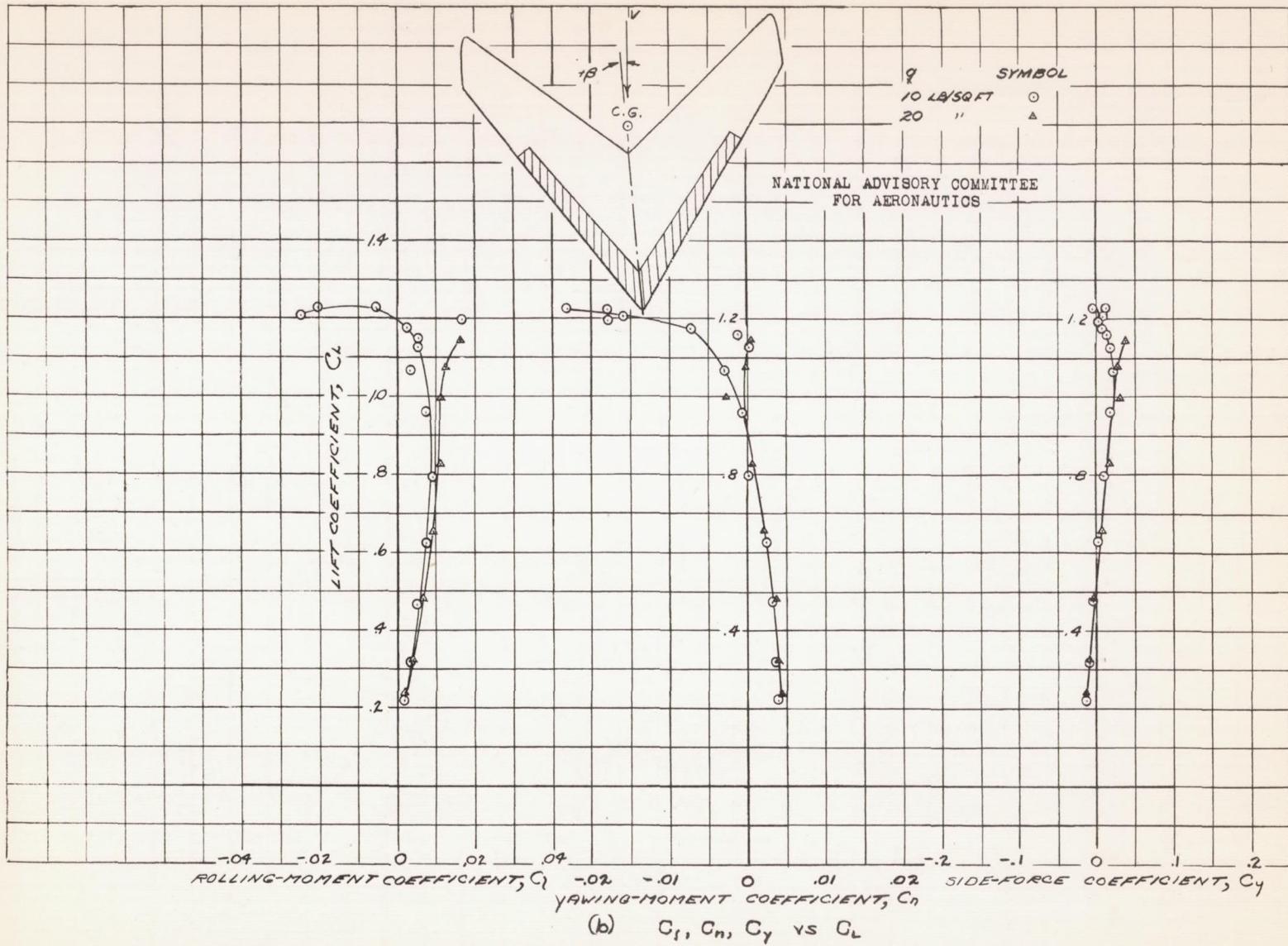


FIGURE 34.- CONCLUDED.

Fig. 35

NACA RM No. A6K15

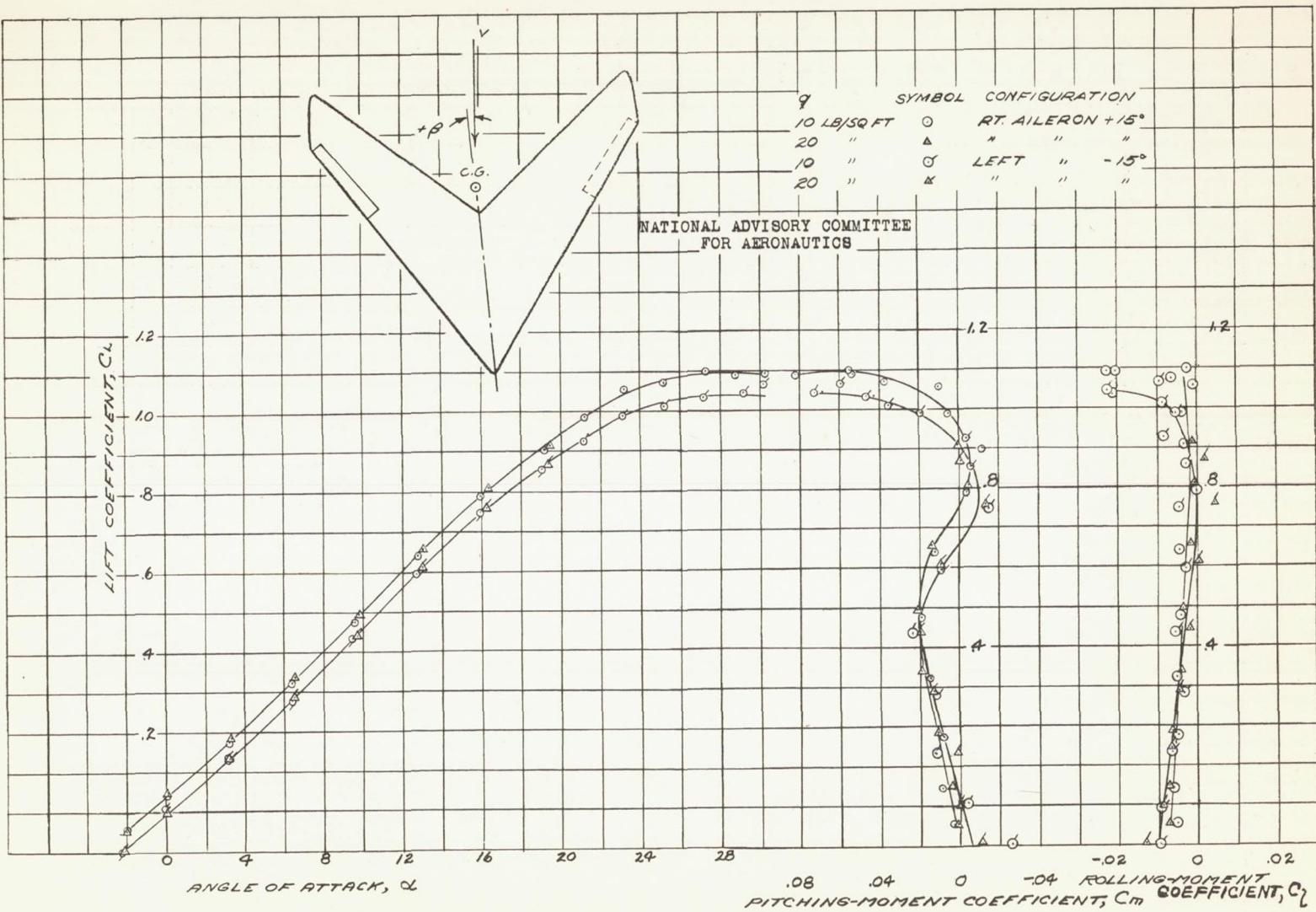


FIGURE 35.—AERODYNAMIC CHARACTERISTICS OF THE 95°
SWEPTFORWARD WING AT 19.5° SIDESLIP 20% CHORD
34.6% SPAN SPLIT FLAP TYPE AILERONS
DEFLECTED $\pm 15^\circ$.

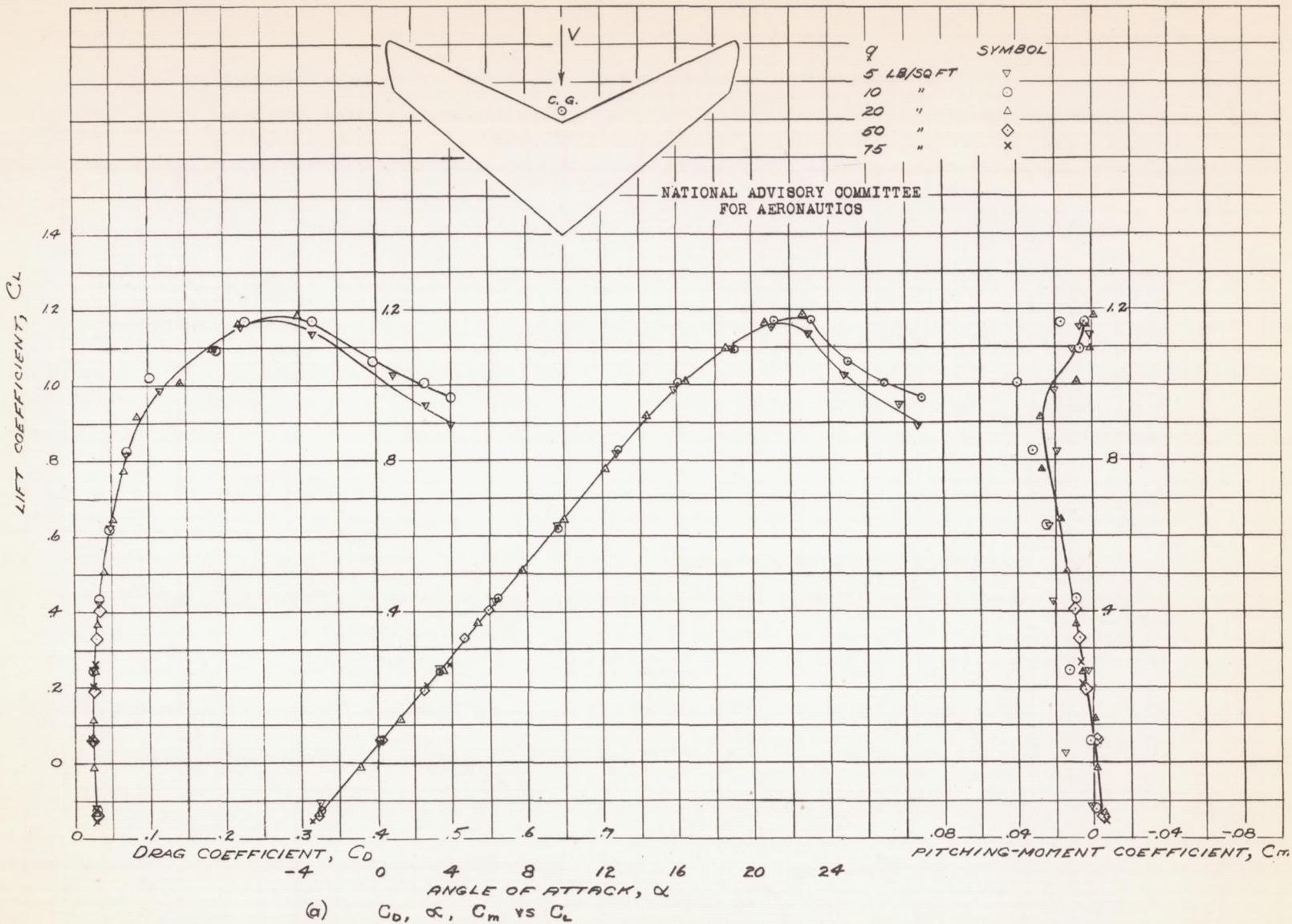


FIGURE 36.-AERODYNAMIC CHARACTERISTICS OF THE 30° SWEEPTFORWARD WING AT -0.2° SIDESLIP.
PLAIN WING.

Fig. 36b

NACA RM No. A6K15

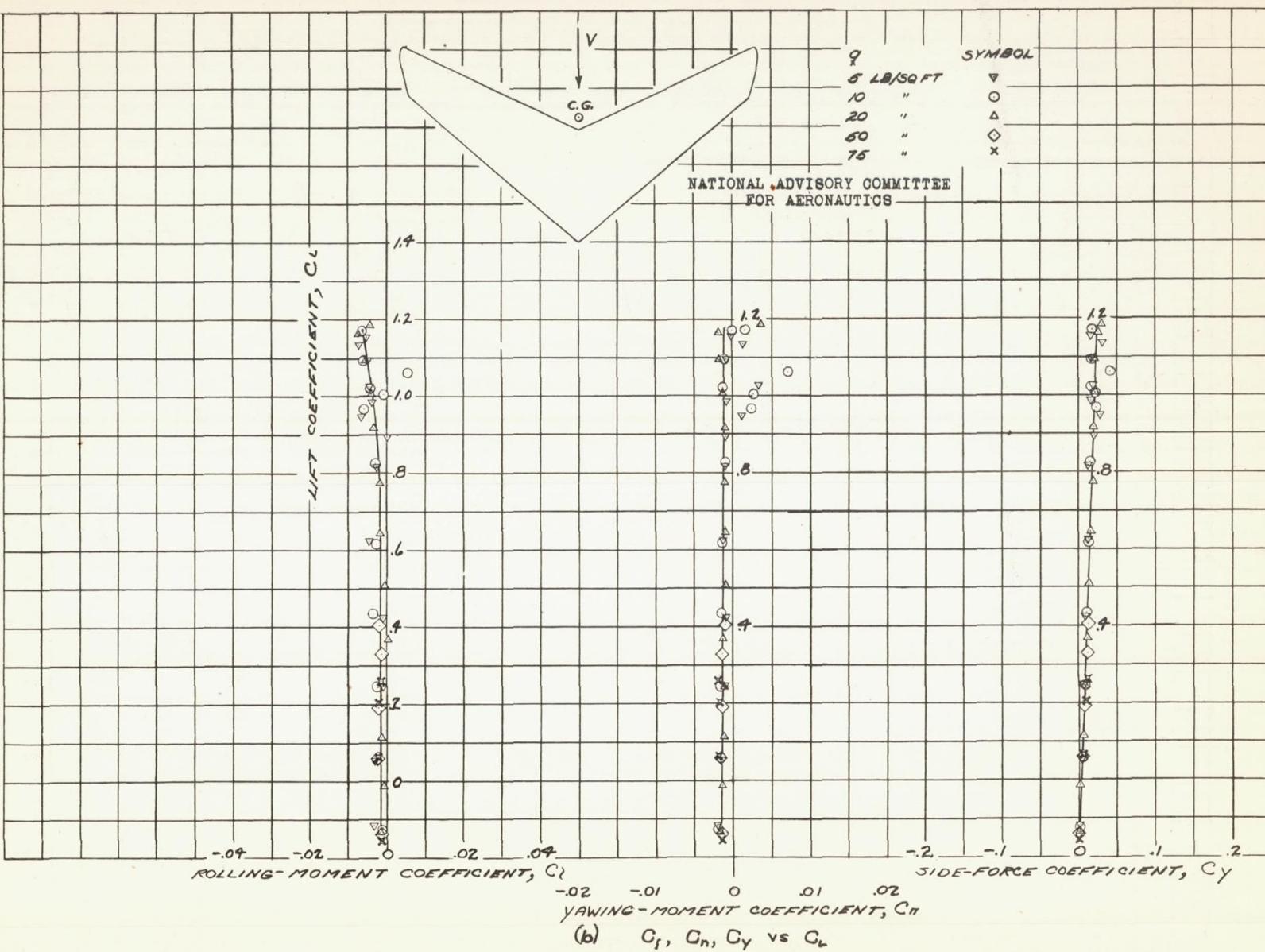


FIGURE 36.-CONCLUDED.

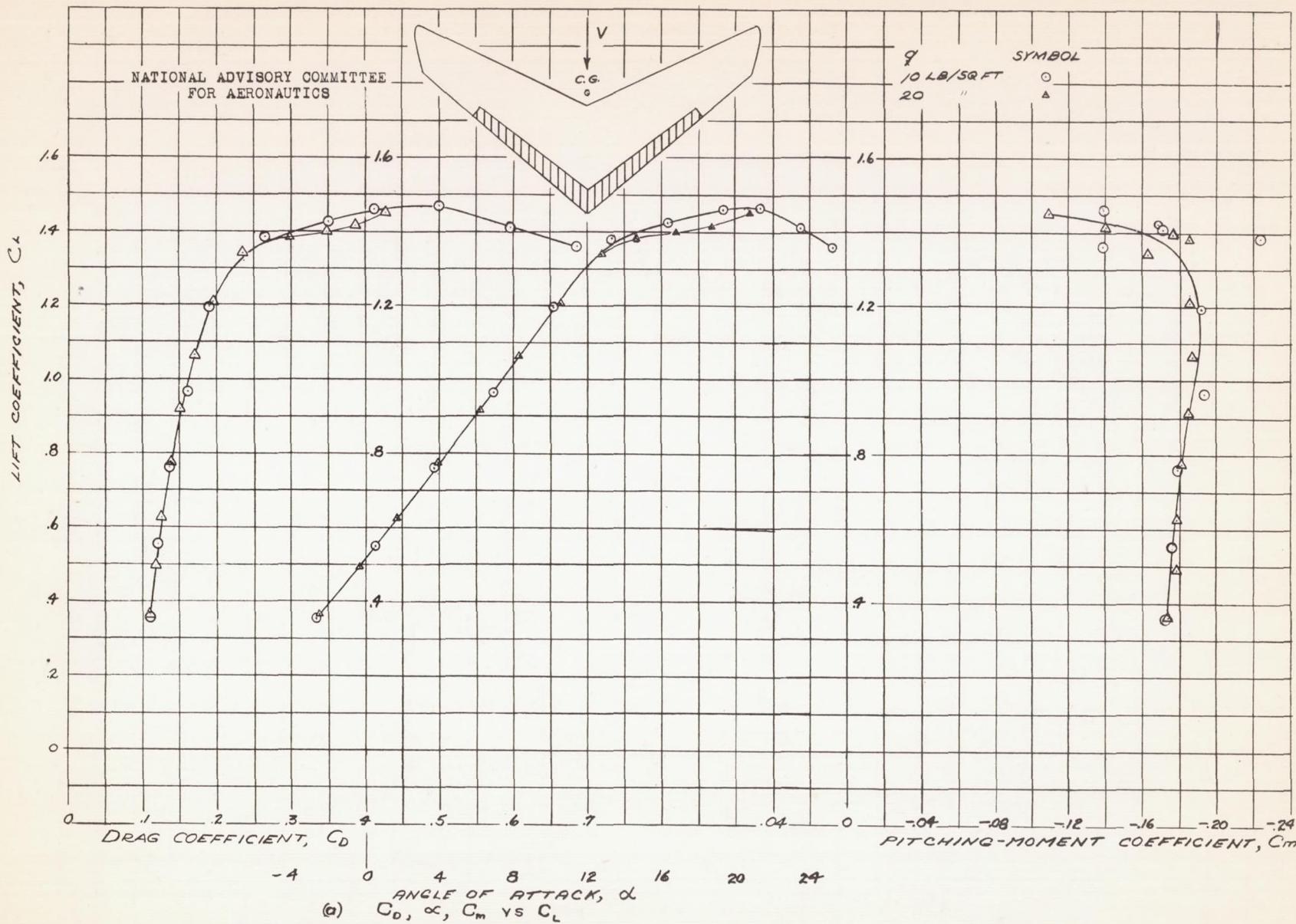


FIGURE 37.- AERODYNAMIC CHARACTERISTICS OF THE 30° SWEEPTFORWARD WING AT -0.2° SIDESLIP.
20% CHORD, 62.3% SPAN SPLIT FLAPS DEFLECTED 60°.

Fig. 37b

NACA RM No. A6K15

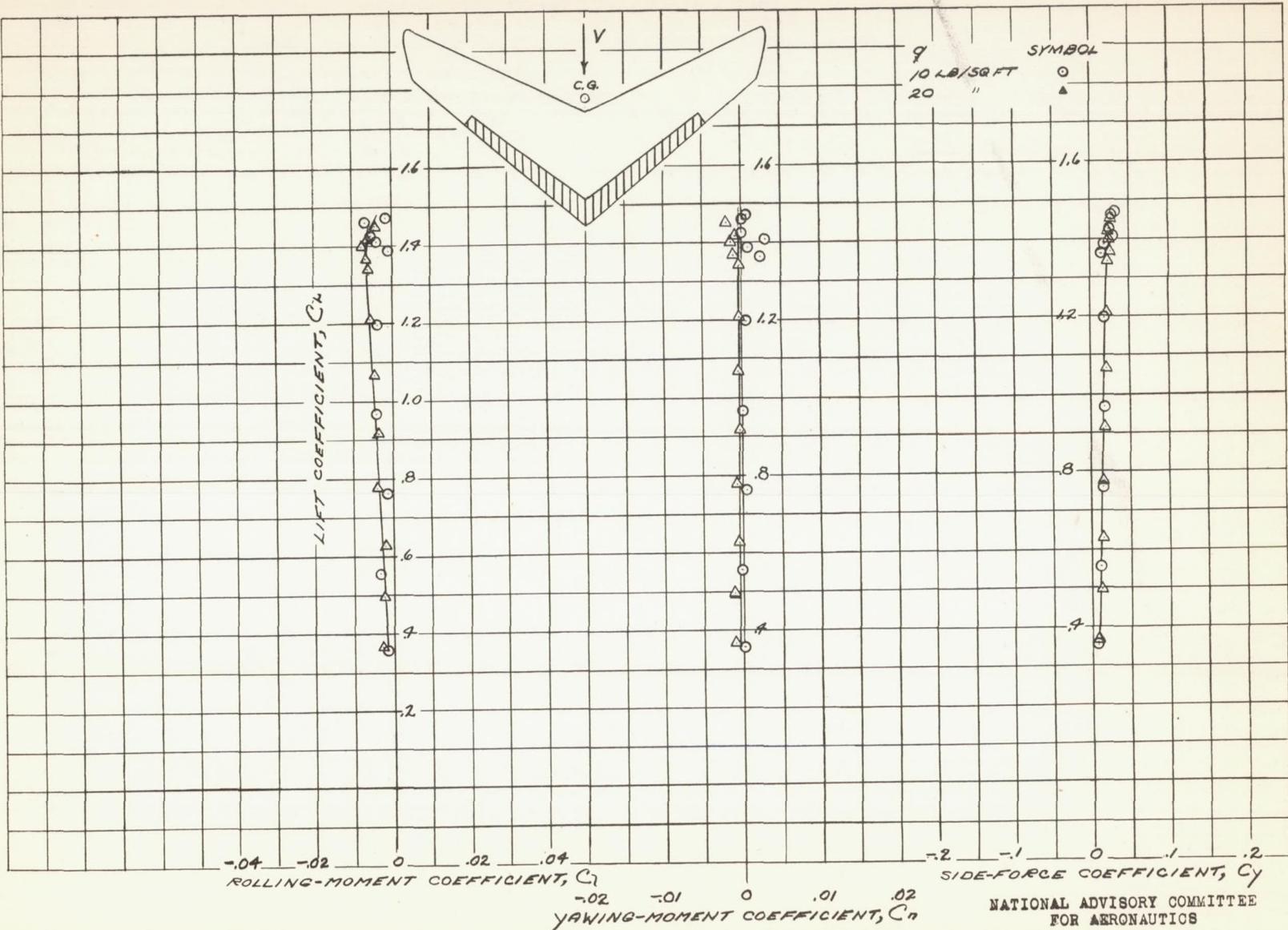
(b) C_r , C_n , C_y vs C_L

FIGURE 37.- CONCLUDED.

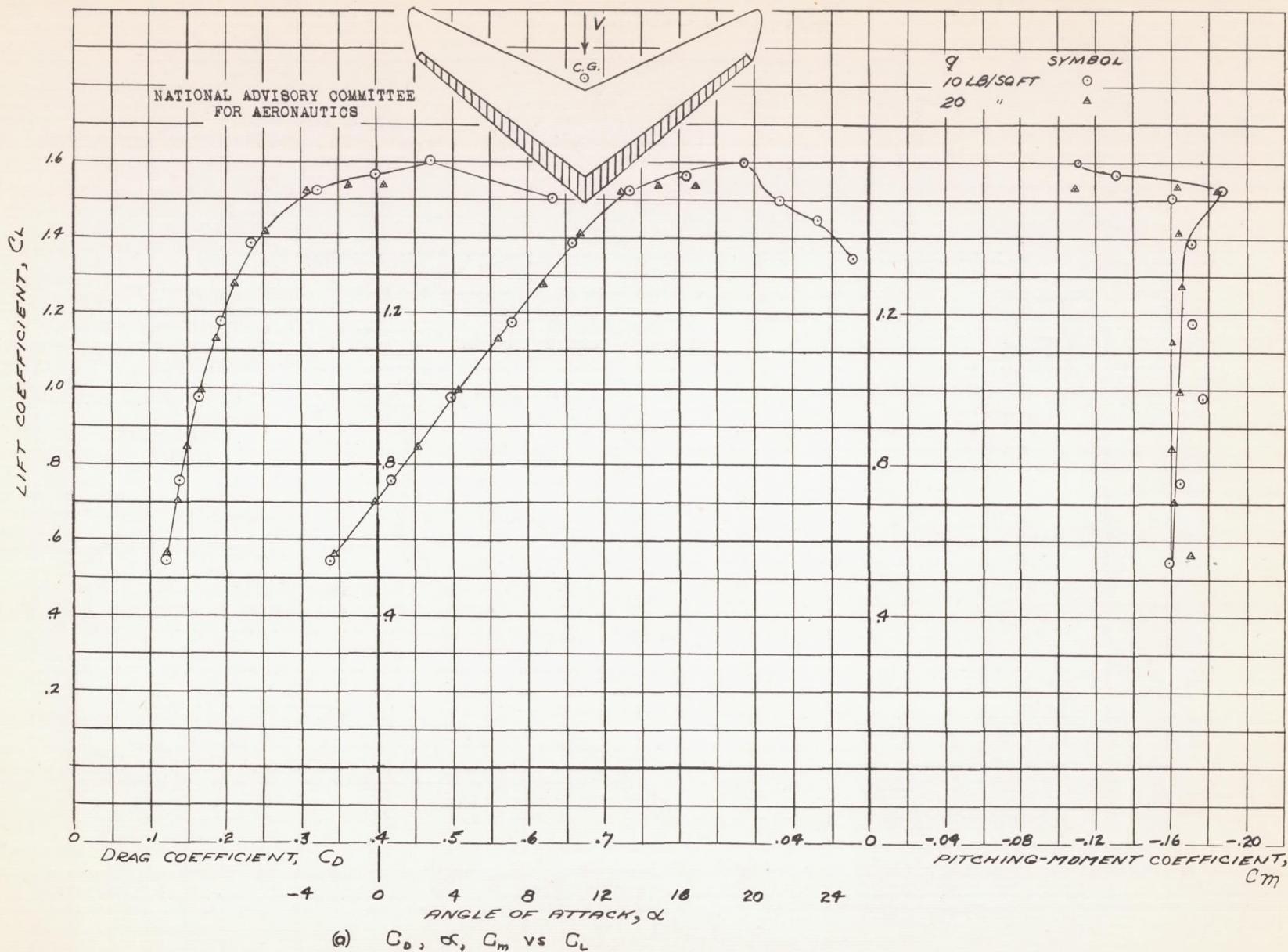


FIGURE 38.-AERODYNAMIC CHARACTERISTICS OF THE 30° SWEPT-FORWARD WING AT -0.2° SIDESLIP
20% CHORD, FULL SPAN SPLIT FLAPS DEFLECTED 60° .

Fig. 38b

NACA RM No. A6K15

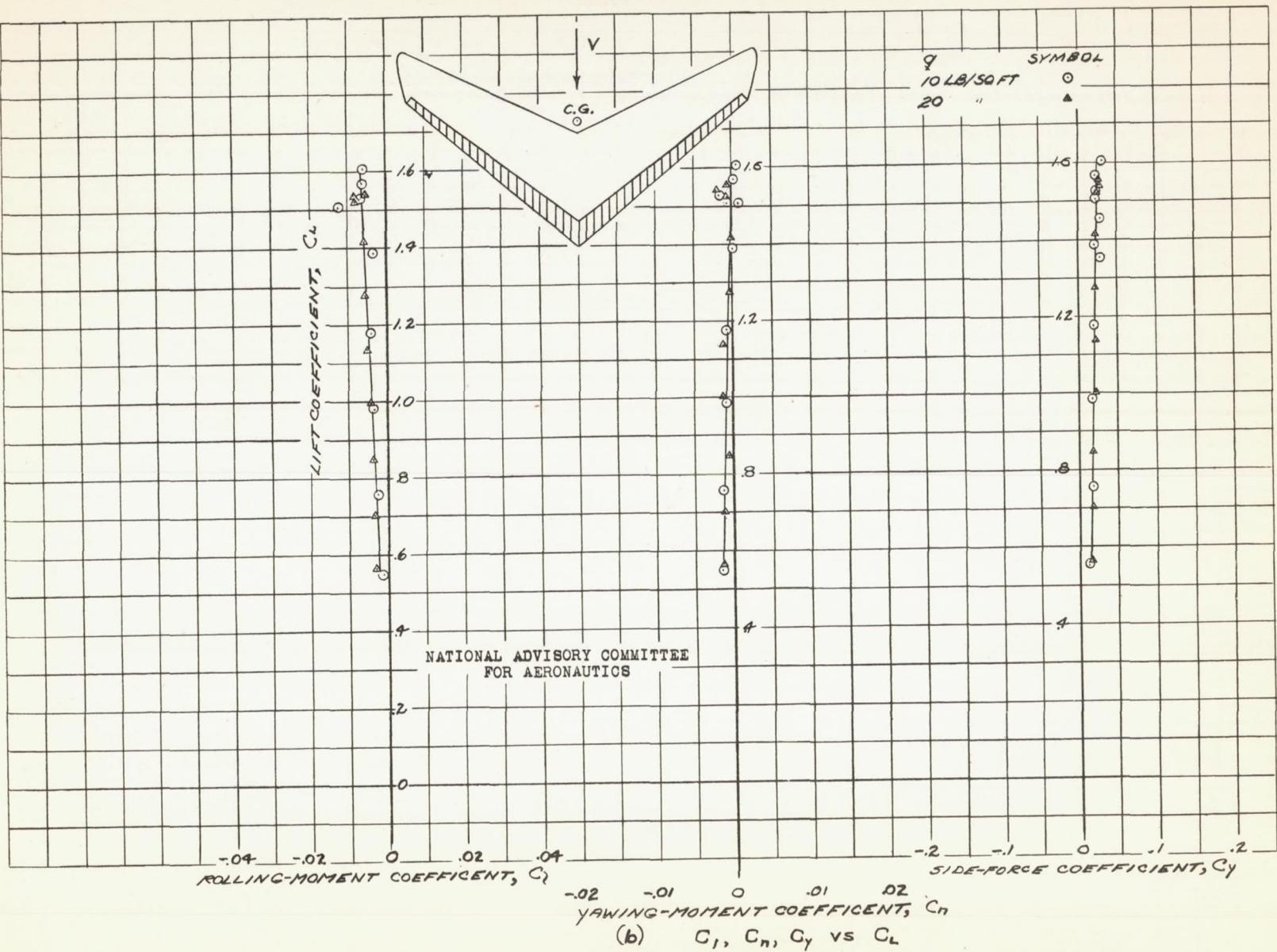


FIGURE 38.- CONCLUDED.

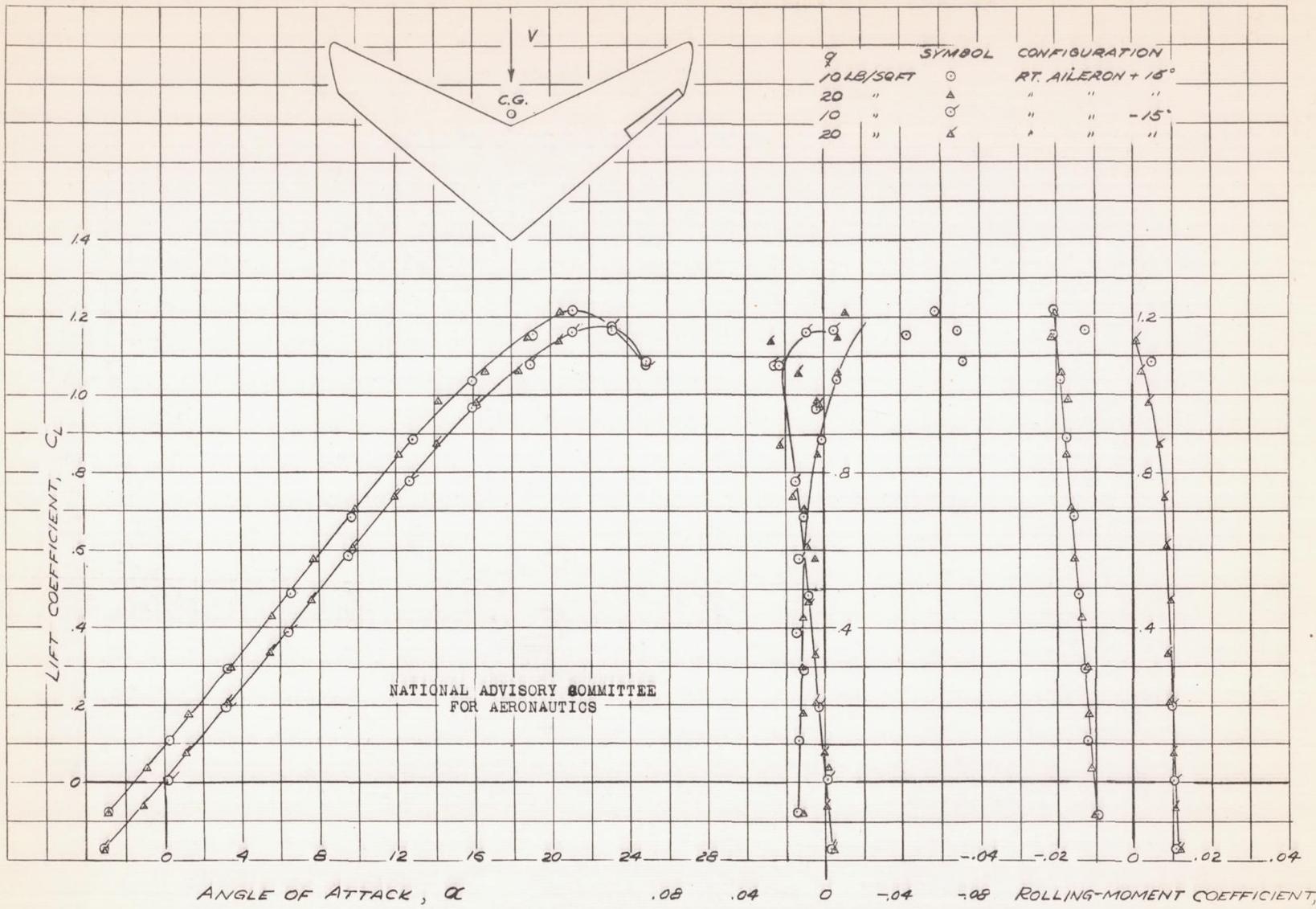


FIGURE 39.—AERODYNAMIC CHARACTERISTICS OF THE 30° SWEEPTFORWARD WING AT -0.2° SIDESLIP.
20% CHORD, 31.3% SPAN SPLIT FLAP TYPE
AILERON ON RIGHT WING DEFLECTED ±15°.

Fig. 40a

NACA RM No. A6K15

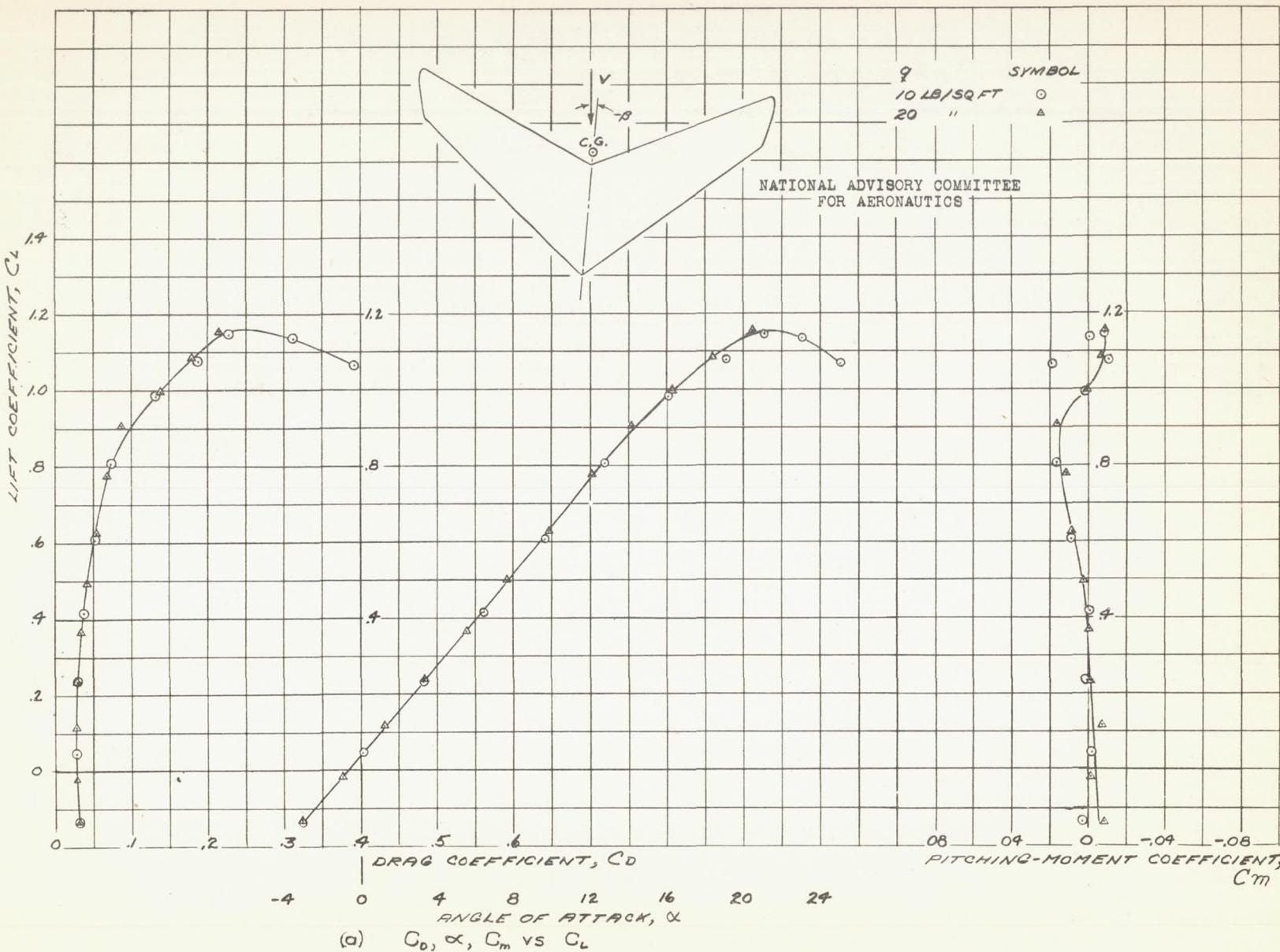


FIGURE 40.-AERODYNAMIC CHARACTERISTICS OF THE 30° SWEEPTFORWARD WING AT -5.3° SIDESLIP.
PLAIN WING.

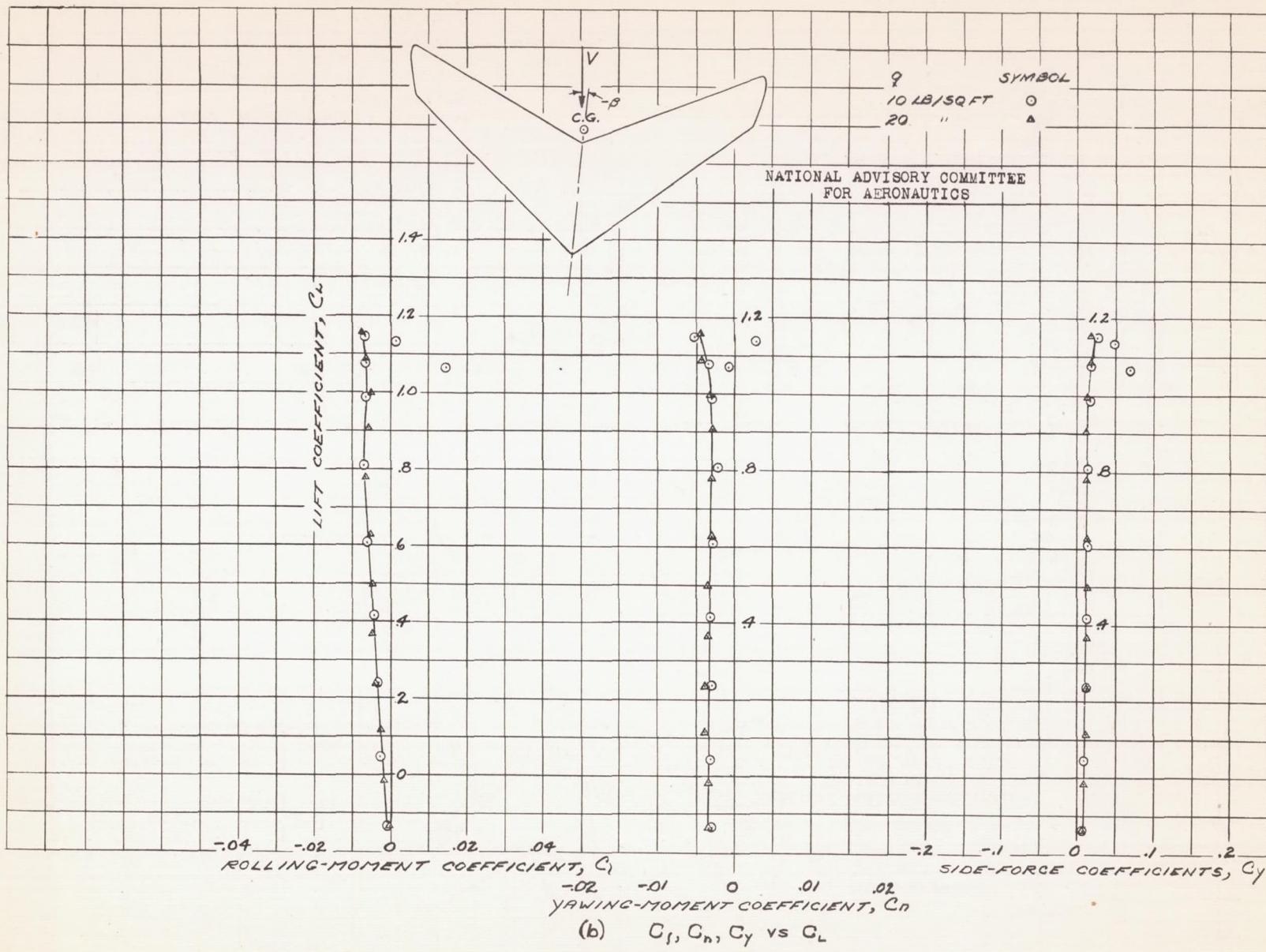
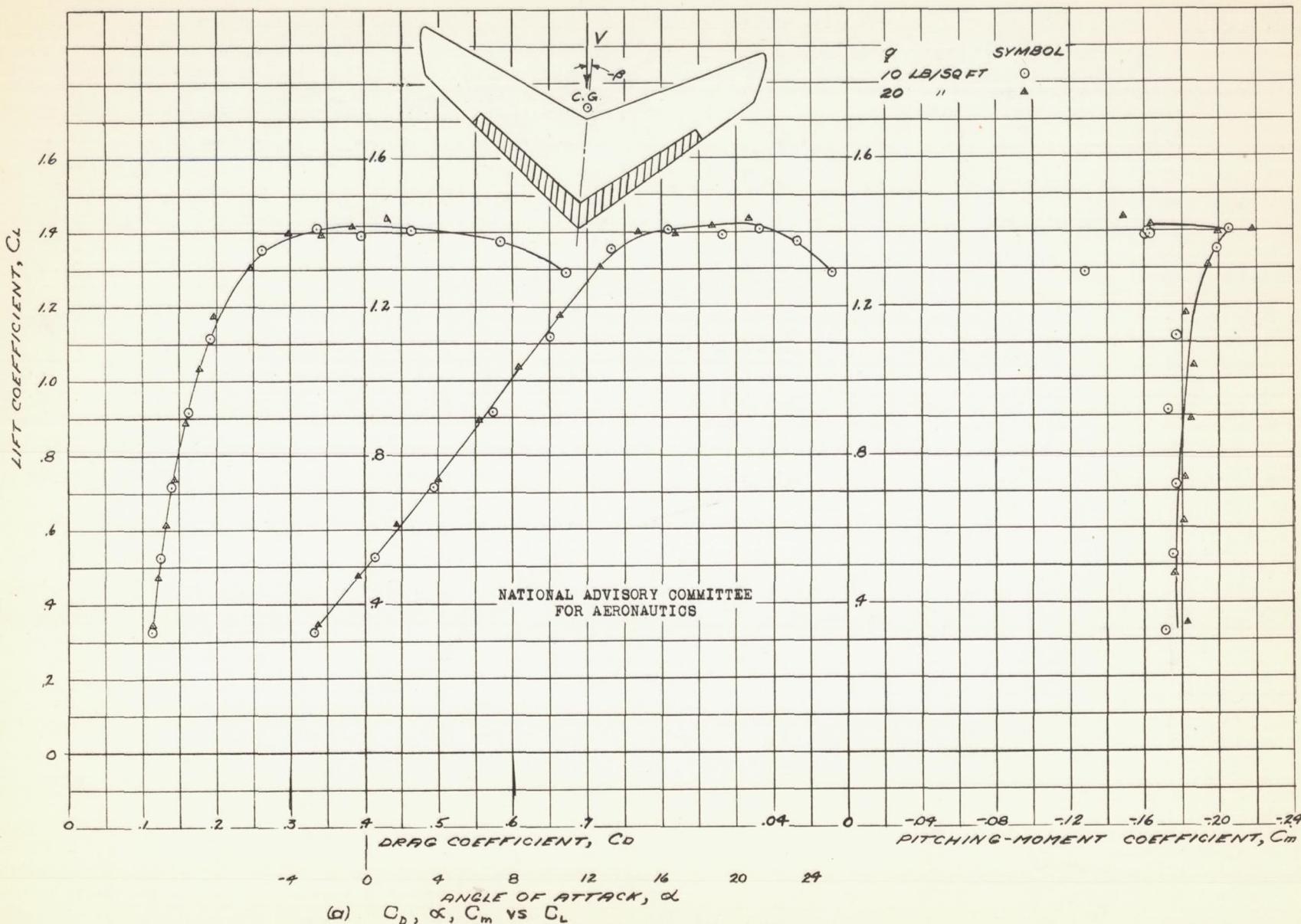


FIGURE 40.- CONCLUDED.

Fig. 41a

NACA RM No. A6K15



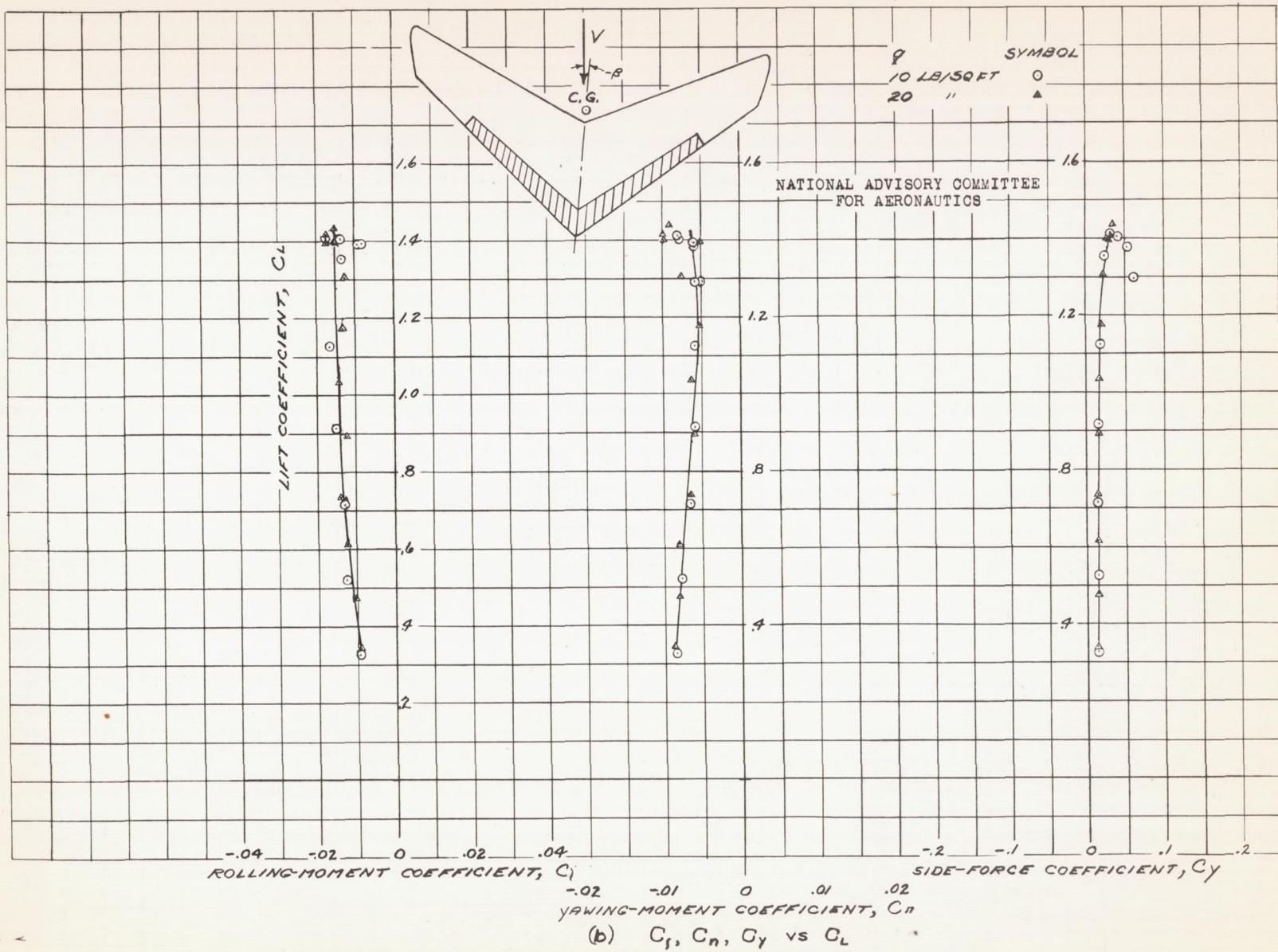


FIGURE 41.- CONCLUDED.

Fig. 42a

NACA RM No. A6K15

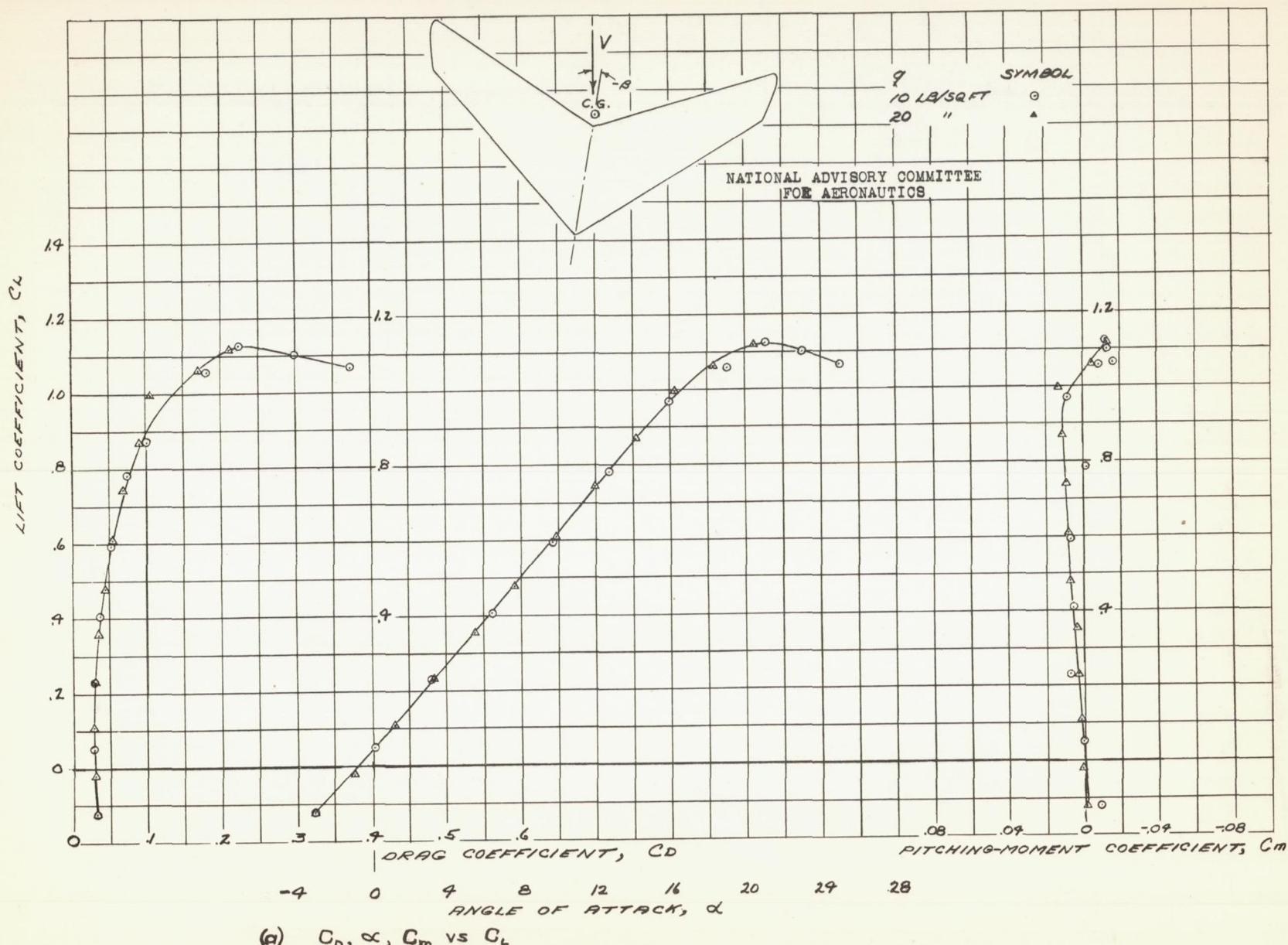


FIGURE 42.- AERODYNAMIC CHARACTERISTICS OF THE 30° SWEEPTFORWARD WING AT -103° SIDESLIP.
PLAIN WING.

Fig. 42b

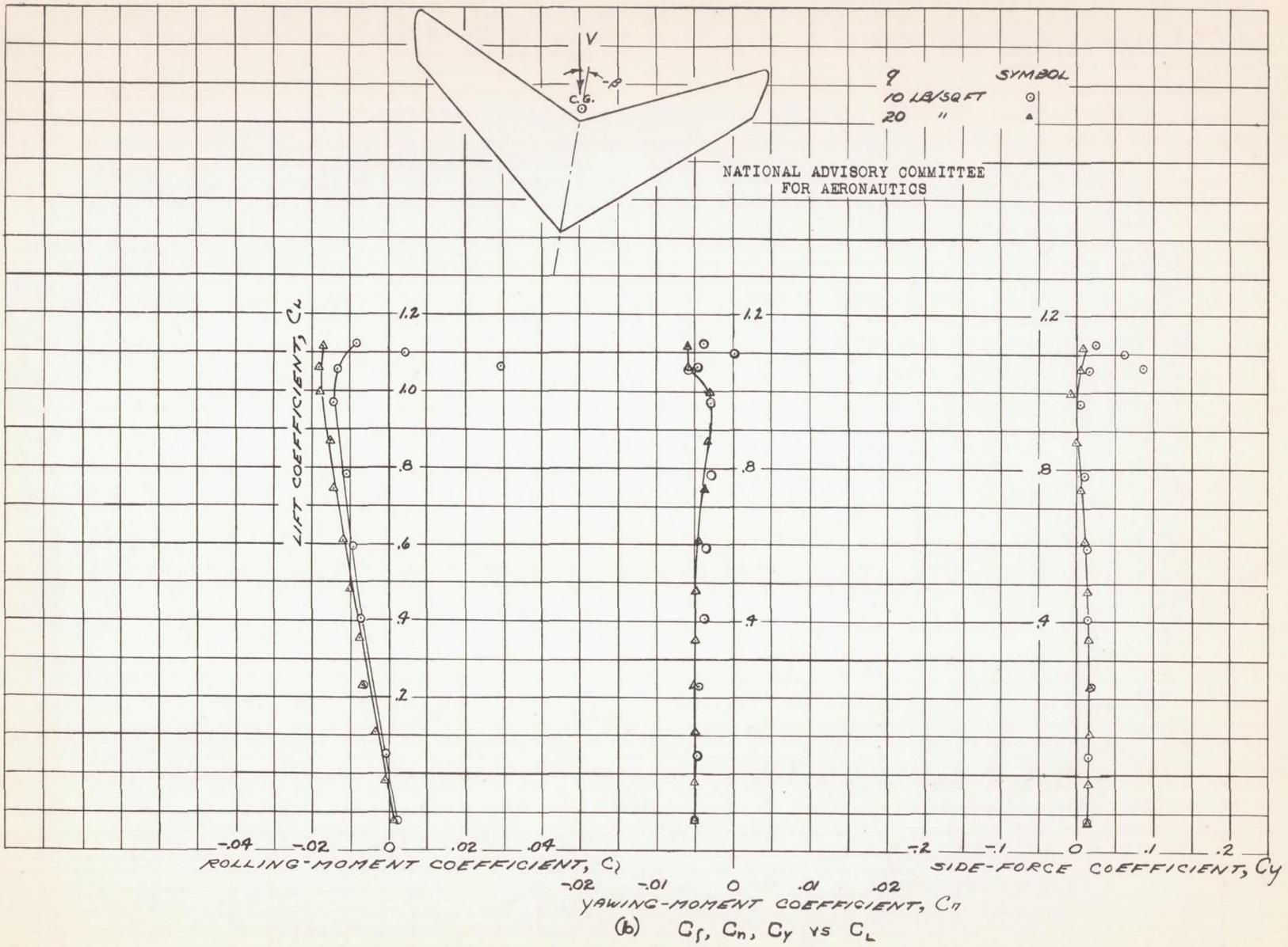


FIGURE 42.-CONCLUDED.

Fig. 43a

NACA RM No. A6K15

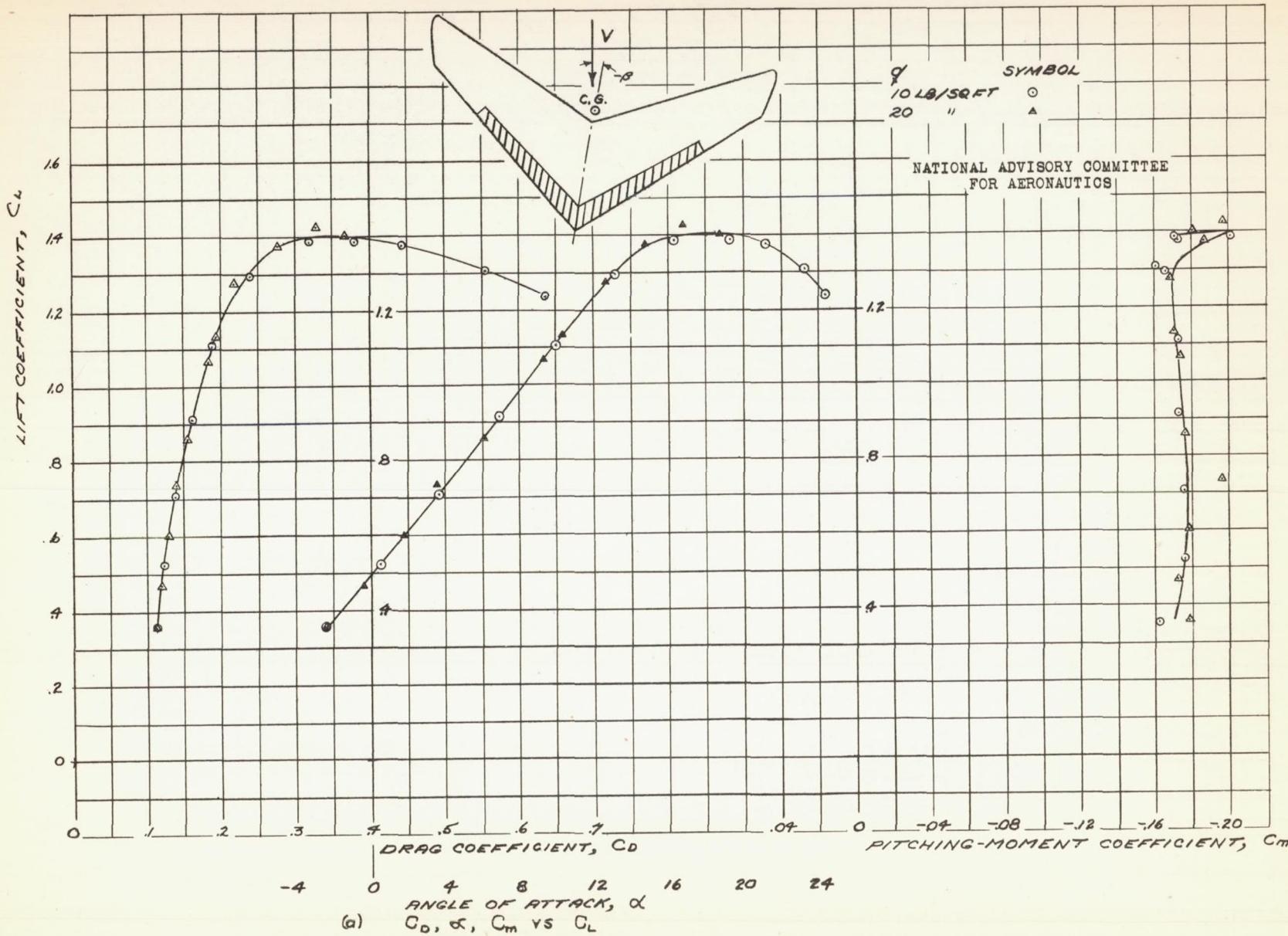


FIGURE 43.—AERODYNAMIC CHARACTERISTICS OF THE 30° SWEEP FORWARD WING AT -10.3° SIDESLIP
20% CHORD, 62.3% SPAN SPLIT FLAPS DEFLECTED 60°

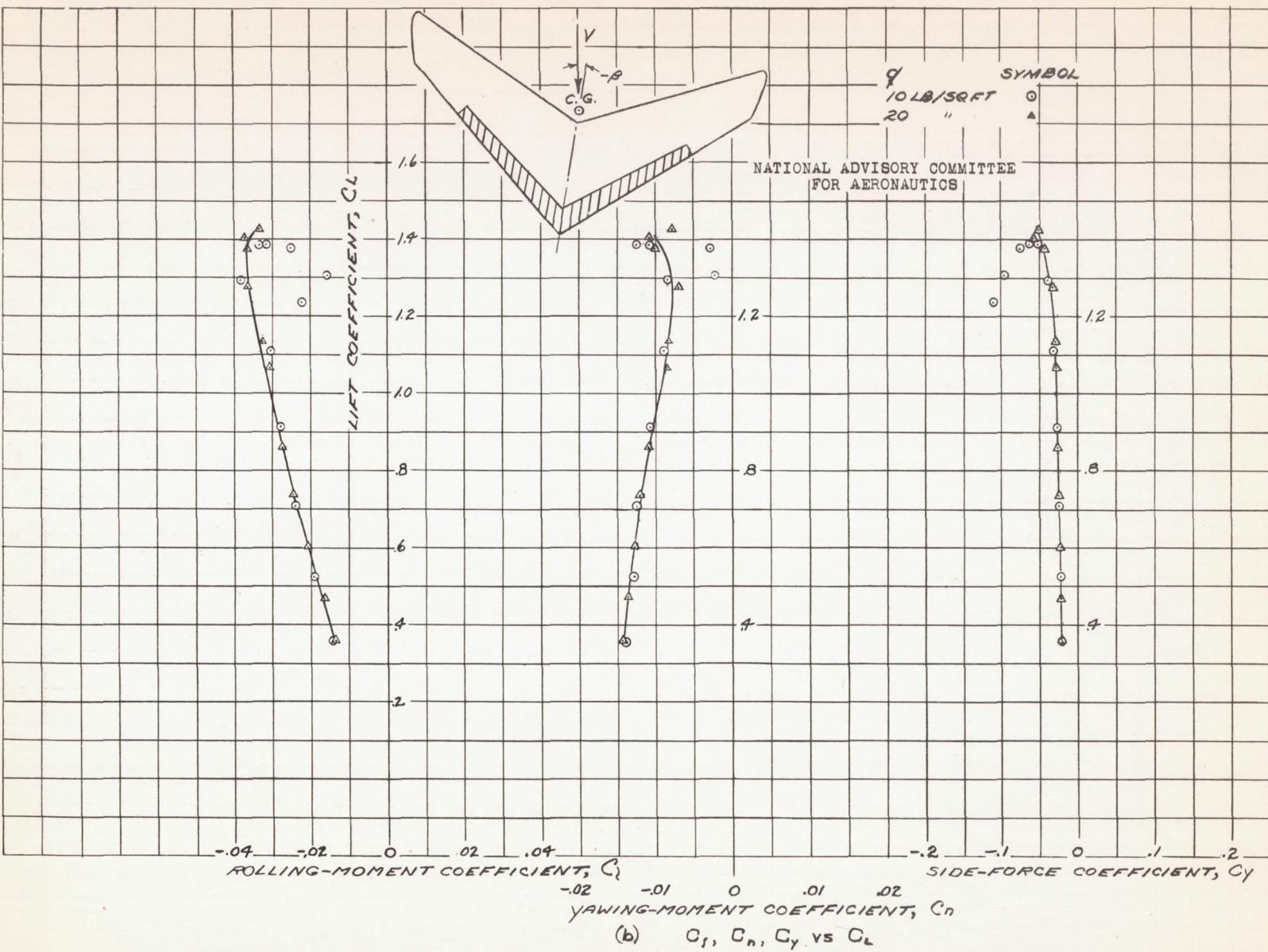


FIGURE 43.— CONCLUDED.

Fig. 44a

NACA RM No. A6K15

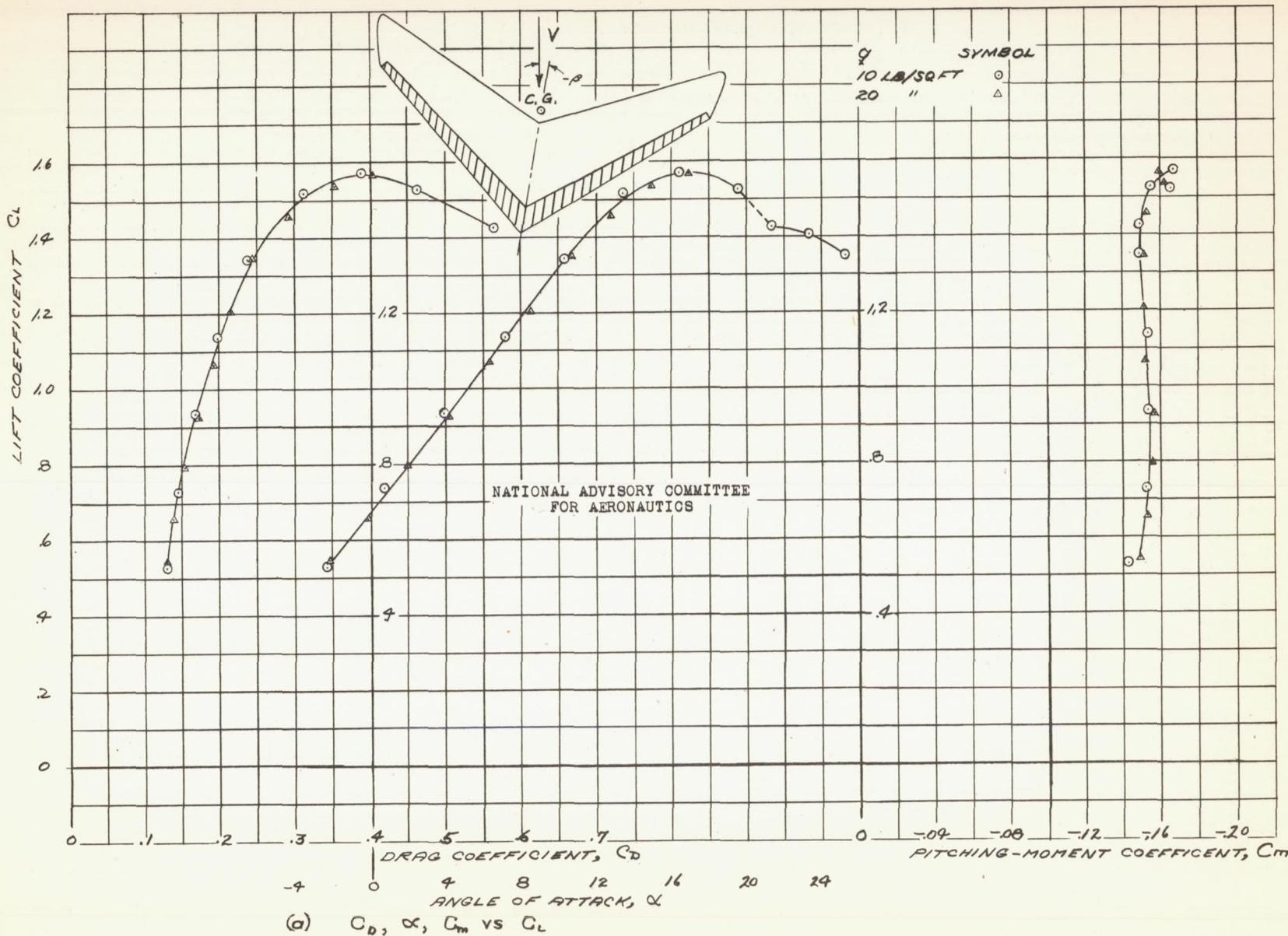


FIGURE 44.—AERODYNAMIC CHARACTERISTICS OF THE 30° SWEEP FORWARD WING AT -10.3° SIDESLIP
20% CHORD FULL SPAN SPLIT FLAPS DEFLECTED 60°

NACA RM No. A6K15

Fig. 44b

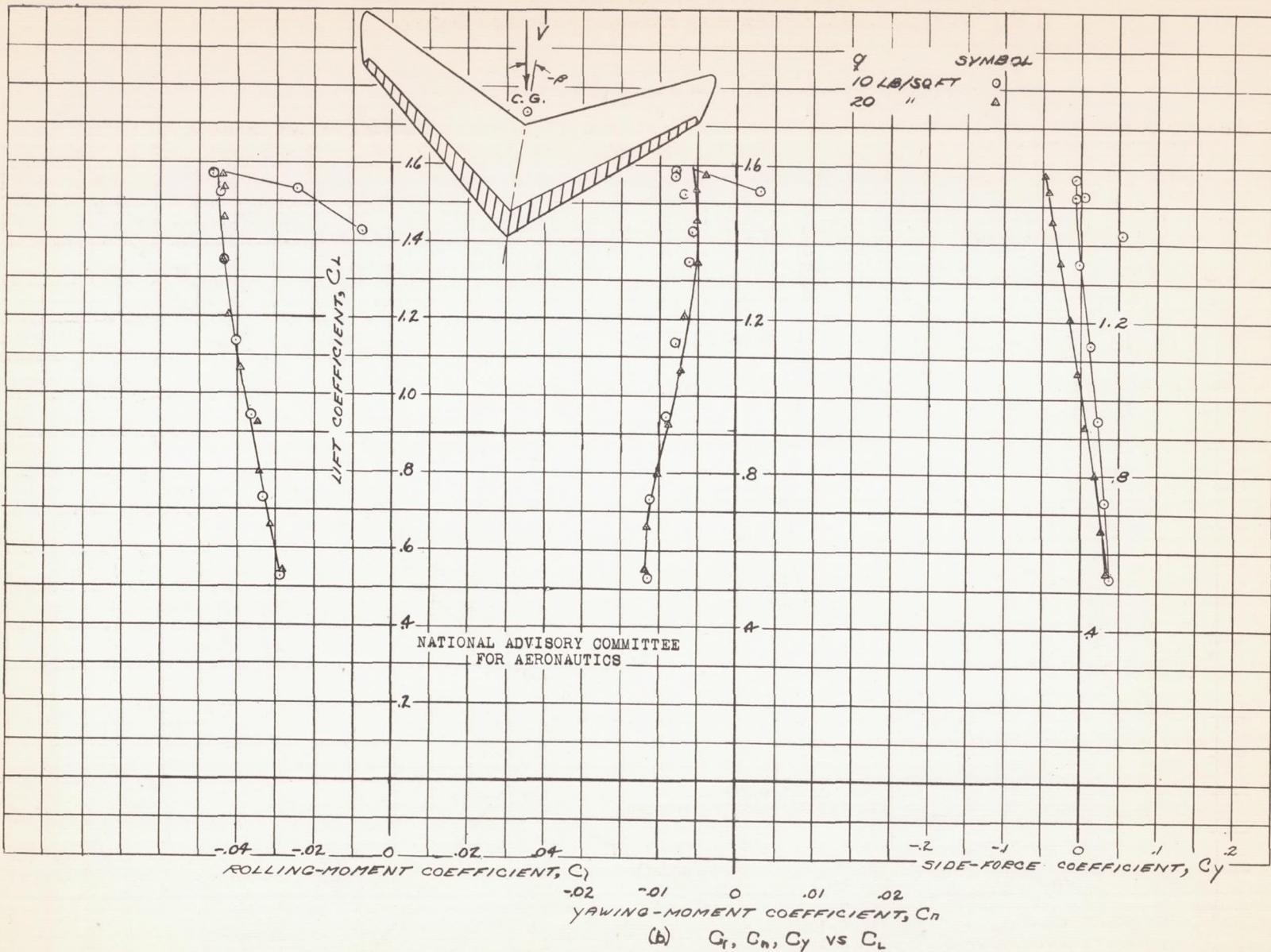


FIGURE 44.- CONCLUDED.

Fig. 45

NACA RM No. A6K15

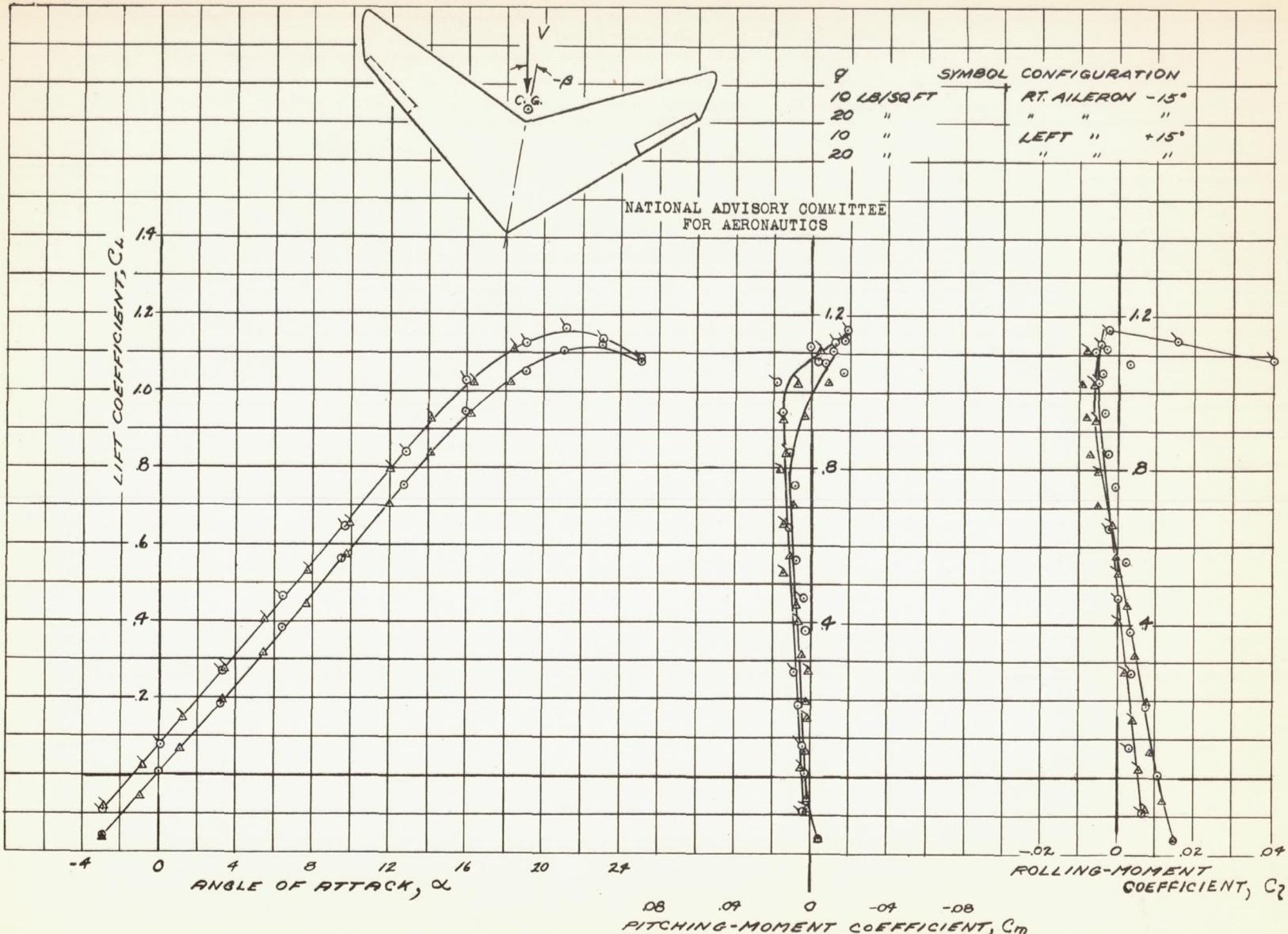


FIGURE 45.—AERODYNAMIC CHARACTERISTICS OF THE 30° SWEEP FORWARD WING AT -10.3° SIDESLIP.
20% CHORD, 31% SPAN SPLIT FLAP TYPE AILERONS
DEFLECTED $\pm 15^\circ$.

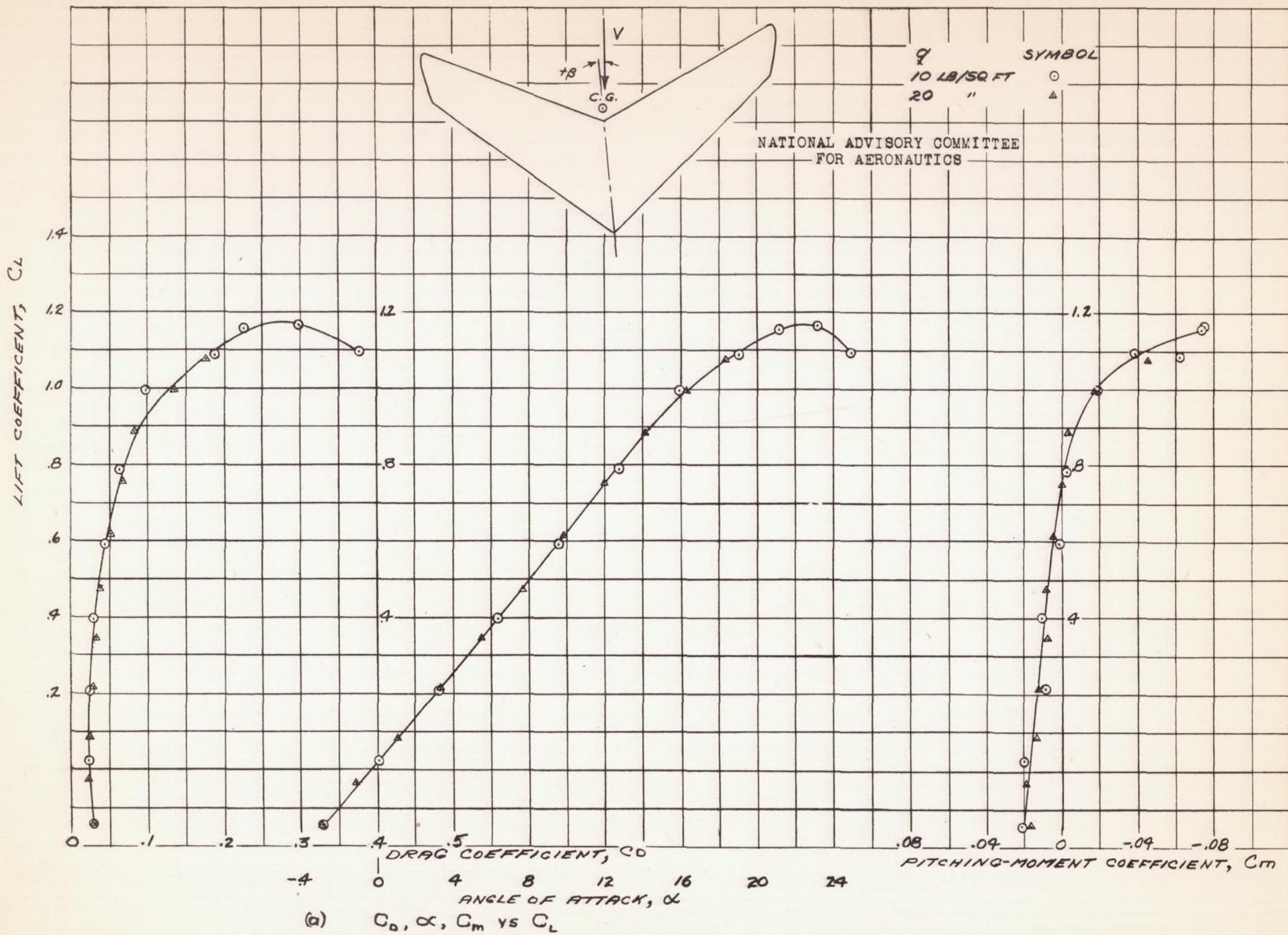


FIGURE 46.—AERODYNAMIC CHARACTERISTICS OF THE 30° SWEEP-FORWARD WING AT +50° SIDESLIP.
PLAIN WING.

Fig. 46b

NACA RM No. A6K15

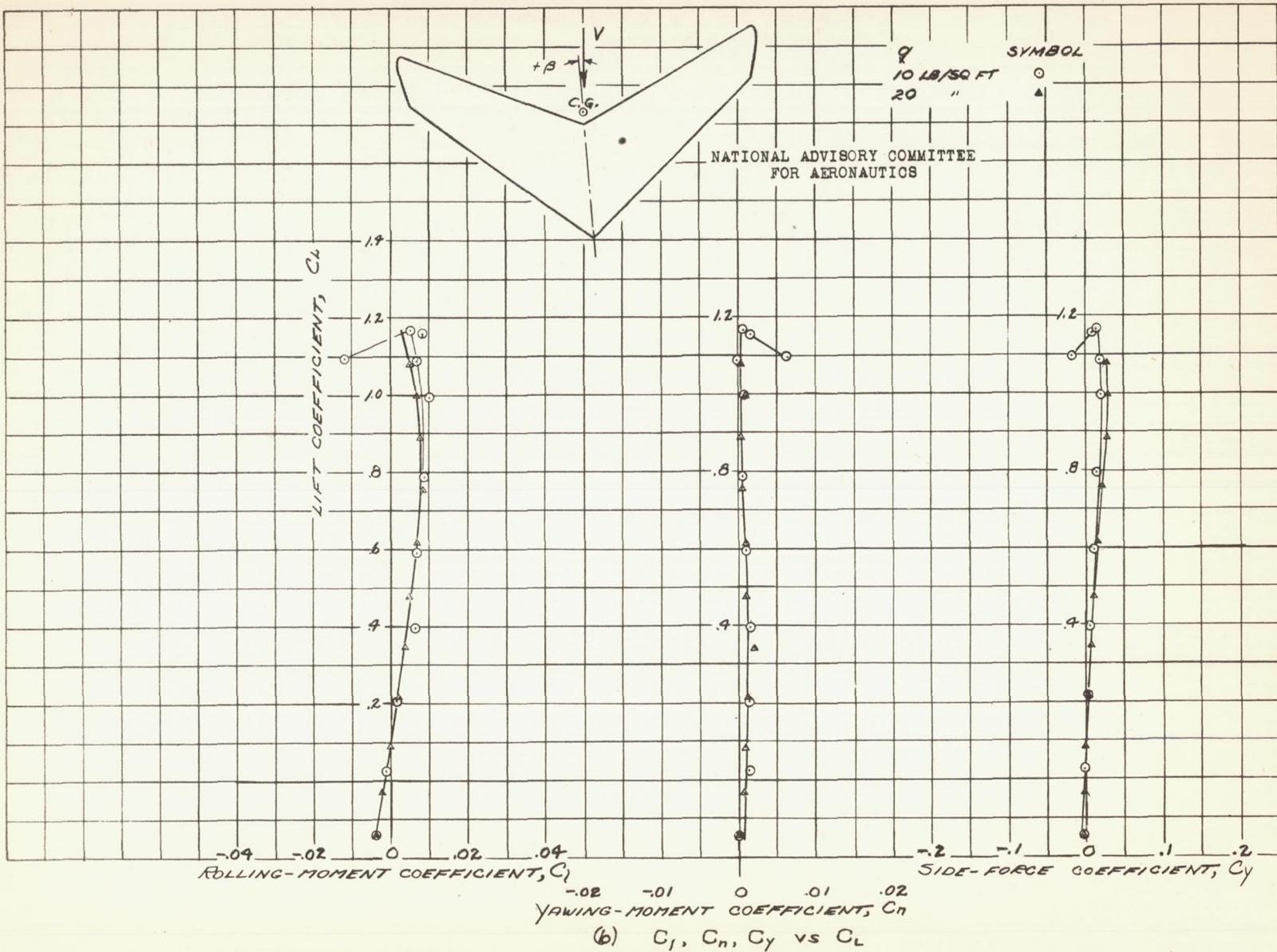


FIGURE 46.- CONCLUDED.

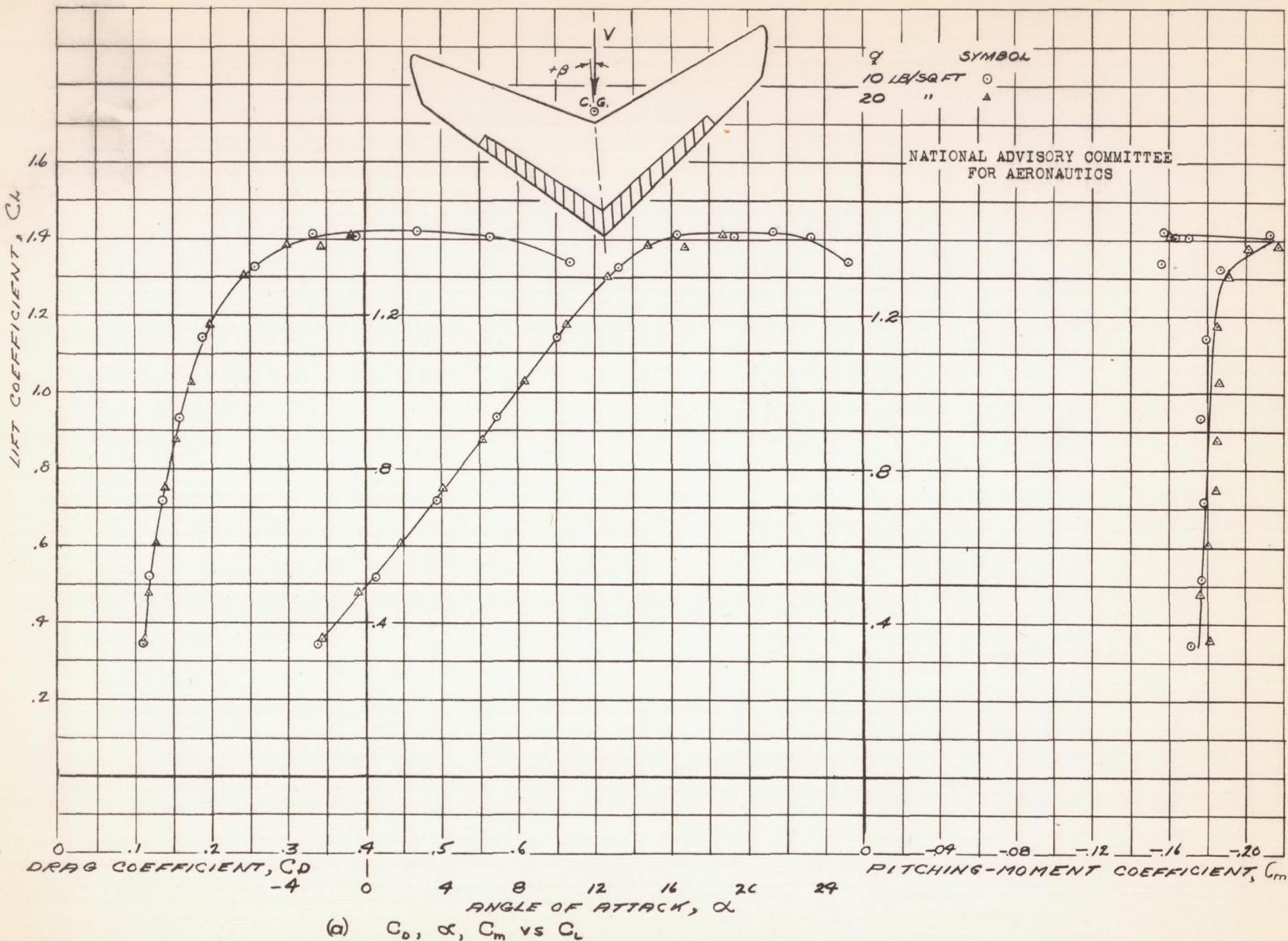


FIGURE 47.- AERODYNAMIC CHARACTERISTICS OF THE 30° SWEEP-FORWARD WING AT +5.0° SIDESLIP.
20% CHORD, 62.3% SPAN SPLIT FLAPS
DEFLECTED 60.°

Fig. 47b

NACA RM No. A6K15

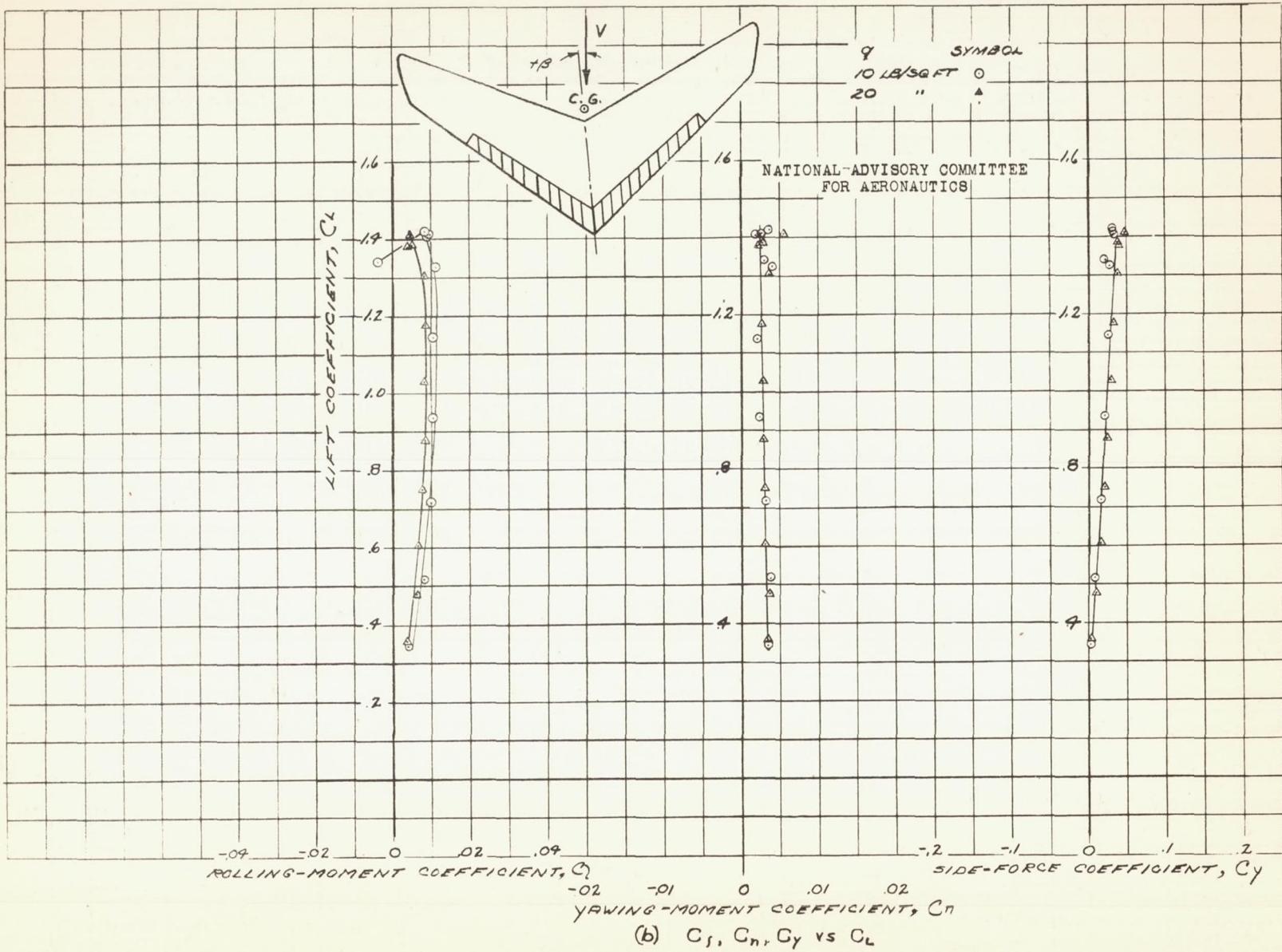


FIGURE 47.— CONCLUDED.

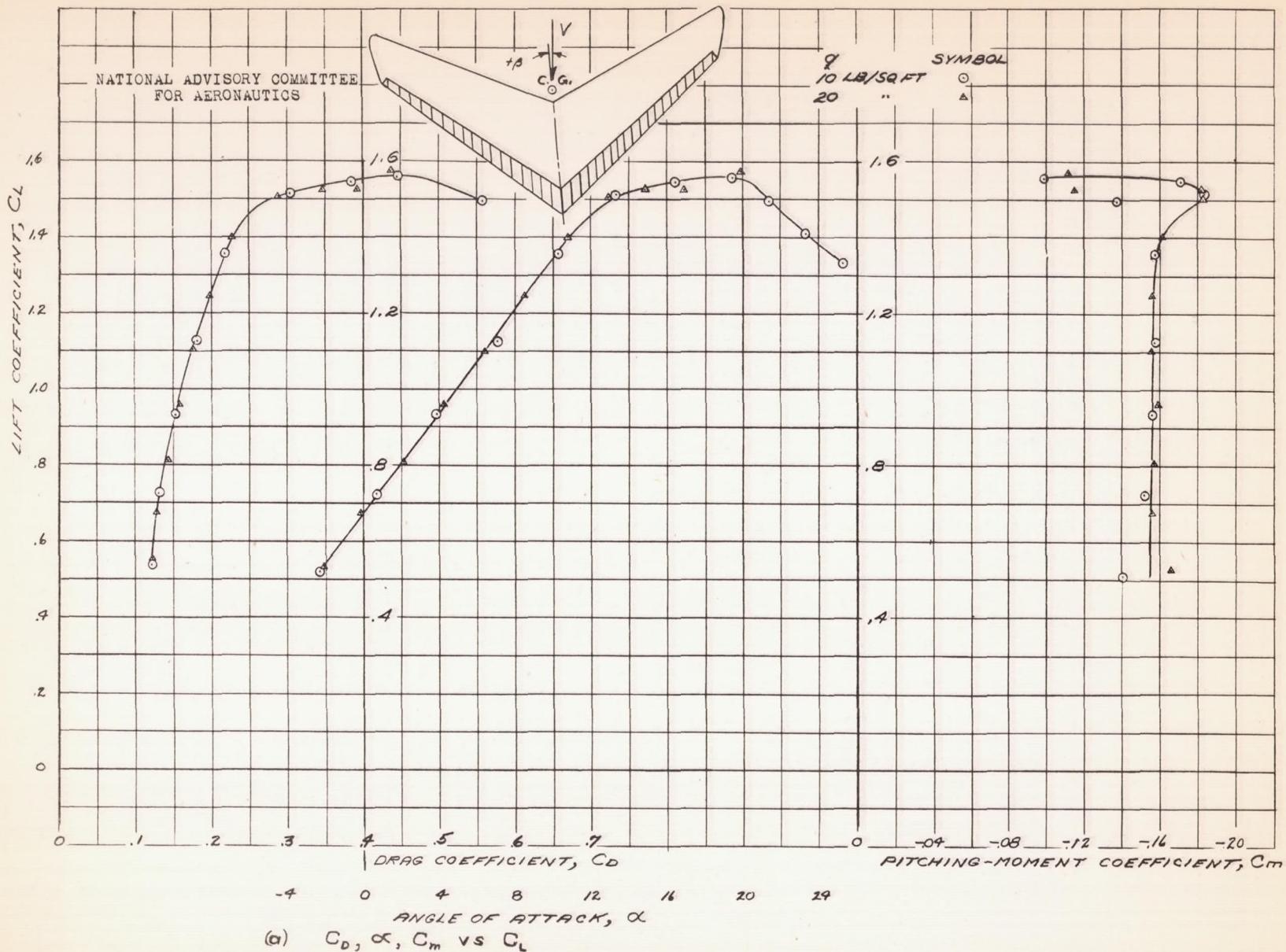


FIGURE 48.-AEROdynamic CHARACTERISTICS OF THE 30° SWEEP FORWARD WING AT +50° SIDESLIP.
20% CHORD FULL SPAN SPLIT FLAPS DEFLECTED 60°.

Fig. 48b

NACA RM No. A6K15

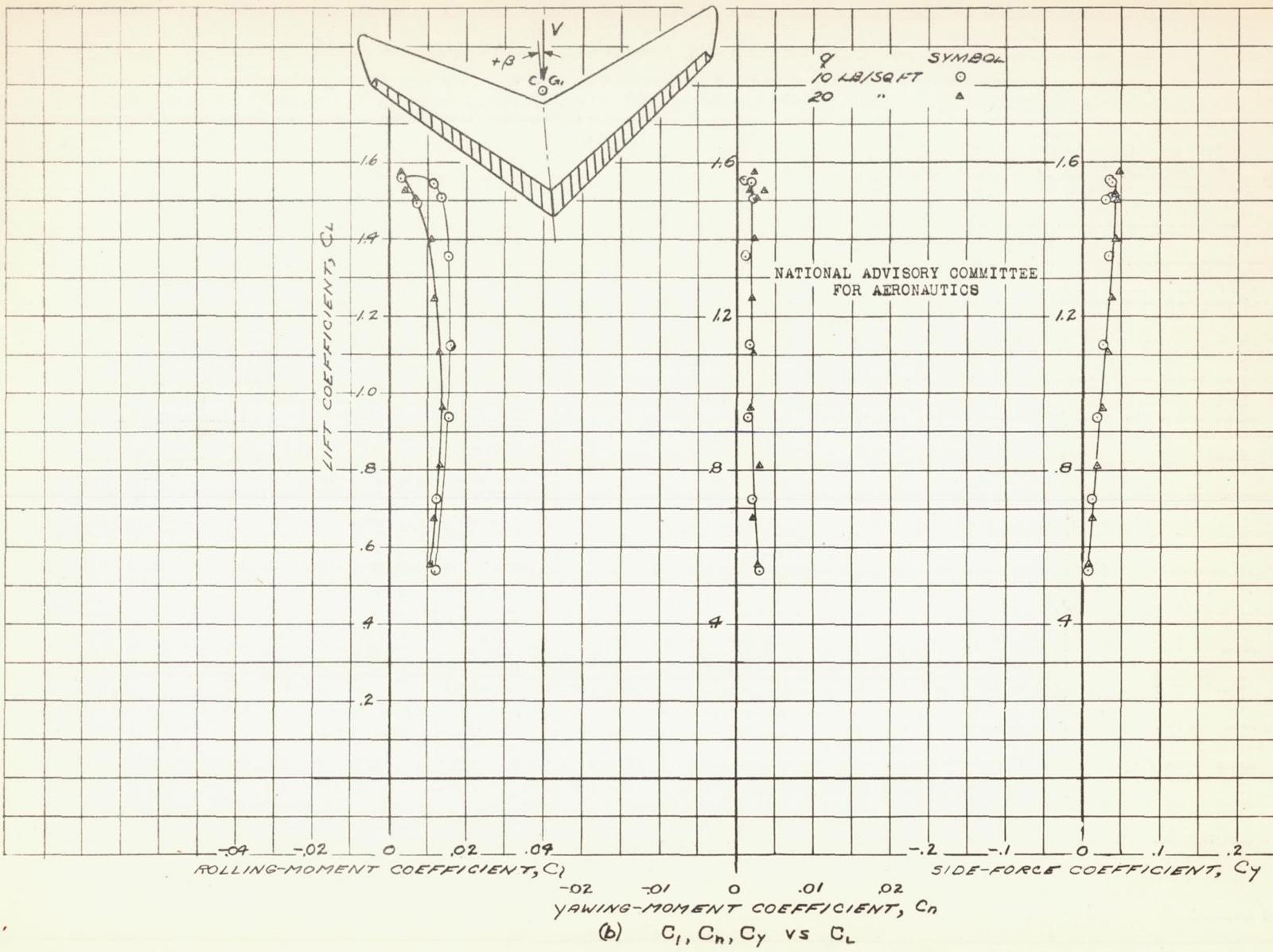


FIGURE 48.- CONCLUDED.

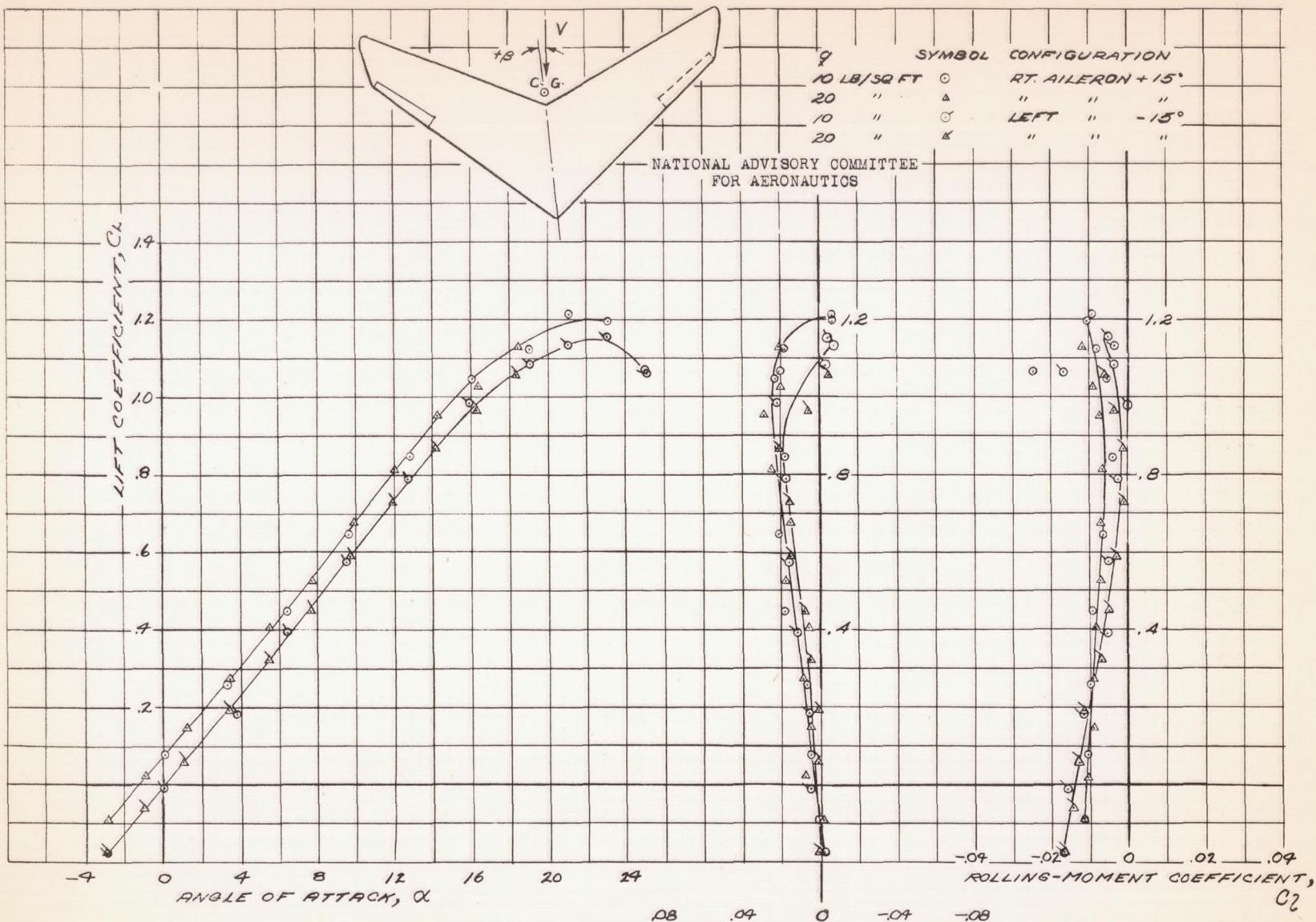


FIGURE 49.—AERODYNAMIC CHARACTERISTICS OF THE 30°
SWEPT-FORWARD WING AT +5.0° SIDESLIP. 20% CHORD
31.3% SPAN SPLIT FLAP TYPE AILERONS DEFLECTED $\pm 15^\circ$.

Fig. 50a

NACA RM No. A6K15

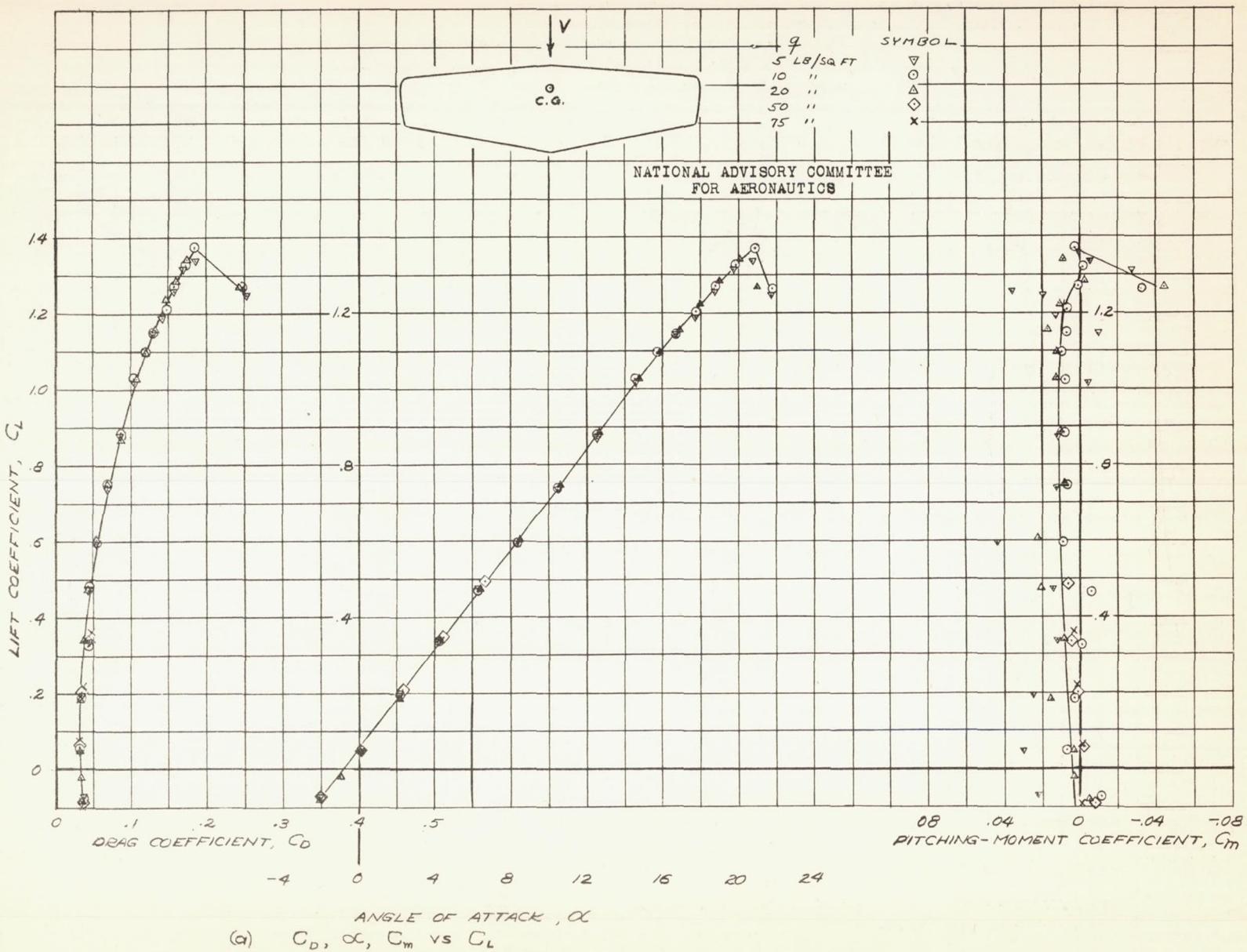
FIGURE 50.-AERODYNAMIC CHARACTERISTICS OF THE UNSWEPT WING AT -0.1° SIDESLIP. PLAIN WING.

Fig. 50b

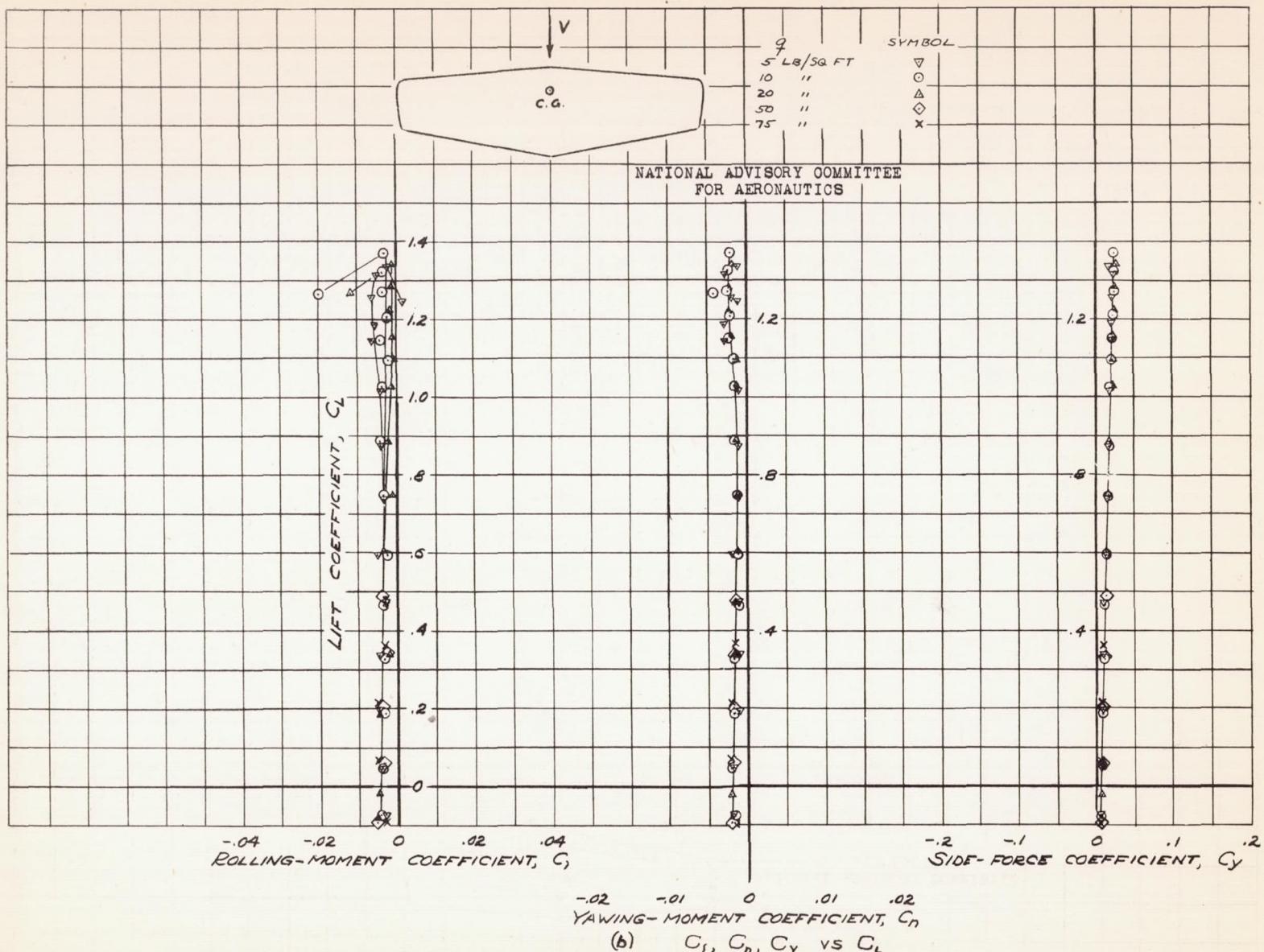


FIGURE 50.- CONCLUDED.

Fig. 51a

NACA RM No. A6K15

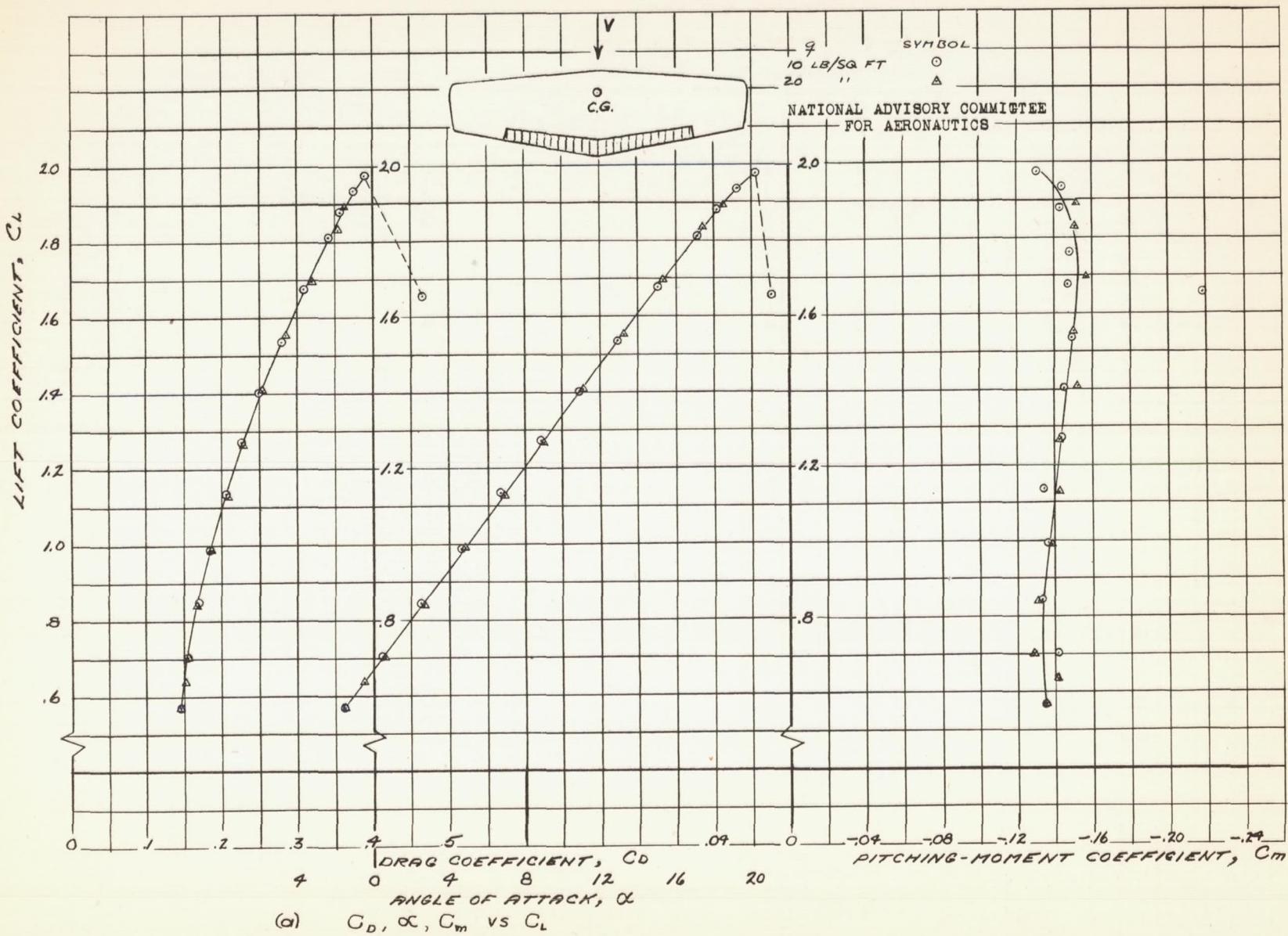


FIGURE 51.- AERODYNAMIC CHARACTERISTICS OF THE 0° SWEEP WING AT -0.1° SIDESLIP. 20% CHORD 62.3% SPAN SPLIT FLAPS DEFLECTED 60°

Fig. 51b

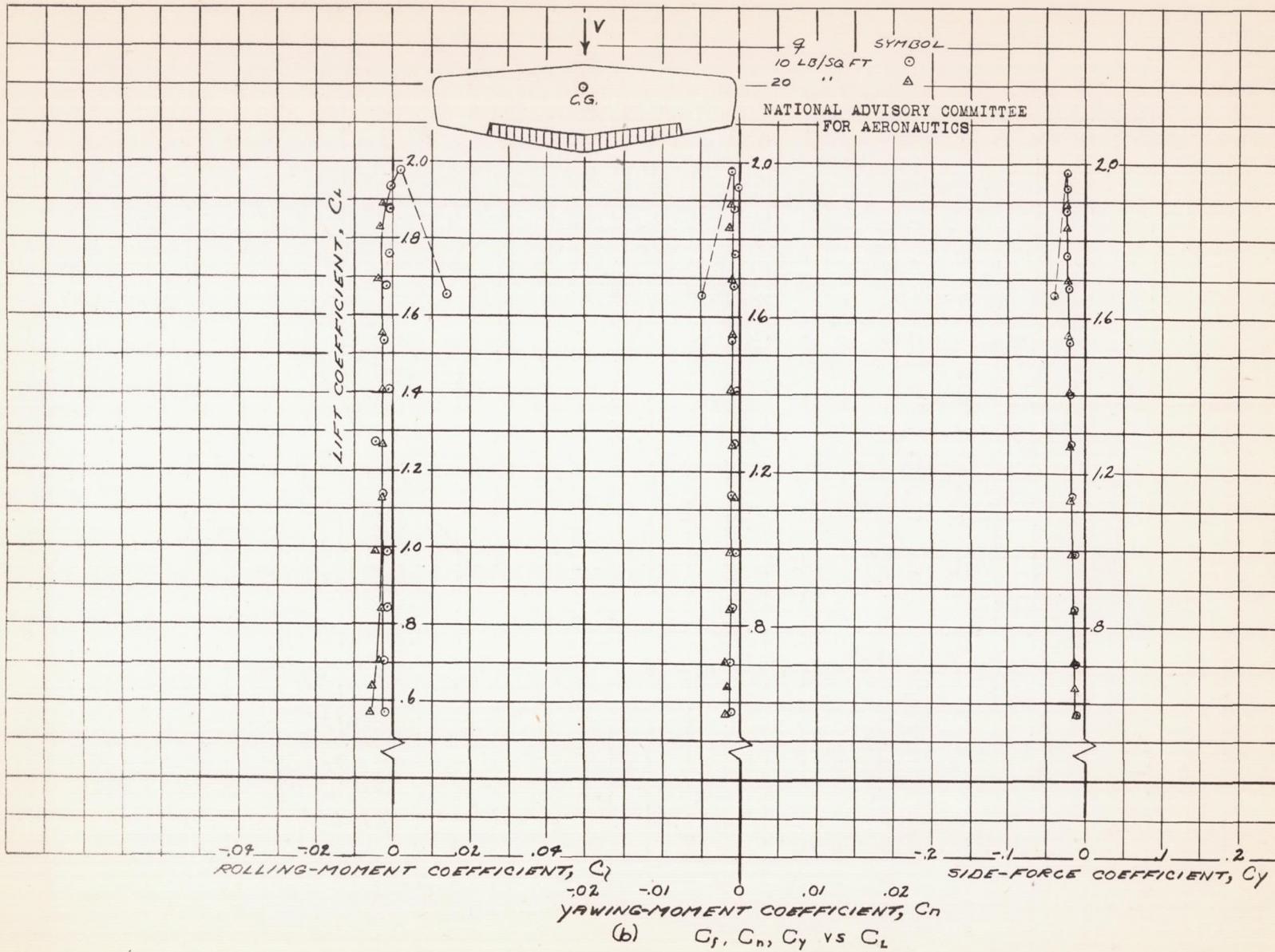
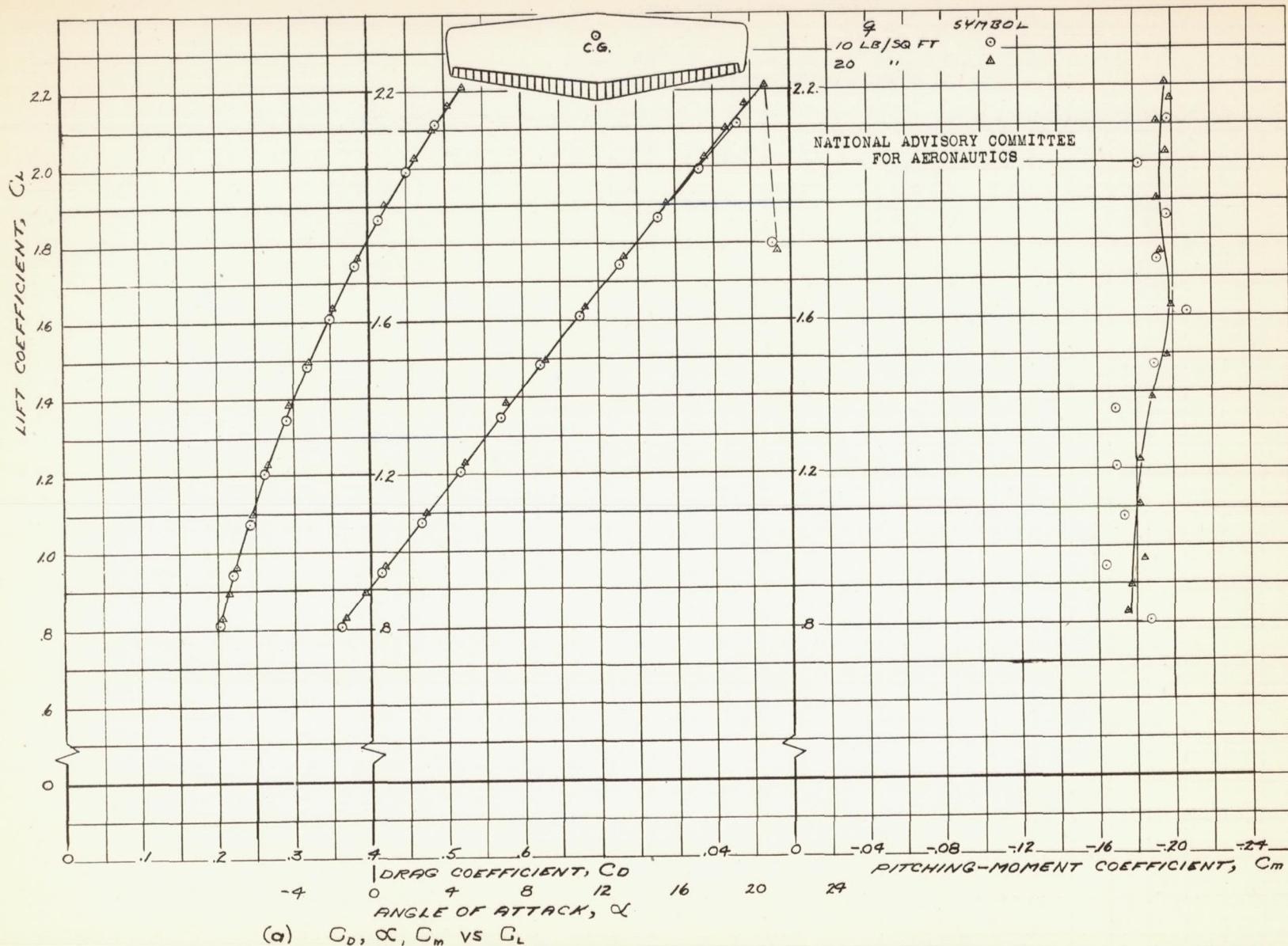


FIGURE 51.- CONCLUDED.

Fig. 52a



NACA RM No. A6K15

FIGURE 52.-AERODYNAMIC CHARACTERISTICS OF
THE 0° SWEEP WING AT -0.1° SIDESLIP, 20% CHORD
FULL SPAN SPLIT FLAPS DEFLECTED 60°.

Fig. 52b

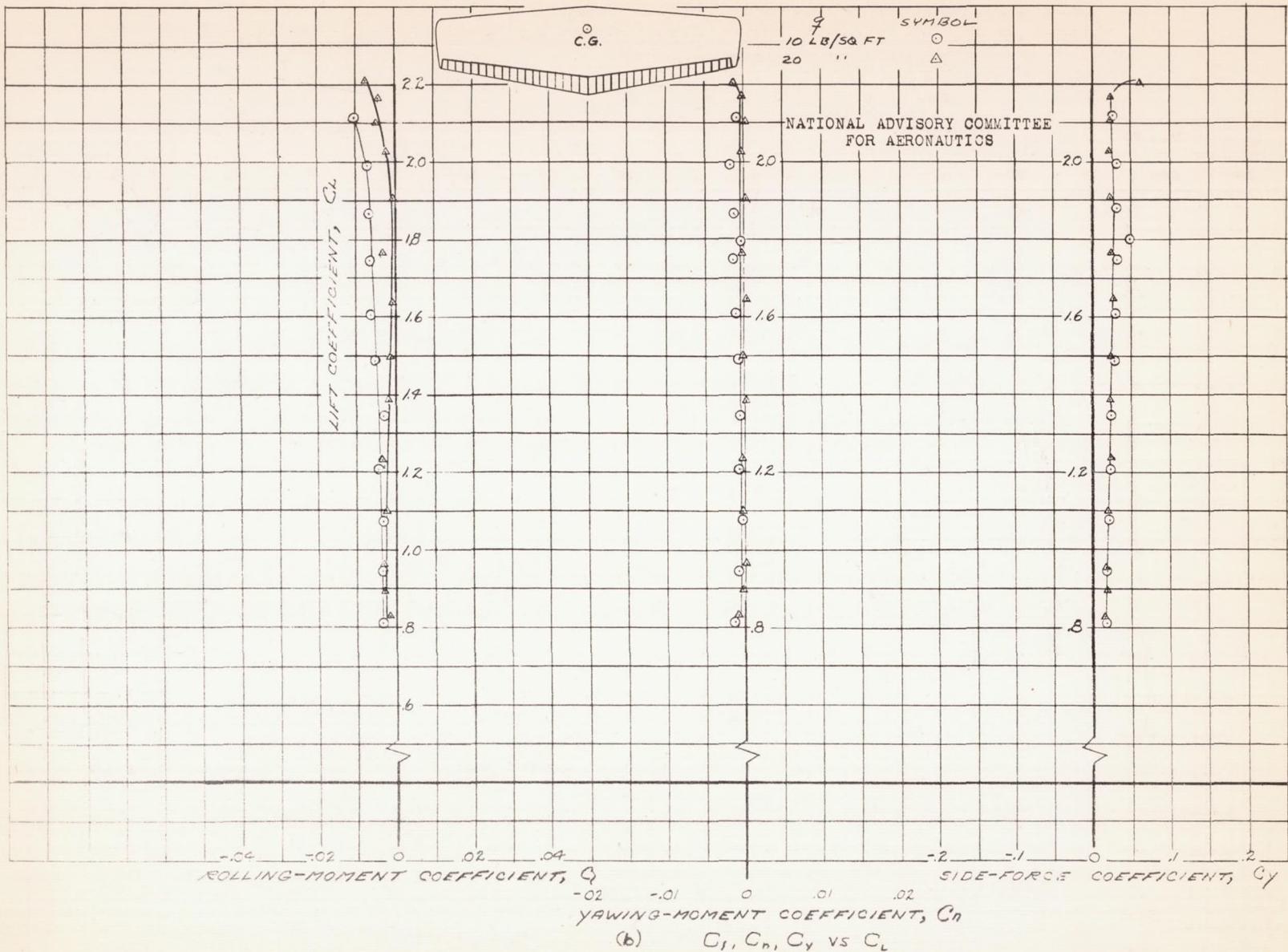


FIGURE 52.-CONCLUDED.

Fig. 53

NACA RM No. A6K15

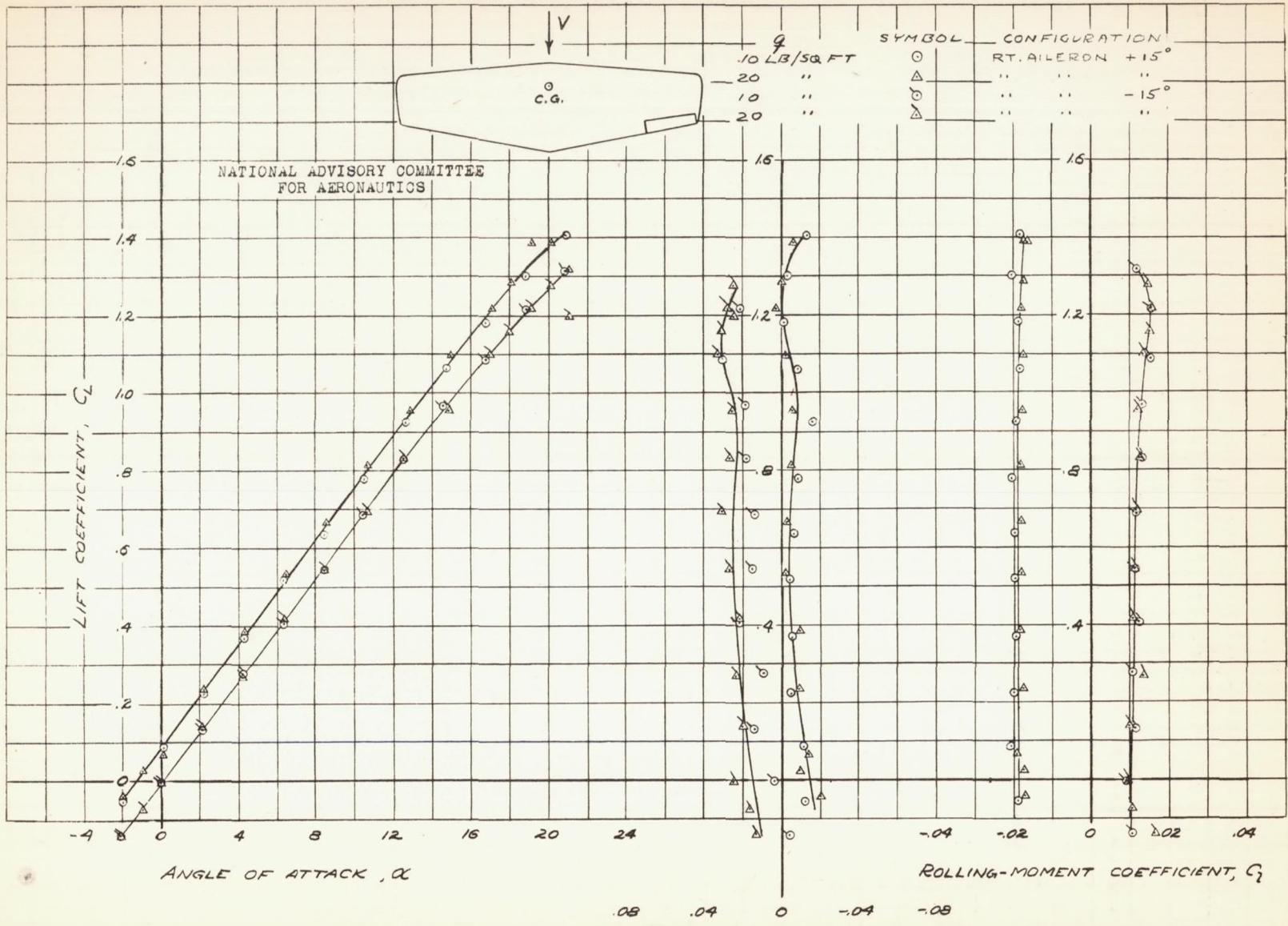


FIGURE 53.—AERODYNAMIC CHARACTERISTICS OF THE 0° SWEEP
WING AT -0.1° SIDESLIP. 20% CHORD, 35.2% SPAN
SPLIT FLAP TYPE AILERON ON RIGHT WING
DEFLECTED $\pm 15^{\circ}$.

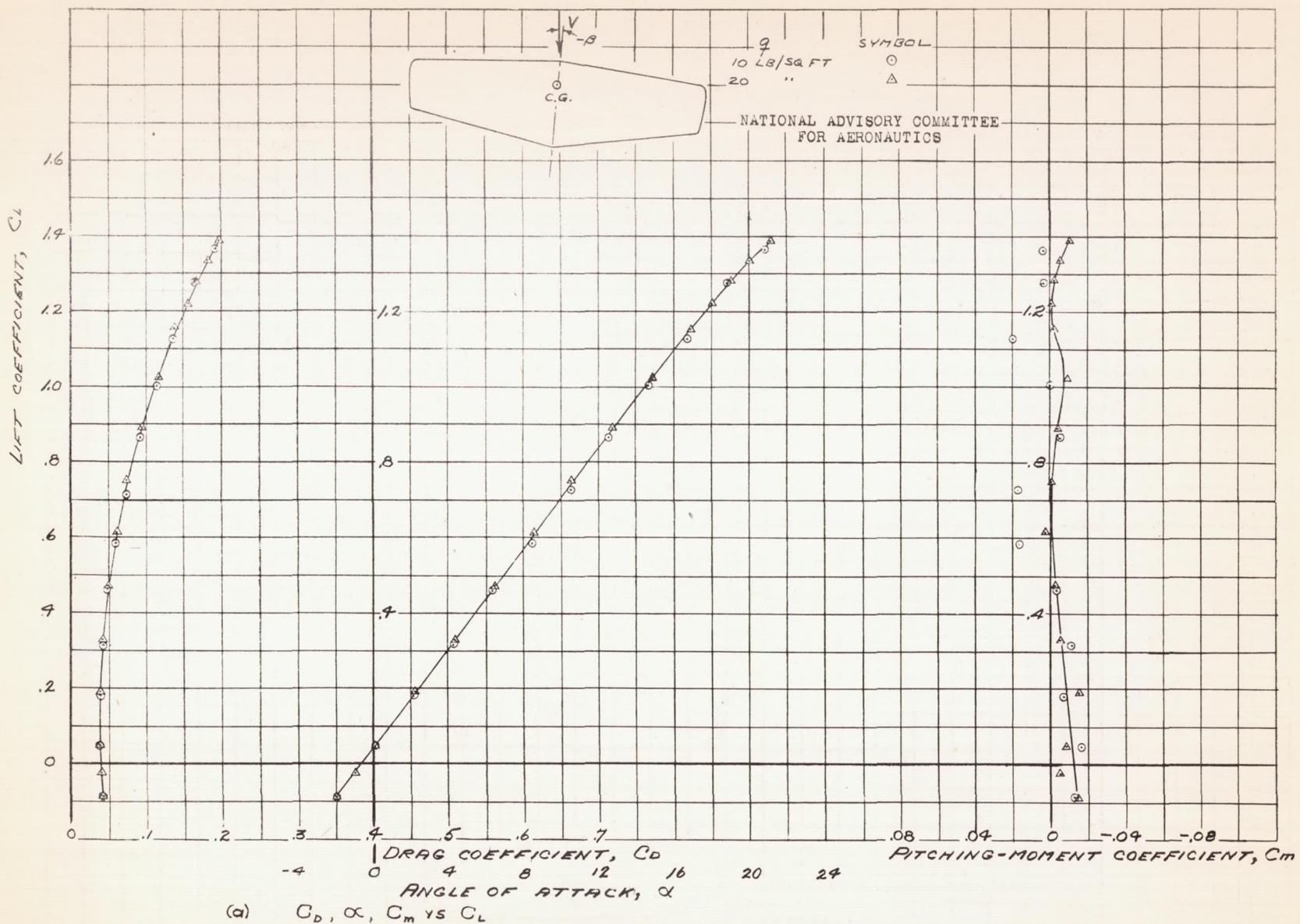


FIGURE 54.-AERODYNAMIC CHARACTERISTICS OF THE 0° SWEEP WING AT -5.2° SIDESLIP. PLAIN WING.

Fig. 54b

NACA RM No. A6K15

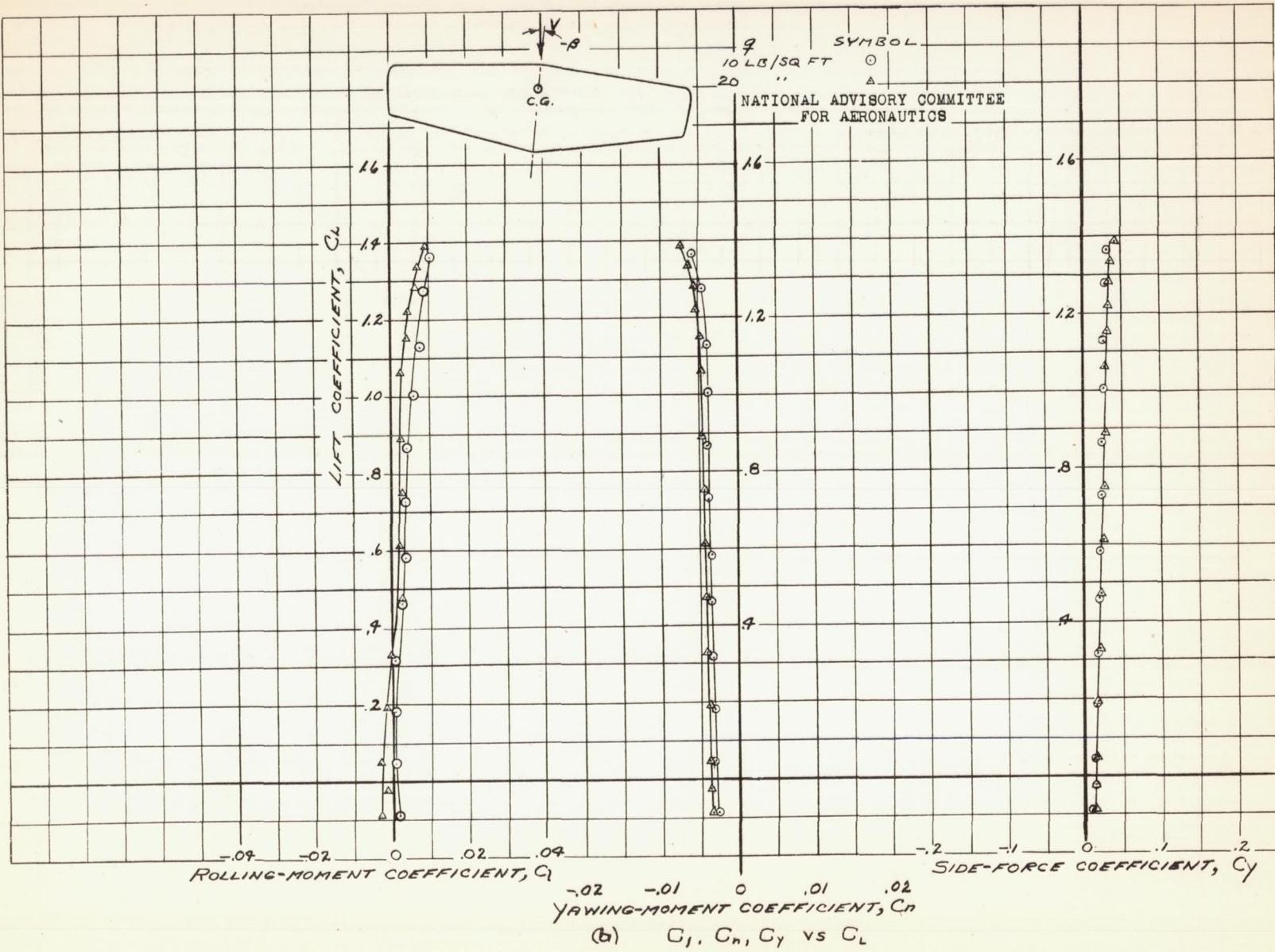


FIGURE 54.-CONCLUDED.

Fig. 55a

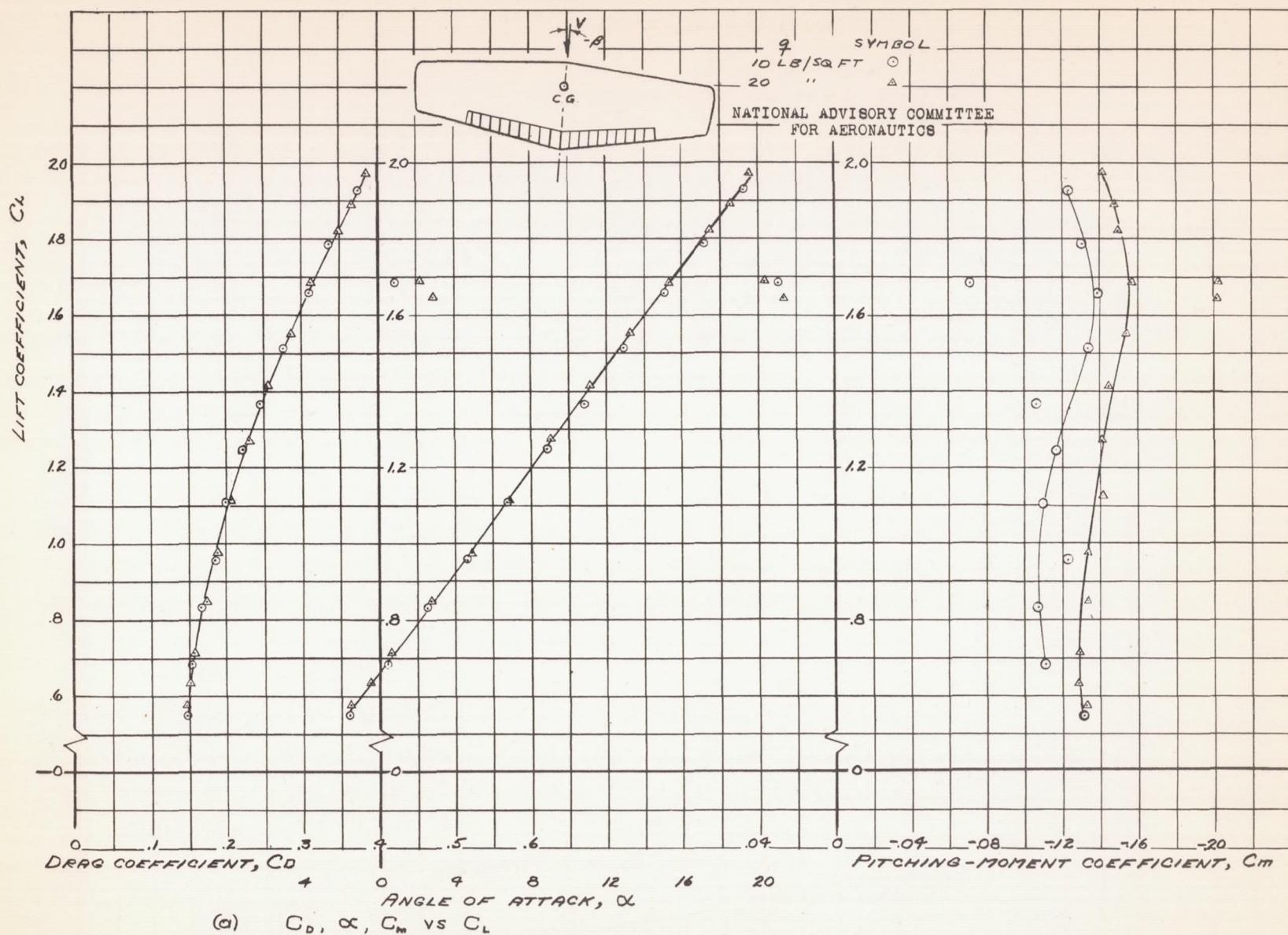


FIGURE 55.-AERODYNAMIC CHARACTERISTICS OF THE 0°
SWEEP WING AT -5.2° SIDESLIP, 20% CHORD
62.3% SPAN SPLIT FLAPS DEFLECTED 60°

Fig. 55b

NACA RM No. A6K15

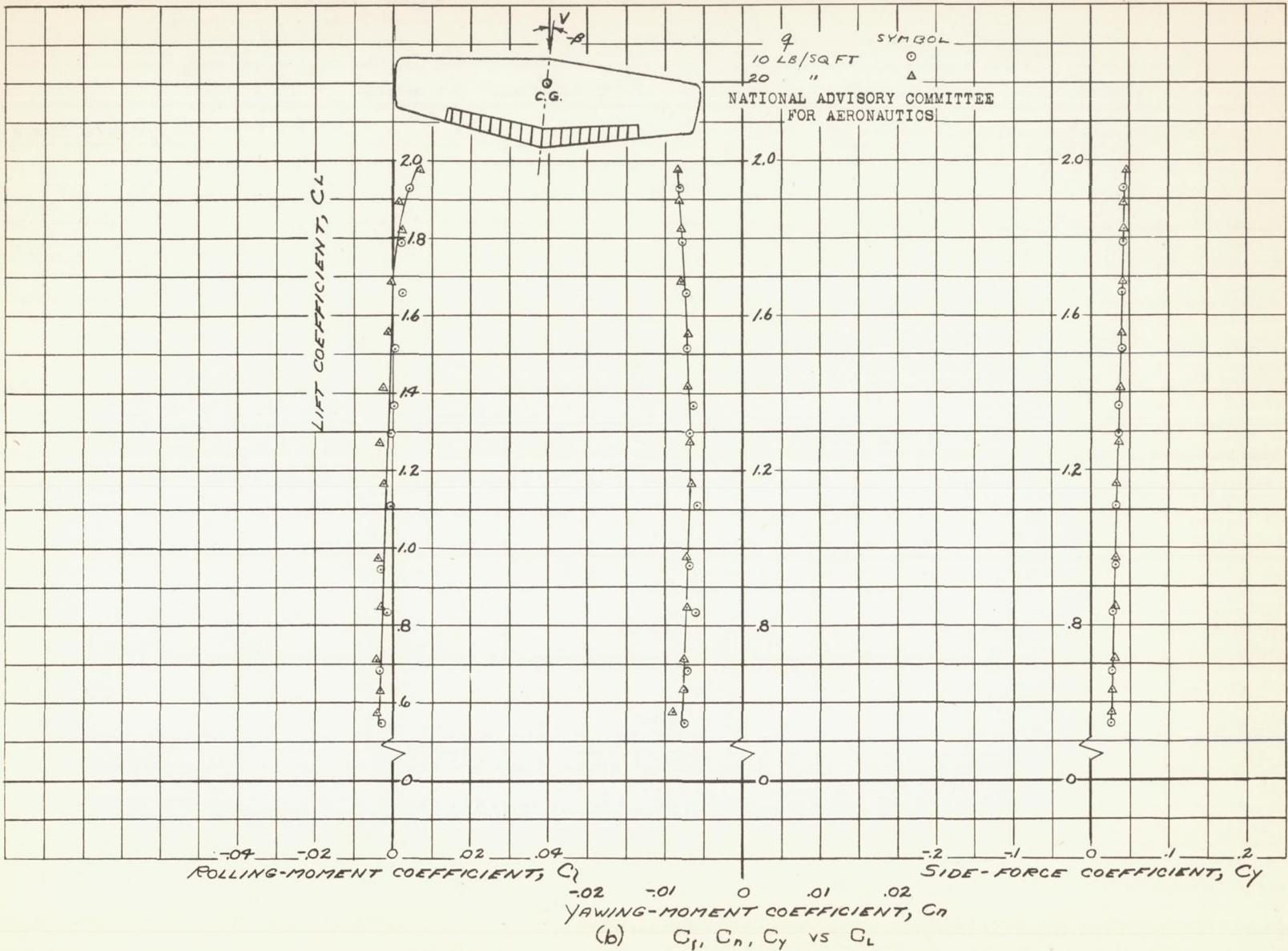


FIGURE 55.- CONCLUDED.

Fig. 56a

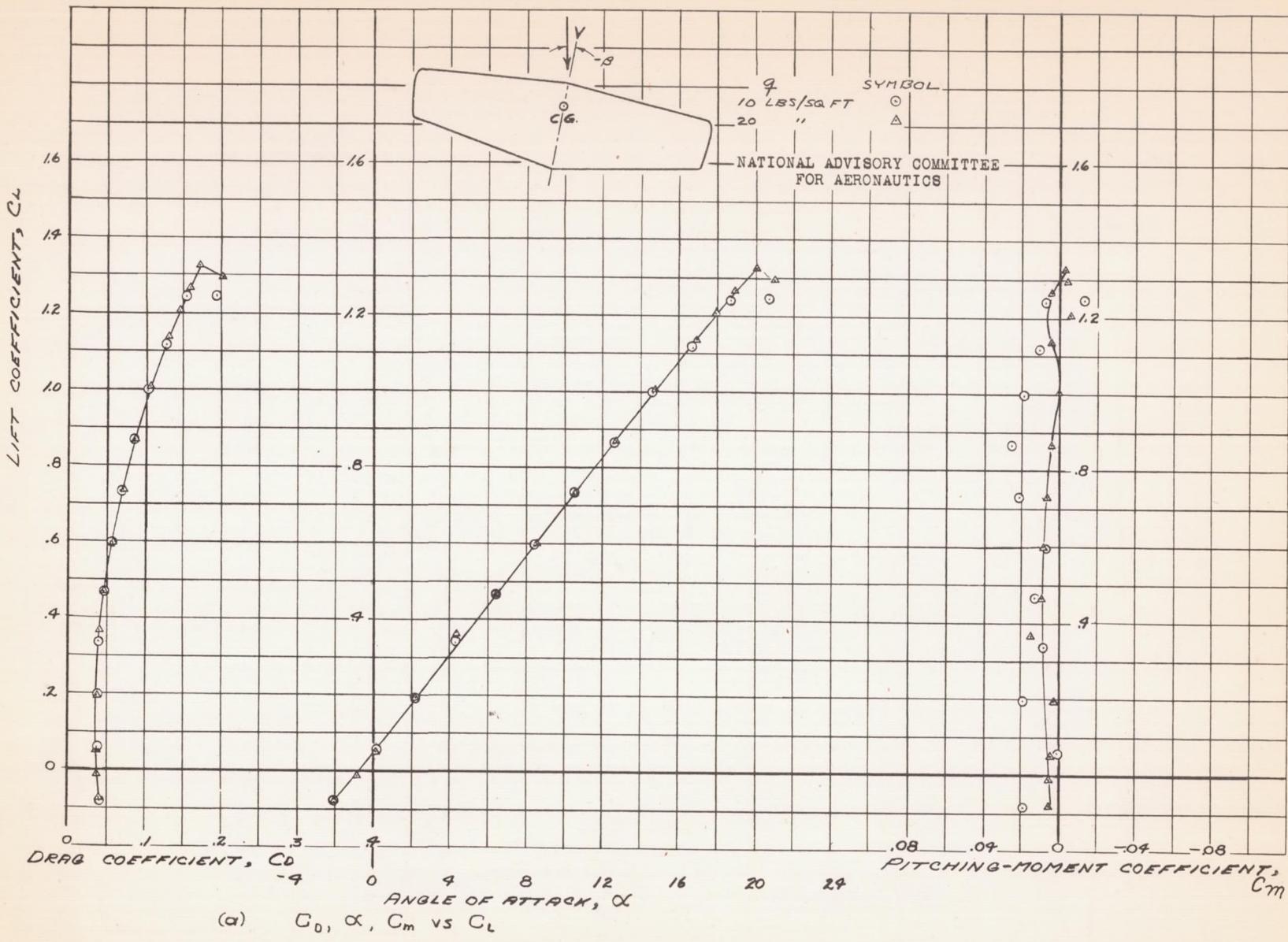


FIGURE 56.- AERODYNAMIC CHARACTERISTICS OF THE 0° SWEEP WING AT -10.1° SIDESLIP.
PLAIN WING.

Fig. 56b

NACA RM No. A6K15

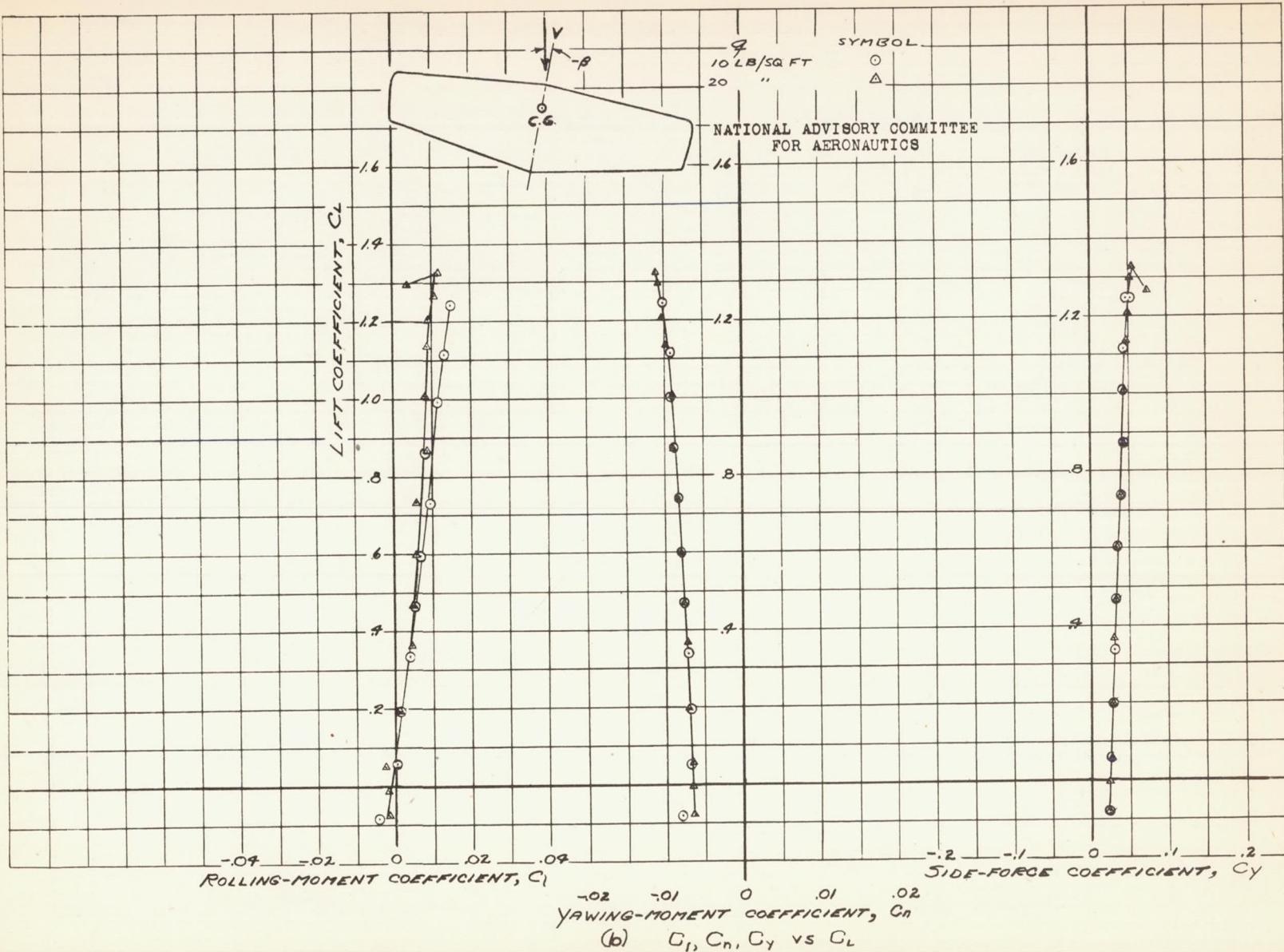


FIGURE 56.-CONCLUDED.

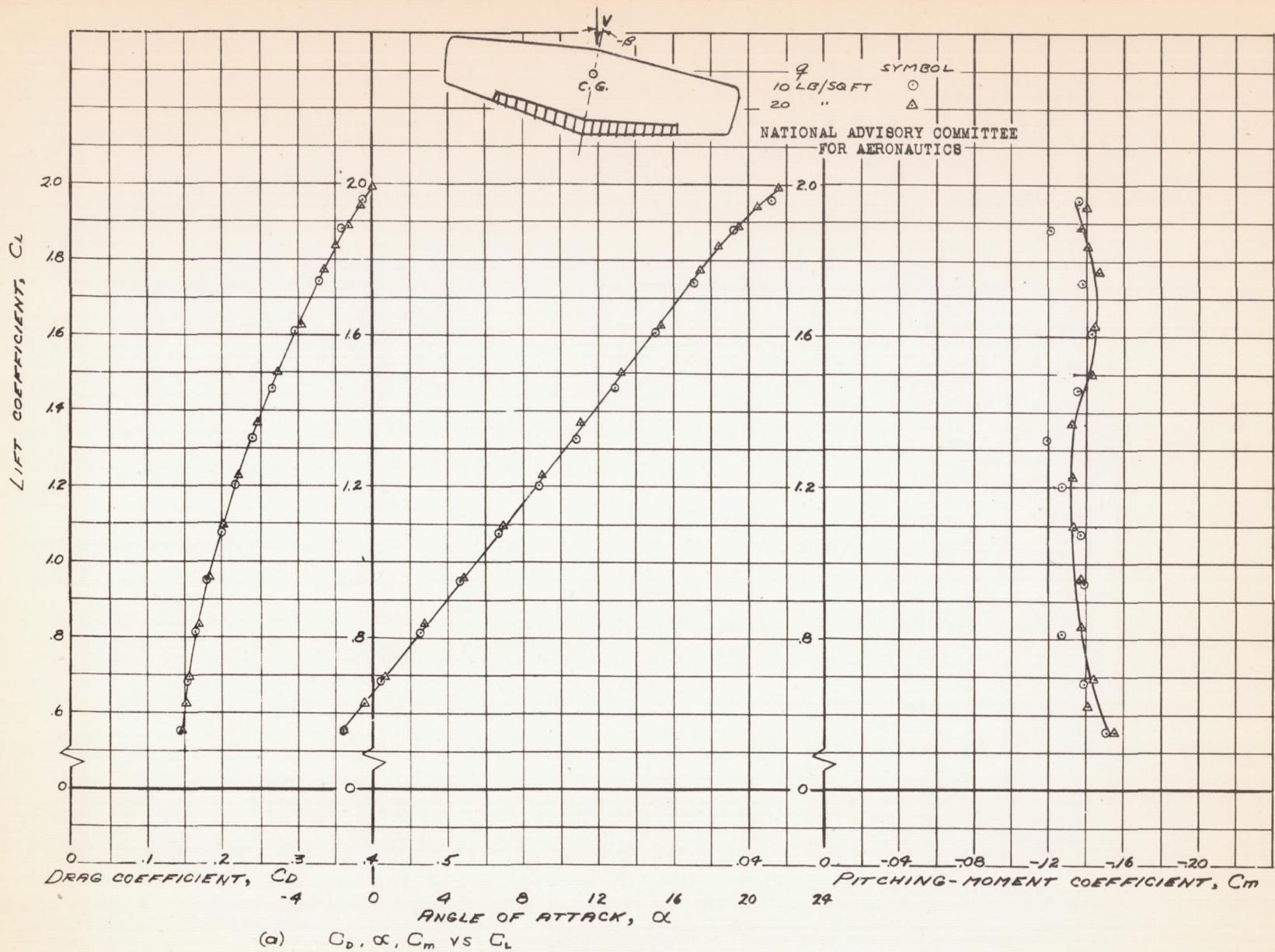
(a) C_D, α, C_m vs C_L

FIGURE 57.—AERODYNAMIC CHARACTERISTICS OF THE 0° SWEEPED WING AT -10.1° SIDESLIP, 20% CHORD 62.3% SPAN SPLIT FLAPS DEFLECTED 60°.

Fig. 57b

NACA RM No. A6K15

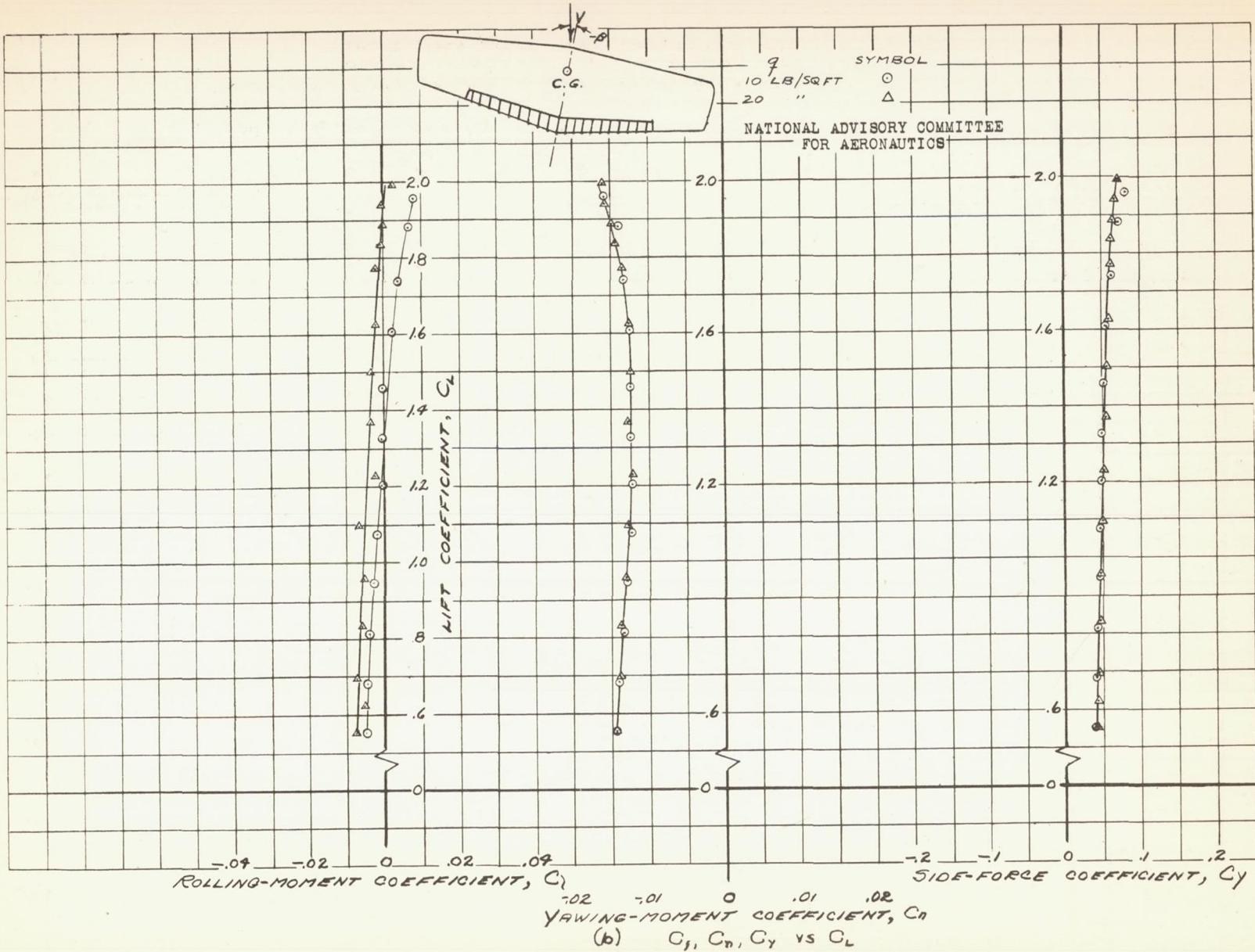


FIGURE 57.- CONCLUDED.

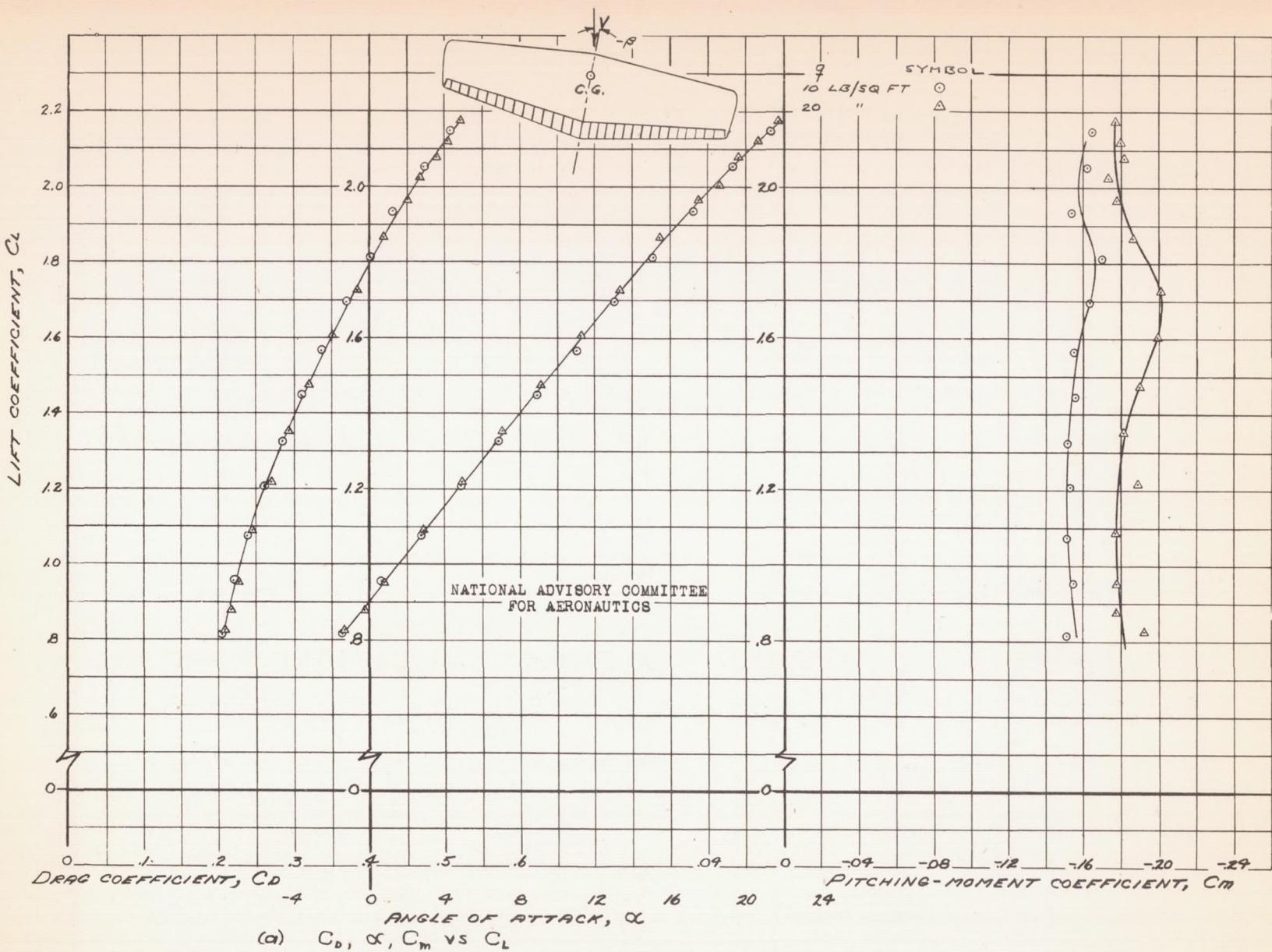


FIGURE 58.- AERODYNAMIC CHARACTERISTICS OF THE 0° SWEEP WING AT -10.1° SIDESLIP, 20% CHORD FULL SPAN SPLIT FLAPS DEFLECTED 60°.

Fig. 58b

NACA RM NO. A6K15

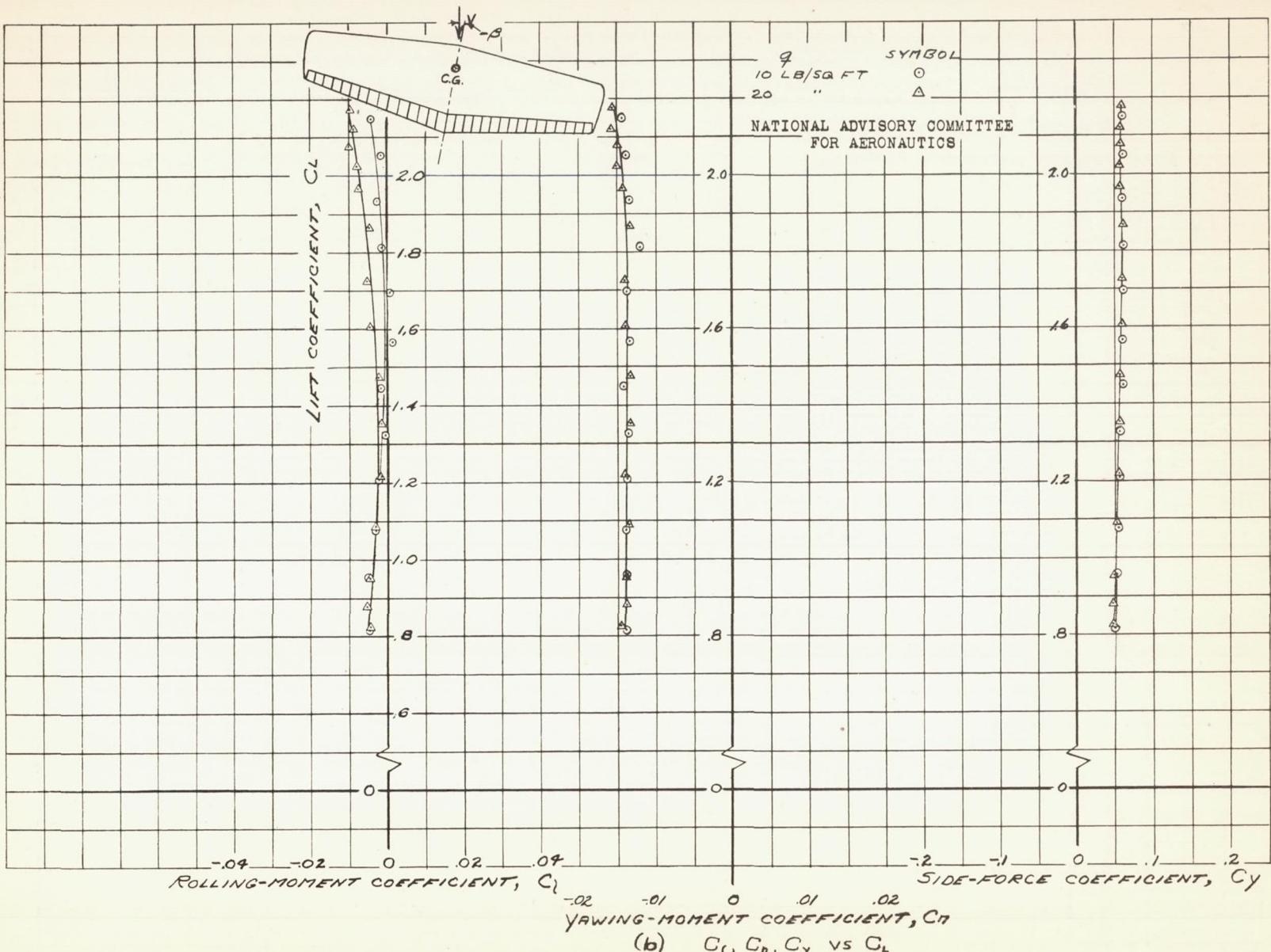


FIGURE 58.- CONCLUDED.

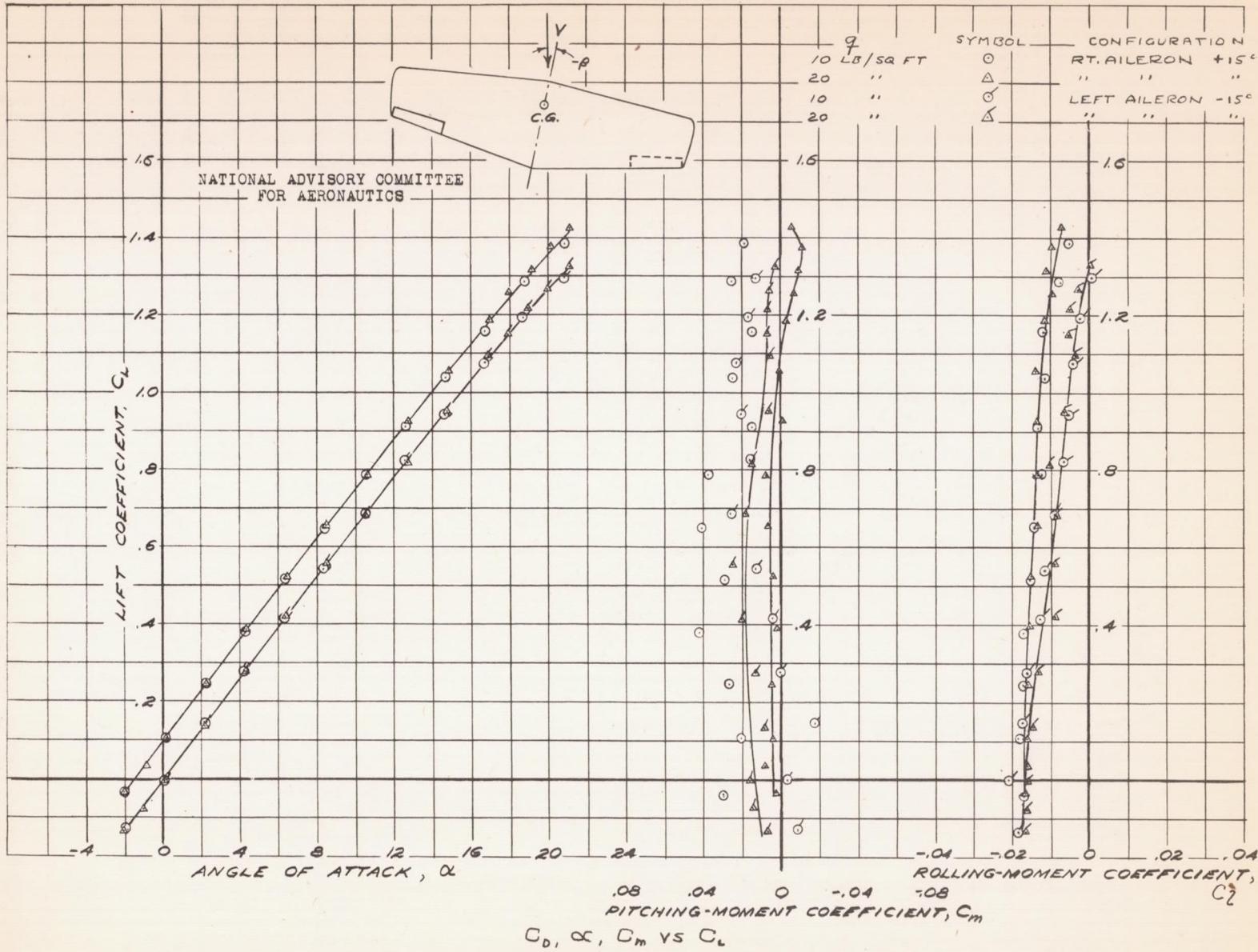


FIGURE 59.-AERODYNAMIC CHARACTERISTICS OF THE 0° SWEEP WING AT -10.1° SIDESLIP. 20% CHORD, 35.2% SPAN SPLIT FLAP TYPE AILERONS DEFLECTED \pm 15°.

Fig. 60a

NACA RM NO. A6K15

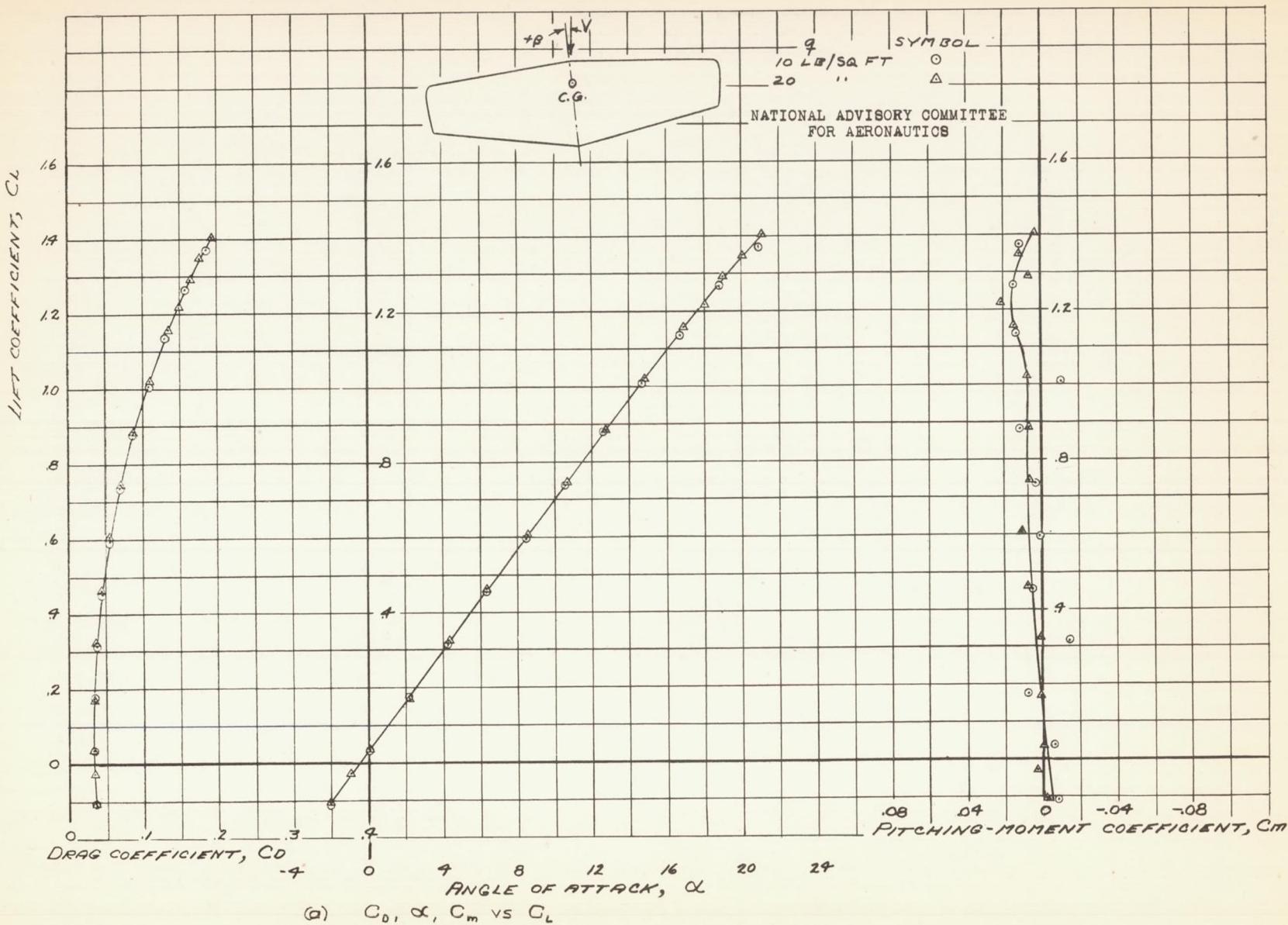
FIGURE 60.- AERODYNAMIC CHARACTERISTICS OF THE
0° SWEEP WING AT +14.4° SIDESLIP. PLAIN WING.

Fig. 60b

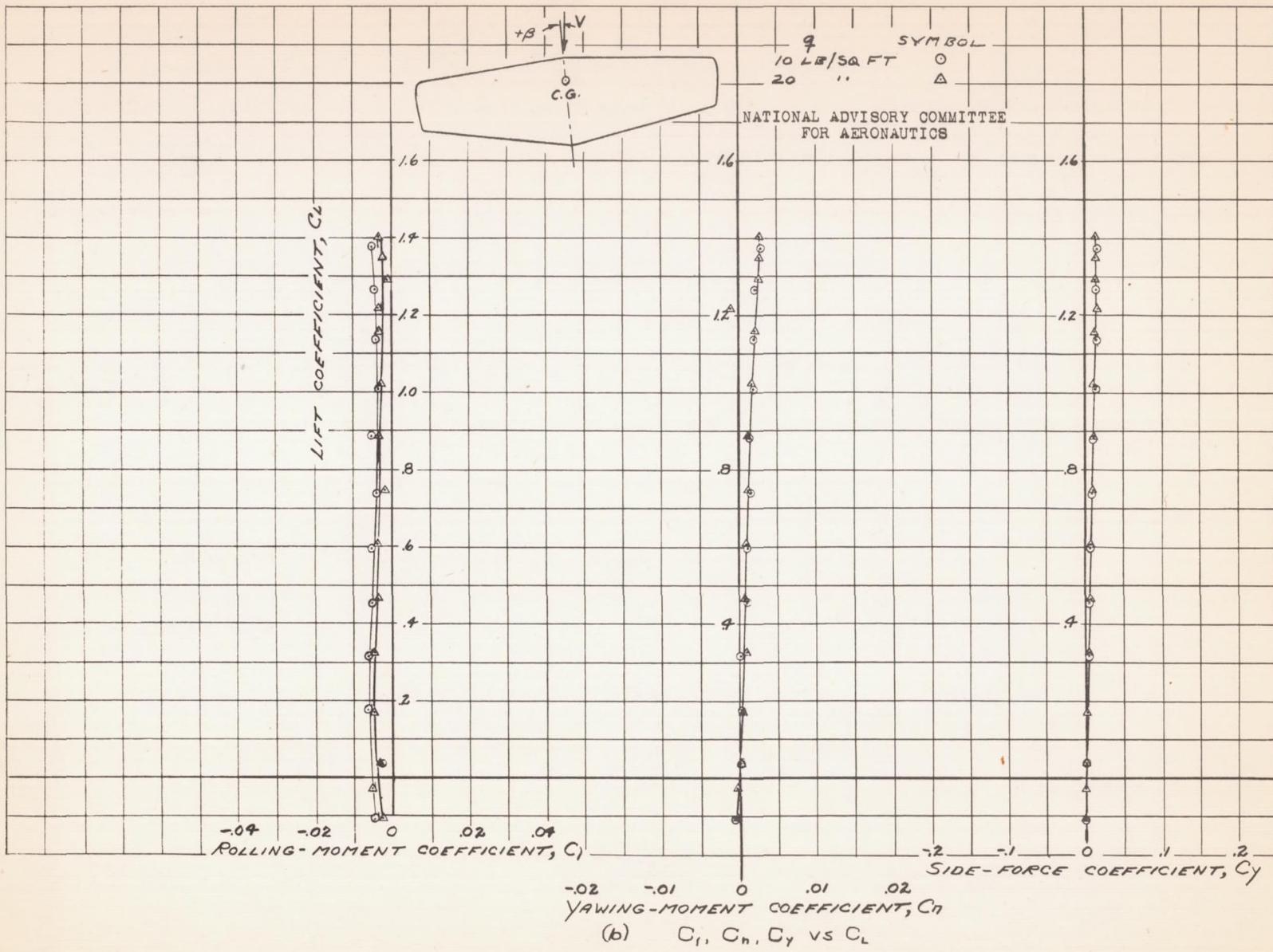


FIGURE 60.-CONCLUDED.

Fig. 61a

NACA RM No. A6K15

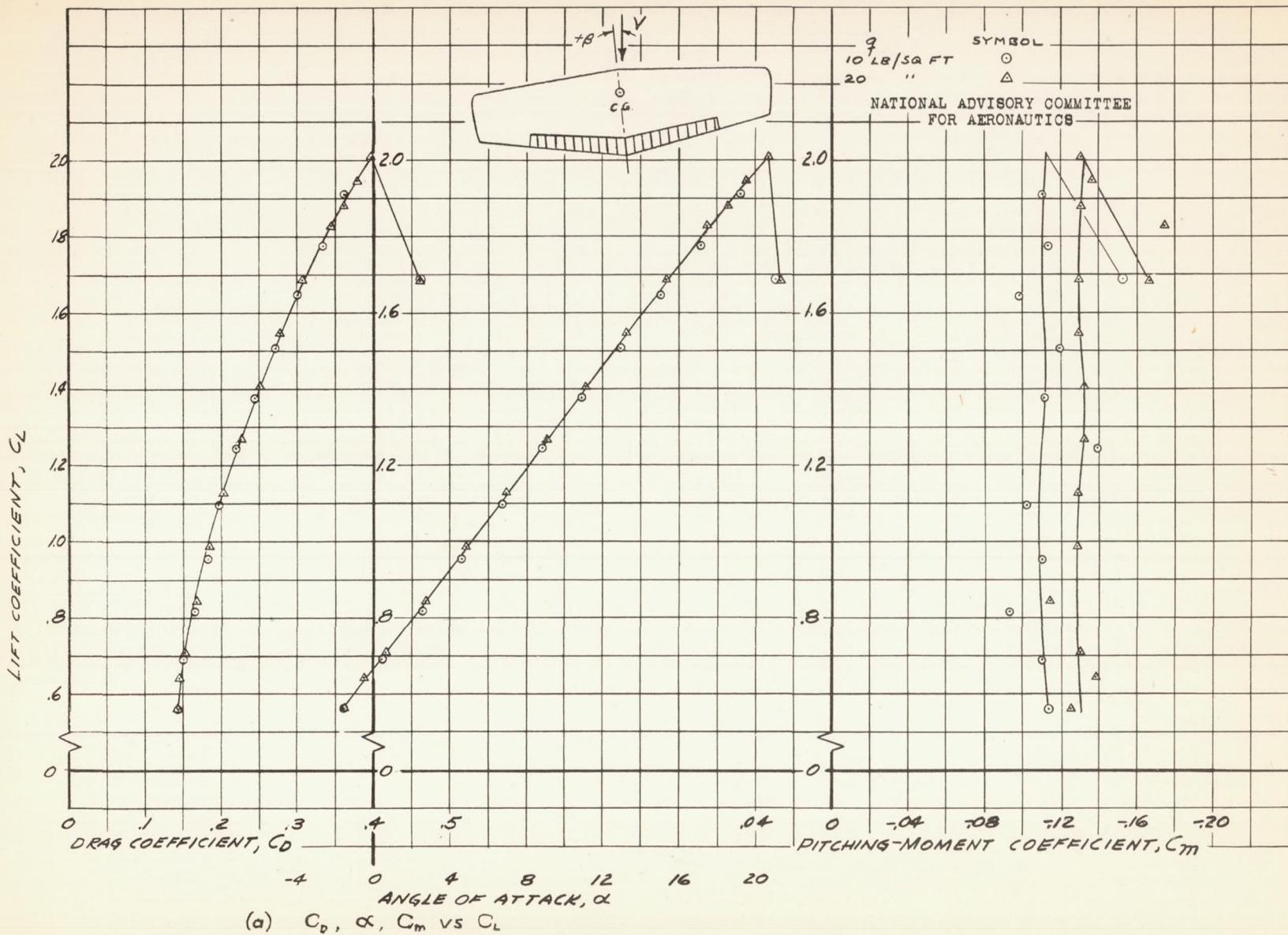


FIGURE 61.-AERODYNAMIC CHARACTERISTICS OF THE 0° SWEEP WING AT +4.4° SIDESLIP. 20% CHORD 62.3% SPAN SPLIT FLAPS DEFLECTED 60°

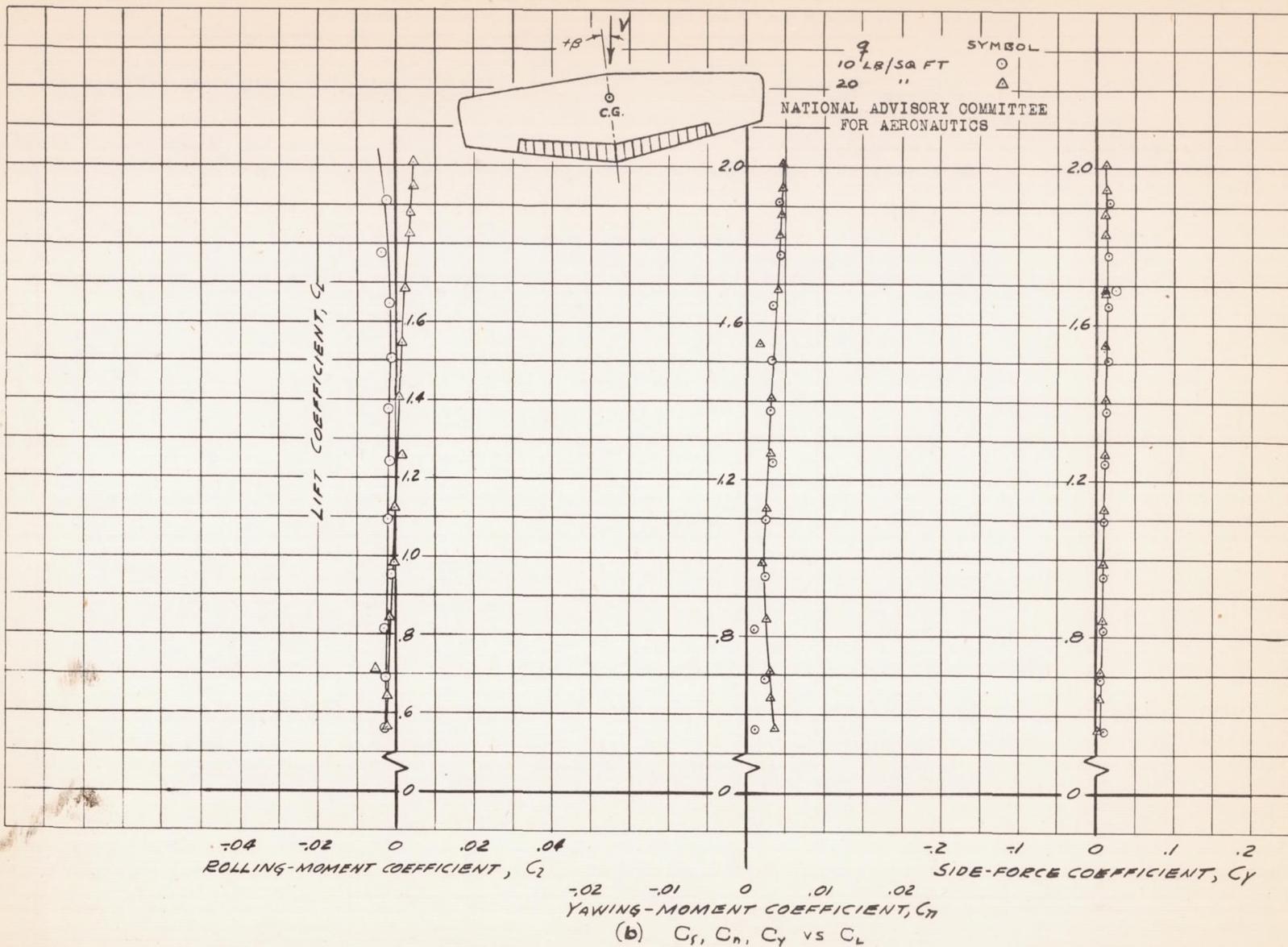


FIGURE 61.- CONCLUDED.

Fig. 62a

NACA RM NO. A6K15

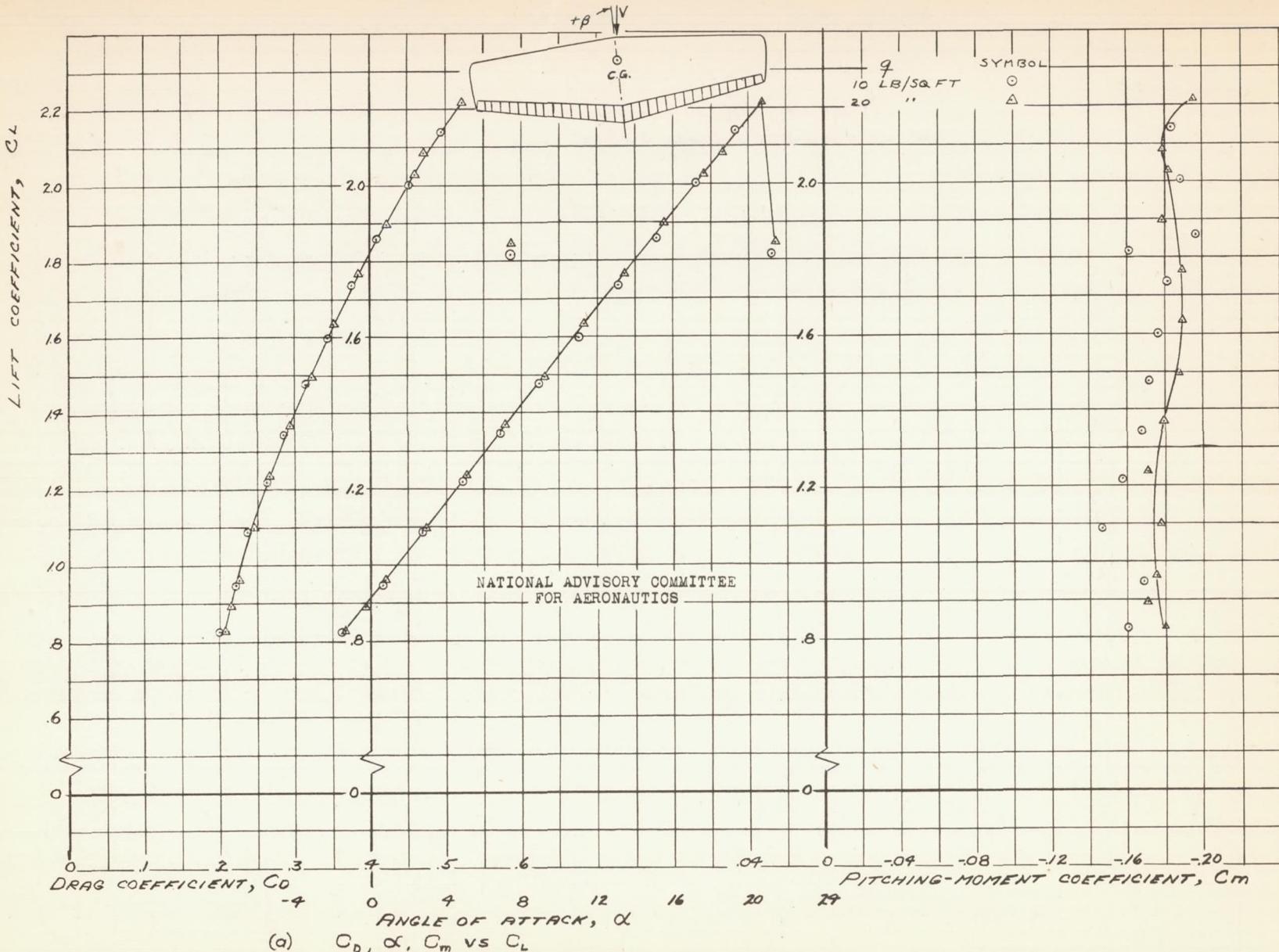


FIGURE 62.—AERODYNAMIC CHARACTERISTICS OF THE
0° SWEPT WING AT +4.4° SIDESLIP, 20% CHORD
FULL SPAN SPLIT FLAPS DEFLECTED 60°.

Fig. 62b

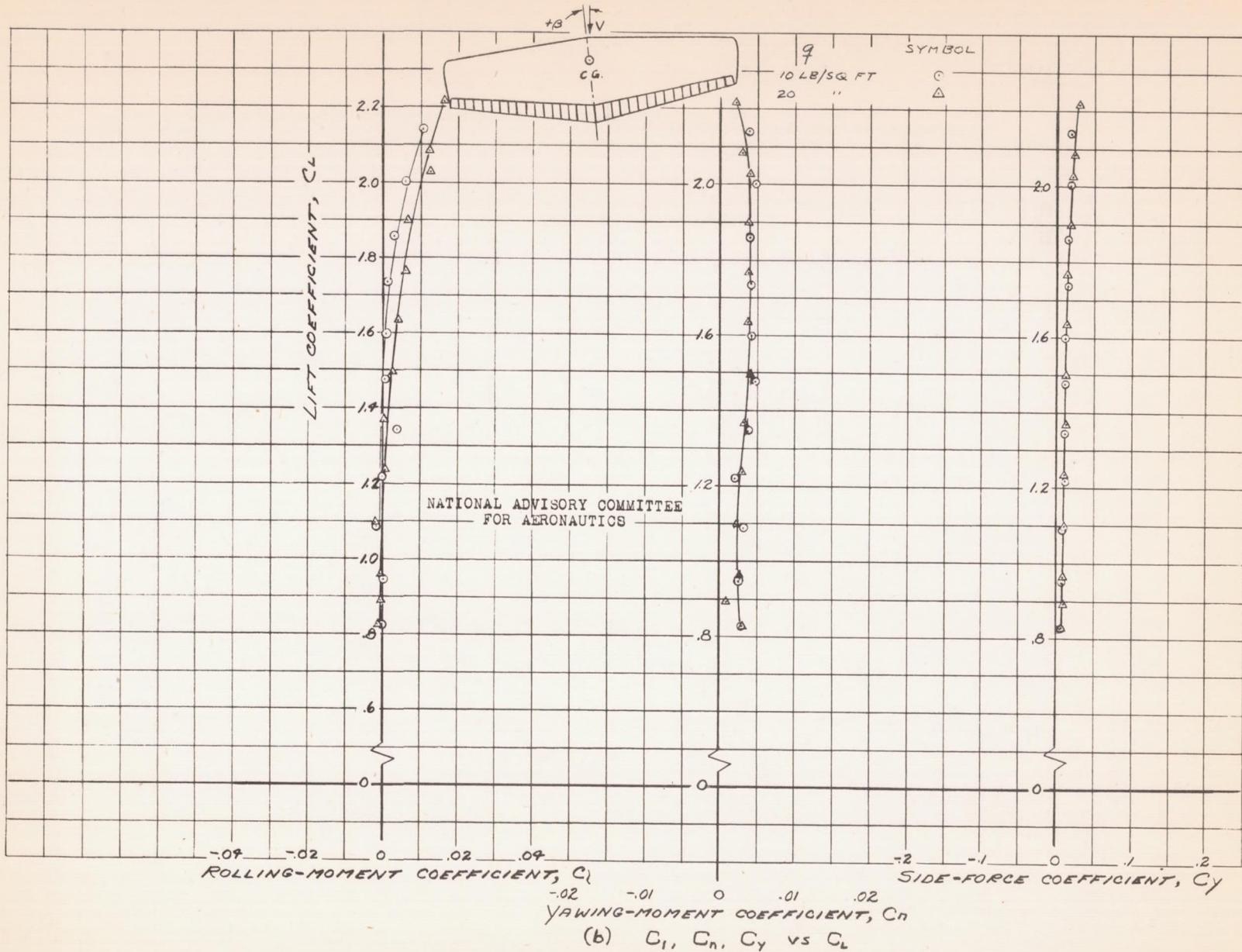


FIGURE 62.- CONCLUDED.

Fig. 63

NACA RM NO. A6K15

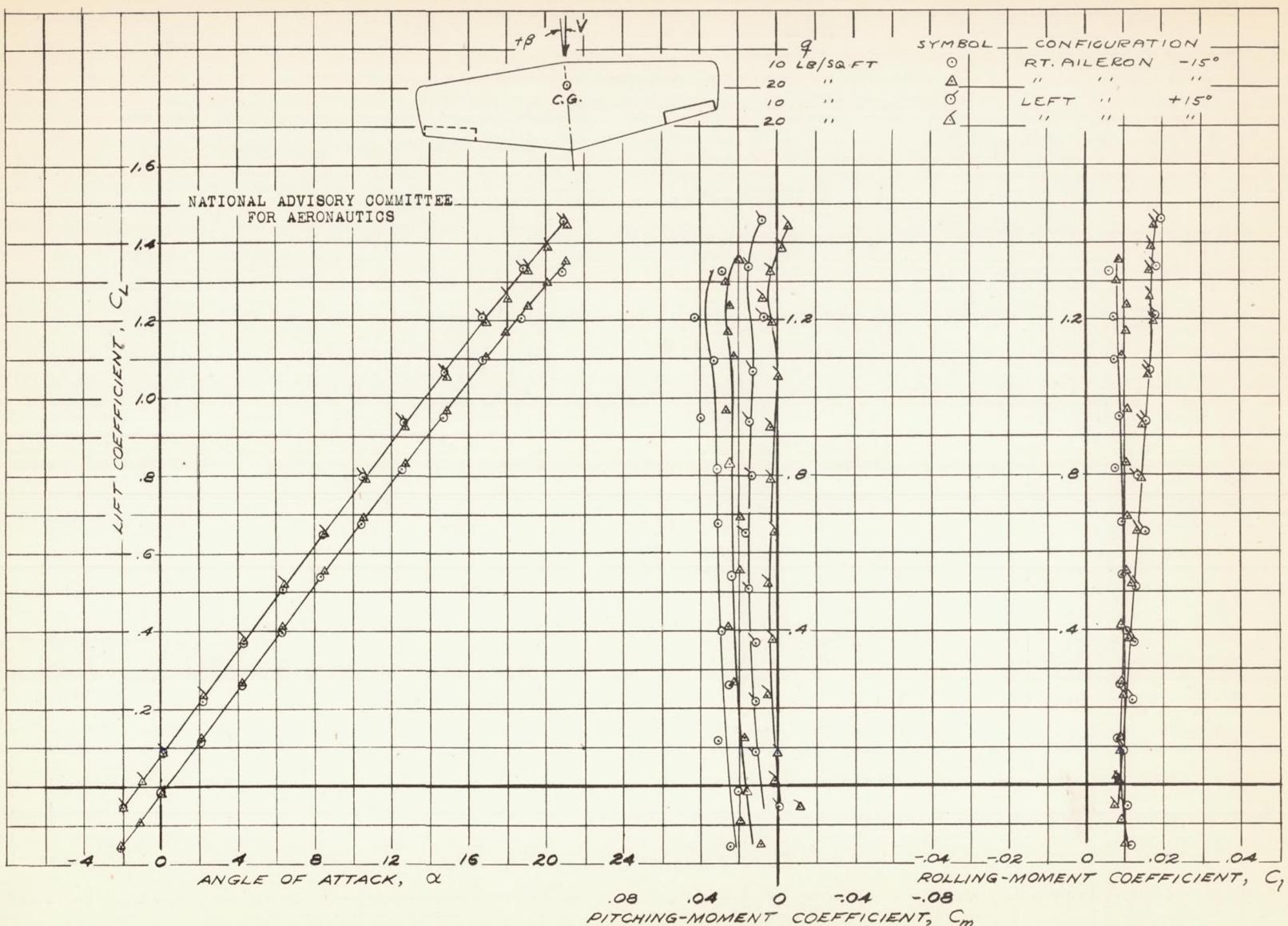


FIGURE 63.—AEROdynamic CHARACTERISTICS OF THE 0° SWept
WING AT $+4.4^\circ$ SIDEslIP, 20% CHORD, 35.2% SPAN
SPLIT FLAP TYPE AILERONS DEFLECTED $\pm 15^\circ$.

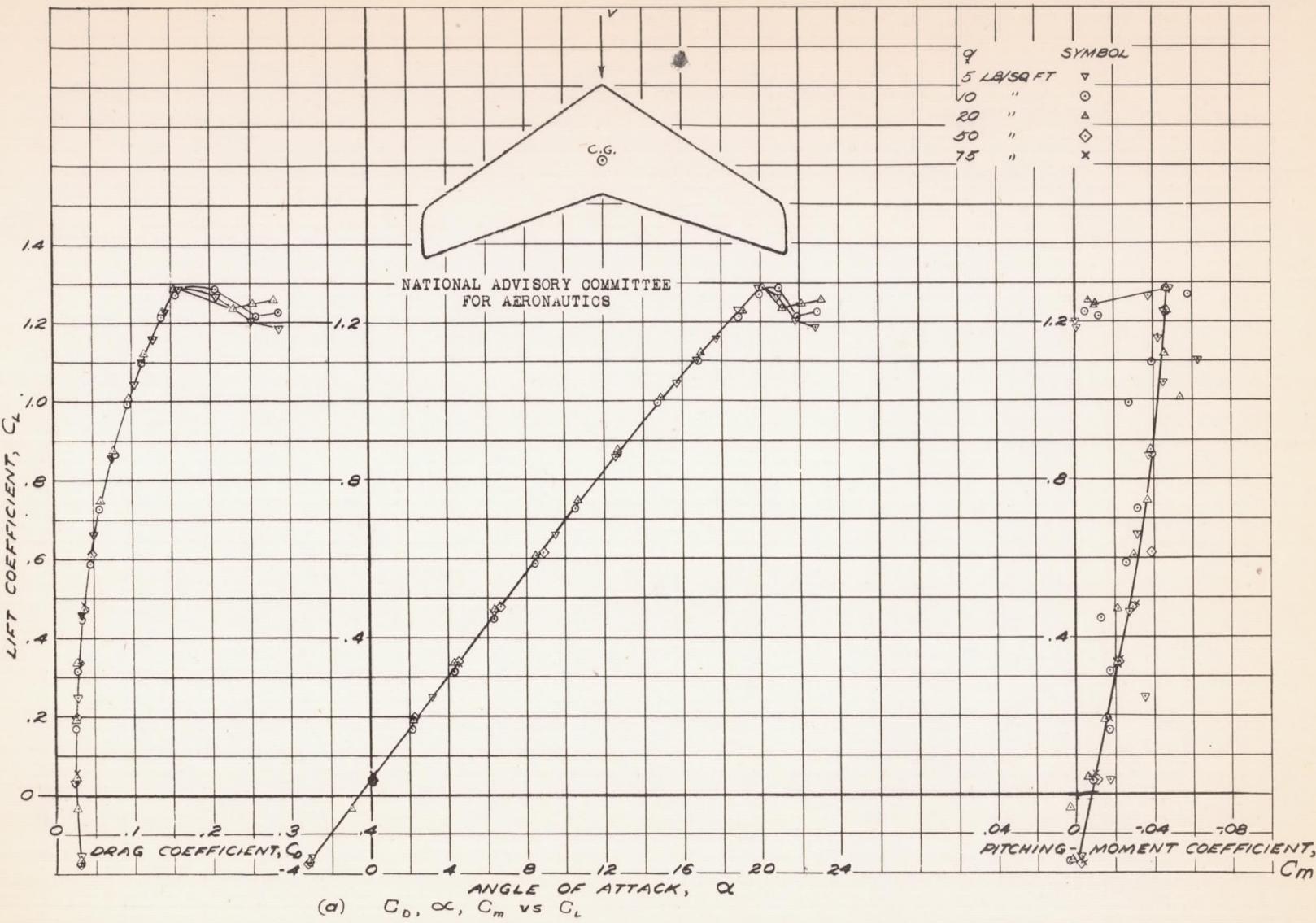


FIGURE 64.-AERODYNAMIC CHARACTERISTICS OF THE 30° SWEEP BACK WING AT -0.3° SIDESLIP. PLAIN WING.

Fig. 64b

NACA RM No. A6K15

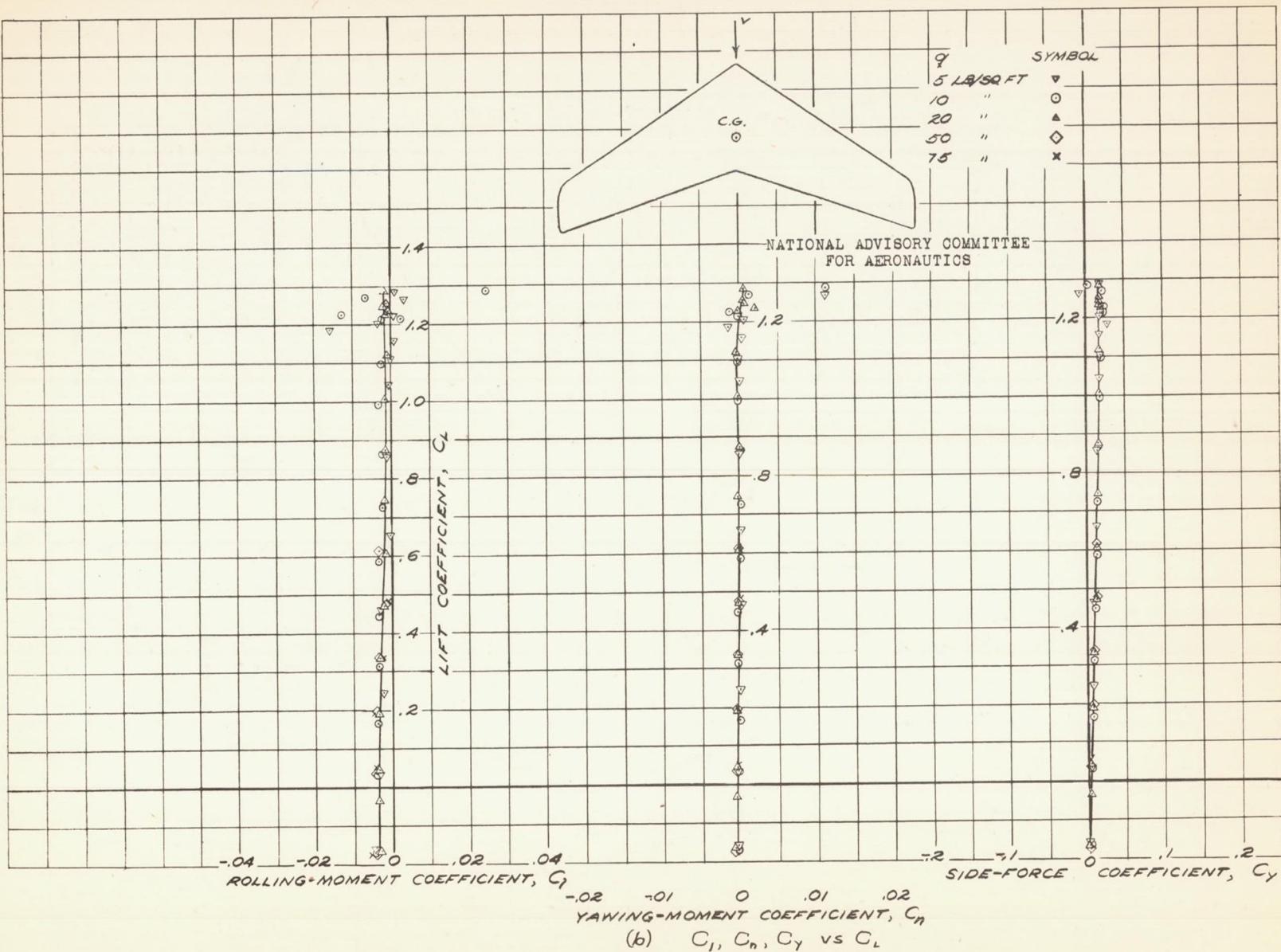


FIGURE 64.-CONCLUDED.

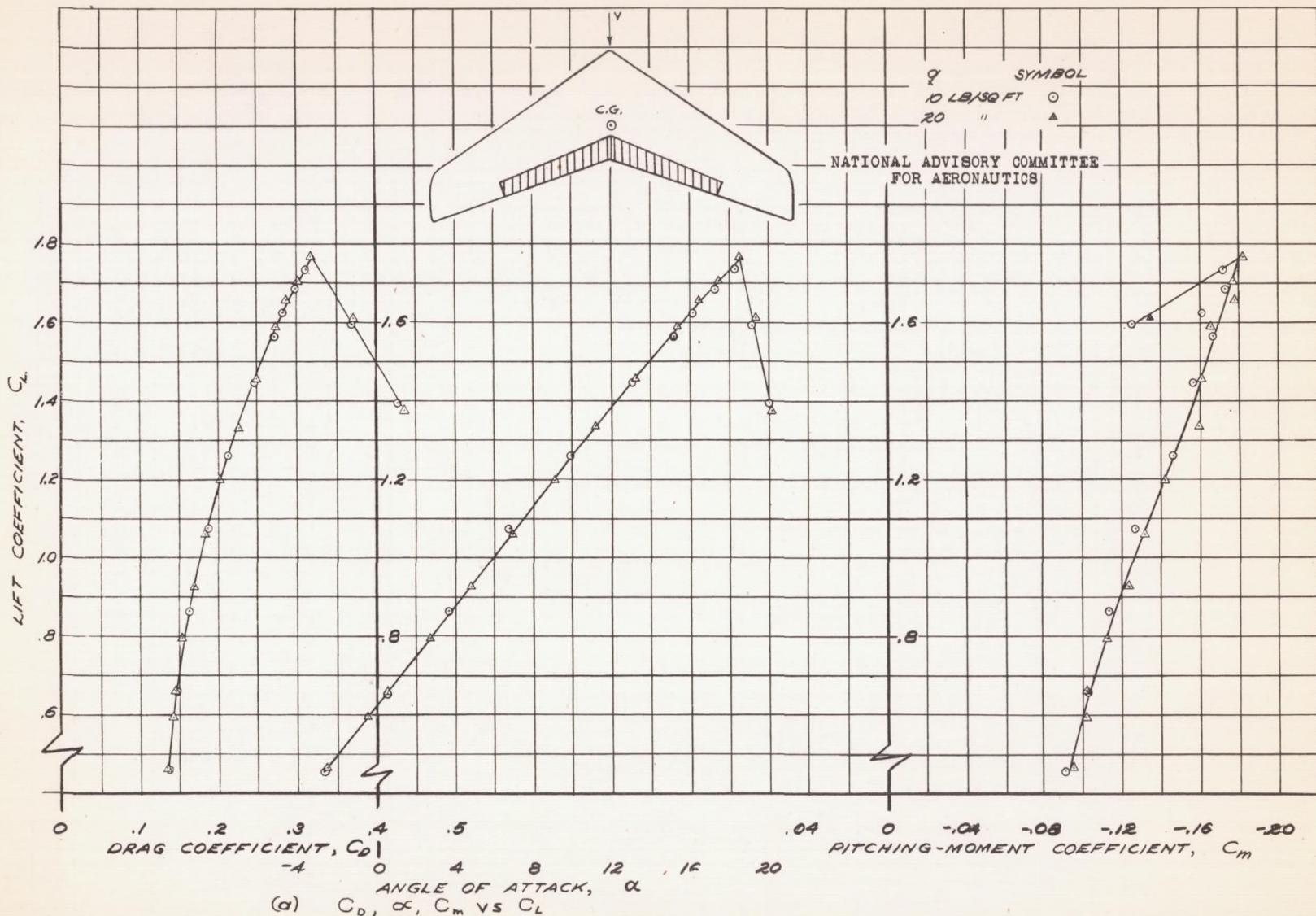


FIGURE 65.—AERODYNAMIC CHARACTERISTICS OF THE 30° SWEEPBACK WING AT -0.3° SIDESLIP, 20% CHORD 62.3% SPAN SPLIT FLAPS DEFLECTED 60°

Fig. 65b

NACA RM No. A6K15

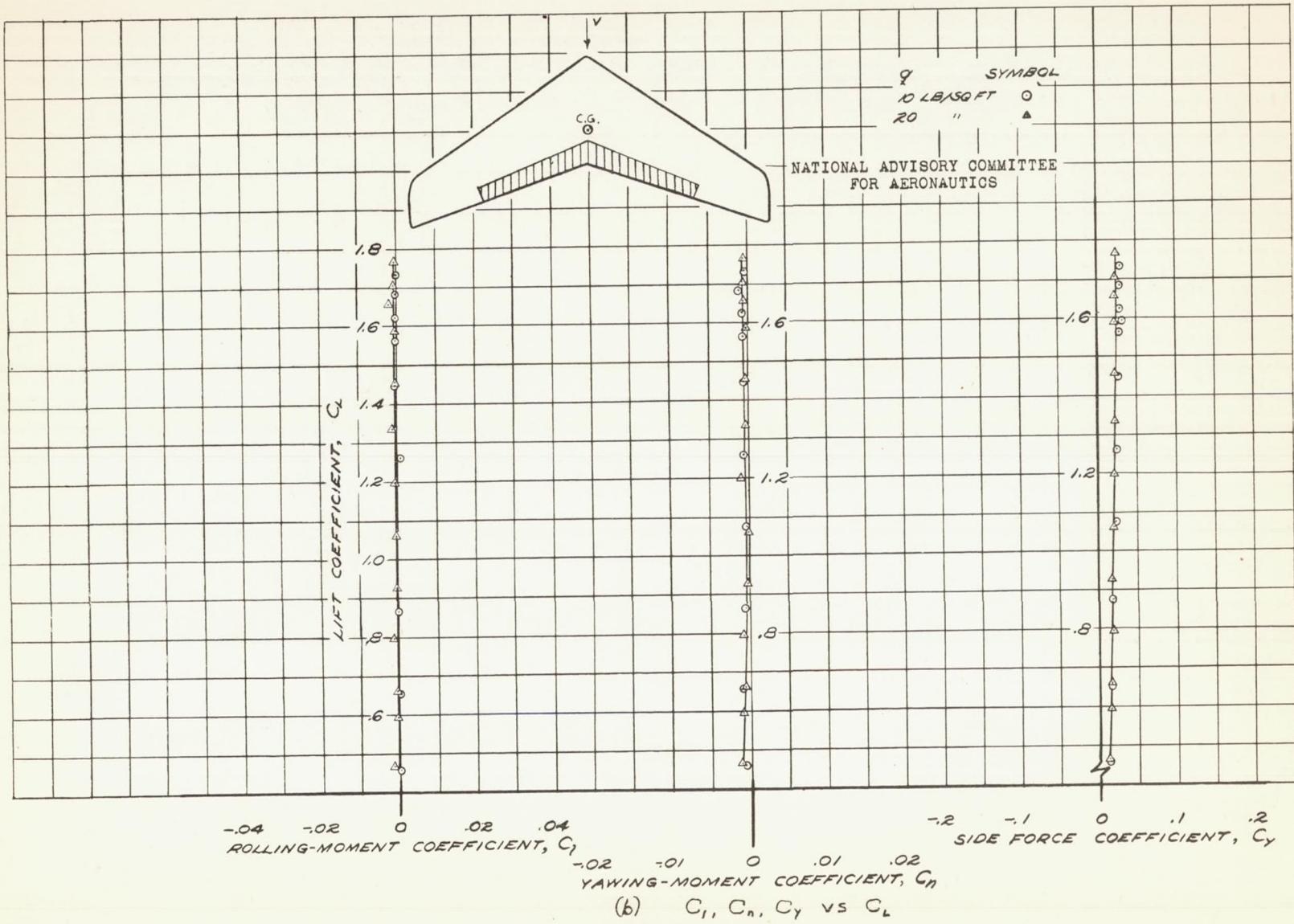


FIGURE 65.-CONCLUDED.

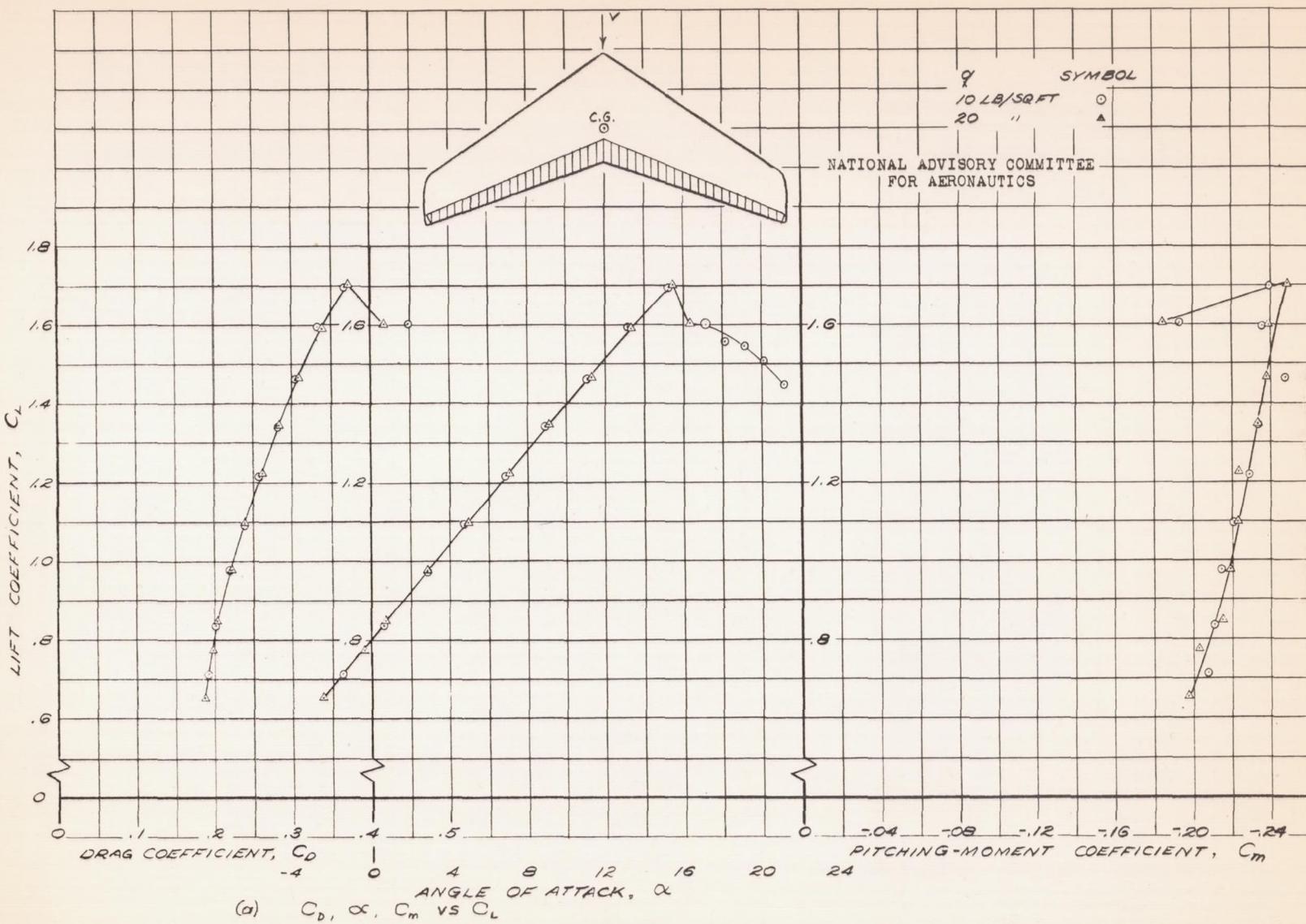
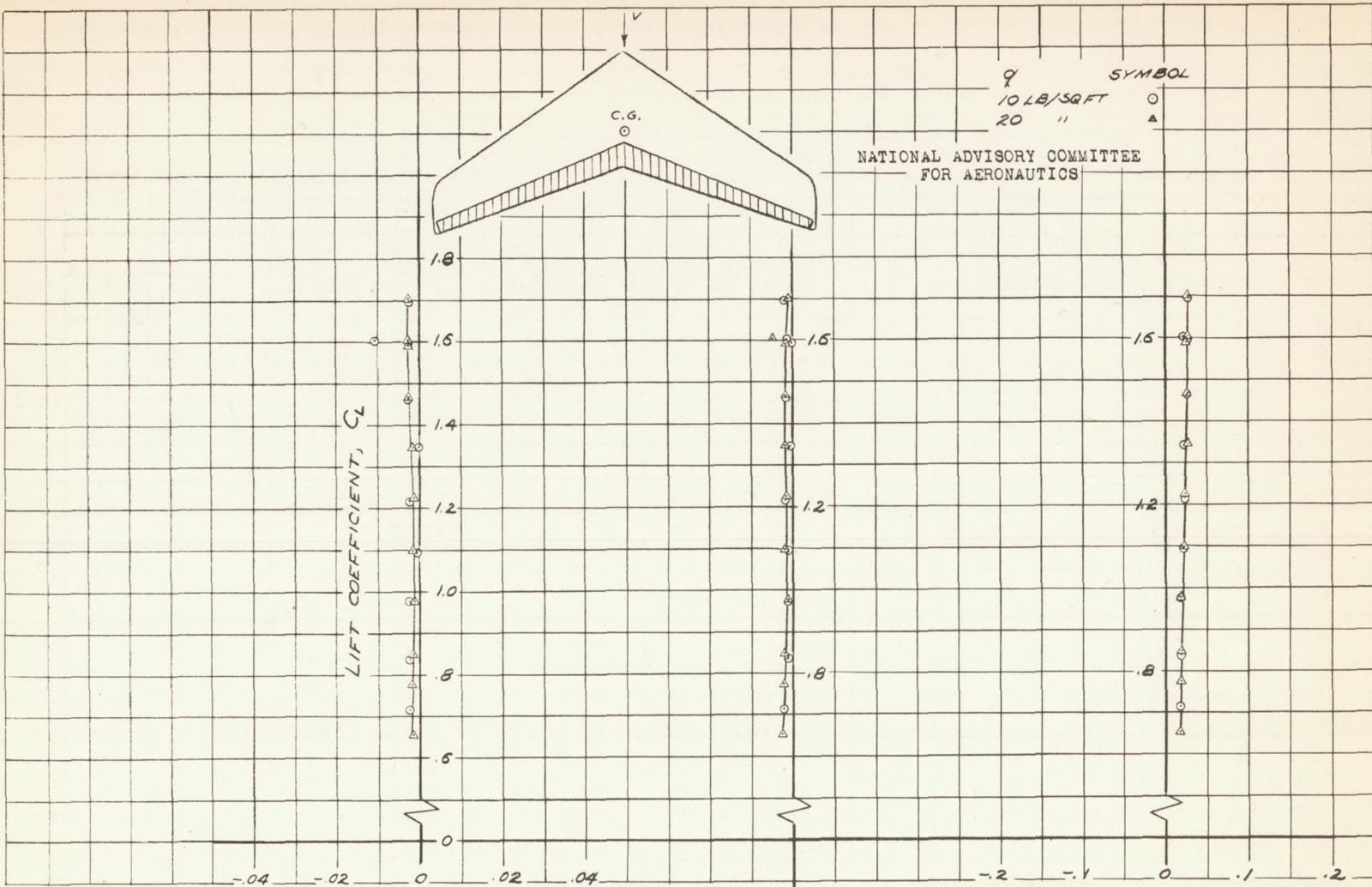


FIGURE 66.- AERODYNAMIC CHARACTERISTICS OF THE 30° SWEEPBACK WING AT -0.3° SIDESLIP, 20% CHORD FULL SPAN SPLIT FLAPS DEFLECTED 60°.

Fig. 66b

NACA RM No. A6K15



YAWING-MOMENT COEFFICIENT, C_n
(b) C_I, C_n, C_y vs C_L

FIGURE 66.-CONCLUDED.

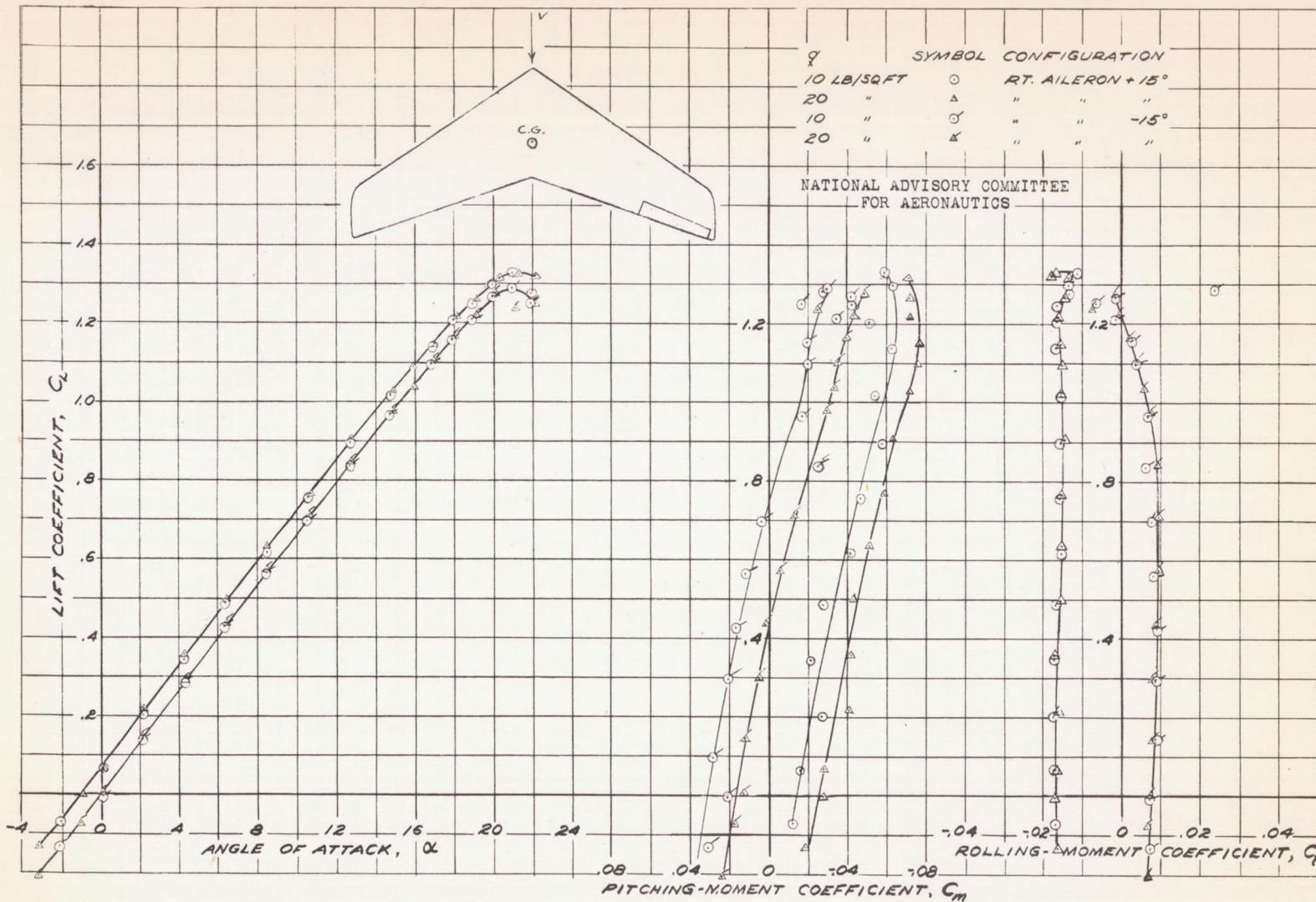


FIGURE 67. - AERODYNAMIC CHARACTERISTICS OF THE 30° SWEEPBACK WING AT -0.3° SIDESLIP. 20% CHORD 36.8% SPAN SPLIT FLAP TYPE AILERON ON RIGHT WING DEFLECTED $\pm 15^\circ$.

Fig. 68a

NACA RM NO. A6K15

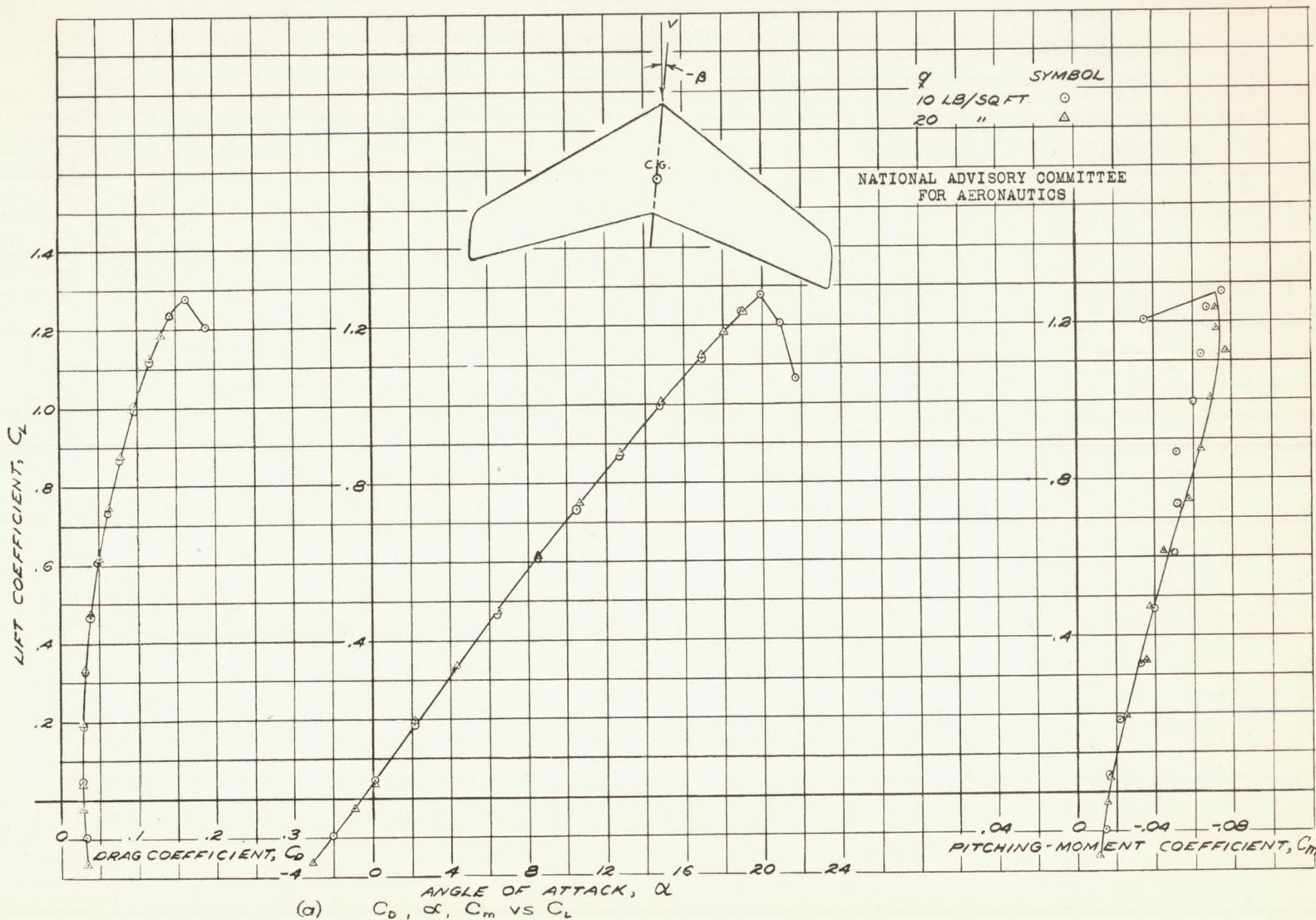


FIGURE 68.- AEROdynamic CHARACTERISTICS OF THE 30° SWEEPBACK WING AT -5.3° SIDESLIP. PLAIN WING.

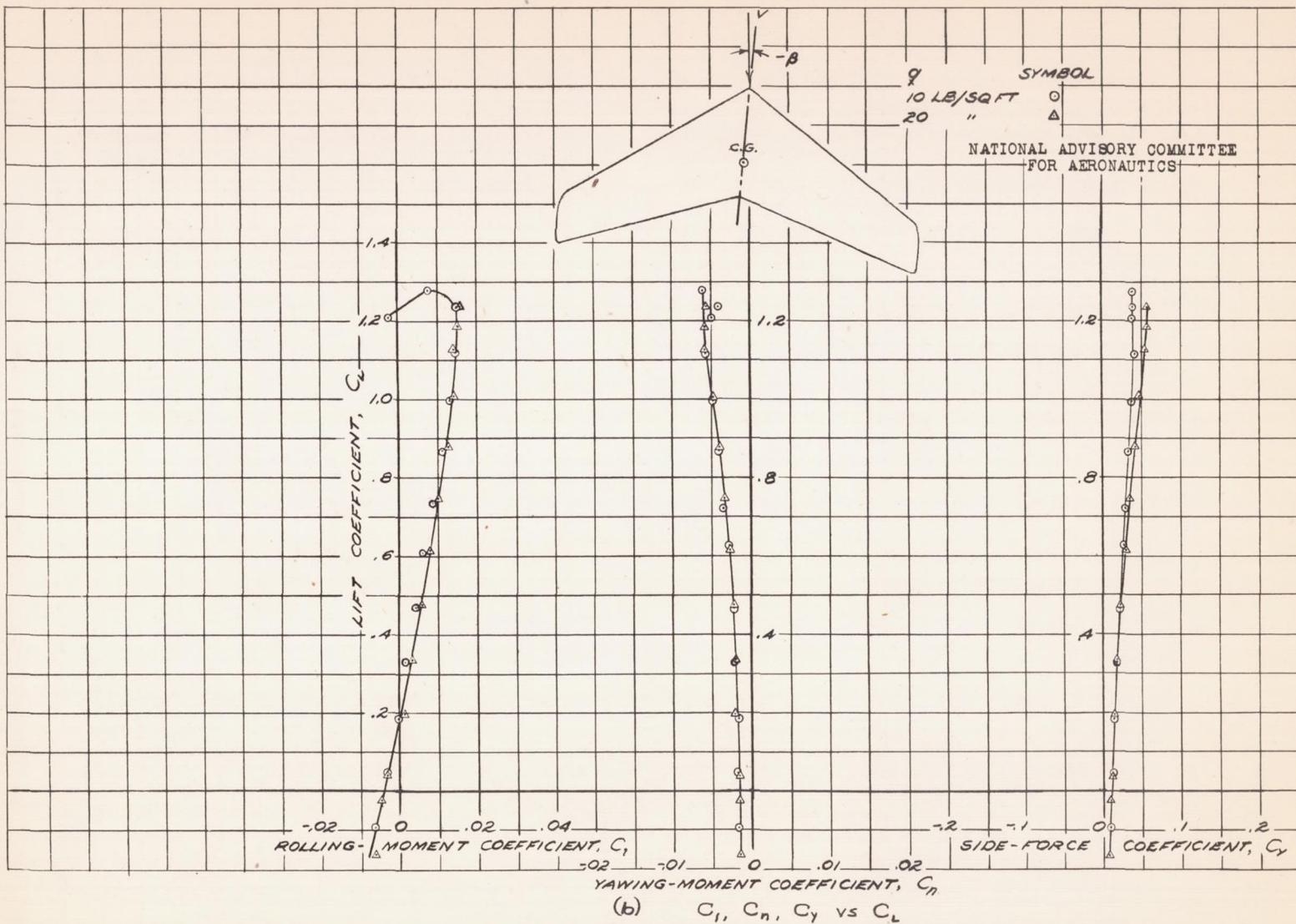


FIGURE 68.- CONCLUDED.

Fig. 69a

NACA RM No. A6K15

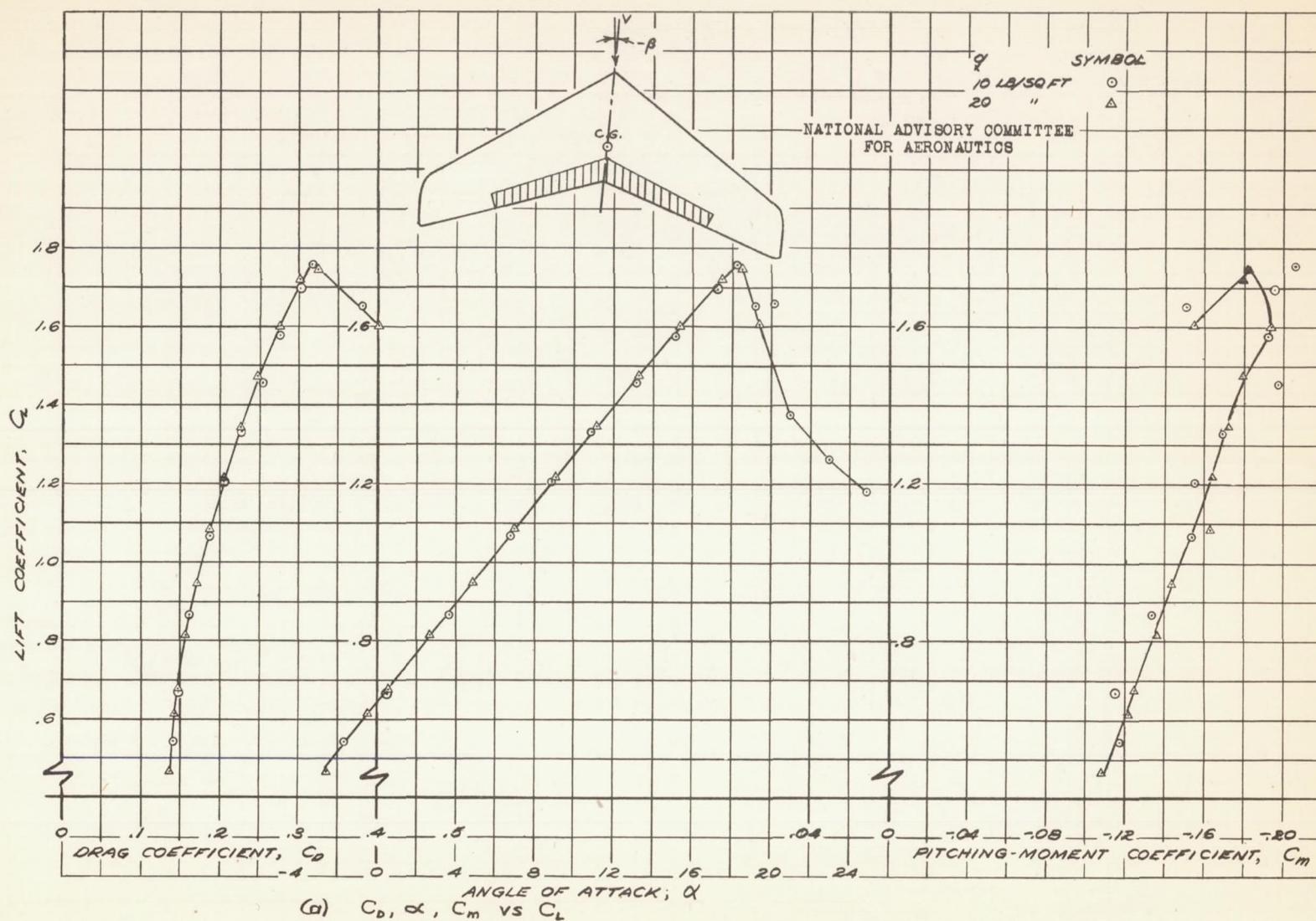


FIGURE 69.— AERODYNAMIC CHARACTERISTICS OF THE 30° SWEEPBACK WING AT -5.3° SIDESLIP. 20% CHORD 62.3% SPAN SPLIT FLAPS DEFLECTED 60°

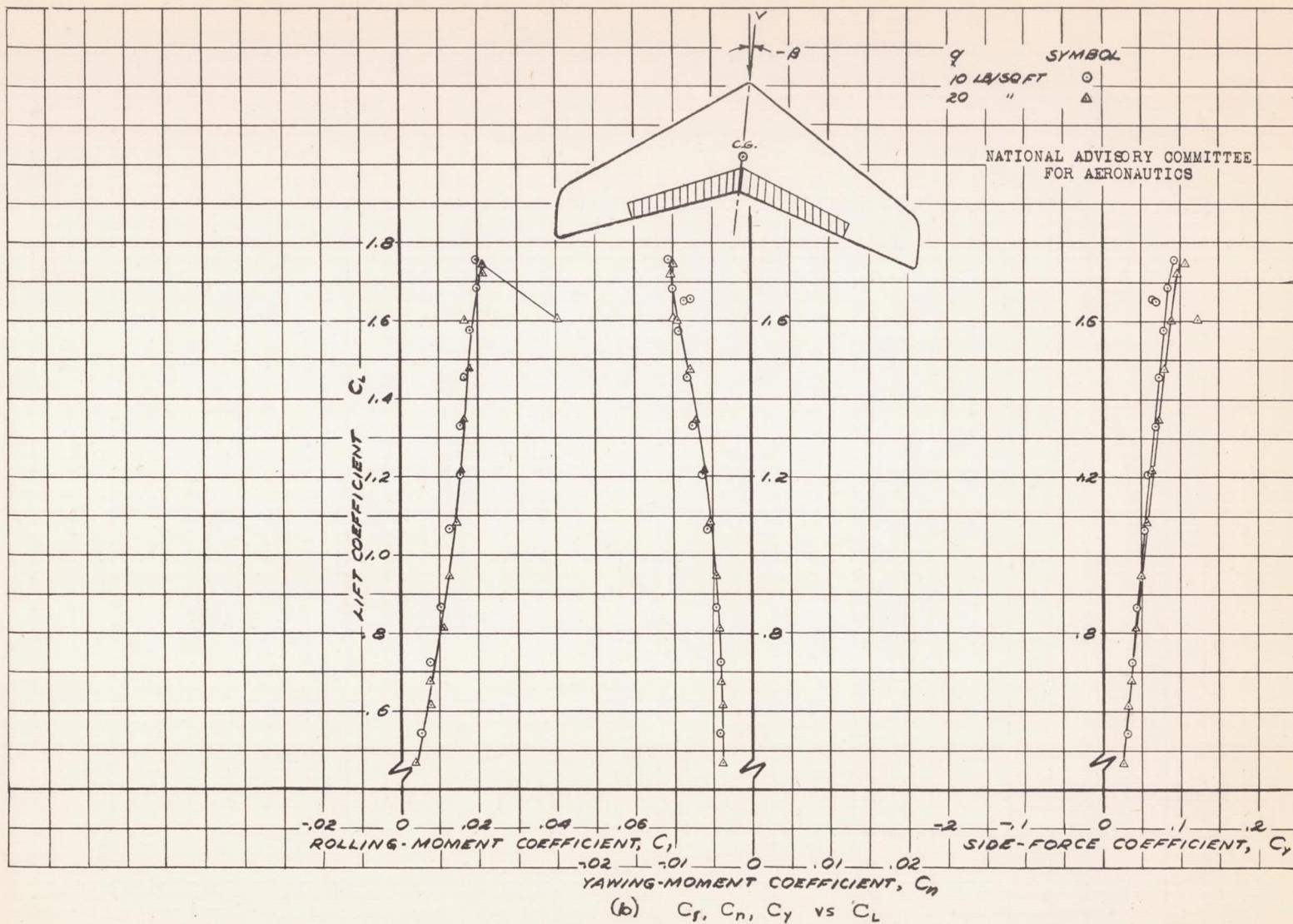


FIGURE 69.- CONCLUDED.

Fig. 70a

NACA RM No. A6K15

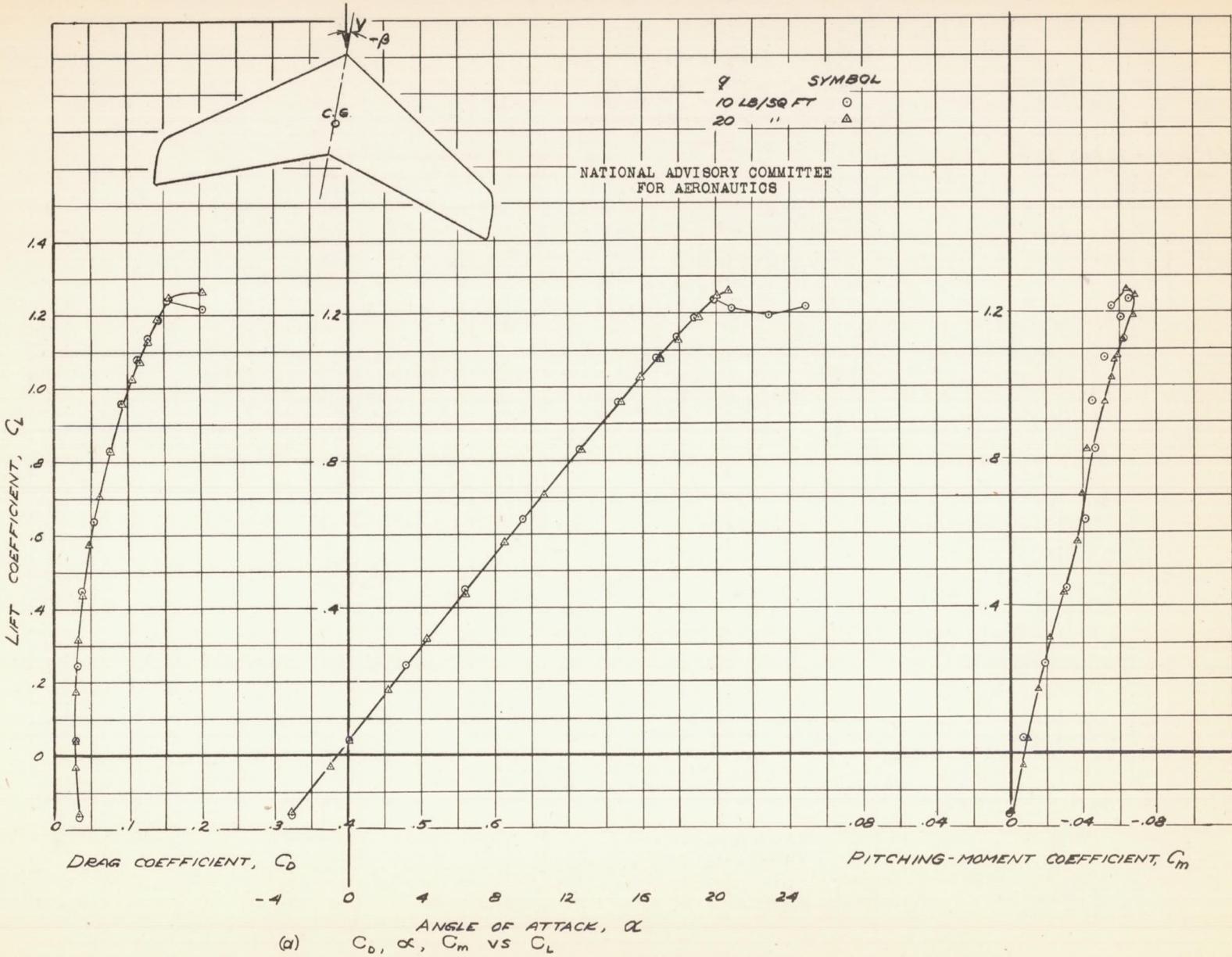


FIGURE 70.- AERODYNAMIC CHARACTERISTICS OF THE 30° SWEEPBACK WING AT -9.5° SIDESLIP. PLAIN WING.

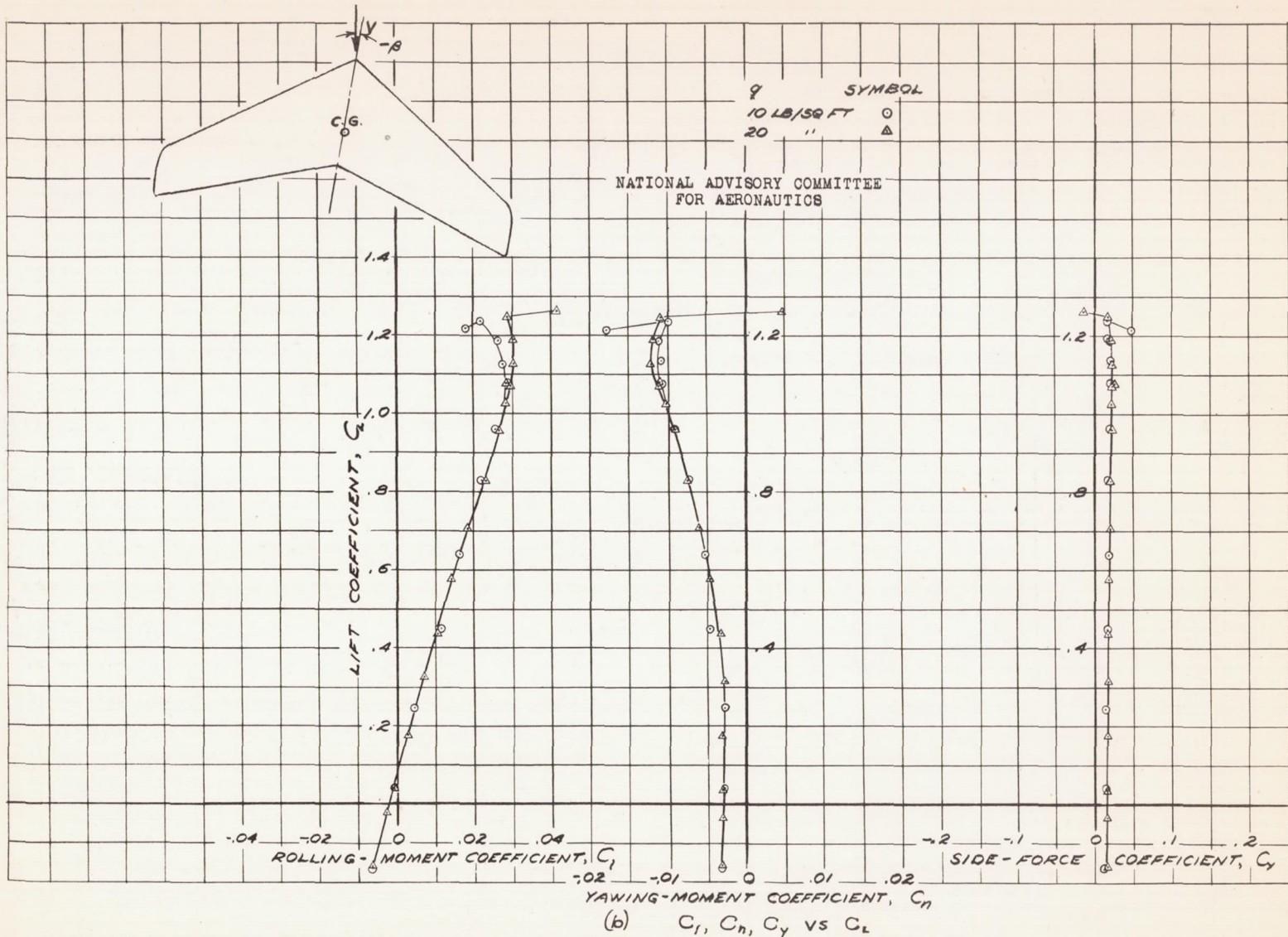


FIGURE 70.— CONCLUDED.

Fig. 71a

NACA RM No. A6K15

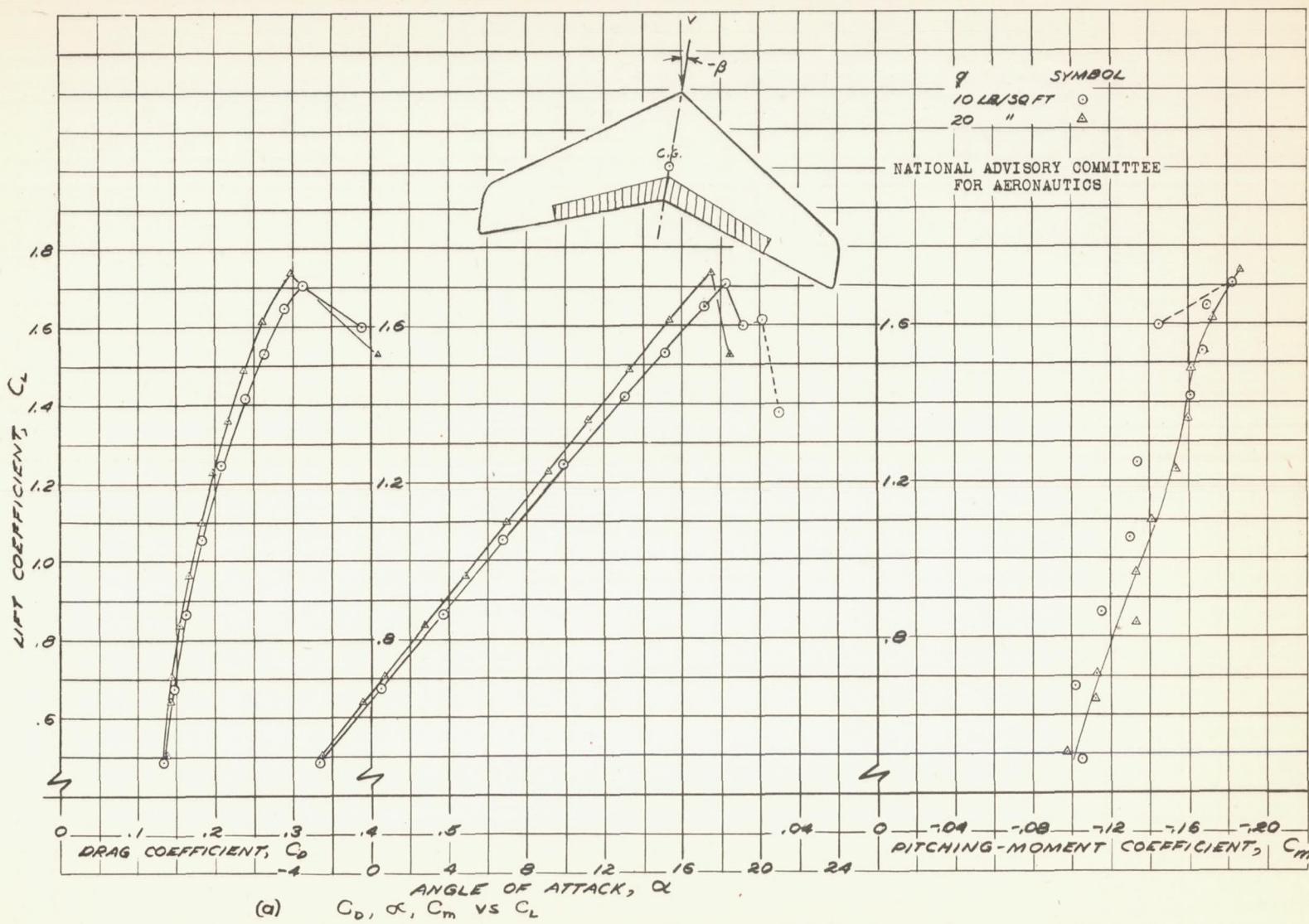


FIGURE 71.— AEROODYNAMIC CHARACTERISTICS OF THE 30° SWEEPTBACK WING AT -9.5° SIDESLIP 20% CHORD 62.3% SPAN SPLIT FLAPS DEFLECTED 60°

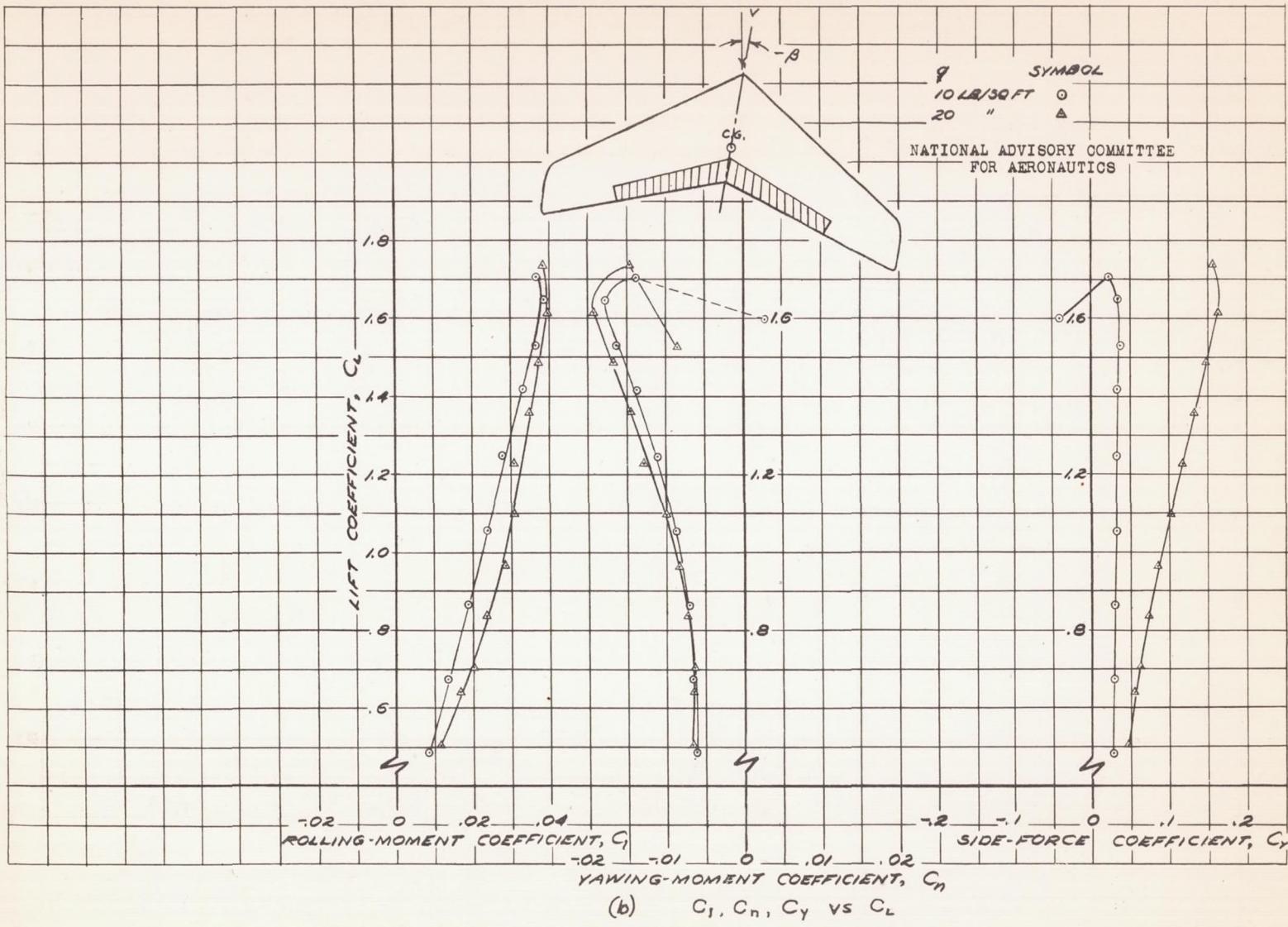


Fig. 72a

NACA RM NO. A6K15

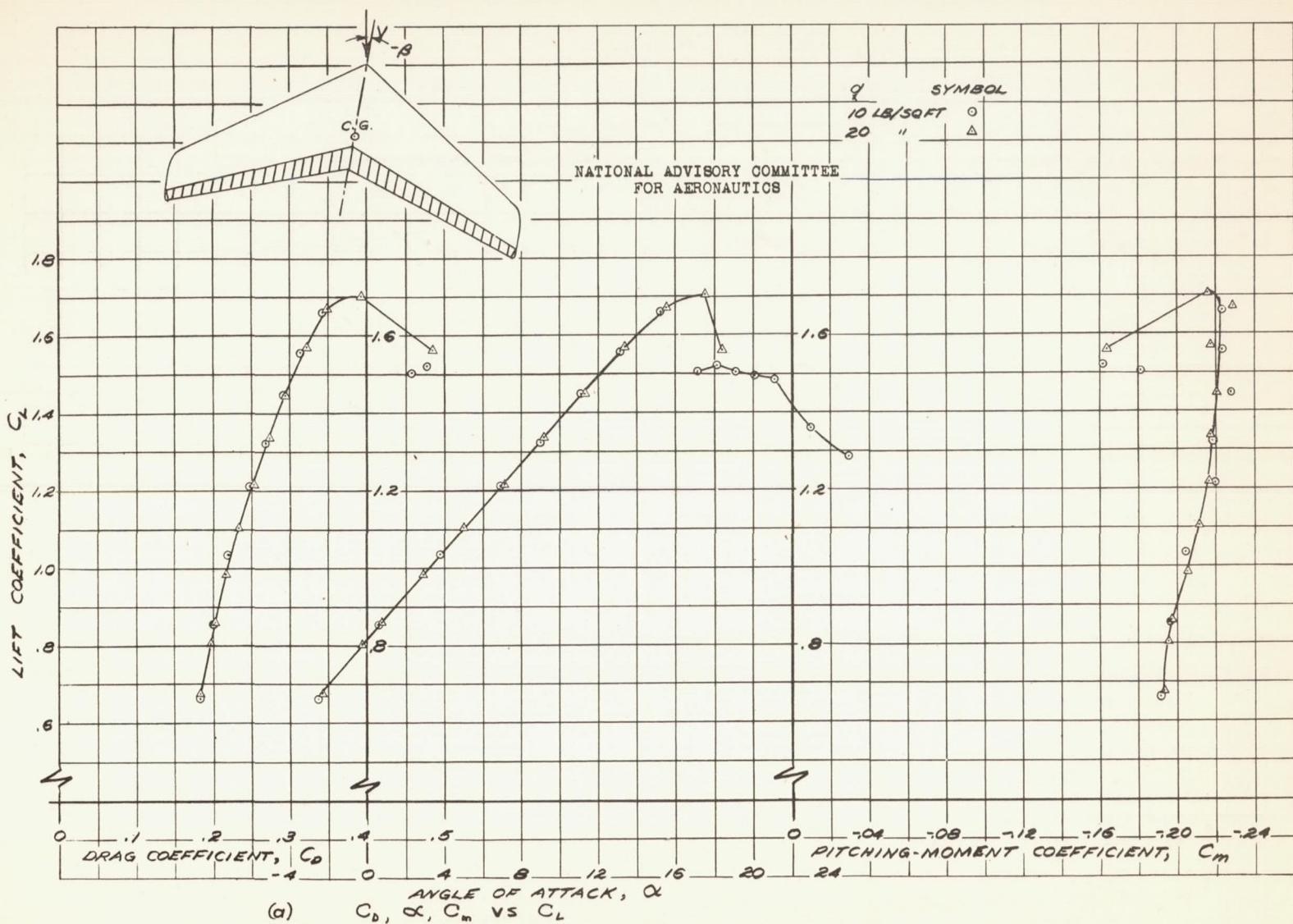


FIGURE 72.— AERODYNAMIC CHARACTERISTICS OF THE 30°
SWEEPBACK WING AT -9.5° SIDESLIP, 20% CHORD
FULL SPAN SPLIT FLAPS DEFLECTED 60°.

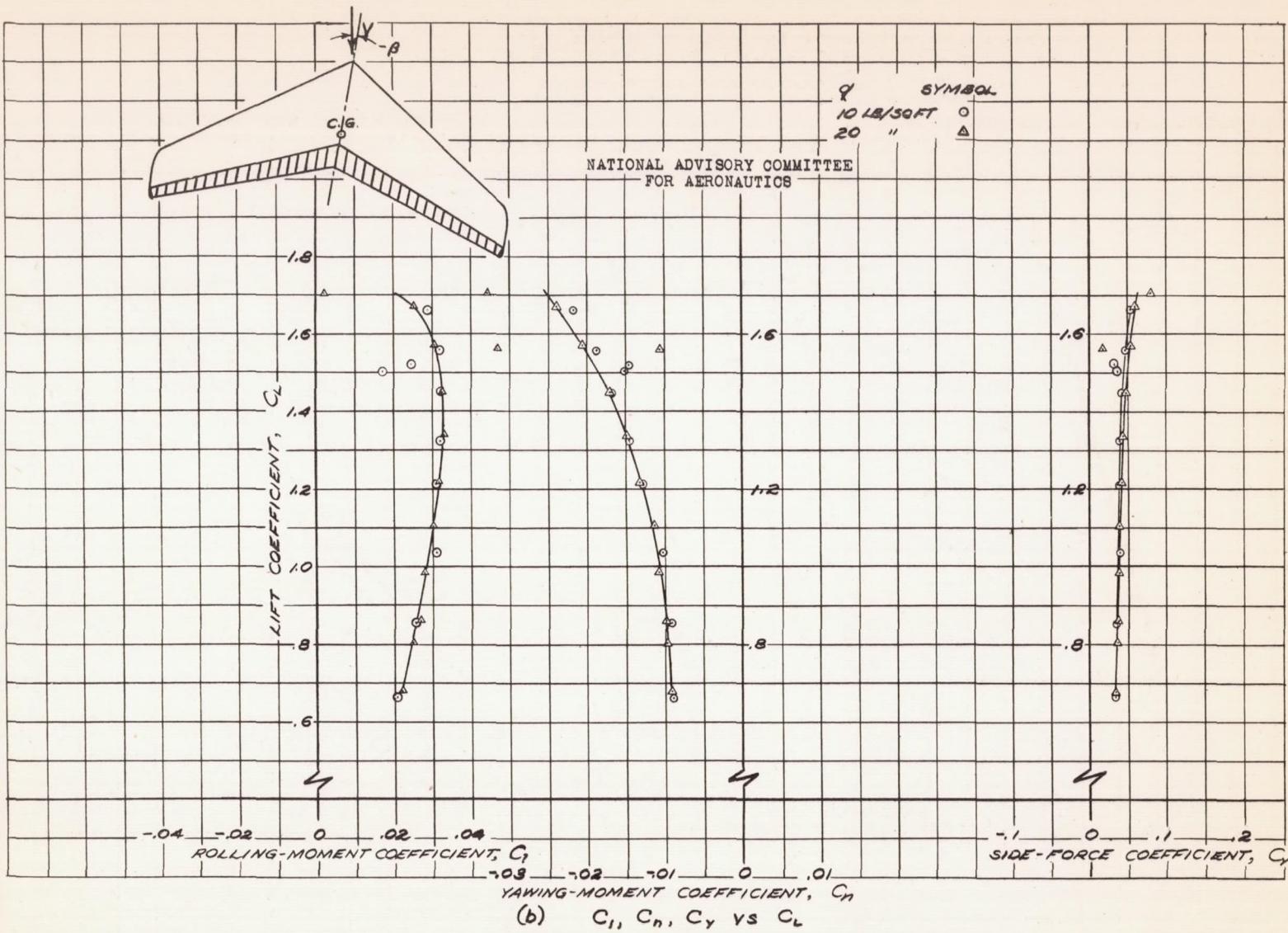


Fig. 73

NACA RM No. A6K15

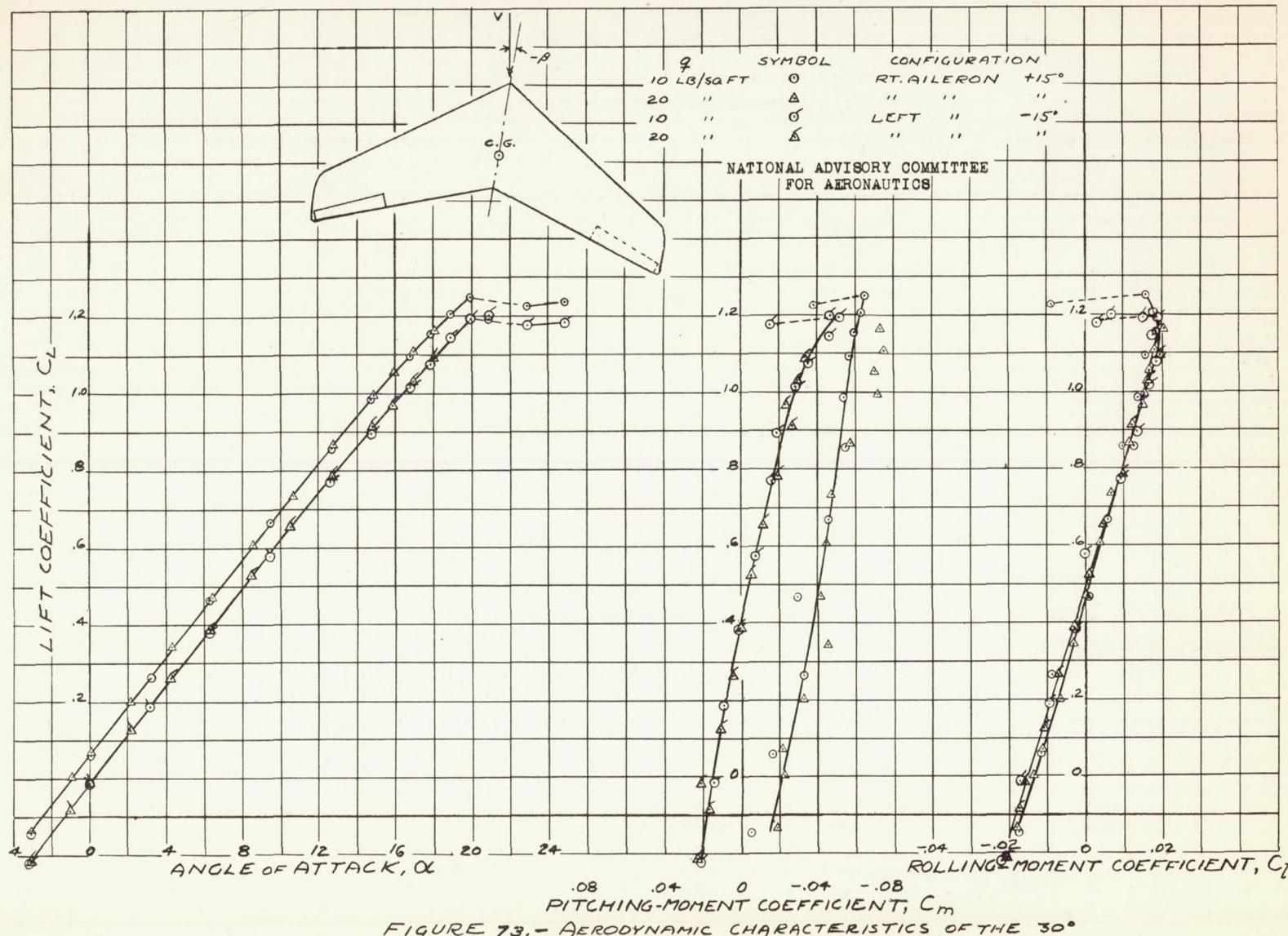


FIGURE 73.—AERODYNAMIC CHARACTERISTICS OF THE 30° SWEEPBACK WING AT -9.5° SIDESLIP, 20% CHORD 36.8% SPAN SPLIT FLAP TYPE AILERONS DEFLECTED $\pm 15^\circ$

Fig. 74a

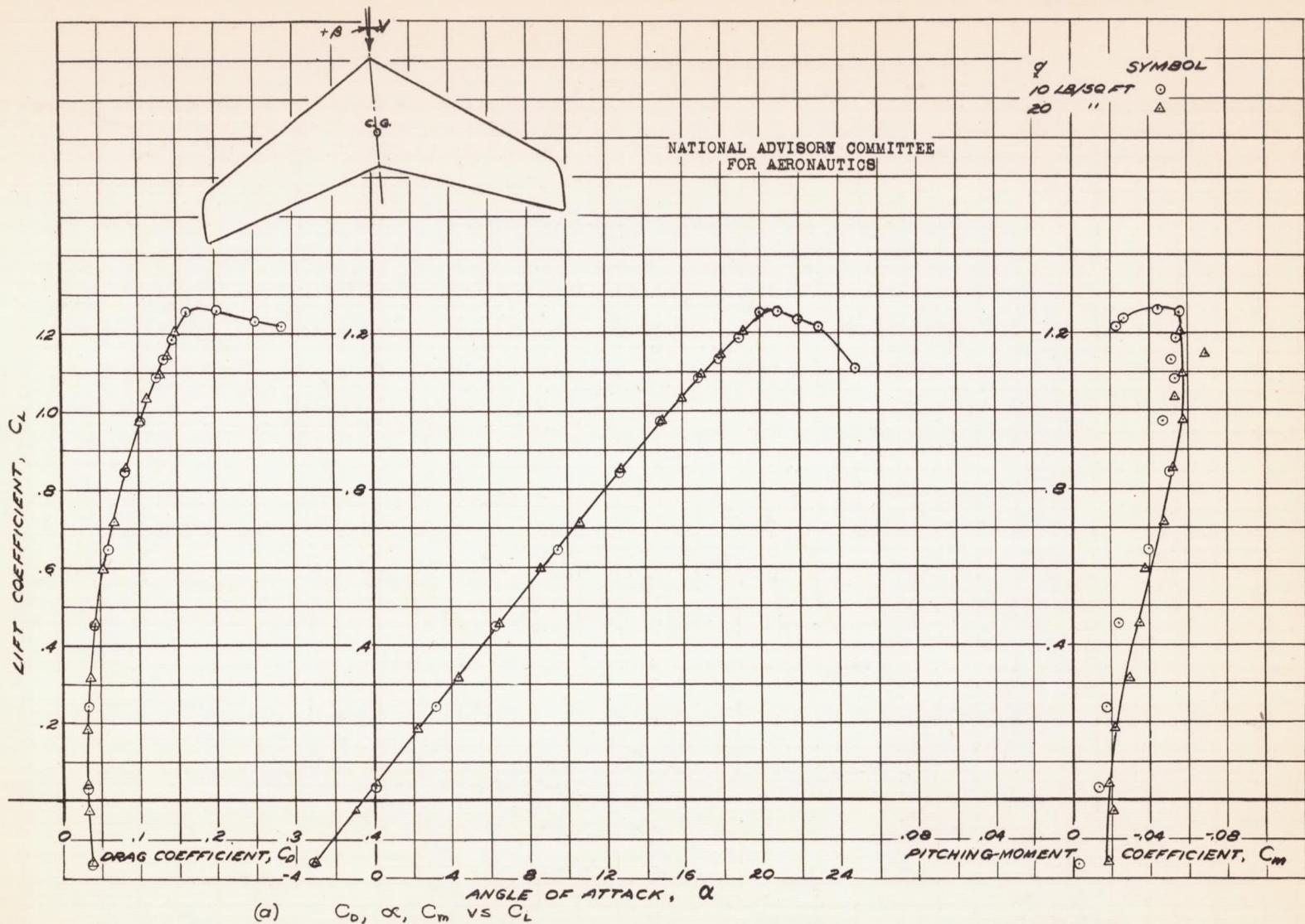
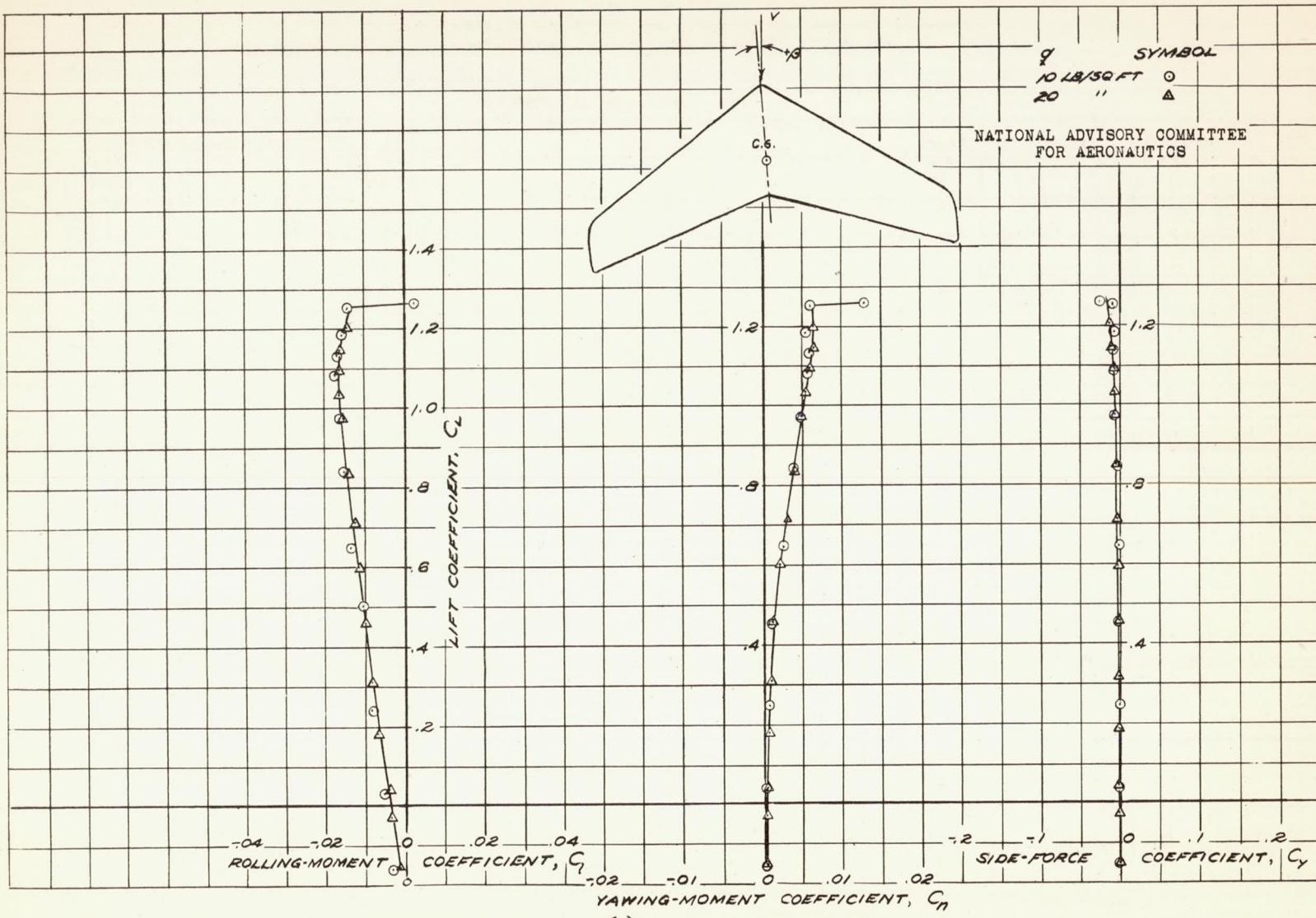


FIGURE 74.— AERODYNAMIC CHARACTERISTICS OF THE 30° SWEEPBACK WING AT +4.1° SIDESLIP, PLAIN WING.

Fig. 74b

NACA RM No. A6K15



(b) C_I, C_n, C_y vs C_L

FIGURE 74.— CONCLUDED.

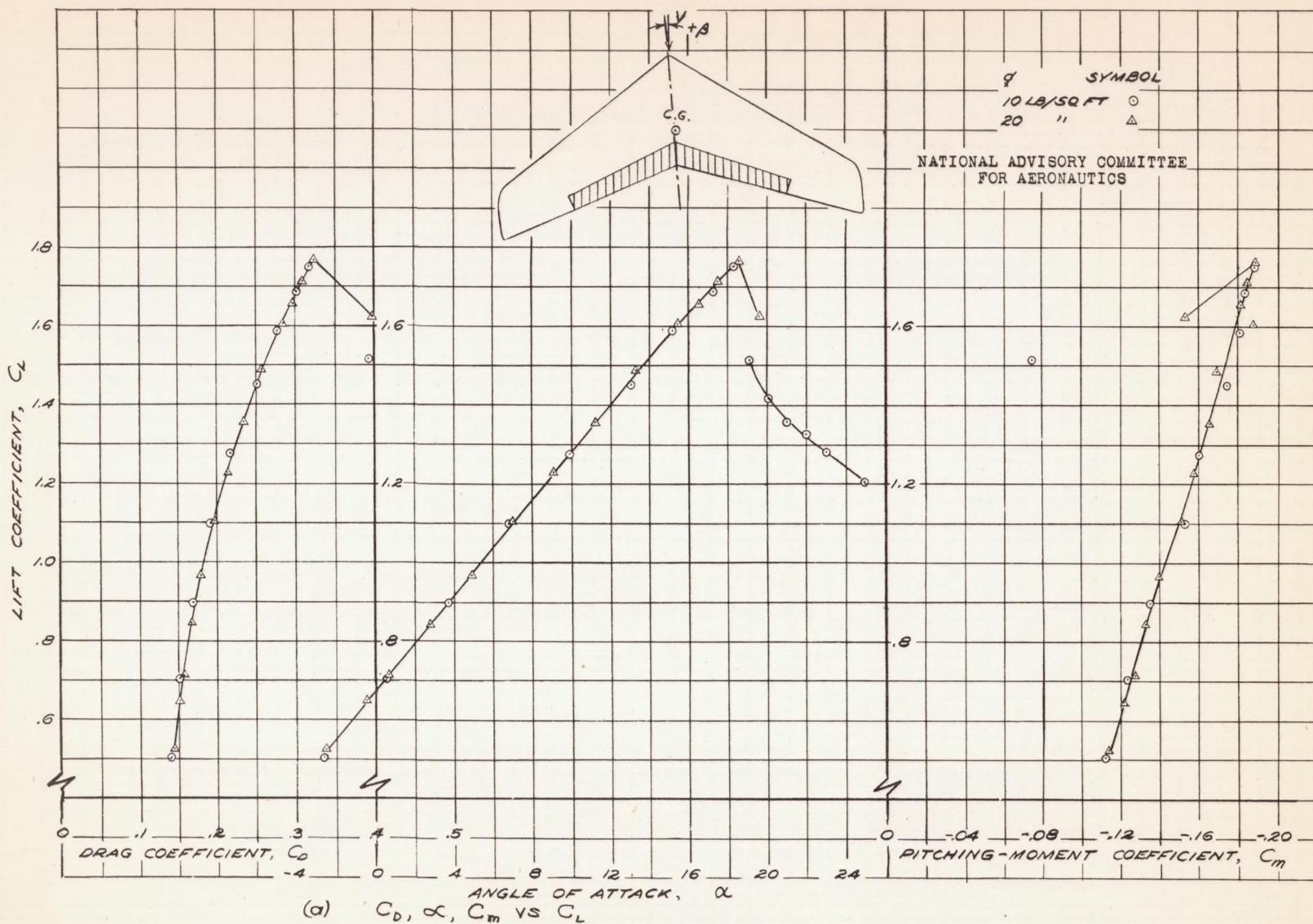
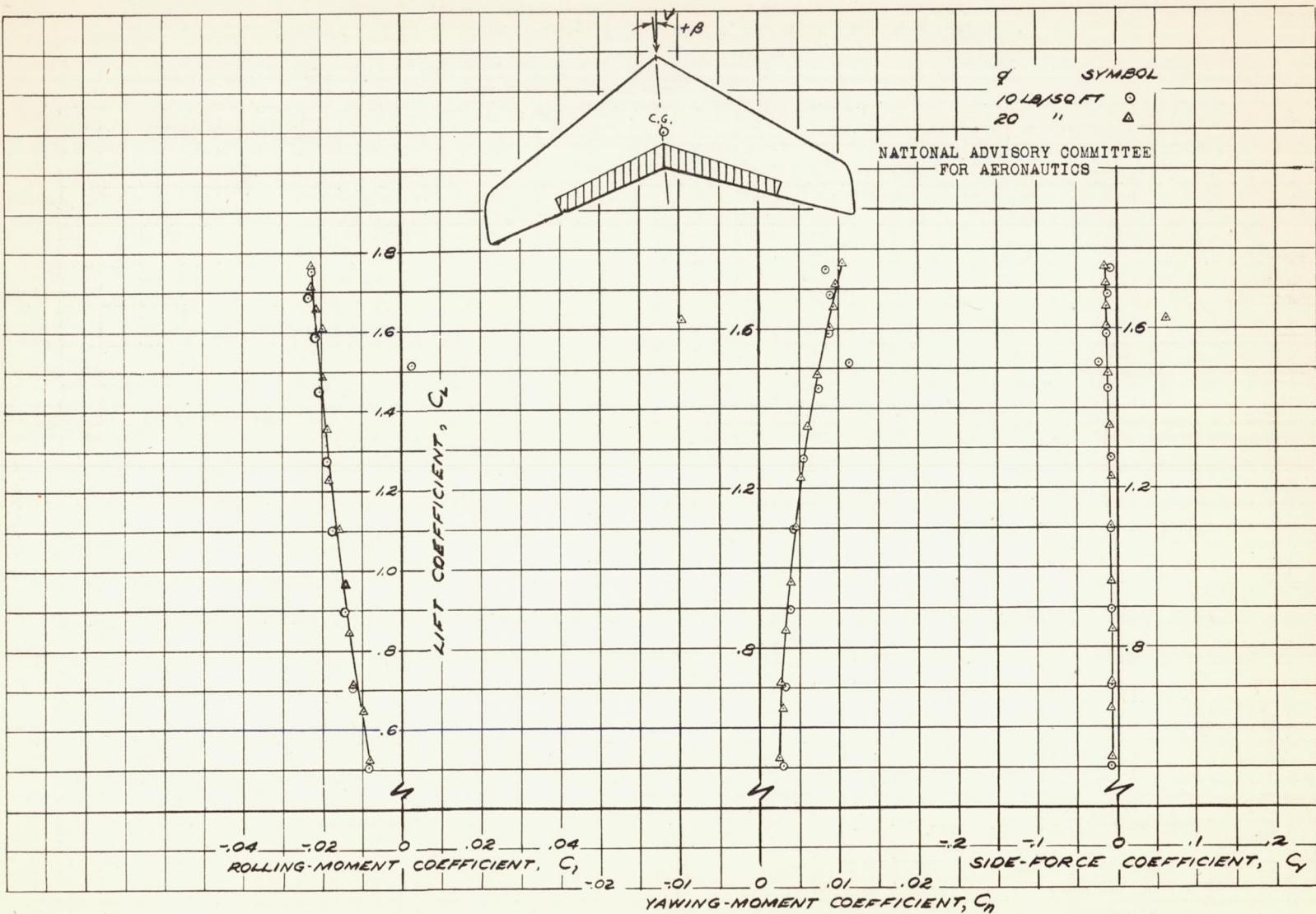


FIGURE 75.— AEROdynamic CHARACTERISTICS OF THE 30° SWEEPBACK WING AT +4.1° SIDESLIP 20% CHORD 62.3% SPAN SPLIT FLAPS DEFLECTED 60°

Fig. 75b

NACA RM No. A6K15



(b) C_L, C_n, C_y vs C_L

FIGURE 75.— CONCLUDED.

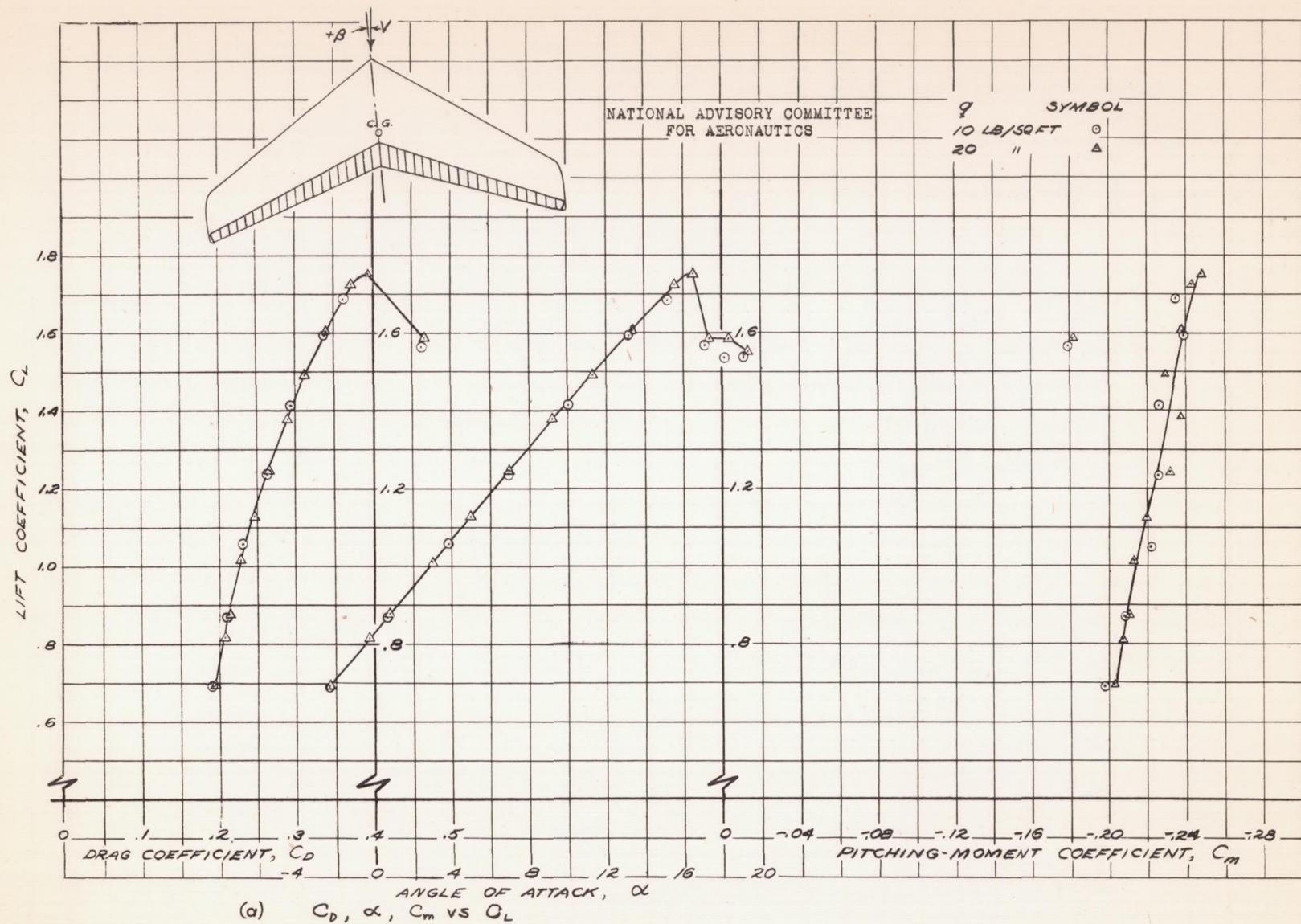


FIGURE 76.- AEROdynamic CHARACTERISTICS OF THE 30° SWEEPBACK WING AT +4.1° SIDESLIP. 20% CHORD FULL SPAN SPLIT FLAPS DEFLECTED 60°.

Fig. 76b

NACA RM No. A6K15

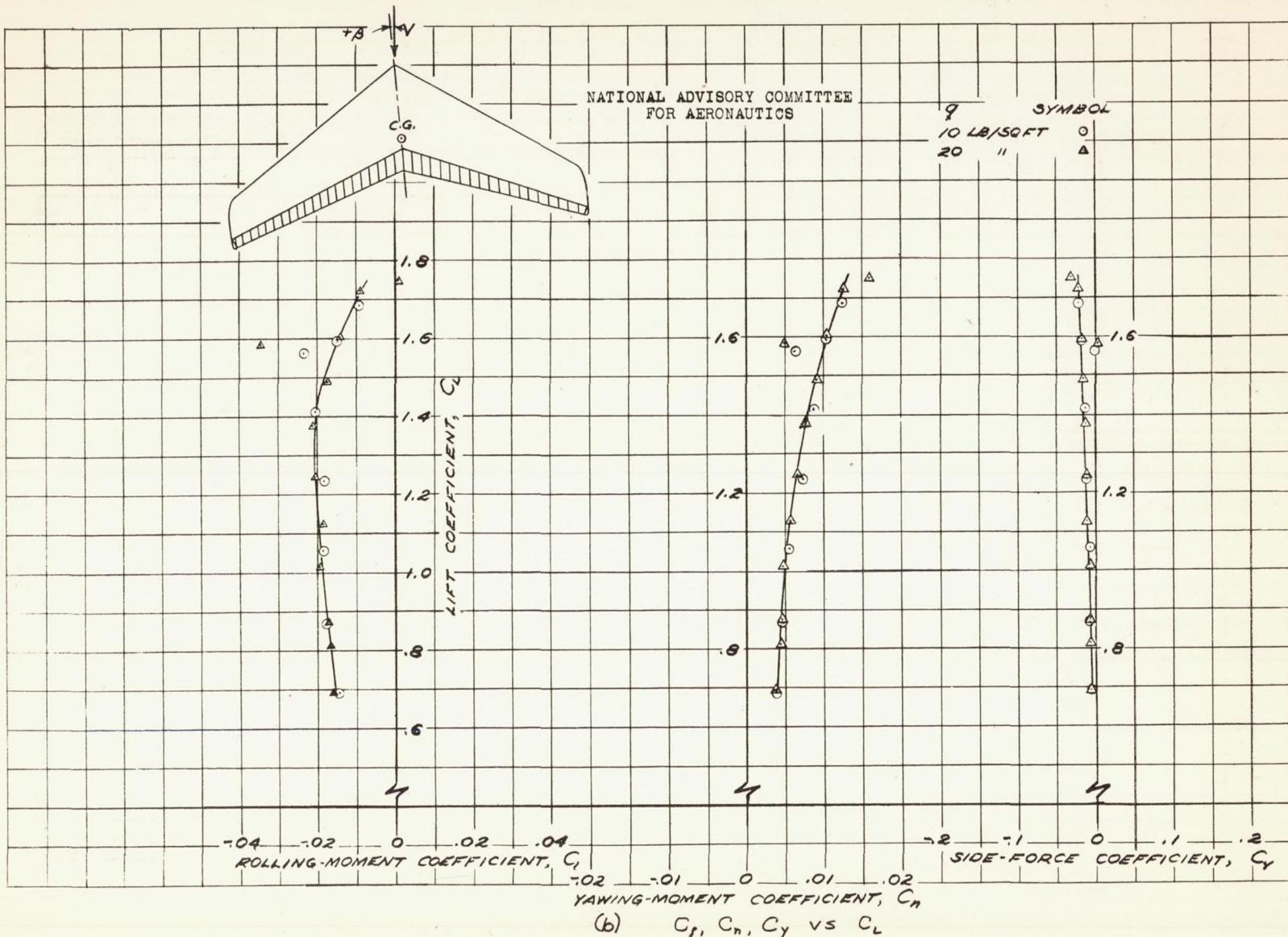


FIGURE 76.- CONCLUDED.

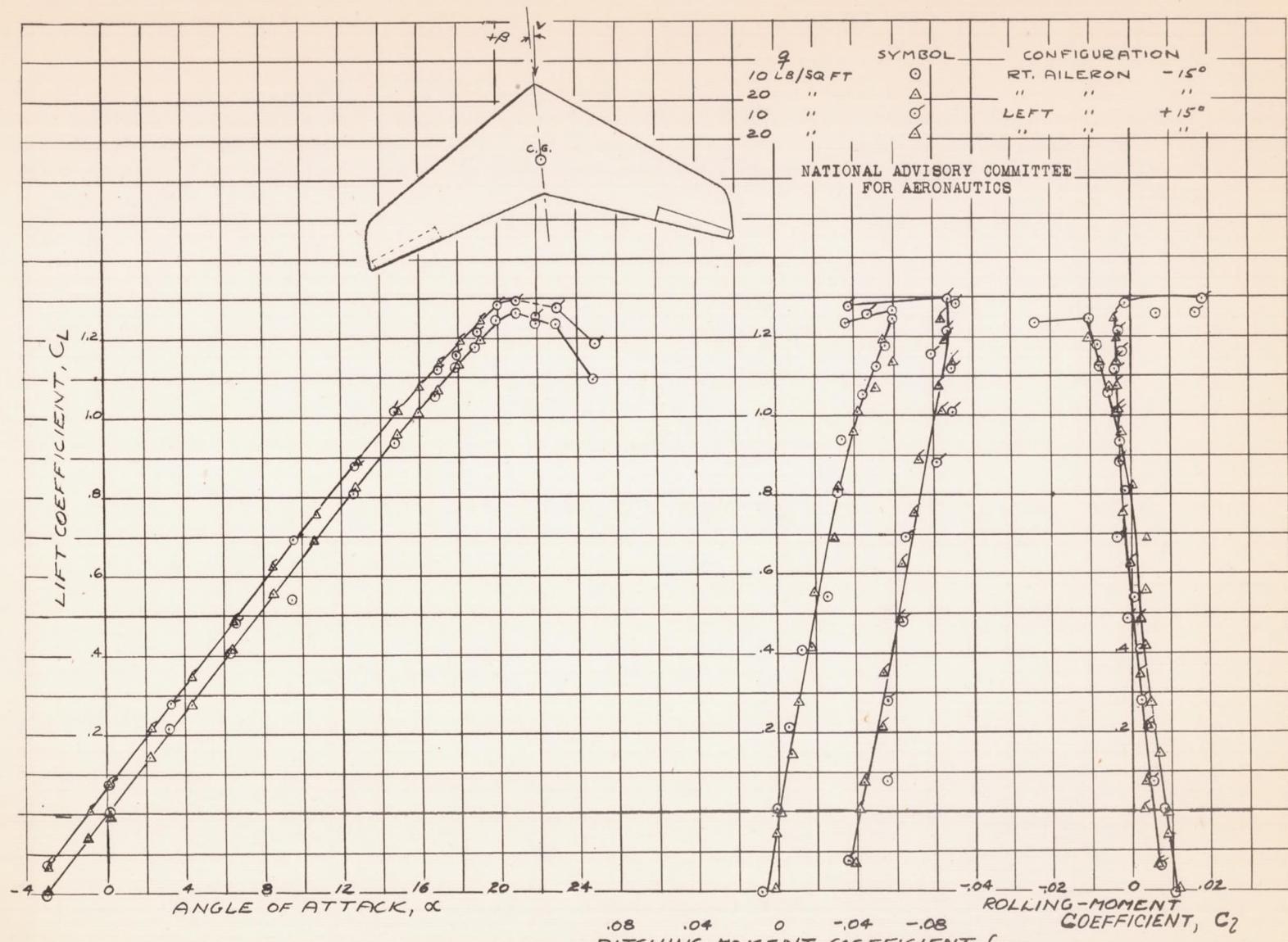


FIGURE 77—AERODYNAMIC CHARACTERISTICS OF THE 30°
SWEPT BACK WING AT $+4.10$ SIDESLIP, 20% CHORD
36.8% SPAN SPLIT FLAP TYPE AILERONS DEFLECTED $\pm 15^\circ$

Fig. 78a

NACA RM No. A6K15

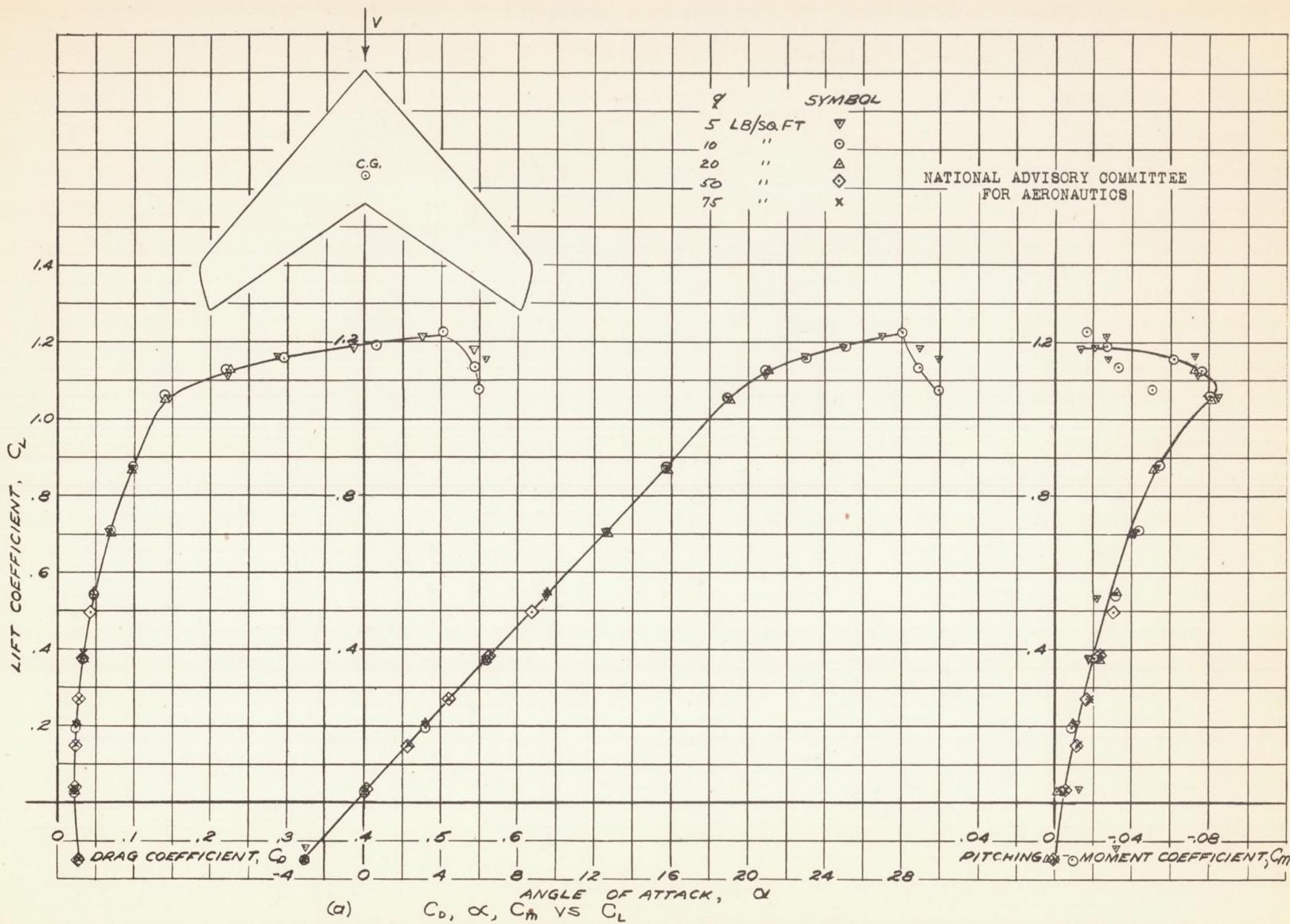


FIGURE 78.-AERODYNAMIC CHARACTERISTICS OF THE 45° SWEEPBACK WING AT -0.1° SIDESLIP. PLAIN WING.

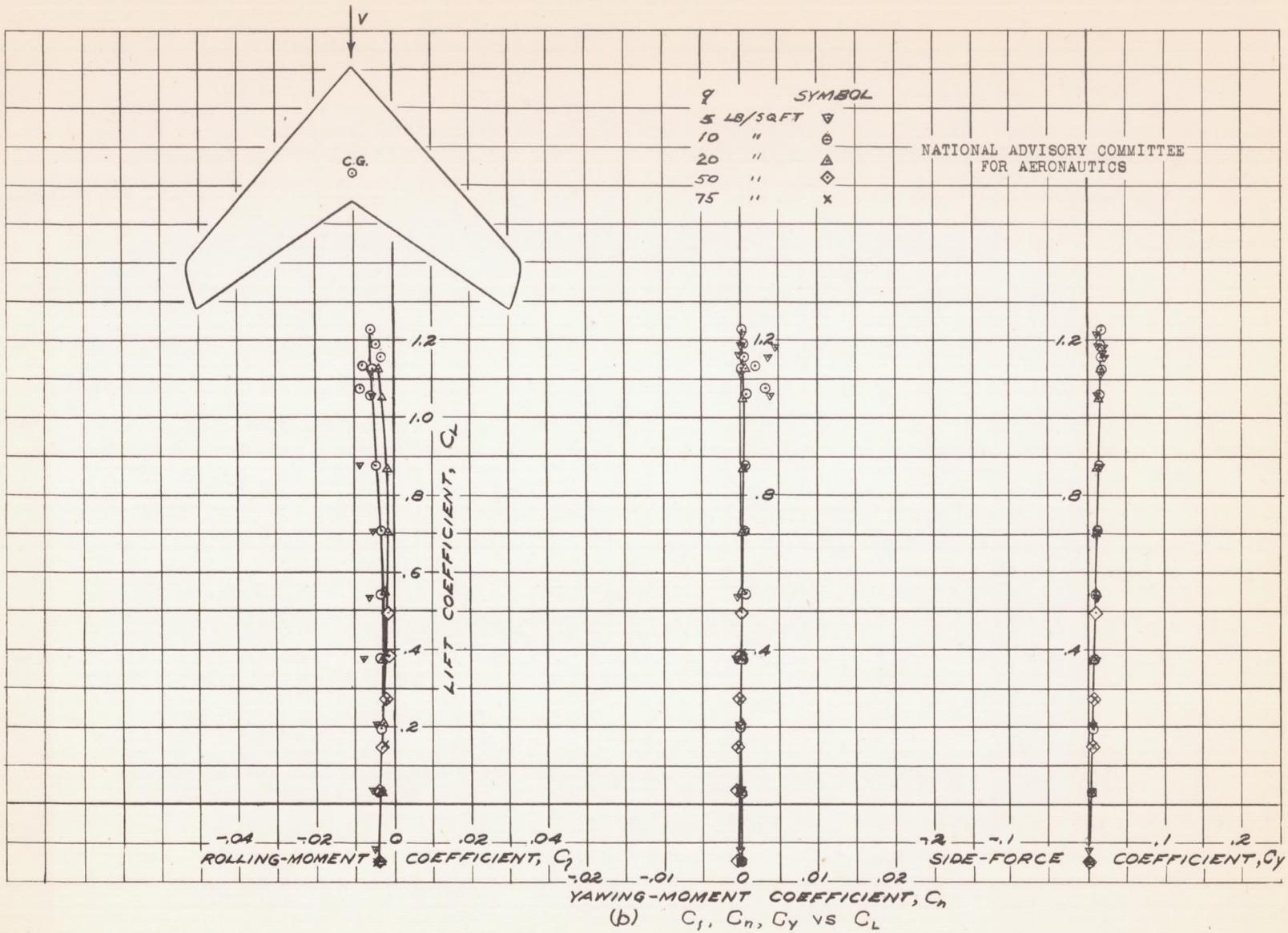


FIGURE 78.-CONCLUDED.

Fig. 79a

NACA RM No. A6K15

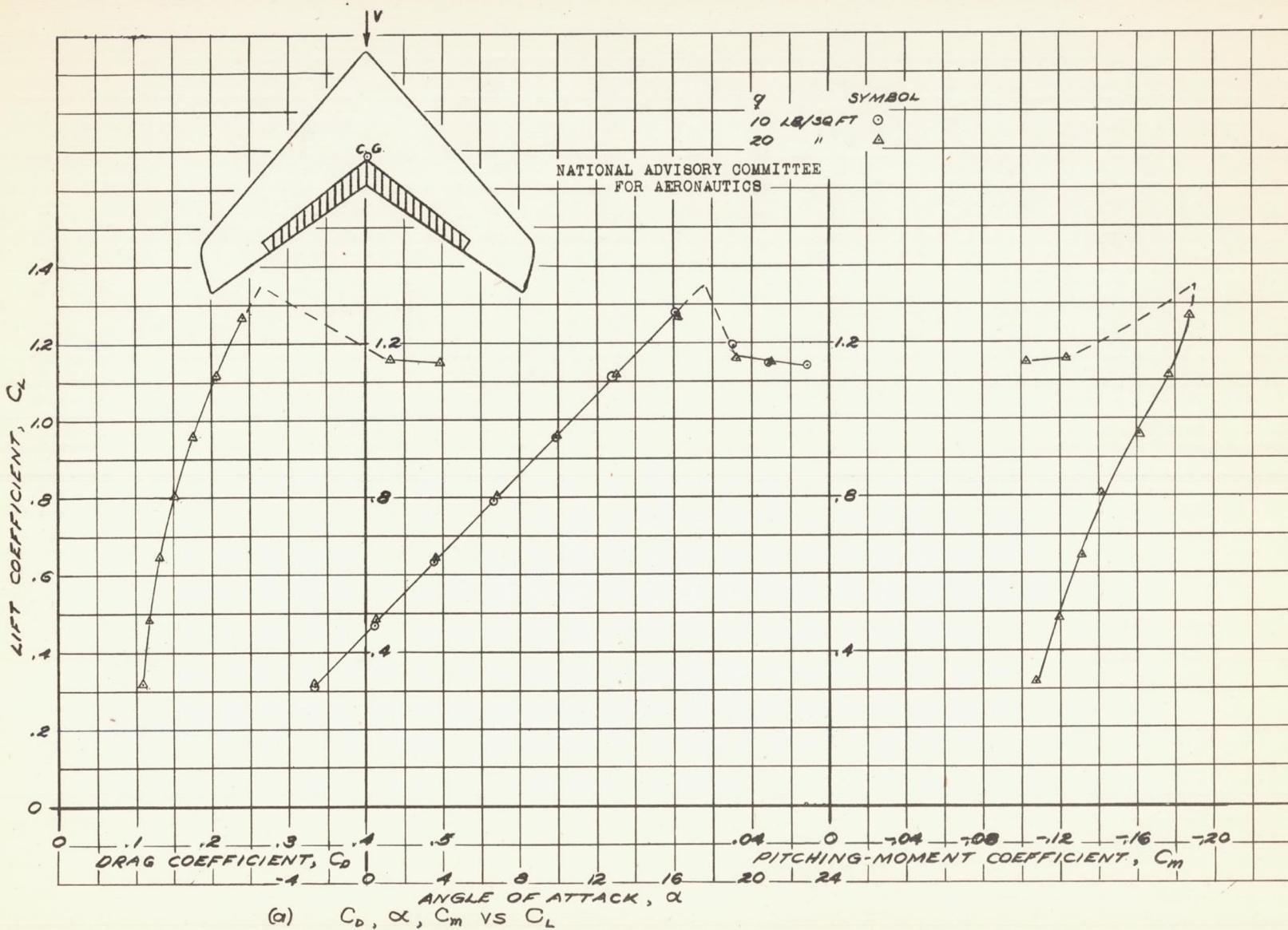


FIGURE 79.—AERODYNAMIC CHARACTERISTICS OF THE 45° SWEEPBACK WING AT -0.1° SIDESLIP, 20% CHORD 62.3% SPAN SPLIT FLAPS DEFLECTED 60°

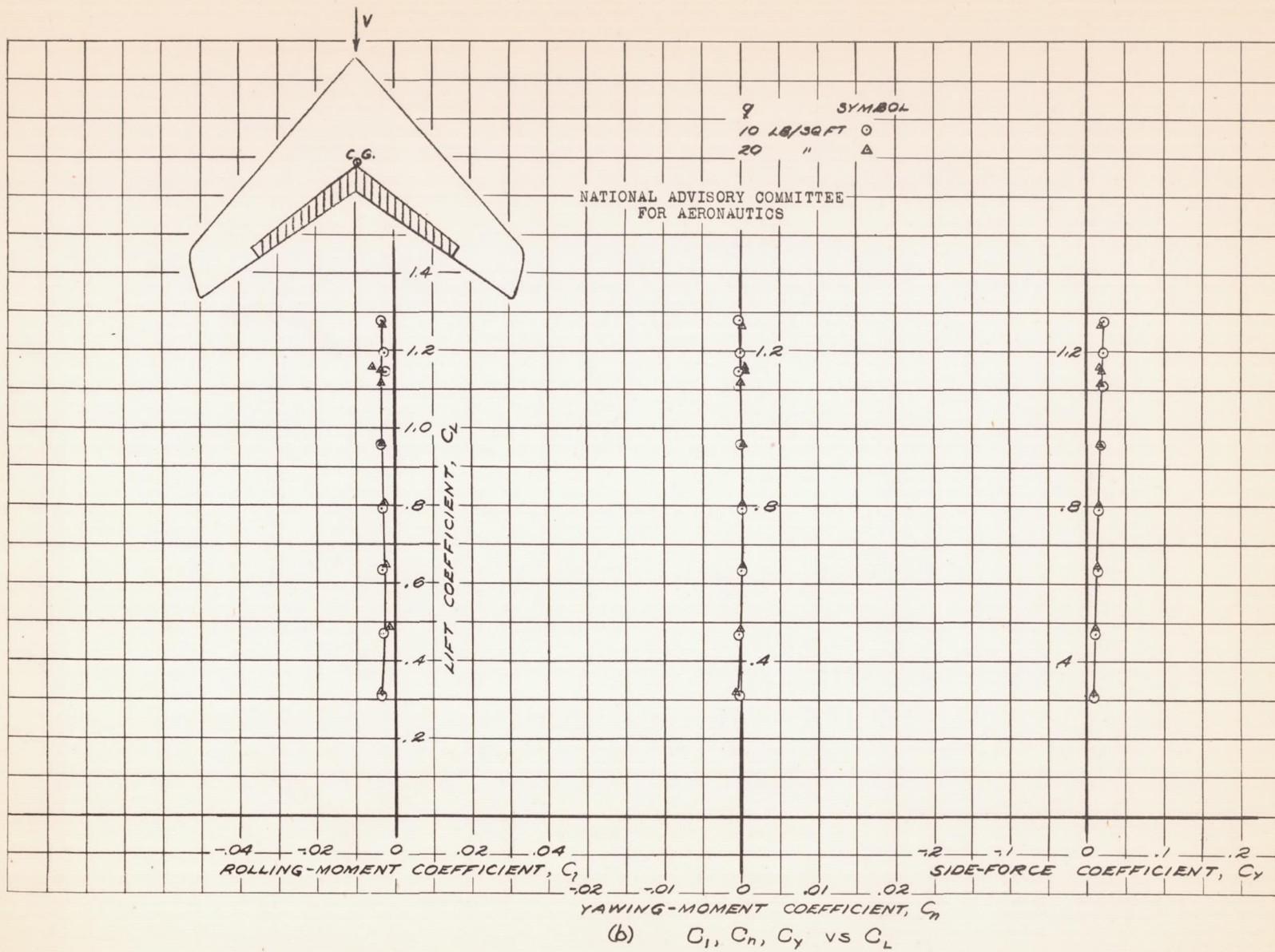


Fig. 80a

NACA RM No. A6K15

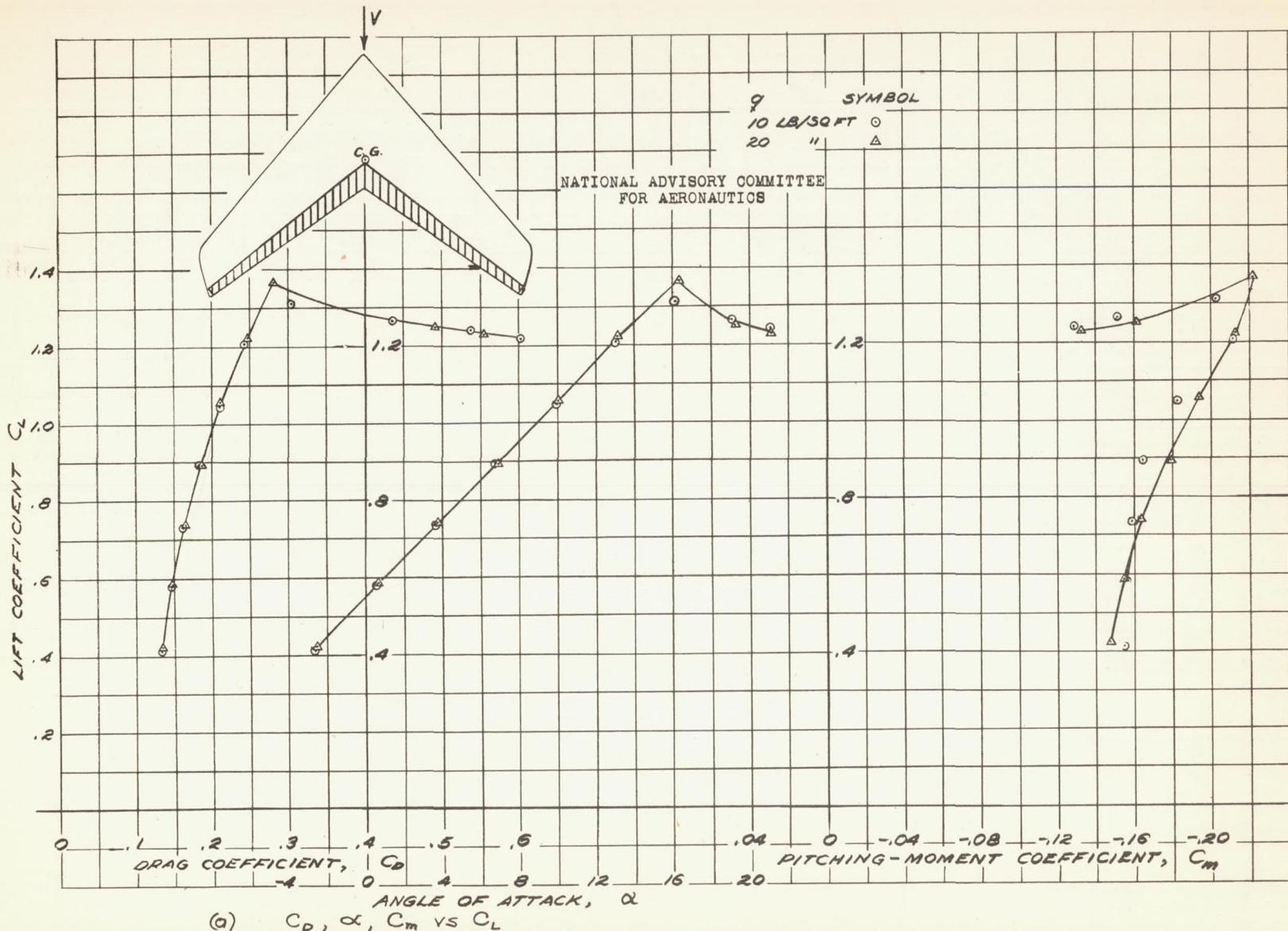


FIGURE 80.—AERODYNAMIC CHARACTERISTICS OF THE 45°
SWEPTBACK WING AT -0.1° SIDESLIP, 20% CHORD
FULL SPAN SPLIT FLAPS DEFLECTED 60°

Fig. 80b

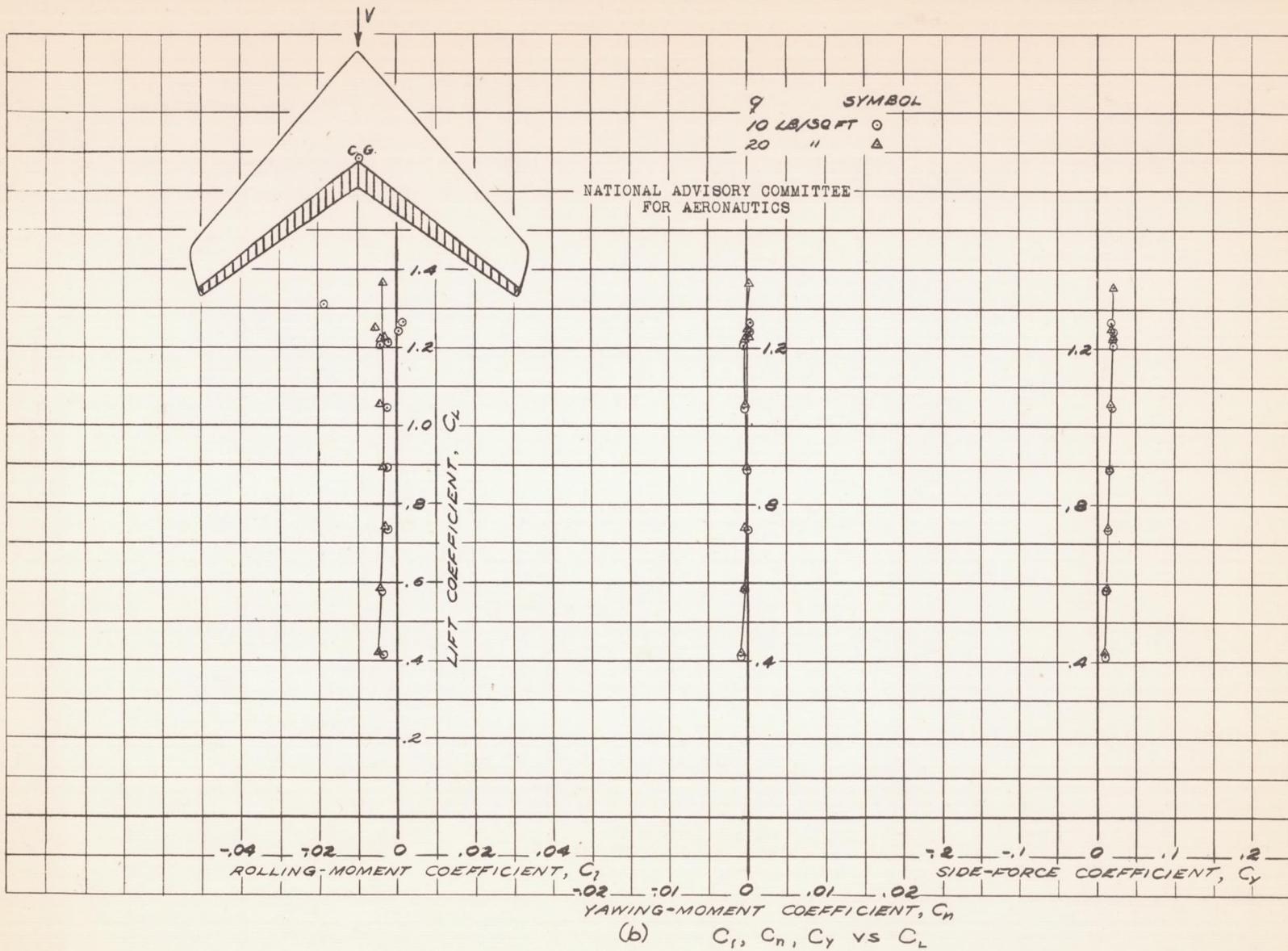


FIGURE 80.- CONCLUDED.

Fig. 81

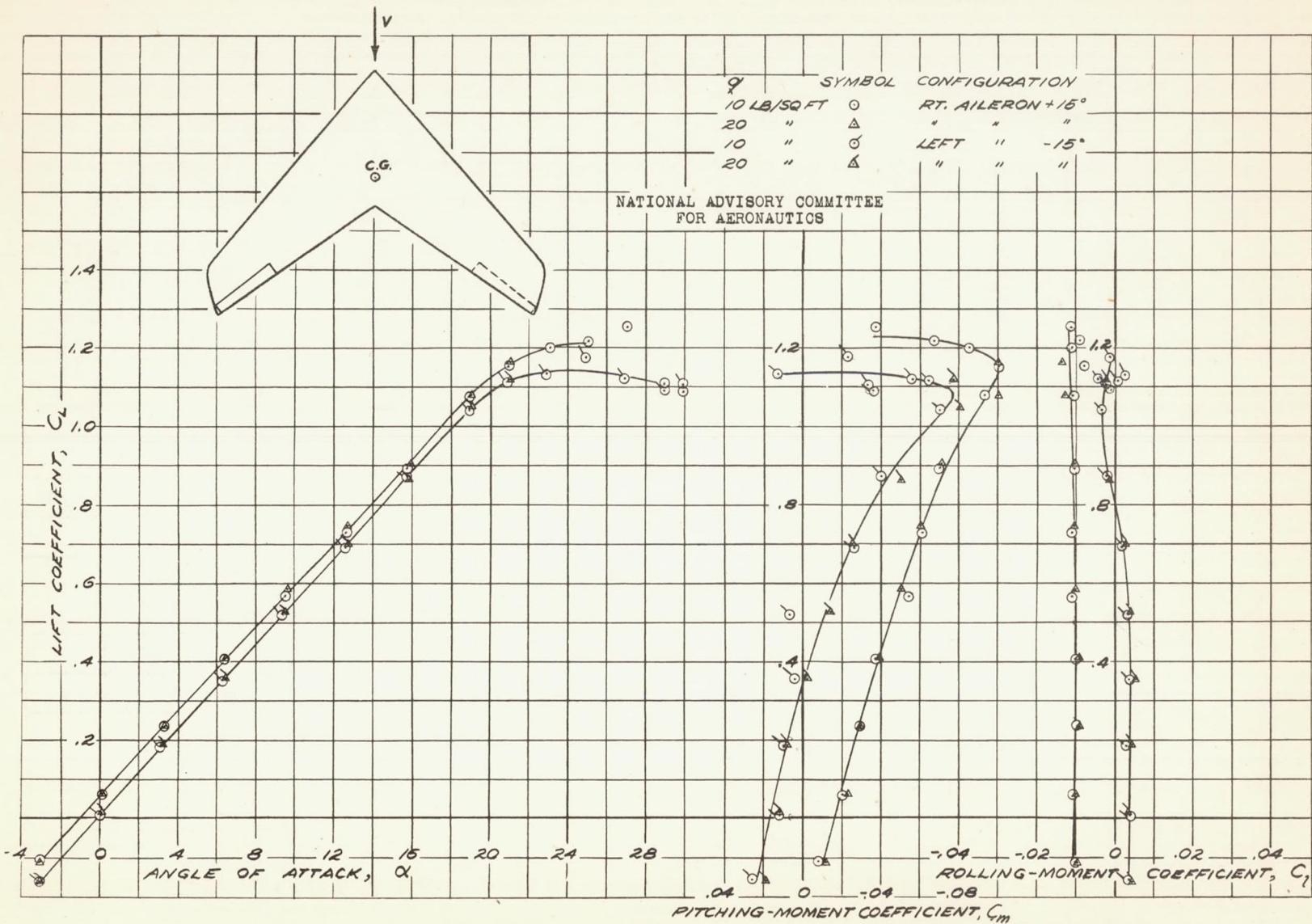


FIGURE 81.— AERODYNAMIC CHARACTERISTICS OF THE 15° SWEEPBACK WING AT -0.1° SIDESLIP, 20% CHORD 34.1% SPAN SPLIT FLAP TYPE AILERONS DEFLECTED $\pm 15^\circ$

NACA RM No. A6K15

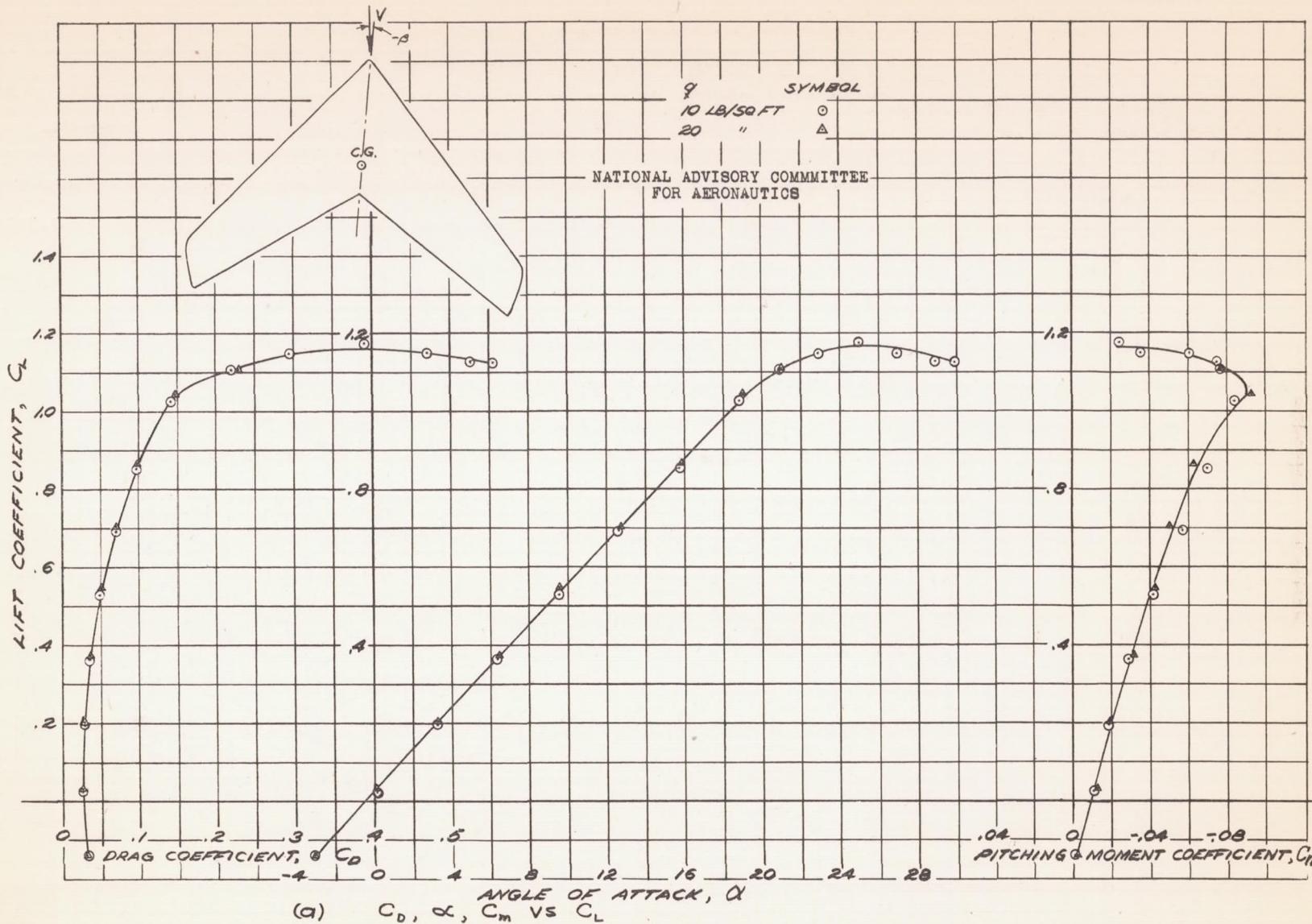


FIGURE 82.- AERODYNAMIC CHARACTERISTICS OF THE 45° SWEEPBACK WING AT -5.2° SIDESLIP, PLAIN WING.

Fig. 82b

NACA RM No. A6K15

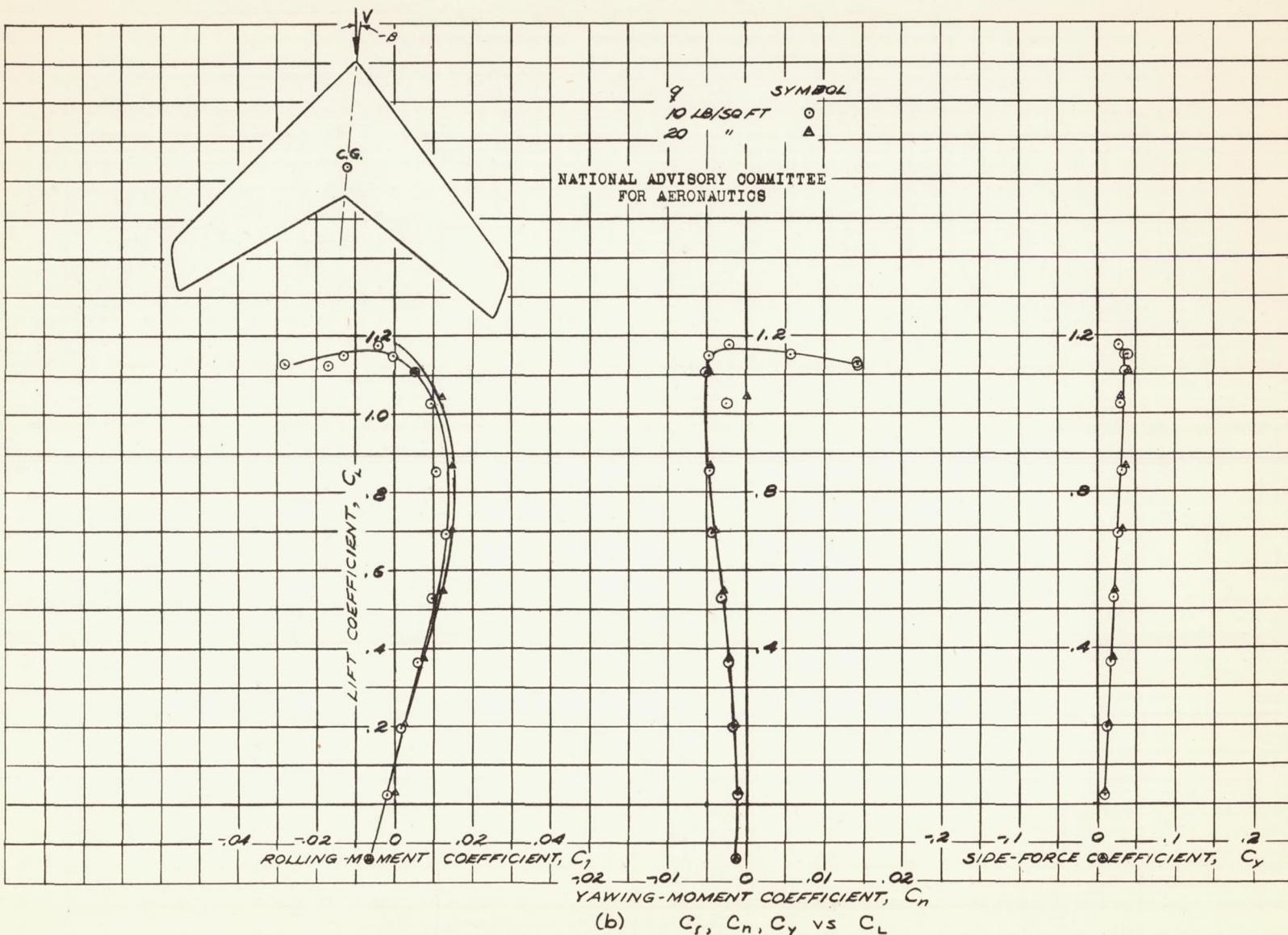


FIGURE 82. - CONCLUDED.

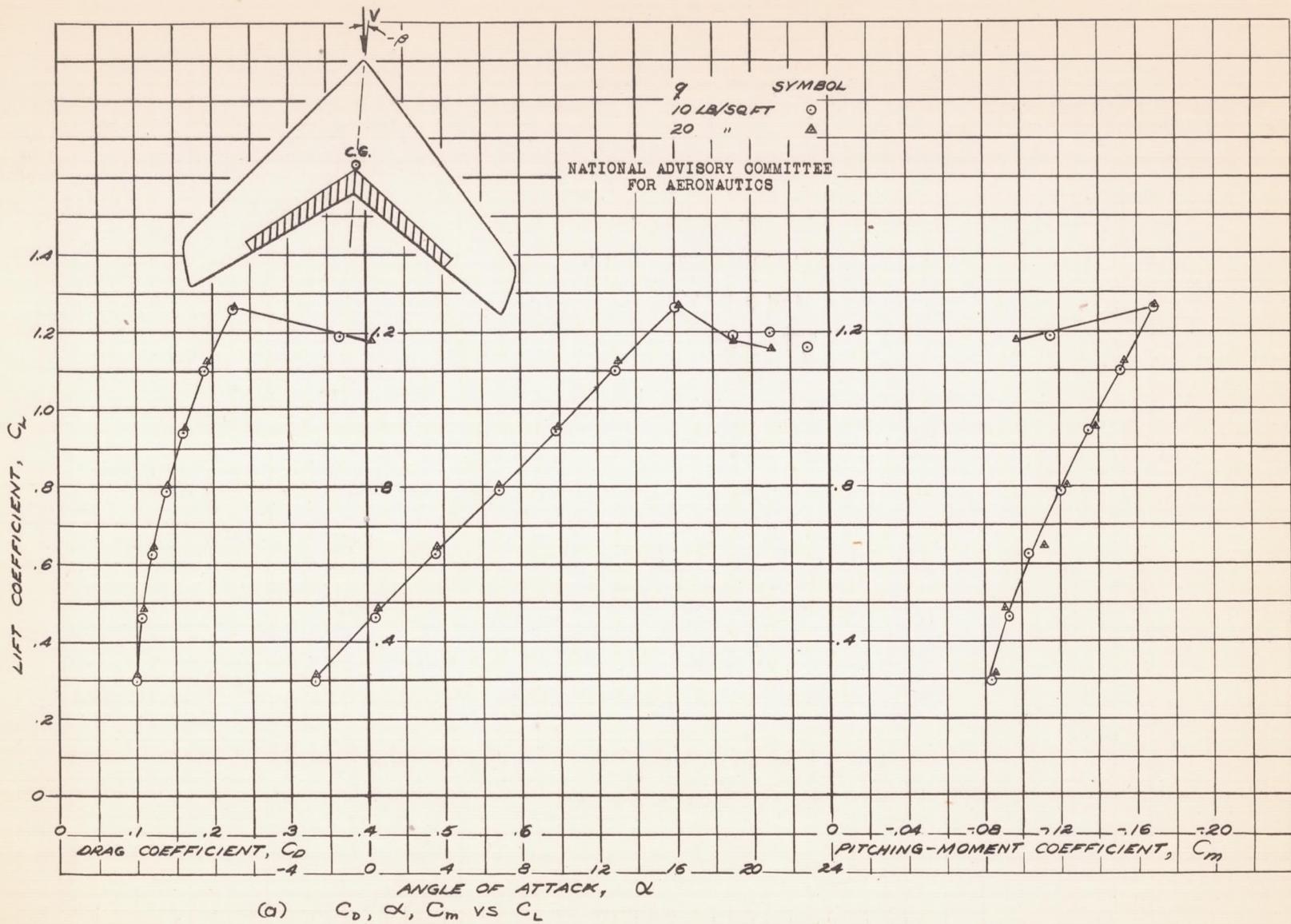


FIGURE 83.- AERODYNAMIC CHARACTERISTICS OF THE 45° SWEEPBACK WING AT -5.2° SIDESLIP. 20° CHORD 62.3 % SPAN SPLIT FLAPS DEFLECTED 60°.

Fig. 83b

NACA RM NO. A6K15

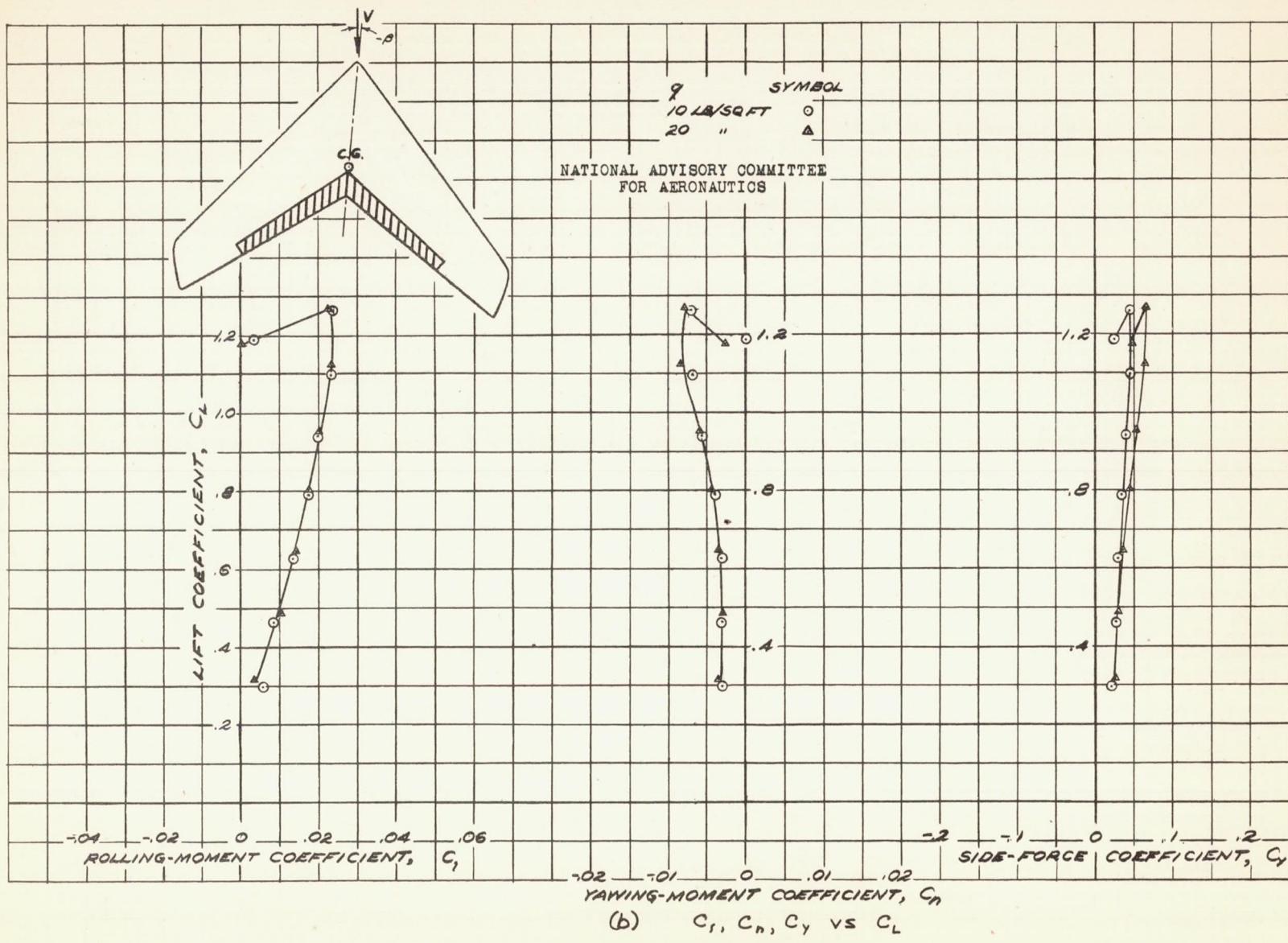


FIGURE 83.— CONCLUDED.

Fig. 84a

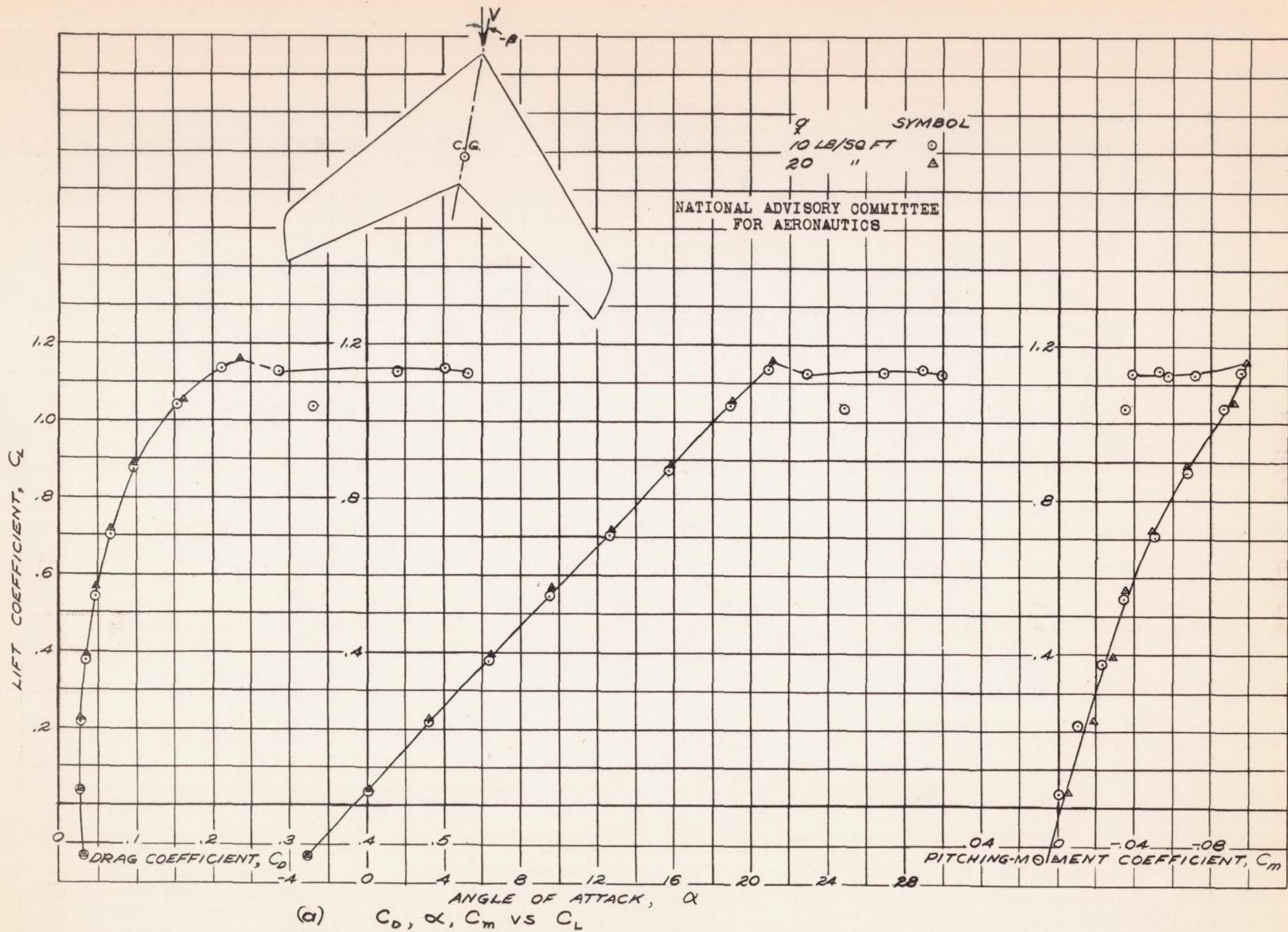


FIGURE 84.- AERODYNAMIC CHARACTERISTICS OF THE 45° SWEEPBACK WING AT -9.9° SIDESLIP,
PLAIN WING.

Fig. 84b

NACA RM No. A6K15

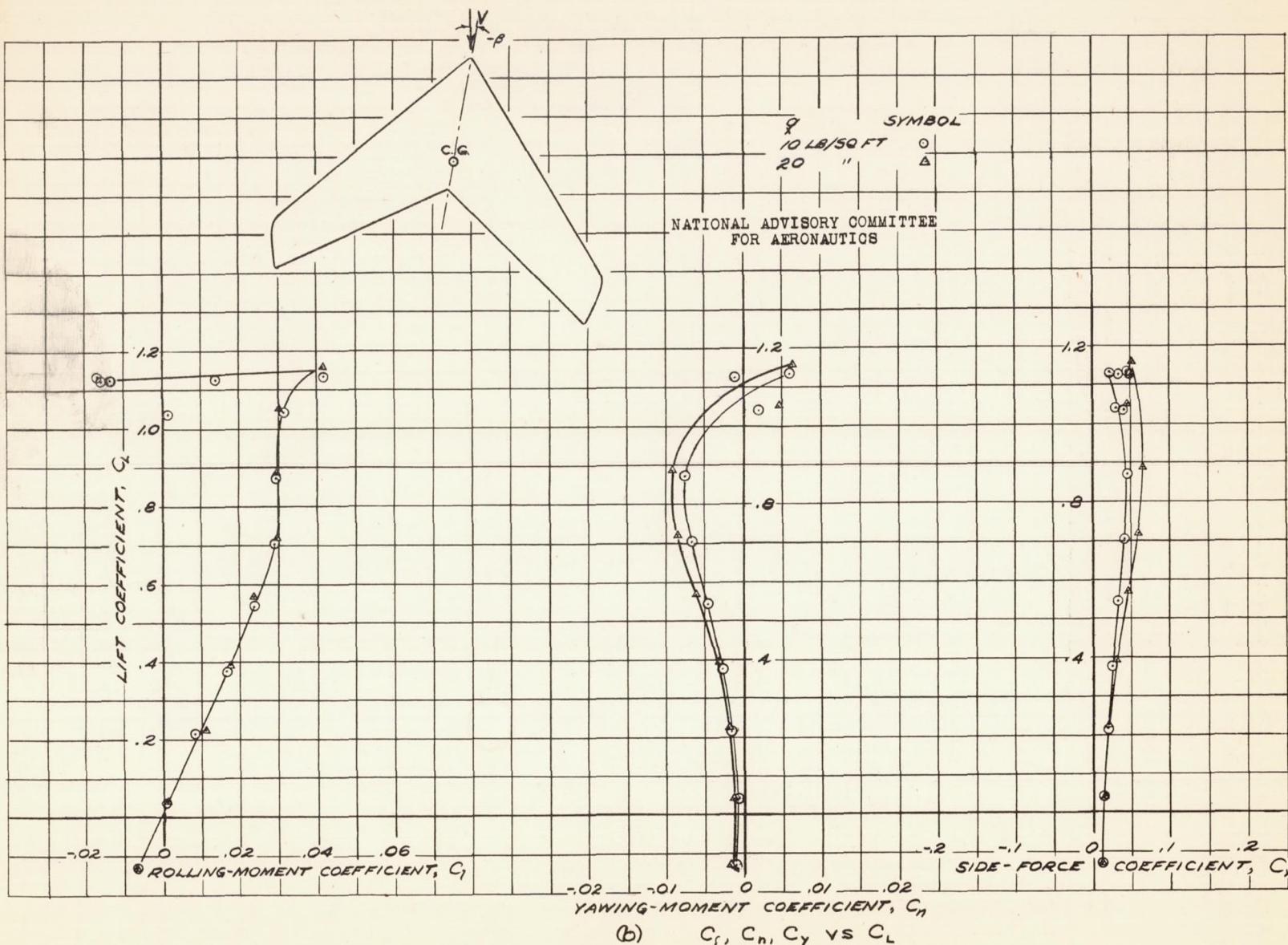


FIGURE 84. - CONCLUDED.

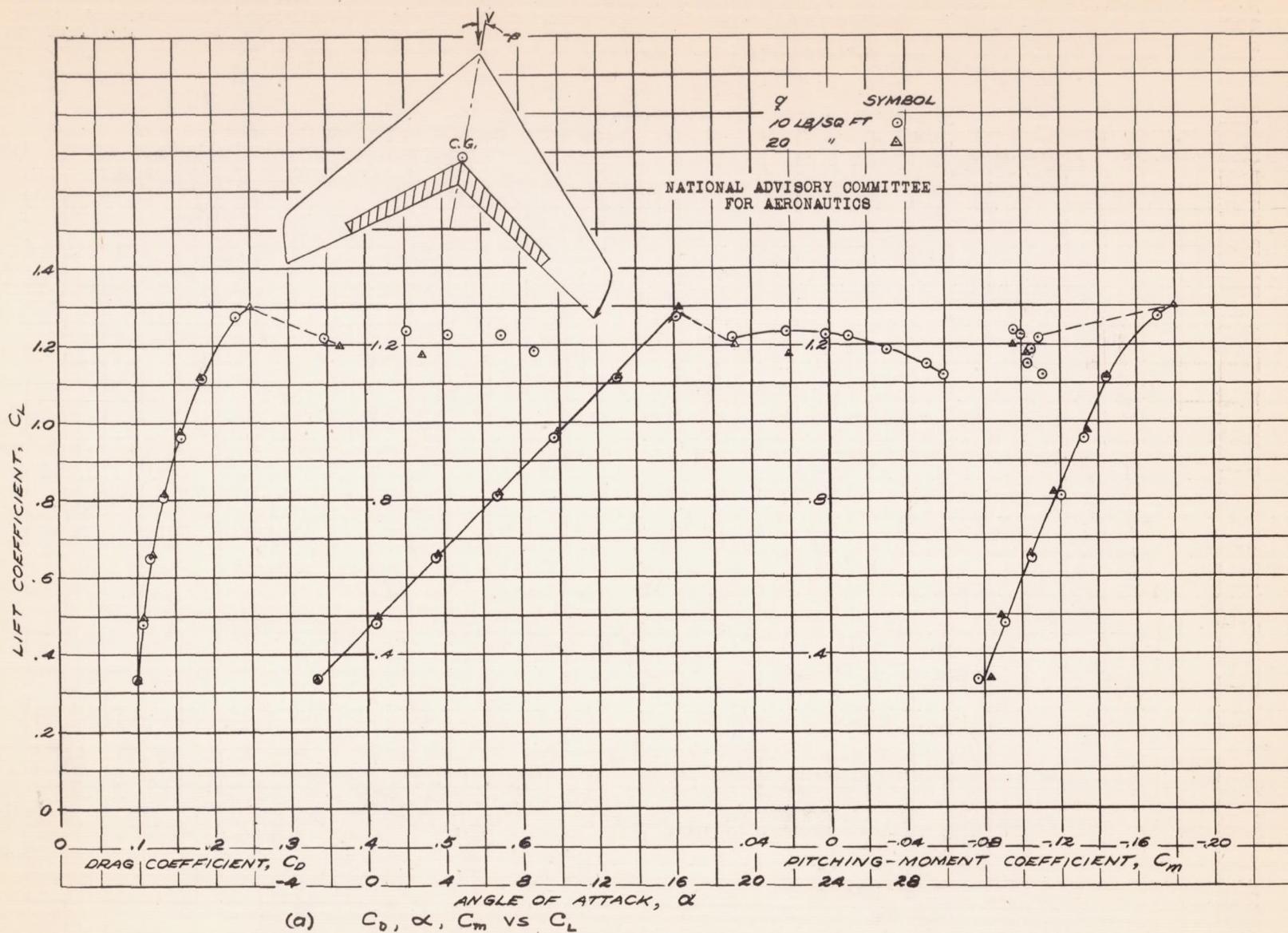


FIGURE 85.—AERODYNAMIC CHARACTERISTICS OF THE 45° SWEEPBACK WING AT -9.9° SIDESLIP. 20% CHORD 62.3% SPAN SPLIT FLAPS DEFLECTED 60°.

Fig. 85b

NACA RM NO. A6K15

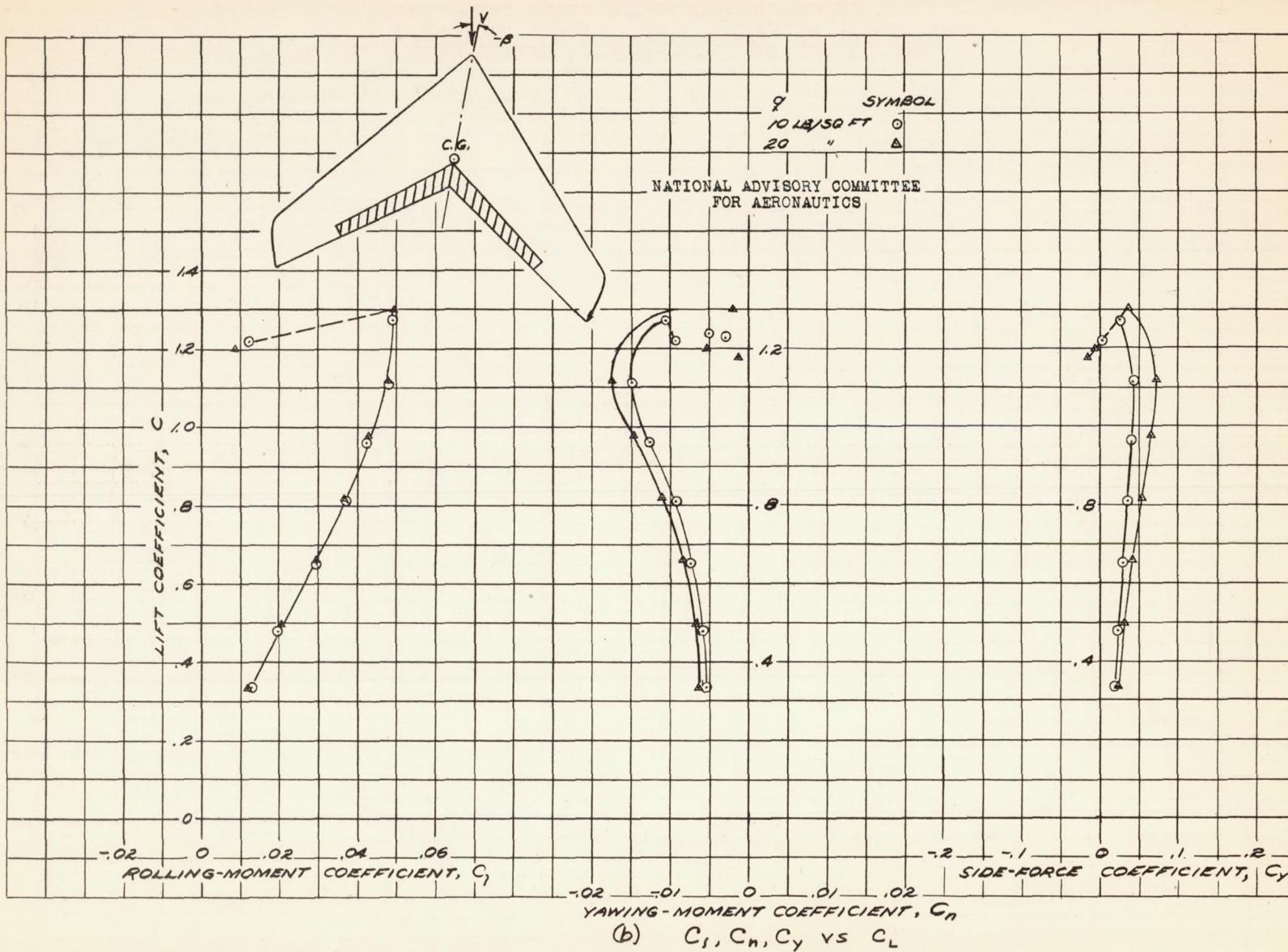


FIGURE 85.- CONCLUDED.

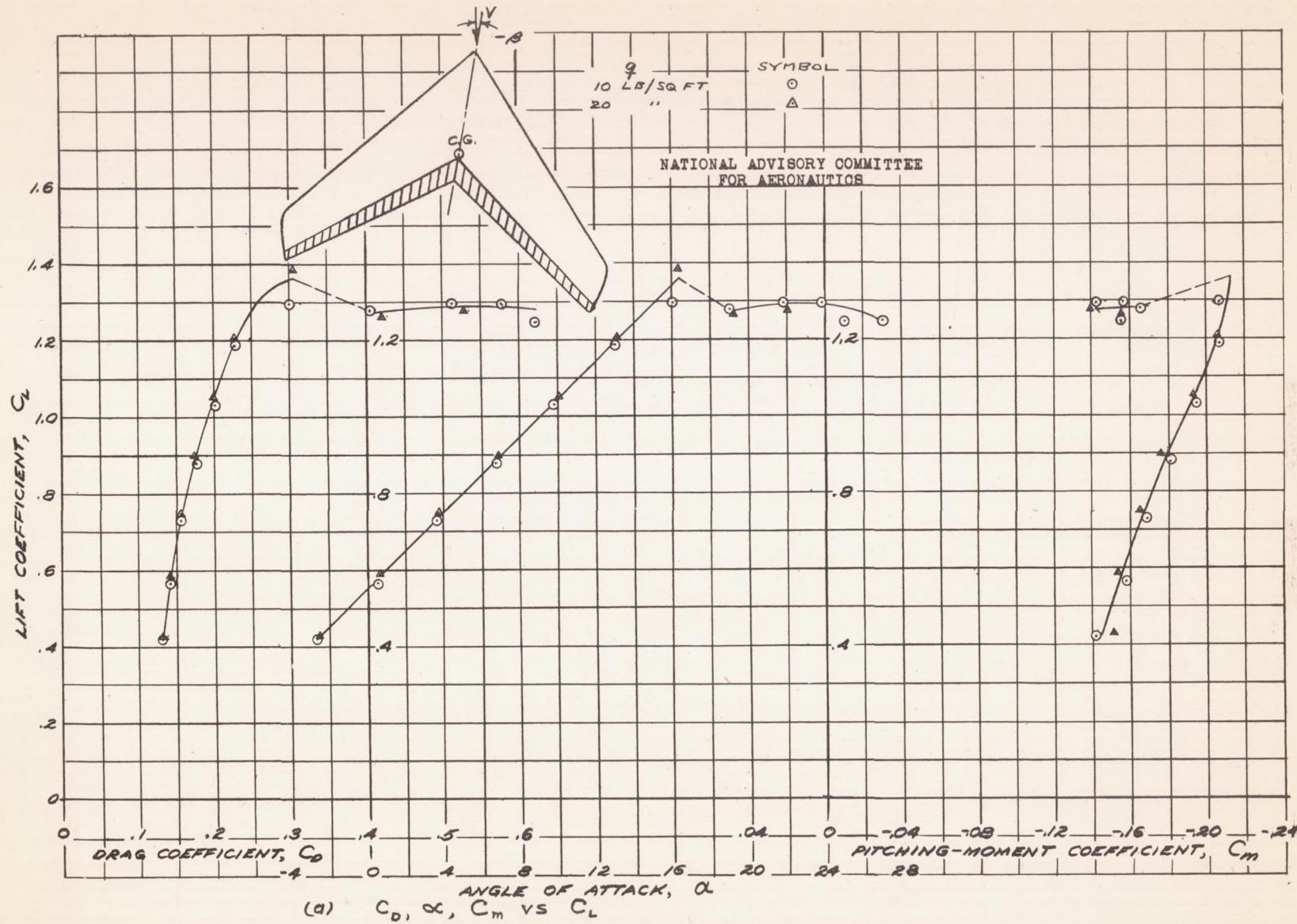


FIGURE 86.—AERODYNAMIC CHARACTERISTICS OF THE 45° SWEEPBACK WING AT -9.9° SIDESLIP. 20% CHORD FULL SPAN SPLIT FLAPS DEFLECTED 60°

Fig. 86b

NACA RM No. A6K15

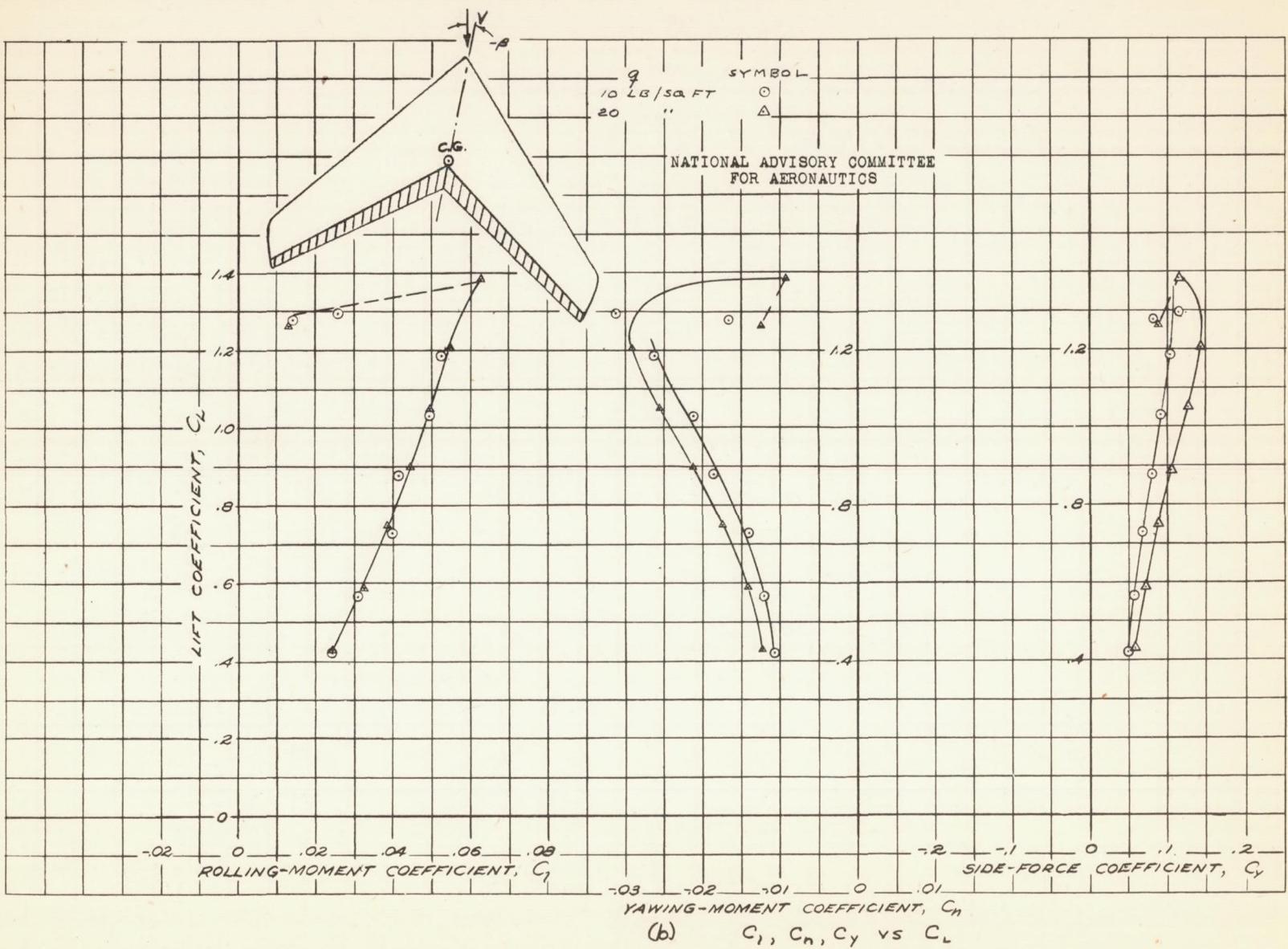


FIGURE 86.- CONCLUDED.

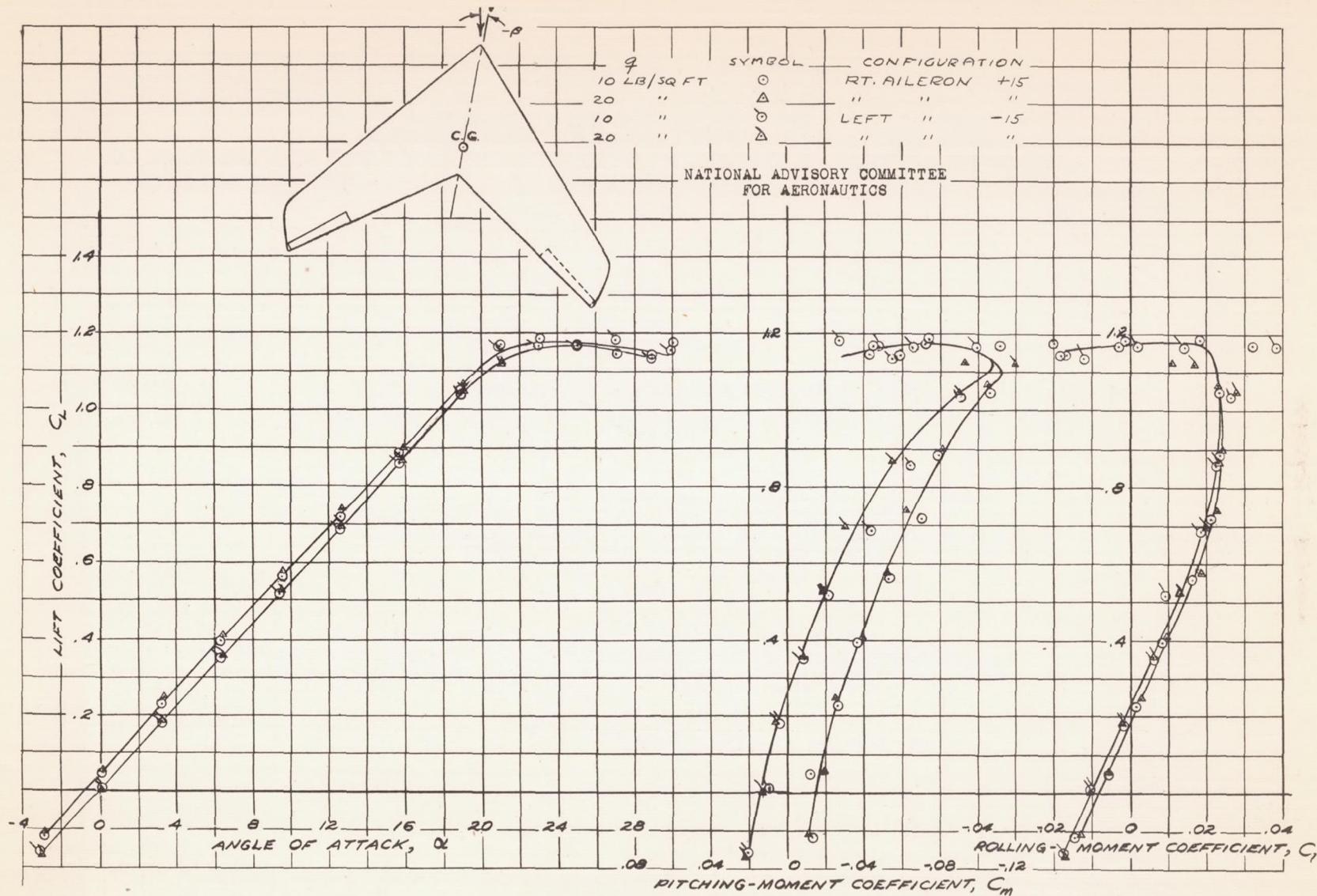


FIGURE 87. - AERODYNAMIC CHARACTERISTICS OF THE 45° SWEEPBACK WING AT -9.9° SIDESLIP, 20% CHORD 34.1% SPAN SPLITFLAP TYPE AILERONS DEFLECTED ± 15.0 .

Fig. 88a

NACA RM No. A6K15

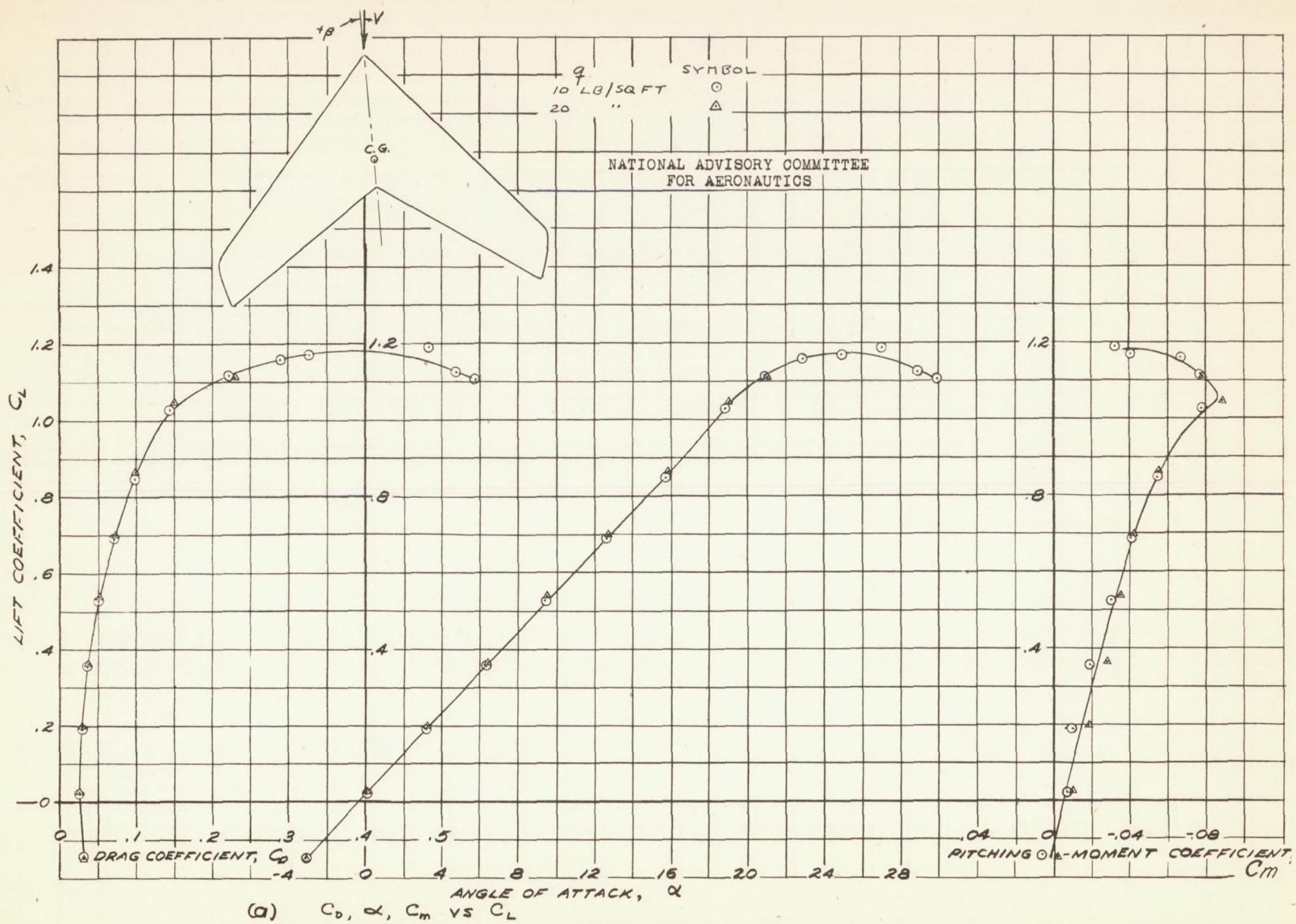


FIGURE 88.- AERODYNAMIC CHARACTERISTICS OF THE 45° SWEEPBACK WING AT +4.1° SIDESLIP.
PLAIN WING.

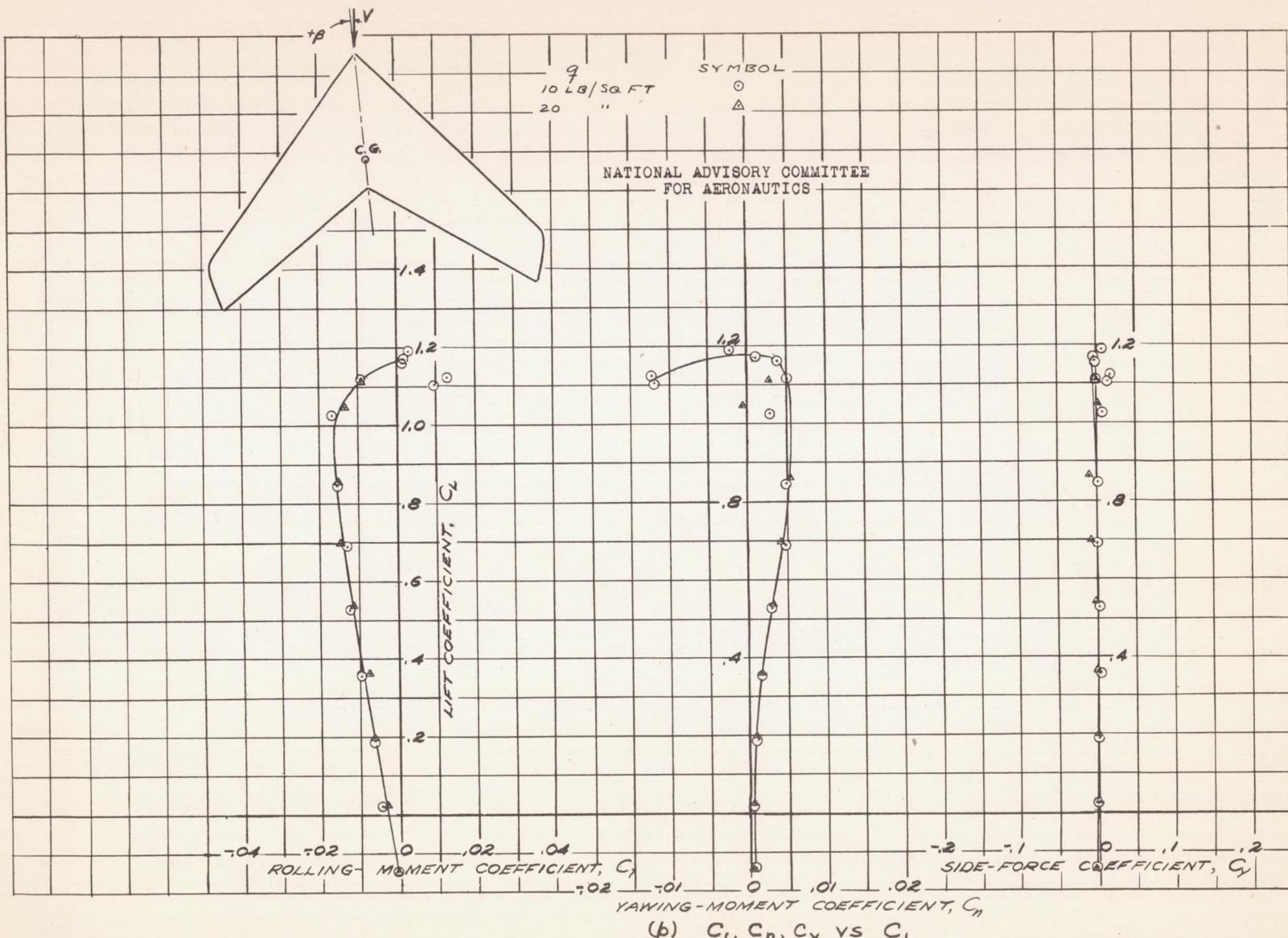


FIGURE 88.- CONCLUDED.

Fig. 89a

NACA RM No. A6K15

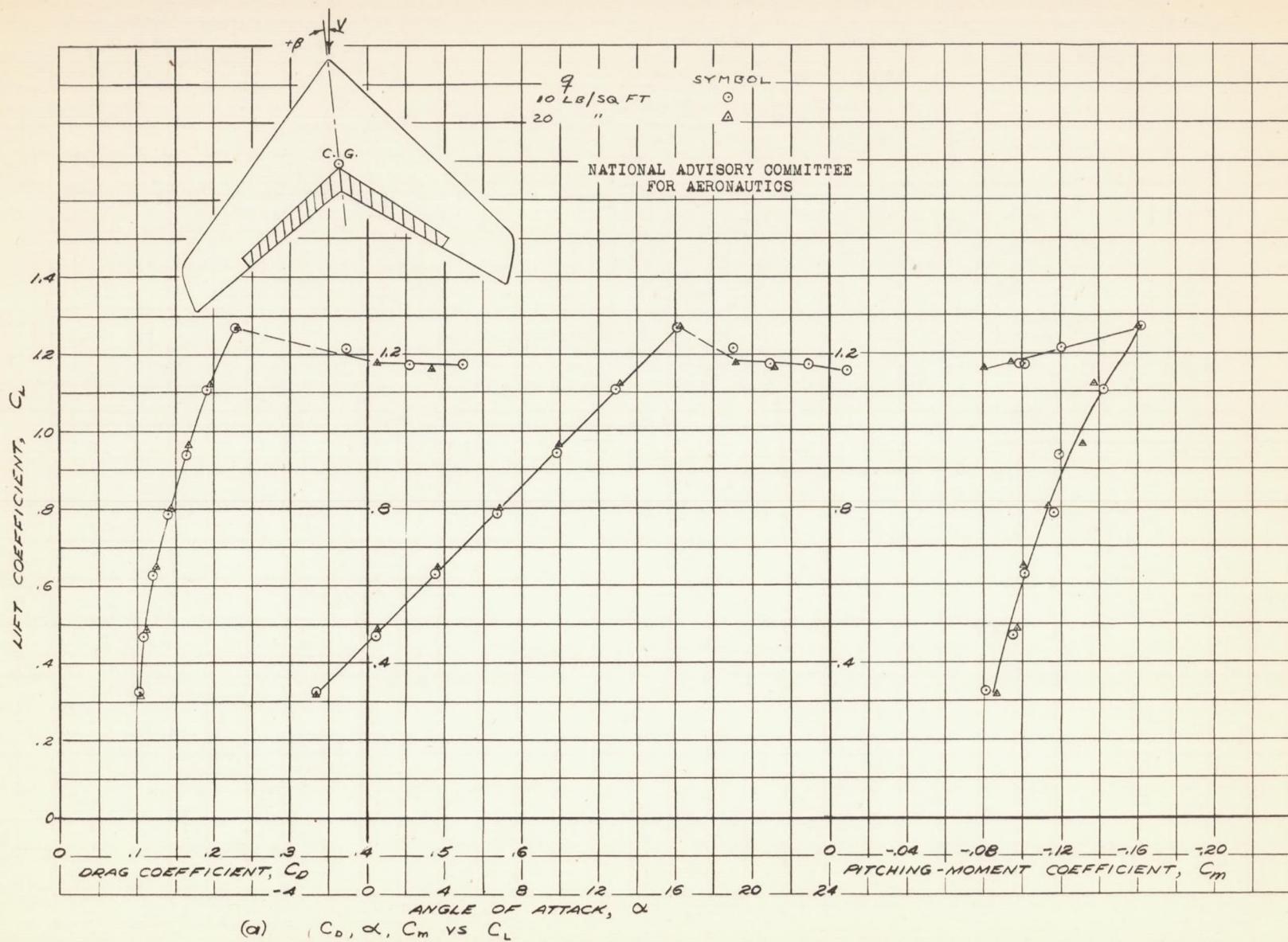


FIGURE 89.-AEROdynamic CHARACTERISTICS OF THE 45° SWEEPBACK WING AT $+41^\circ$ SIDESLIP. 20% CHORD 62.3% SPAN SPL. - FLAPS DEFLECTED 60° .

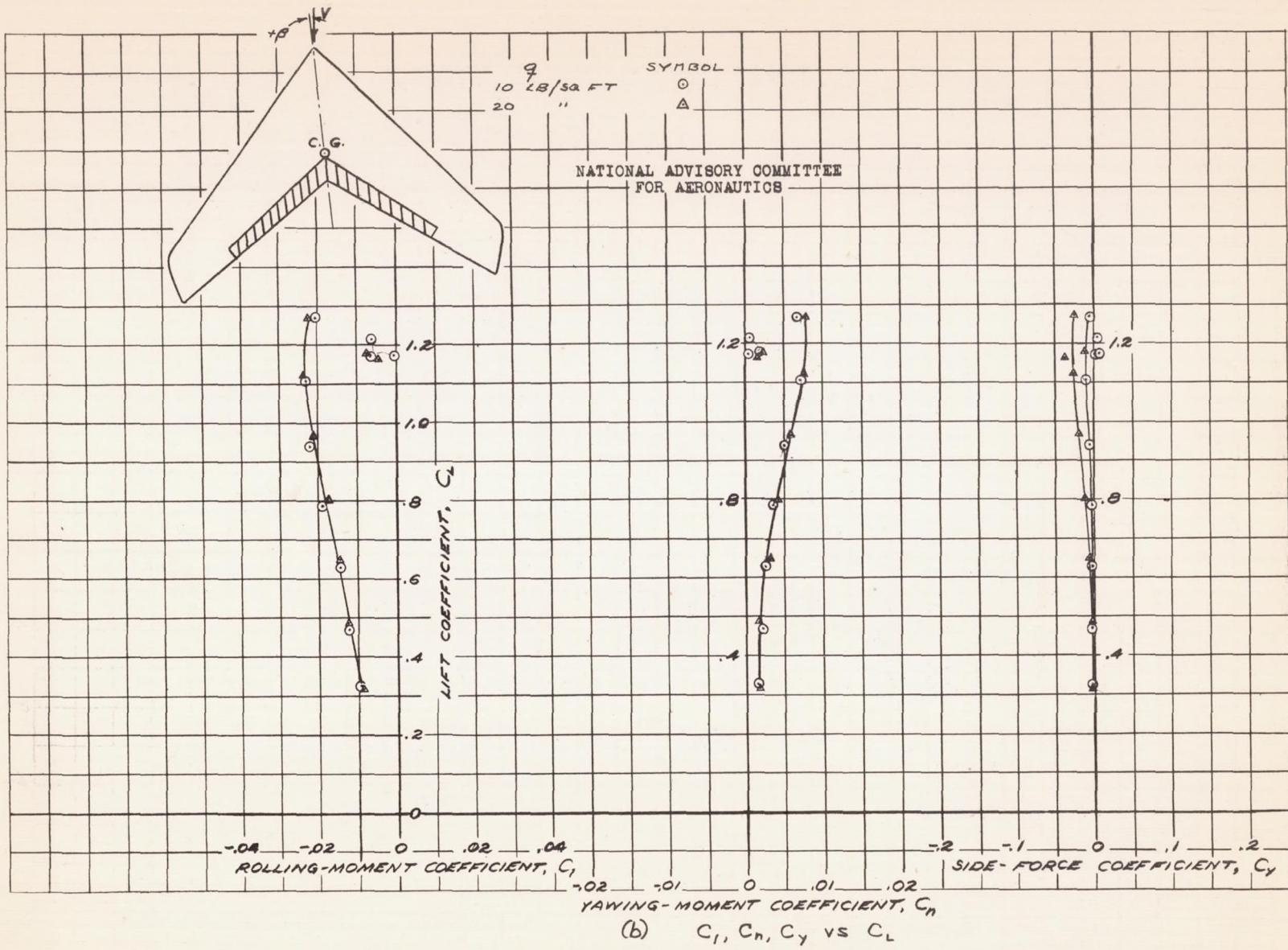


FIGURE 89.- CONCLUDED

Fig. 90a

NACA RM No. A6K15

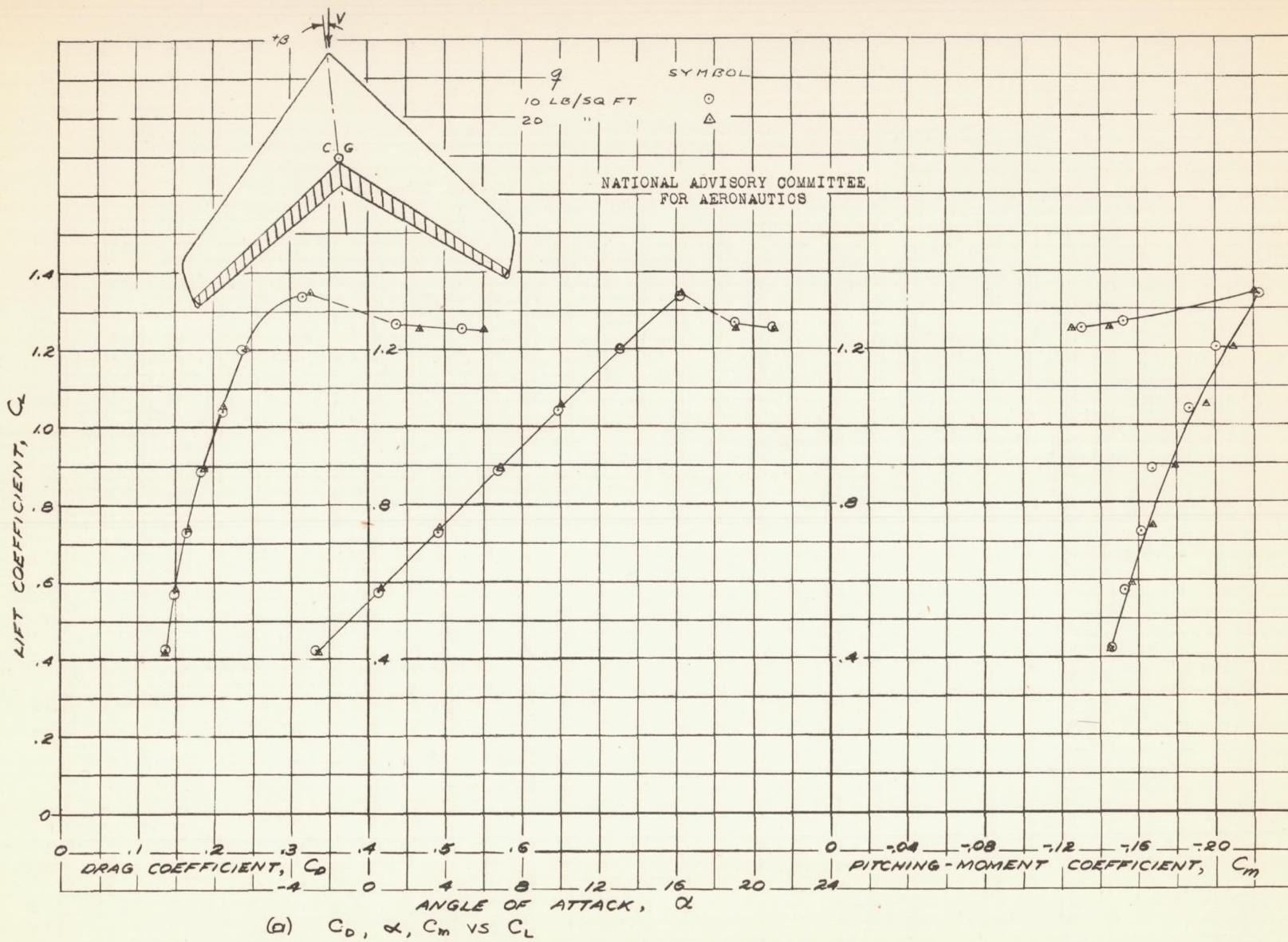


FIGURE 90.— AERODYNAMIC CHARACTERISTICS OF THE 45°
SWEPTBACK WING AT +4.1° SIDESLIP,
20% CHORD FULL SPAN SPLIT FLAPS DEFLECTED 60°

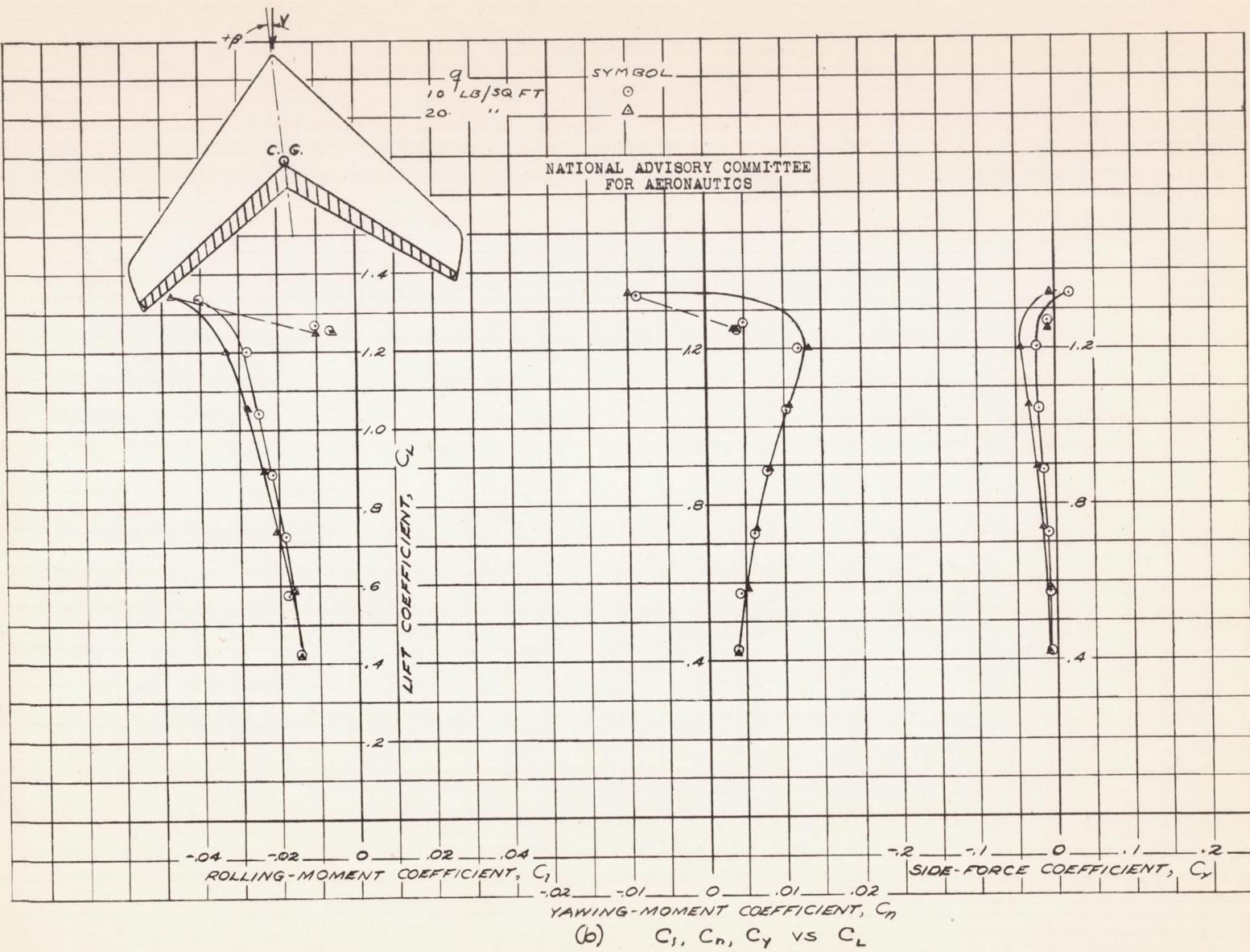


FIGURE 90.- CONCLUDED.

Fig. 91

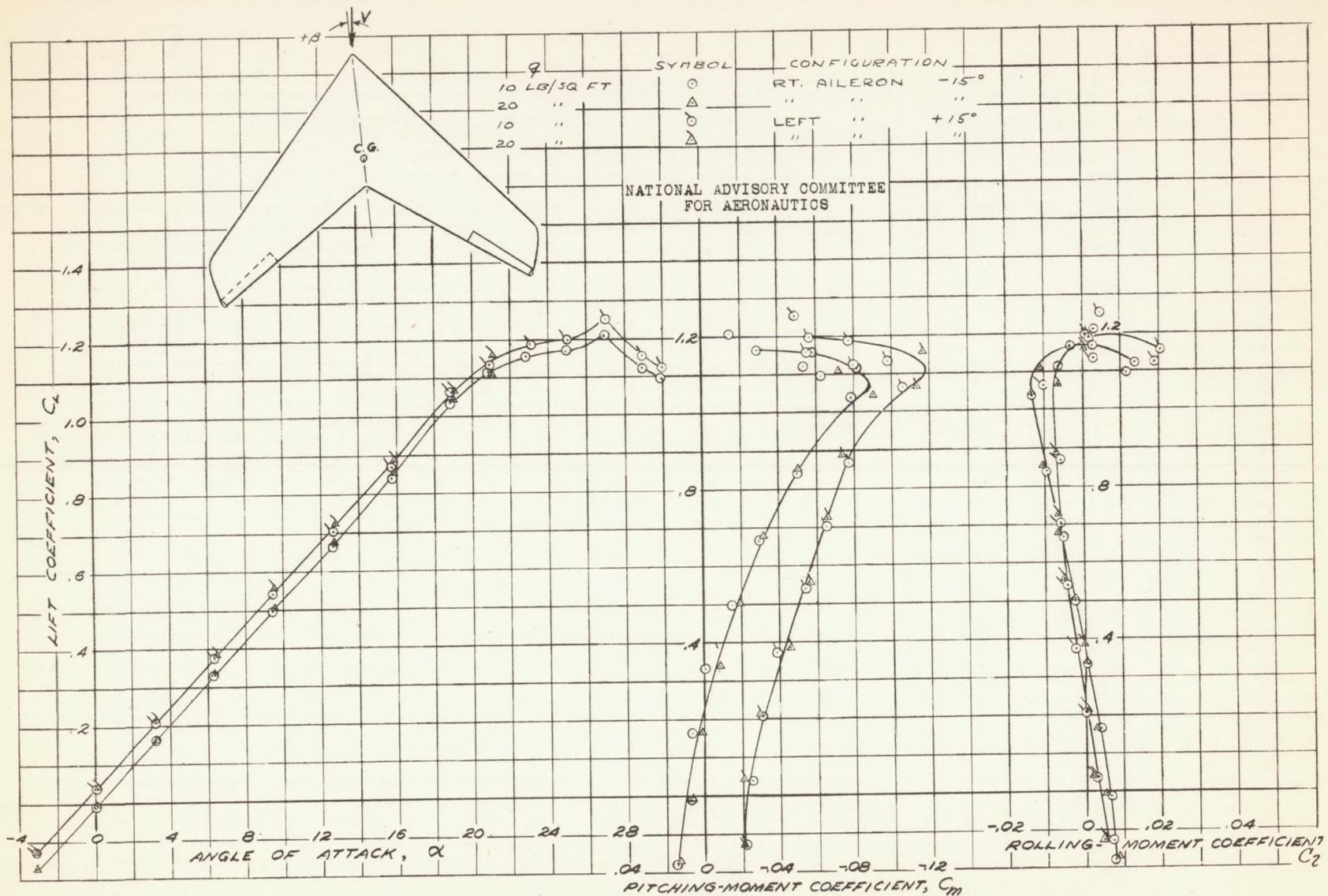


FIGURE 91.— AEROdynamic CHARACTERISTICS OF THE 45° SWEEPBACK WING AT $+4.1^\circ$ SIDESLIP, 20% CHORD 34.1% SPAN SPLIT FLAP TYPE AILERONS DEFLECTED $\pm 15^\circ$

NACA RM No. A6K15

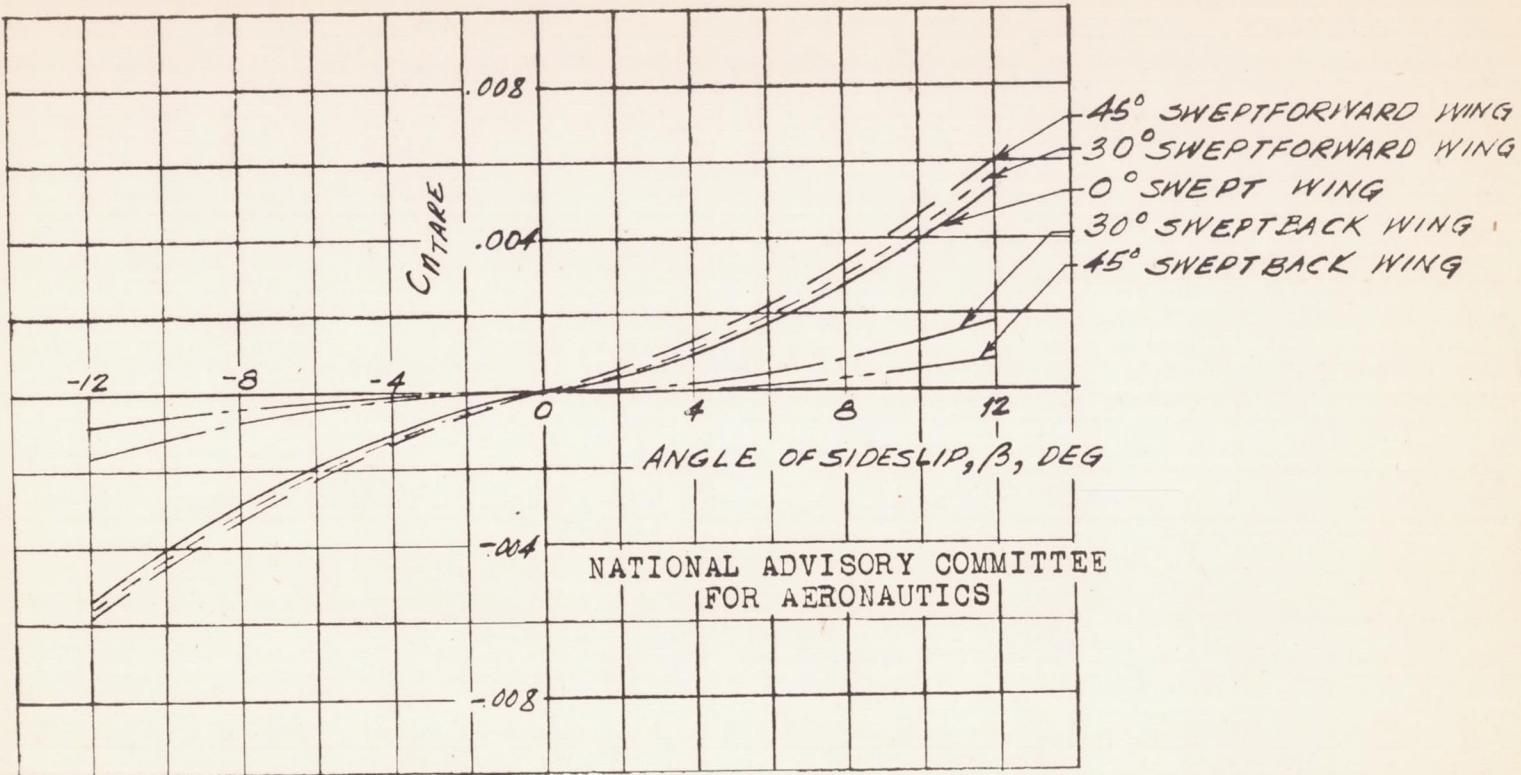


FIGURE 92.-YAWING-MOMENT COEFFICIENT TARE OF THE
FIVE SWEEP WINGS. (APPLIED TO BASIC DATA
TO OBTAIN SUMMARY DATA.)

